PENETRATION OF HARMFUL SUBSTANCES INTO THE SKIN: POLYCYCLIC AROMATIC HYDROCARBONS AND METAL ALLERGENS

Dissertation

submitted to the

Department of Biology, Chemistry, Pharmacy

Freie Universität Berlin

to obtain the degree

Doctor rerum naturalium

(Dr. rer. nat.)

Konstantin Simon

2024

This work with the title *Penetration of harmful substances into the skin: polycyclic aromatic hydrocarbons and metal allergens* was submitted to the Department of Biology, Chemistry, Pharmacy of Freie Universität Berlin as a dissertation to obtain the academic degree *Doctor rerum naturalium* (Dr. rer. nat.). The experimental work of this thesis was carried out at the German Federal Institute for Risk Assessment (BfR) in Berlin, Germany, from September 2019 to August 2022 under supervision of Prof. Dr. Dr. Andreas Luch.

1st reviewer: Prof. Dr. Dr. Andreas Luch

2nd reviewer: Prof. Dr. Daniel Klinger

Date of defense: 26.11.2024

I hereby declare that I alone am responsible for the content of my doctoral dissertation and that I have only used the sources or references cited in the dissertation.

Berlin,

Foreword

In 2019, I was offered the opportunity to carry out a doctoral research project at the Federal Institute for Risk Assessment (BfR) on skin penetration of harmful substances. The focus of the subject has shifted over time and has resulted in the publications presented in this thesis. I would like to thank all of the people who have made this possible and accompanied me along the way.

Alexander Roloff was of immense help during each stage of my doctoral research project. I am grateful for the fortnightly progress reports that made me reflect upon the results I had generated. It gave me valuable feedback for future experiments. He was always available for discussions on projects and critically reviewed the manuscripts as well as this thesis. These correction rounds helped me hone my writing skills, which have greatly improved over the course of my doctoral research. Thank you, Alex!

I want to thank Christoph Hutzler, Nastasia Bartsch and Ralph Pirow. Christoph Hutzler contributed to my project before working for a different department. During this time, he critically reviewed my work in the progress reports and helped me out with his extensive knowledge on gas chromatography coupled to mass spectrometry (GC-MS/MS). Nastasia Bartsch was my predecessor on the skin penetration subject and took the time to patiently show me how to employ the Franz diffusion cell (FDC) assay. There is a lot to take into consideration, which would have taken me a long time to learn without her help. Ralph Pirow had the idea for my first research project concerning partition and diffusion coefficients of polycyclic aromatic hydrocarbons (PAH) through the skin. He helped me with writing code in R and the mathematical side of the project.

Special credit goes to Lidia Schneider. Together with her, I carried out most of the FDC assays. These experiments are a lot of work and very time consuming. With Lidia, they were less burdensome. I was able to discuss the experiments and projects with her and she gave me her honest and valuable opinion.

Gila Oberender carried out a internship and a bachelor thesis under my supervision. I could not have ask for a better student. She was of great help especially for the tape stripping experiments and FDC assays for PAH penetration experiments.

Coming to the BfR, I had not used GC-MS/MS before, now I have quite a deep knowledge of this analytical technique, to which Klaudia Michna and Svetlana Kruschinski contributed a great deal. They explained this method patiently and were always at hand when I needed help or the machine failed to work correctly.

I want to thank all of Department 7 and especially unit 77 for a supportive work environment. Special thanks goes to Philipp Reichardt, Nadine Dreiack, Roman Schmidt and Mohammad Al-Khatib who helped with the microwave-assisted digestion and inductively-coupled plasma mass spectrometry measurements. Sandra Schiewe and Nadine Dreiack were of great help when it came to the use of the cryo-microtome, which is not always easy to handle. Katherina Siewert had a great impact on the project on skin penetration of metal allergens, for which I am grateful. I also want to thank Elke Kerstan and Gabriele Wothe in the laboratory scullery, who provided me and everybody else with clean laboratory glassware.

I want to especially thank Andreas Luch, who is head of Department 7, for providing a work environment where I had scientific freedom to pursue my research projects. Furthermore, I thank him for the critical review of my publications and my thesis. I also thank Daniel Klinger for accepting to review my thesis.

I was not the only doctoral student during my time at the BfR. I want to thank my peers who experienced the same troubles that I did and we almost all managed to get through together. These include Aline Rosin, Maya Kissner, Nadja Mallock, Manah Kaveh, Benjamin Krause, Tessa Höper, Markus Kirchner, Luise Klein, Emeka Emecheta and Amelie Vogel.

There are two names among those at the BfR, which deserve special recognition: Franziska Riedel and Charlotte Kromer. We have spent a lot of time together and have grown to become more than mere colleagues. I regard you as two of my closest friends. The times were not always easy, but you made them weigh lighter.

I also have people outside of the academic world to thank. My parents, Helga and Lubens Simon, have always supported and guided me along the way, long before I even started this project.

My friends Henrik Hupatz, Leo Grothe and Vico Adjedje have supported me during this phase of my life that was not always easy. Thank you for being there when I needed you!

Finally, I want to thank Paul Nentwig, my partner, who has supported me during the last stretch of this long project. He endured me during these sometimes somewhat stressful times.

This thesis was proof read by Alexander Roloff, Henrik Hupatz, Vico Adjedje, Charlotte Kromer, Franziska Riedel and Andreas Luch. Thank you for helping me with this manuscript!

Contents

Foreword . . . 3

Zusammenfassung . . . 7

Abstract . . . 9

Abreviations . . . 11

1 Introduction . . . 13

2 Skin . . . 17
Tape stripping: studying individual layers of the *startum corneum* . . . 19

3 Polycyclic aromatic hydrocarbons . . . 25
Metabolism of polycyclic aromatic hydrocarbons in mammals . . . 28
Dermal exposure to polycyclic aromatic hydrocarbons . . . 29

4 Metal-induced allergic contact dermatitis . . . 43
Dermal penetration of metal allergens . . . 45

5 Conclusion . . . 51

References . . . 53

A Publications . . . 73
A.1 Continuous removal of single cell layers by tape stripping the *stratum corneum* — a histological study . . . 73
A.2 Polycyclic aromatic hydrocarbon skin permeation efficiency *in vitro* is lower through human than pigskin and decreases with lipophilicity . . . 85
A.3 Migration of polycyclic aromatic hydrocarbons from a polymer surrogate through the *stratum corneum* layer of the skin . . . 103
A.4 Less efficient skin penetration of the metal allergen Pd^{2+} compared to Ni^{2+} and Co^{2+} from patch test preparations . . . 127

Zusammenfassung

Die folgende Arbeit beschäftigt sich eingehend mit der Barrierefunktion der Haut, indem sie die Hautpenetration von zwei toxikologisch wichtigen Stoffklassen untersucht: polyzyklische aromatische Kohlenwasserstoffe (PAK) und die Metallallergene Nickel, Kobalt und Palladium. Darüber hinaus wurde die Methode des *tape strippings* genutzt, um die Abtragungsrate des *Stratum corneum* (s.c.) mit jedem Klebestreifen zu ermitteln.

Hautkontakt zu schädlichen Stoffen kann durch Verbraucherprodukte, die diese enthalten, auftreten. Die Schadstoffe sind den Verbraucherprodukten entweder absichtlich — beispielsweise als Zusatzstoffe in Kunststoffen oder bestimmte Metalle in Legierungen — oder unbeabsichtigt als Kontaminanten zugesetzt. PAK können Kunststoffe kontaminieren, die Mineralöle als Weichmacher oder *Carbon Black* als Färbemittel enthalten. Nickel, Kobalt und Palladium, die allergische Kontaktdermatitis hervorrufen können, werden in Legierungen für Schmuck zugesetzt, um bestimmte Eigenschaften wie beispielsweise Farbe und Korrosionsbeständigkeit zu erhalten.

Studien zur Hautpenetration stützen sich auf die bewährte Methode des *in vitro* Franz-Diffusionszellenassay (FDC-Assay). Eine Hautprobe oder ein Hautmodel wird über eine Rezeptorkammer gespannt und eingeklemmt. Die Rezeptorkammer ist mit einem wässrigen Medium befüllt. Der zu untersuchende Stoff wird in einer Matrix aufgetragen, beispielsweise in Lösemittel, in Petrolatum oder direkt im Verbraucherprodukt. Nach einer bestimmten Inkubationszeit werden die Kompartimente analysiert, um die Penetrationsraten dieses Stoffes in die Haut zu ermitteln.

Um die Menge des Stoffes in den einzelnen s.c.-Schichten zu quantifizieren, spielt die Technik des *tape stripping* mit Klebestreifen eine wichtige Rolle. Ein Klebestreifen wird auf die Haut gedrückt und entfernt eine Schicht des s.c. wenn er wieder abgezogen wird. Allerdings ist die Menge des mit jedem Klebestreifen entfernten s.c. noch immer Gegenstand wissenschaftlicher Debatten. In einer hier vorgestellten histologischen Studie wurde das s.c. durch *tape stripping* von Schweinehaut entfernt und das verbleibende s.c. mikroskopisch quantifiziert. Die Studie ergab eine lineare Abnahme des s.c. in Bezug auf die Dicke und die Anzahl der Zellschichten bei bis zu zwanzig abgenommenen Klebestreifen. Jeder Klebebandstreifen entfernte etwa eine Zellschicht, was einer Dicke von 0,4 µm entspricht.

Im Rahmen dieser Arbeit wurde das Eindringen von PAK durch das s.c. untersucht. Dabei wurde der Einfluss der Lipophilie — ausgedrückt durch den Oktanol-Wasser-Verteilungskoeffizienten ($\log P$) — auf die Durchlässigkeit dieser toxischen Verbindungen gezeigt. Die Auftragung 24 ver-

schiederner PAK (152–302 g/mol, log*P*: 3.9–7.3) in Acetonitril in einem FDC-Assay ergab, dass PAK mit höherer Lipophilie eine geringere Penetrationsrate aufweisen. Außerdem wurde die Penetration für Zeitpunkte zwischen 2 und 48 Stunden untersucht. Hoch-lipophile, sechsringige PAK wie die Dibenzopyrene dringen überhaupt nicht durch die Haut, während weniger lipophile, dreiringige PAK wie Acenaphthen die Haut bereits nach zwei Stunden durchdringen.

Die Auswertung von FDC-Assays die mit Menschen- und Schweinehaut durchgeführt wurden, ermöglichte den Vergleich dieser beiden Hauttypen. Es wurde gezeigt, dass das menschliche s.c. einen größeren Anteil der in die Haut eingedrungenen PAK zurückhält als das s.c. von Schweinen.

Die Abhängigkeit der Hautpenetration von der Lipophilie der PAH wurde auch durch Experimente untermauert, die darauf abzielten, die Verteilungs- und Diffusionskoeffizienten von fünf ausgewählten PAK aus einer Polypropylenersatzmatrix (Squalan) in das s.c. von Schweinen zu ermitteln. Der PAK-Gehalt in den Hautkompartimenten wurde durch Gaschromatographie in Verbindung mit Tandem-Massenspektrometrie bestimmt. Die Anwendung des *tape strippings* erlaubte das Erstellen eines Konzentrationsprofils im s.c. Dieses Profil wurde an eine mathematische Lösung des zweiten Fickschen Gesetzes angepasst, was die Berechnung der Verteilungs- und Diffusionskoeffizienten ermöglichte. Die Verteilungskoeffizienten korrelierten positiv mit dem log*P*, während der Diffusionskoeffizient für Naphthalin am höchsten und für die anderen PAK etwa gleich hoch war.

Nickel und Kobalt sind im Gegensatz zu Palladium Teil der Standardreihe von Epikutantests, die zur Diagnose von Kontaktallergien verwendet werden. Entsprechend werden Palladiumallergien selterner diagnostiziert als solche gegen Nickel und Cobalt. Pd^{2+} zeigte jedoch in einem *in vitro* Aktivierungs-induzierten Marker-Assay in menschlichen Blutproben eine höhere Frequenz an $CD154^{+}$ T-Zellen als Ni^{2+} oder Co^{2+}. Ein Grund für die niedrigere Zahl an diagnostizierten Palladiumallergien könnte neben der geringeren Anzahl an Epukutantests eine geringere Hautpenetrationsrate von Pd^{2+} im Vergleich zu Ni^{2+} oder Co^{2+} sein.

Um diese Hypothese zu testen, wurden FDC-Assays mit Schweinehaut durchgeführt. Für die klinische Diagnose verwendete Epikutantest-Präparate (das jeweilige Metallsalz in Petrolatum) wurden auf Schweinehaut aufgetragen und 48 Stunden inkubiert, was dem Zeitrahmen eines Epikutantests entspricht. Zusätzlich wurden FDC-Assays mit den drei Ionen Ni^{2+}, Co^{2+} und Pd^{2+} in einer wässrigen Lösung durchgeführt, um Penetrationsraten unabhängig von der Ionen-Löslichkeit zu bestimmen. Die Wiederfindungen in den Hautkompartimenten wurden durch Massenspektrometrie mit induktiv gekoppeltem Plasma quantifiziert. Pd^{2+} zeigte geringere Penetrationsraten als Ni^{2+} und Co^{2+}, unabhängig von der Anwendung in Petrolatum oder wässriger Lösung.

Insgesamt trägt die vorliegende Arbeit zum Verständnis und der Untersuchung der Barrierefunktion des s.c. und der Faktoren bei, die die dermale Penetration von zwei unterschiedlichen Klassen toxikologisch relevanter Stoffe beeinflussen.

Abstract

The present thesis provides an in-depth study of the barrier function of the skin by investigating the penetration of two toxicologically important substance classes: polycyclic aromatic hydrocarbons (PAH) and the metal allergens nickel, cobalt and palladium. Furthermore, the method of tape stripping was scrutinized to reveal the removal rate of *stratum corneum* (s.c.) with each tape strip.

Skin contact to harmful substances can occur through consumer products containing them. Harmful substances are added to consumer products either by design — for example, as additives in plastic or certain metals in alloys — or inadvertently as contaminants. PAH were found to contaminate those plastics that are dyed with carbon black or contain mineral oils used as plasticizers. Nickel, cobalt and palladium, known to cause allergic contact dermatitis, are added into alloys in jewelry to attain certain characteristics such as color or corrosion resistance.

Skin penetration studies rely on the well-established *in vitro* Franz diffusion cell (FDC) assay. A skin sample or model is fixed over a receptor chamber containing an aqueous medium. The substance of interest is applied onto the skin in a matrix, for example, in solvents, petrolatum or in the consumer products themselves. After a certain incubation time, the compartments are analyzed to reveal the penetration rates of that substance into the skin.

In order to quantify the amount of substance in separate s.c. layers, the technique of tape stripping plays an important role. A tape strip is pressed onto the skin and removes a layer of the s.c. when taken off. However, the amount of s.c. removed with each tape strip is still subject of scientific debate. In a histological study presented here, the s.c. was removed by tape stripping of pigskin and the remaining s.c. was quantified microscopically. The study revealed a linear decrease in s.c. in terms of thickness as well as number of cell layers up to 20 removed tape strips. Each tape strip removed about one cell layer, corresponding to 0.4 µm.

In this thesis, the penetration of PAH through the s.c. was extensively studied. The influence of lipophilicity — expressed by the octanol-water partition coefficient (log$P$) — on the permeability of these toxic compounds was demonstrated. Applying 24 different PAH (152–302 g/mol, log$P$: 3.9–7.3) in acetonitrile in an FDC assa, revealed that more lipophilic PAH exhibit lower penetration rates. Furthermore, the penetration was investigated for time intervals ranging from 2 h to 48 h. Highly lipophilic, six-ringed PAH like the dibenzopyrenes did not permeate the skin at all, whereas the less lipophilic, three-ringed PAH like acenaphthene permeate after 2 h already.

The evaluation of FDC assays using human and pigskin allowed for the comparison of these two skin types. Human s.c. was shown to retain a greater share of the PAH that partition into the skin than porcine s.c.

The dependence on lipophilicity of PAH skin penetration is further supported by experiments that aimed to determine partition and diffusion coefficients of five selected PAH from a polypropylene surrogate (squalane) into porcine s.c. The PAH content in the skin compartments was quantified by gas chromatography coupled to tandem mass spectrometry. The use of tape stripping resulted in a concentration profile along the s.c. This profile was fitted to a solution of Fick's second law, allowing the calculation of partition and diffusion coefficients. The partition coefficients positively correlated with the log$P$, while the diffusion coefficient was highest for naphthalene and about the same for the other PAH.

Nickel and cobalt are, contrary to palladium, part of the standard patch test used as diagnostic tool to detect contact allergies. Therefore, fewer allergies against palladium are diagnosed than those against nickel and cobalt. Nonetheless, Pd^{2+} exhibited higher frequencies of $CD154^{+}$ in an *in vitro* activated marker assay in human blood samples than Ni^{2+} and Co^{2+}. A reason for the lower number of diagnosed palladium allergies next to fewer tests could be a lower penetration rate of Pd^{2+} as compared to Ni^{2+} or Co^{2+}.

To test this hypothesis, FDC assays using pigskin were employed. Patch test preparations used for clinical diagnosis (the respective metal salt dispersed in petrolatum) were given onto the skin and incubated for 48 h, which corresponds to the time frame of a patch test. Additionally, FDC assays with the three ions in an aqueous solution were carried out to evaluate penetration rates independent of ion solubility. The recoveries in the skin compartments were quantified by inductively coupled plasma mass spectrometry. Pd^{2+} showed lower penetration rates than Ni^{2+} and Co^{2+}, regardless of application in petrolatum or aqueous solution, thus confirming the hypothesis.

Collectively, these studies contribute to the understanding and analysis of the s.c. barrier function and the factors influencing the dermal penetration of two distinct classes of toxicologically relevant substances.

Abbreviations

The following list includes all abbreviations and symbols used throughout this thesis.

ACD	allergic contact dermatitis
AhR	aryl hydrocarbon receptor
B[*a*]P	benzo[*a*]pyrene
BSA	bovine serum albumin
CAS	Chemical Abstracts Service Registry Number
CYP	cytochrome P450 dependent monooxygenases
DB[*a,h*]P	dibenzo[*a,h*]pyrene
DB[*a,l*]P	dibenzo[*a,l*]pyrene
dG	deoxyguanosine
DNA	deoxyribonucleic acid
doi	digital object identifier
EFSA	European Food Safety Authority
et al.	and others
FDC	Franz diffusion cell
GC-MS/MS	gas chromatography coupled to tandem mass spectrometry
HE	hematoxylin-eosin
ICP-MS	inductively coupled plasma mass spectrometry
mEH	microsomal expoxide hydrolase
NER	nucleotide excision repair pathway
NIAS	non-intentionally added substances
OECD	Organisation for Economic Co-Operation and Development
PAH	polycylic aromatic hydrocarbons
PBS	phosphate-buffered saline
PTP	patch test preparation
s.c.	*stratum corneum*
SCCS	Scientific Committee on Consumer Safety
TEWL	trans-epidermal water loss
TLR4	Toll-like receptor 4
UV	ultraviolet light
VIS	visible light

Symbols and units

°C	degree Celsius
c	before units: centi
Co	cobalt
c_A	molar surface concentration
c_m	concentration in the matrix
c_n	molar concentration
$c_{rel,x,t}$	relative concentration in the *stratum corneum*
$c_{x,t}$	concentration in the *stratum corneum*
D_{sc}	diffusion coefficient in the *stratum corneum*
g	gram
h	hour
Hg	mercury

H_{sc}	total thickness of the *stratum corneum*
k	before units: kilo
$K_{sc/m}$	partition coefficient from a matrix into the *stratum corneum*
l	liter
log*P*	dedadic-logarithmic octanol-water partition coefficient
M	molar mass
M	mole per liter
m	mass
m	before units: milli
m	meter
Me	metal in molecular formula
mol	mole
m/z	mass-to-charge ratio
n	number of replicates
n	before units: nano
Ni	nickel
n_{sc}	number of *stratum corneum* layers
n_{TS}	number of tape strips
Pd	palladium
ppm	parts per million
r^2	coefficient of determination
t	time
u **and** w	parameters of exponential equation
x	depth in the *stratum corneum*
x	number of atoms/charges in molecular formula
y	dependent parameter of exponential equation
β	mass concentration
β_A	mass surface concentration
δ_{sc}	thickness of remaining *stratum corneum*
ζ	mass pecentage
µ	before units: micro
Å	Ångström (10^{-10} m)
ℵ	variable in exponential equation
%	percent

1 Introduction

In 1996, a chemistry professor at Dartmouth college in New Hampshire spilled only a few drops of dimethylmercury onto her hand protected by two layers of gloves.[1] Less than a year later, she died of mercury poisoning.[2] Fortunately, most substances that come into contact with human skin are not as dangerous as to cause death from a single drop. However, some can still lead to adverse health effects after coming into contact with human skin, for example, from consumer products.

Consumer products are made of many different materials, ranging from wood over metals and rubber to synthetic materials such as plastics. They contain a plethora of different substances, some of which might be harmful to humans. These can be divided into two major categories: intentionally and non-intentionally added substances (NIAS). Substances may be added to a material to change its properties, such as plasticizers, dyes or flame retardants in plastics or certain metals in alloys. Nickel, cobalt and palladium, for example, are commonly used in jewelry, where they can come into contact with the skin.[3–8] All three of these metals are known to cause allergic contact dermatitis (ACD).[9]

NIAS can be detected in consumer products because of contamination or due to degradation of the material itself or of the intentionally added substances. One important class of NIAS are the polycyclic aromatic hydrocarbons (PAH), which have been found in consumer products in concerningly high amounts.[10,11] Some PAH are classified carcinogens[12] and the class as a whole is linked to many different health risks.[13–17] Understanding the mechanism and the general exposure of these potentially harmful substances to the skin is of key importance for risk assessment.

The skin covers almost the whole human body, which gives it a surface area of around 2 m^2.[18] In contrast to most other organs, it is in regular contact to the outside world. One of its main functions is to protect the inner lying organs from pathogens and substances that humans are exposed to. The outermost layer of the skin, the *stratum corneum* (s.c.), consists of multiple layers of dead keratinocytes, the main cell type in the epidermis.[19] For substances to reach the viable parts of our bodies, they must overcome this lipophilic barrier.

The Franz diffusion cell (FDC) assay is an important method for *in vitro* skin penetration research. It is named for its inventor, Thomas Franz. The cell was first described in their publication from 1975, aiming at standardizing *in vitro* skin penetration studies and providing a systematic comparison to *in vivo* data.[20] Since then, the FDC has been used in numerous studies and remains an

important instrument for *in vitro* skin penetration experiments.[21–23]

The bottom of the FDC consists of a receptor chamber, filled with a liquid that mimics bodily fluids. The receptor chamber is enclosed by a water jacket that keeps a consistent temperature, corresponding to the skin surface temperature (31 °C).[24] The skin or skin model is laid atop the receptor chamber and fixed with the donor cap (donor compartment). The skin used is ideally donated from humans either from plastic surgery patients or corpses.[25–28] Because human skin is not always readily available, synthetic or lab-grown alternatives are sometimes used.[23,29] A more common substitute is pigskin, which shares crucial properties with human skin.[30–33] An application medium such as a solution or a sample is administered to the skin in the donor chamber and after a given incubation time, the setup is disassembled. The compartments (donor, skin, receptor) can then be extracted and analyzed.

To investigate how substances penetrate the s.c. during the FDC assay, tape stripping is a commonly used technique to remove the s.c. layer by layer. They can then be analyzed individually or pooled.[34,35] A tape strip is pressed onto the skin and then torn off in order to remove a portion of the s.c. It is imperative to scrutinize this method, because the amount of s.c. removed with each tape strip remains unclear as reflected by conflicting literature.[36–43] Hence, the histological investigation of the s.c. after tape stripping represents an important building block in the field of skin penetration. It serves as a basis for the other studies under the umbrella of this thesis.

The extraction of the analytes for quantification poses a main challenge to skin penetration studies because of the different matrices present after the FDC assay (application medium, tape strips, skin, receptor fluid). Depending on the investigated substance, various analysis methods are used that have differing requirements to the nature of the injection sample. For the analysis with gas chromatography coupled to tandem mass spectrometry (GC-MS/MS) — a common quantification method for volatile organic compounds, for example PAH — the substance should be solved in an organic solvent free of interfering matrix. Therefore, the sample preparation demands the extraction with organic solvents that ideally do not extract too much of the matrix to achieve clean injection solutions. Inductively coupled plasma mass spectrometry (ICP-MS), used for the quantification of metals, demands highly acidic aqueous solutions for efficient ionization. A common method of sample preparation is the total destruction of the matrix using microwave-assisted digestion in mineral acids. Difficulties with both sample preparations have to be overcome during the method development phase of the skin penetration studies.

PAH are ubiquitous persistent organic pollutants that are released into our environment by incomplete combustion of organic material of natural or anthropogenic origin.[44] PAH are found in consumer products from rubber utensils to make-up due to the contamination of source materials such as mineral oils or carbon black.[10,11,45] They pose a risk to human health because they are known to penetrate the skin[25] and many are toxic besides their carcinogenic potential.[15–17] The dependence of the penetration rate on the lipophilicity of a broad range of PAH was explored by means of FDC assays. A special focus was laid on five exemplary PAH from the two-ringed

naphthalene to the six-ringed dibenzo[*a,h*]pyrene (DB[*a,h*]P). For these, the partition and diffusion coefficients through the s.c. from the polypropylene surrogate squalane were determined to mimic consumer products made from this material. They are important input parameters for *in silico* approaches to skin penetration.

The final project of this thesis is concerned with the skin penetration behavior of the metal allergens nickel, cobalt and palladium.[46,47] Especially nickel is a well investigated allergen that is responsible for about half of all diagnosed contact allergies.[9] The clinical symptom of contact allergies is ACD, leading to loss of quality of life and economical damages.[48,49] In an *in vitro* activated marker assay, Pd^{2+} showed higher frequencies of $CD154^{+}$ than Ni^{2+} and Co^{2+} in human blood samples, which should indicate a strong potency as allergen.[50] However, palladium allergies are not detected as often as nickel or cobalt contact allergies.[47,50] Apart from lower test rates, a lower skin penetration rate of Pd^{2+} compared to Ni^{2+} and Co^{2+} could contribute to this discrepancy. Here, the skin penetration rate of Pd^{2+} was experimentally compared to those of Ni^{2+} and Co^{2+} in an FDC assay to answer this question.

2 Skin

Unlike most human organs, the skin is exposed to the elements. In fact, its main function is to protect the other organs against a wide variety of attacks of biological, physical and chemical nature. The skin is the largest organ of the human body and as such an important entry point for potentially harmful chemicals, organic and inorganic alike.[51]

The outermost layer of the skin is the epidermis. With the exception of vitamin D production, all functions of the epidermis are protective, for example, against UV radiation, water loss and microorganisms.[19,52] The cells of the epidermis are connected by desmosomes — cell structures that adhere cells to each other — with a fluid in between, allowing nutrients to flow in from the dermis.[53] This is necessary because the epidermis is not connected to blood vessels. In the lower part of the epidermis, fresh keratinocytes, the main cell type of the epidermis, are formed. They gradually move to the surface of the skin, creating keratin on the way. When these keratin-rich keratinocytes die, they form the s.c., the upper part of the epidermis and the outer layer of the skin.[54]

The s.c. is often compared to a brick wall with the bricks being the dead keratinocytes and the mortar being the intercellular fluid (Figure 2.1).[55] The intercellular fluid is mainly composed of ceramides, cholesterol and free fatty acids.[56] The s.c. is the main barrier for substances permeating into the skin.[57]

The upper most layer of the s.c. is the *stratum disjunctum*. This layer is subject to constant desquamation. The European Food Safety Authority (EFSA) recommends to exclude substances quantified in the *stratum disjunctum* in skin penetration studies, because the folds and furrows of the *stratum disjunctum* can accommodate the application medium. This can in turn lead to an overquantification of the substance in the s.c.[58]

Below the epidermis lies the dermis. It is supplied with blood and thus, substances that reach the dermis can be considered bioavailable.[53] The dermis is composed of mainly collagen in connection with glycosamingylcans.[53] These structures are capable of absorbing large quantities of water, maintaining the turgidity of the skin.[53] The dermis is the thickest part of the skin, about 1.5 to 4 mm thick, corresponding to 90% of skin thickness.[54] Its main roles are protection against physical stress, supply of nutrients to the epidermis, temperature regulation and tasks related to the immune system.[51,54]

The lowest layer of the skin is the hypodermis, also called subcutis. It consists mainly of adipocytes,

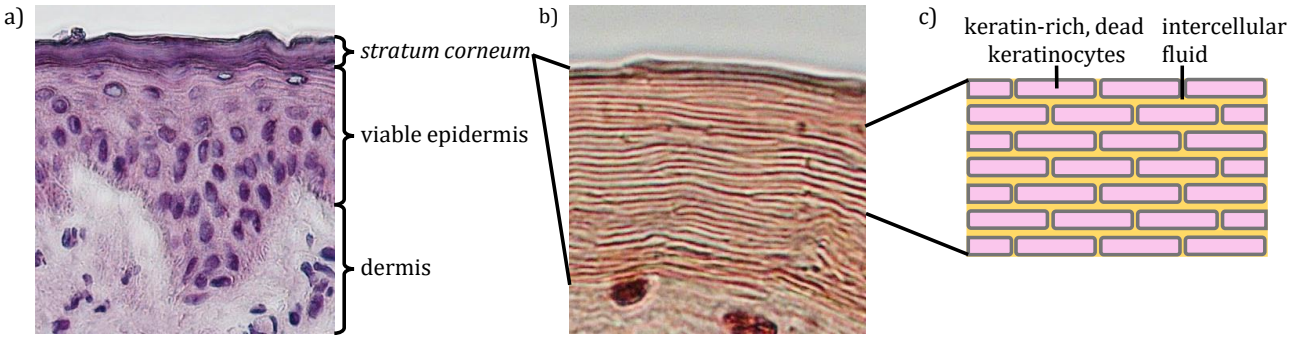

Figure 2.1: The skin with the *stratum corneum*. a) Microsopic image of pigskin with *stratum corneum* (s.c.), viable epidermis and dermis. The dermis is not shown in its entirety, which expands far beyond the lower bound of the image. 40-fold magnification, hematoxylin-eosin stain. b) The s.c. bloated with potassium hydroxide solution (2%) to enhance visibility of the individual, dead keratinocytes and to demonstrate the brick-and-mortar like structure of the s.c. 40-fold magnification, safranin stain. c) Brick-and-mortar model of the s.c. Dimensions not to scale.

a type of cell responsible for storing fat. The hypodermis represents the greatest deposit of fat in the human body,[59] with its roles including heat conservation and absorption of physical damage such as punches.[54] In *in vitro* skin penetration studies, the hypodermis generally does not play a role because it is removed before the experiments. Since the dermis is supplied with blood, the permeation into the hypodermis is not as relevant for skin penetration research: substances that have reached the dermis are already considered bioavailable.

Skin models for *in vitro* studies Wherever possible, human skin should be used in *in vitro* penetration studies because it mimics exposure to human beings most closely.[60] Sources include plastic surgery or corpses.[21,26–28] Nevertheless, availability is limited and an ethics vote for its use is necessary. Synthetic or lab-grown skin models have been used as feasible substitutes in past studies,[23,29] although in the regulatory context they are not recommended for skin penetration studies.[61]

Pigskin represents a viable alternative: procurement is relatively easy and it shares crucial characteristics with human skin.[60,62] Studies have shown pigskin to provide comparable results to human skin in permeation experiments concerning lag time and diffusion or partition coefficients.[30–32] Hence, the use of pigskin is also recommended by guideline 428 on *in vitro* skin absorption studies of the Organisation for Economic Co-operation and Development (OECD)[61] and by the Scientific Committee on Consumer Safety (SCCS).[33]

Nonetheless, human and pigskin are not identical.[63] It was demonstrated that pigskin is more permeable to certain compounds than human skin, such as the highly lipophilic compounds heptane, hexadecane and xylene ($\log P > 3$).[32,64,65] In the studies summarized in this dissertation, pigskin was used as the model skin of choice. In one of the four publications discussed in this thesis, the differences between human and pigskin are discussed for the permeation of PAH. In the other three studies, pigskin was exclusively used.

Transepidermal water loss Besides its role to prevent substances from entering the body, the epidermis and specifically the s.c. also control the release of water from the human body to the environment.[66] This water loss through the skin — not including sweat — is called *transepidermal water loss* (TEWL).[67] In general, the TEWL depends on external factors and the skin itself: the temperature and humidity, but also the site on the body can impact the TEWL.[68] Average TEWL in healthy humans *in vivo* was reported between 3 and 15 g/($m^2 \cdot h$).[68–70] When skin is damaged, the TEWL is elevated in comparison to healthy skin. It can therefore be used as a marker for skin integrity.

In vitro, the TEWL is commonly used to verify the integrity of the skin. However, in 2002, Chilcott *et al.* showed no connection between the TEWL measured in an open chamber system and the gold standard of skin barrier testing: the flux of tritiated water through the skin.[71] Since then, a new system for TEWL measurement was patented and provides more reliable results.[72] Contrary to the older systems using open chambers, the new system applies a closed chamber with a water condenser. The instrument is thus less influenced by external factors, making it more precise and easier to calibrate.[73,74] Using such a system, the TEWL was indeed correlated with the flux of tritiated water.[75] The TEWL was elevated if the skin was damaged and established that using a closed chamber system to measure the TEWL is an adequate approach to test skin integrity.[75]

In the publications summarized in the present dissertation, the TEWL was measured to verify the skin barrier function, as recommended by the OECD.[61] Since a closed chamber system was applied, it was possible to use these values to exclude skin specimens that exceeded a certain threshold. Depending on the study, the value for the threshold was either determined by previous validation studies or compared to literature values.

Tape stripping: studying individual layers of the *startum corneum*

This section summarizes one of the four publications relevant for this dissertation: *Continuous removal of single cell layers by tape stripping the stratum corneum — a histological study.* The published version is available in the appendix, Section A.1.

Scientific basis

Due to s.c.'s composition of loosely bound dead keratinocytes, the layers can be individually separated from each other and from the underlying skin layers. The technique used most commonly for this feat is the rather unassuming use of tape strips. In 1939, Jan Wolf published a study where they investigated the use of adhesive tape strips to study individual layers of the s.c.[34] Wolf accurately pointed out that the s.c. is resistant against the then customary method of scratching off of skin layers because that is part of the s.c.'s purpose. A non-destructive removal of cell layers

could not be achieved this way. However, the s.c. is rather vulnerable against an upward force. This upward force could only be achieved if it where possible to *grab* the s.c. layers individually. Wolf somewhat ingeniously thought of an adhesive tape strip. This made it possible to prepare the cell layers for microscopy with subsequent staining of the layers.

The method described in the paper from 1939 has not changed fundamentally to this date. Since then, tape stripping has been widely applied in an abundance of studies. The aim of these studies ranges from investigation of the nature of the s.c.[76–80] to studies interested in the penetration of substances into the s.c.[21,25,32,81,82] First applications for skin penetration studies are recorded in the 1970s.[81] The method has been used either to remove the s.c. from the underlying skin, completely or partially, or to analyze the layers of the s.c. individually.[76,83,84] Because tape stripping is less invasive than skin biopsies, it can be applied *in vivo* and *in vitro*.[35]

An important debate surrounds this simple technique: how many cell layers are removed with each and every tape strip? Is the removal linear or does it change with increasing s.c. depth? These questions are important, because their answers allow to determine the depth into the s.c. attained after a given amount of tape strips. Together with the surface of the stripped skin, the volume of s.c. removed can be defined, which in turn allows the calculation of the concentration of a given substance in this layer. These concentrations can be used to establish a concentration profile. Several studies have been published trying to solve these questions, but no definitive answer has been found so far.

The removal of the s.c. by tape stripping had been determined by multiple methods, including weighing,[43] microscopy,[36] infrared spectroscopy,[36,80,85] UV/VIS-spectroscopy[40,41] or the measurement of the TEWL,[86] to name a few. Direct measurement of the s.c. by cryo-transmission electron microscopy uncovered that the s.c. itself does not greatly vary in thickness with increasing depth.[87,88] This does not allow the conclusion that each tape strip removes an equal amount of s.c. Nonetheless, laser scanning microscopy revealed a constant thickness of s.c. layers removed (0.5 µm) up to 30 tape strips deep *in vivo*.[36] When measuring the cumulative amount of s.c. stripped, the data show a linear increase of s.c. removed with plateauing beginning at about 20 tape strips.[37,38] These data lead to the conclusion that the s.c. is indeed removed at a constant rate up to a certain depth. When this depth is attained, most of the s.c. is probably removed and no more cells adhere to the tape strips. Studies also measured other quantities besides the weight of the s.c. One focused on the protein absorption in a colorimetric assay[37] and the other on the TEWL,[38] both also displaying a constant removal of s.c.

There are, however, also studies that imply the opposite. The group of Jürgen Lademann studied tape stripping extensively, introducing the term *pseudo-absorption*. This protologism describes the sum of the absorption, reflection, scattering and diffraction — in total: the non-transmitted light. They used *pseudo-absorption* to quantify the amount of s.c. on each tape strip. These studies found that the amount of s.c. removed decreases with increasing depth.[39–42] An independent study confirmed these findings weighing tape strips individually: the mass of s.c. on each tape

strip decreased.[43]

Aim and method

All these studies set out to quantify the amount of s.c. removed by measuring the amount attached to the tape strip. Here, a different approach was chosen — the direct measurement of the s.c. left behind on the skin. The idea is quite straightforward: At successive points in the tape stripping process, samples of the skin were taken and prepared as cryo-sections with subsequent staining for microscopy. Two different staining methods were used: hematoxyline-eosin (HE) stain and safranin with ensuing bloating of cell layers by potassium hydroxide solution (2%). The first staining method allowed the measurement of the thickness of the s.c. The second method of staining and bloating served the counting of the individual cell layers.[89] When plotting the remaining thickness and cell layers versus the number of tape strips, a direct determination of the attained s.c. depth was possible.

In this study, pigskin was used as a adequate substitute for human skin. To ensure the integrity of the skin, the skin was mounted onto an FDC and the TEWL was measured. Skin punches were excluded and replaced if the TEWL exceeded 10 $g/(h \cdot m^2)$.[90] Histological measurements of the s.c. thickness and the number of cell layers were performed after every second tape strip taken from the skin.

Results and discussion

The overall thickness of the s.c. amounted to 11.0 ± 2.0 µm and was reduced to 3.2 ± 0.8 µm after 20 tape strips (Figure 2.2 a). This corresponds to 27.1 ± 3.2 and 7.7 ± 2.6 layers of s.c., respectively (Figure 2.2 b). Thus, the s.c. was not completely removed after 20 tape strips. These numbers are in agreement with measurements from other publications measuring the thickness of s.c.[32,78,91]

When the thickness of the remaining s.c. (δ_{sc}) is plotted against the number of the tape strips (n_{TS}), the correlation can be fitted linearly (Figure 2.3 a, coefficient of determination $r^2 = 0.975$) and is described by

$$\delta_{sc} = -(0.4 \pm 0.02)\ \mu m \cdot n_{TS} + (10.4 \pm 0.2)\ \mu m. \tag{2.1}$$

Accordingly, when the number of the remaining s.c. layers (n_{sc}) is plotted against the number of the tape strips (n_{TS}), the linear correlation (Figure 2.3 b, $r^2 = 0.968$) is described by

$$n_{sc} = -(0.9 \pm 0.05) \cdot n_{TS} + (27.0 \pm 0.6). \tag{2.2}$$

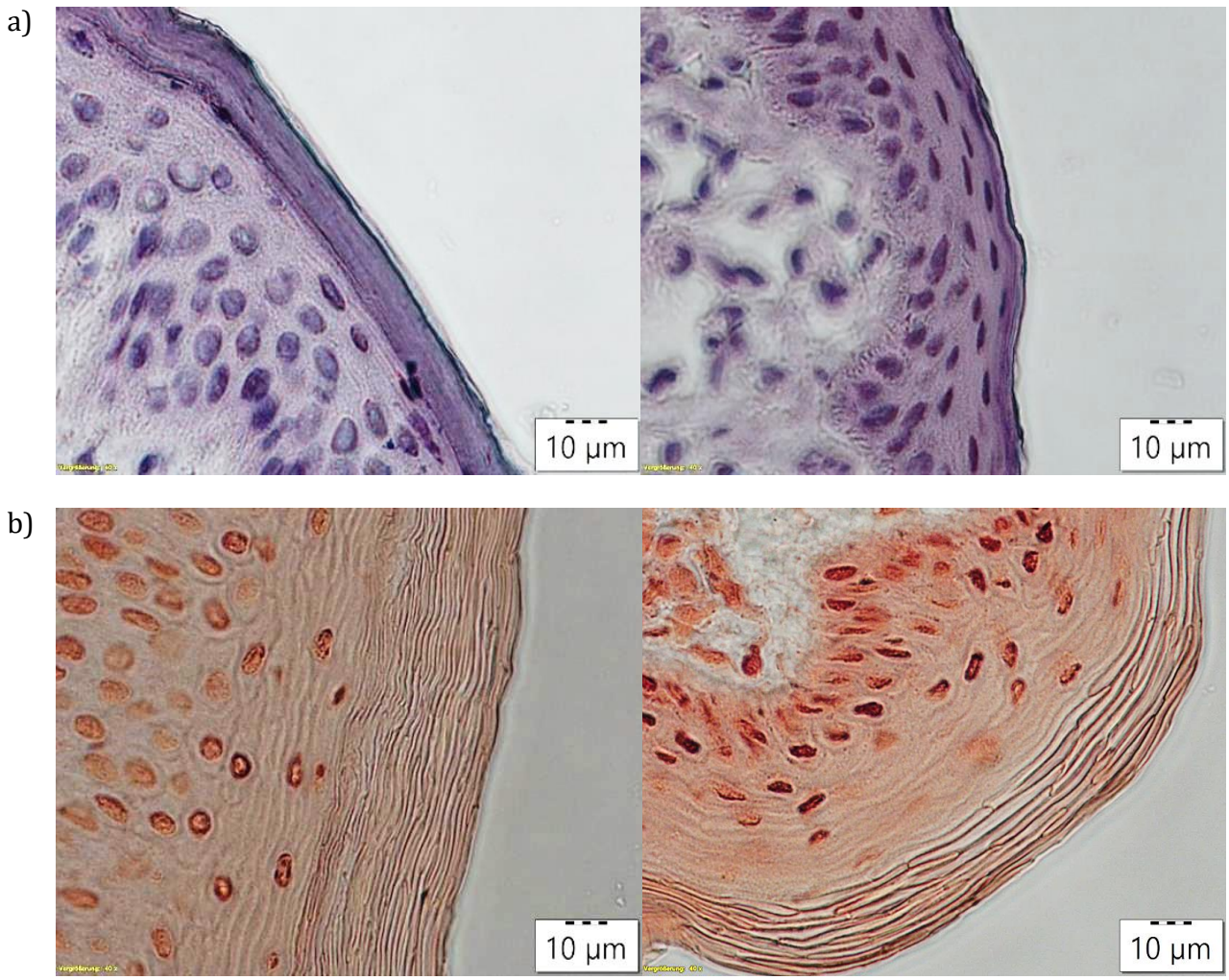

Figure 2.2: Microscopy images before and after tape stripping of the *stratum corneum*. a) Hematoxylin-eosin stain at 40-fold magnification. b) Safranin stain and bloating with potassium hydroxide solution (2%) at 40-fold magnification. Left: before tape stripping; right: after 20 tape strips taken off. Image adapted from Simon *et al.* 2023a licensed under CC BY-NC-ND 4.0.[92]

Plotted against each other, the resulting linear fit (Figure 2.3 c, $r^2 = 0.977$) is described by

$$\delta_{sc} = -(0.4 \pm 0.02)\ \mu\text{m} \cdot n_{sc} + (0.1 \pm 0.4)\ \mu\text{m}. \tag{2.3}$$

The y-axis intercepts of equations (2.1) and (2.2) represent the thickness and number of layers, respectively, of the s.c. before tape stripping. The slope describes the depth attained as a function of the thickness and layers. The slope of equation (2.3) can be interpreted as the thickness of a single s.c. cell layer. The determined thickness (0.40 ± 0.02 µm) corresponds approximately to the thickness of a human s.c. cell layer determined by scanning laser microscopy imaging (0.5 µm).[36]

The data show a clear linear trend with high coefficients of determination for the removal of s.c. by tape stripping. This indicates that the depth attained during tape stripping can be determined

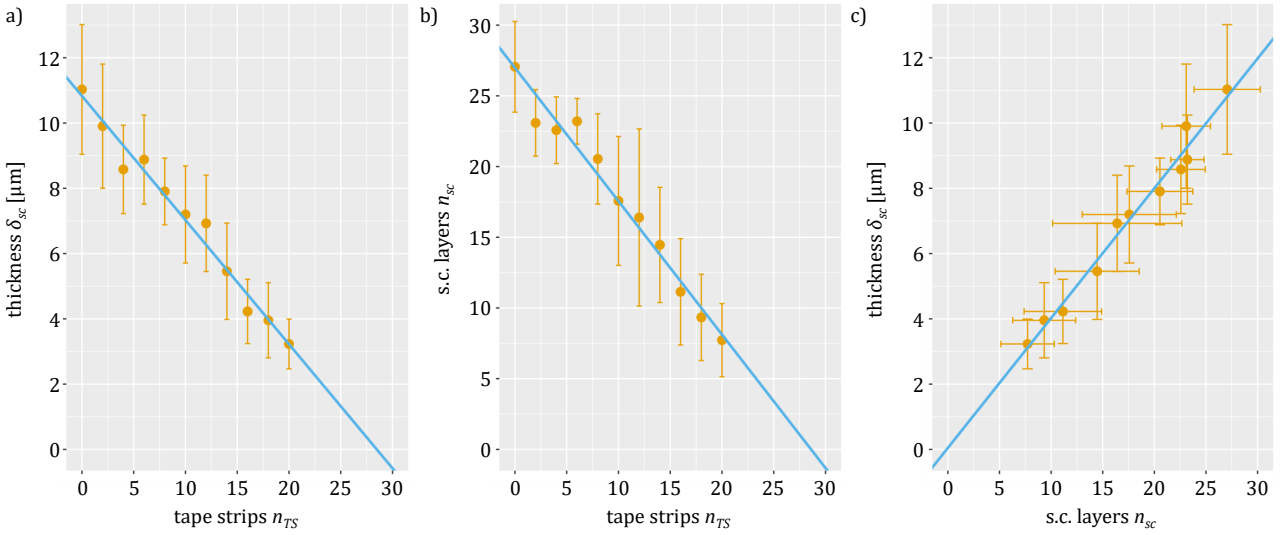

Figure 2.3: Linear regressions of tape stripping. a) Thickness of the *stratum corneum* (s.c., δ_{sc}) versus the number of tape strips taken off (n_{TS}), equation (2.1); b) number of s.c. layers (n_{sc}) versus n_{TS}, equation (2.2); c) δ_{sc} versus n_{sc}, equation (2.3). Image adapted from Simon *et al.* 2023a licensed under CC BY-NC-ND 4.0.[92]

easily by microscopic imaging of two scrap pieces of skin collected before and after tape stripping. Division by the number of tape strips determines the thickness of s.c. removed with each one. In the case described above, this quick calculation yields a value of 0.39 µm per tape strip compared to 0.4 ± 0.02 µm determined by linear regression.

And yet, studies in the past have demonstrated that the removal of s.c. by tape stripping seams to be dependent on the depth into the s.c. In a study with an ample amount of replicates ($n = 240$), the protein content and weight of s.c. material on tape strips was quantified. The results showed a decrease of s.c. removed with an increase of tape strips.[43] This was explained with a stronger cohesion of the s.c. layers near the *stratum granulosum*. However, a different interpretation of the data is possible, which would harmonize with the results presented here.

The s.c. predominantly consists of water (35–75%), proteins (25–55%) and lipids (2–5%).[93–95] An *in vivo* study of infant s.c. revealed that the protein content decreased from the surface of the s.c. to the s.c./viable epidermis boundary layer.[93] The water content also increases linearly dependent with s.c. depth.[73] This effect would explain why the protein content on the tape strips of deeper layers is lower. When it is furthermore considered that proteins are generally more dense than water,[96] the decreasing mass determined gravimetrically in other studies can also be explained.[43]

Conclusion

This study provided the first direct measurement of the depth attained with tape stripping whereas previous studies have relied on indirect quantification of the s.c. on the tape strips. The resulting

linear regression showed conclusively that the s.c. is indeed removed evenly up to 20 layers deep and that each tape strip removes about one s.c. layer, corresponding to circa 0.4 µm per cell layer. Microscopy imaging before and after tape stripping of skin scraps can provide a quick estimate of the removal rate per tape strip that is feasible in any scientific or medical laboratory.

3 Polycyclic aromatic hydrocarbons

When Percivall Pott described scrotal cancer as being especially common among chimney sweeps in 1775, he knew nothing about PAH.[97,98] It would take more than 150 years until it was clear to the scientific community that PAH are the main drivers of cancer in soot. In 1915, the repeated application of soot and tar to skin had produced cancer in mice after many unsuccessful attempts.[99] The carcinogenity was strongly multiplied by exclusively using the high boiling fraction of coal tar — free of other carcinogens such as arsenic.[100–102] Further experiments using pure PAH produced from pyrolysis of isoprene and acetylene induced cancer in mice after regular application to a higher degree than coal tar.[103–105] Finally, in 1932, the hitherto most potent carcinogen found in coal tar was discovered by synthesis and also by isolation from two tons of coal tar: benzo[*a*]pyrene (B[*a*]P, Figure 3.1).[106,107] In the following years, many more PAH were synthesized or isolated and tested on mice.[103]

Chemically, PAH are a group of organic substances with two or more condensed aromatic systems that do not include heteroatoms or substitutents (Figure 3.1). The simplest PAH is naphthalene, consisting of two condensed aromatic rings.[108,109] PAH are rather lipophilic (octanol-water partition coefficient $\log P > 3.3$, Table 3.1) and thus not well soluble in water (< 50 mg/l[110]). PAH are formed by the incomplete combustion of organic matter, either natural or anthropogenic, for example in forest fires, cigarette smoke or combustion engines.[44] The anthropogenic sources are by far the greatest contributor of PAH in the environment.[111] In recent decades, emissions from developed nations have decreased due to more efficient burning of fossil fuels, however, developing countries contribute increasingly to global PAH emissions.[112,113]

Almost all human cell types are capable of metabolizing PAH, including skin cells.[114,115] The metabolism serves their elimination, but in the case of PAH, it also unlocks their carcinogenic potential.[116,117] The studies included in this thesis used skin that was frozen at –20 °C for storage and thawed for use. This procedure deactivates the metabolism of the viable skin cells.[118] Storage at lower temperatures, which would have potentially retained skin viability, is not advised by the OECD because it was shown to enhance permeability.[119] The objective of the studies presented here was to investigate skin permeability and not metabolism. For this reason, a temperature of –20 °C was chosen for storage. Nonetheless, the metabolism of PAH is briefly introduced since it plays an important role in their carcinogenicity.[116,117]

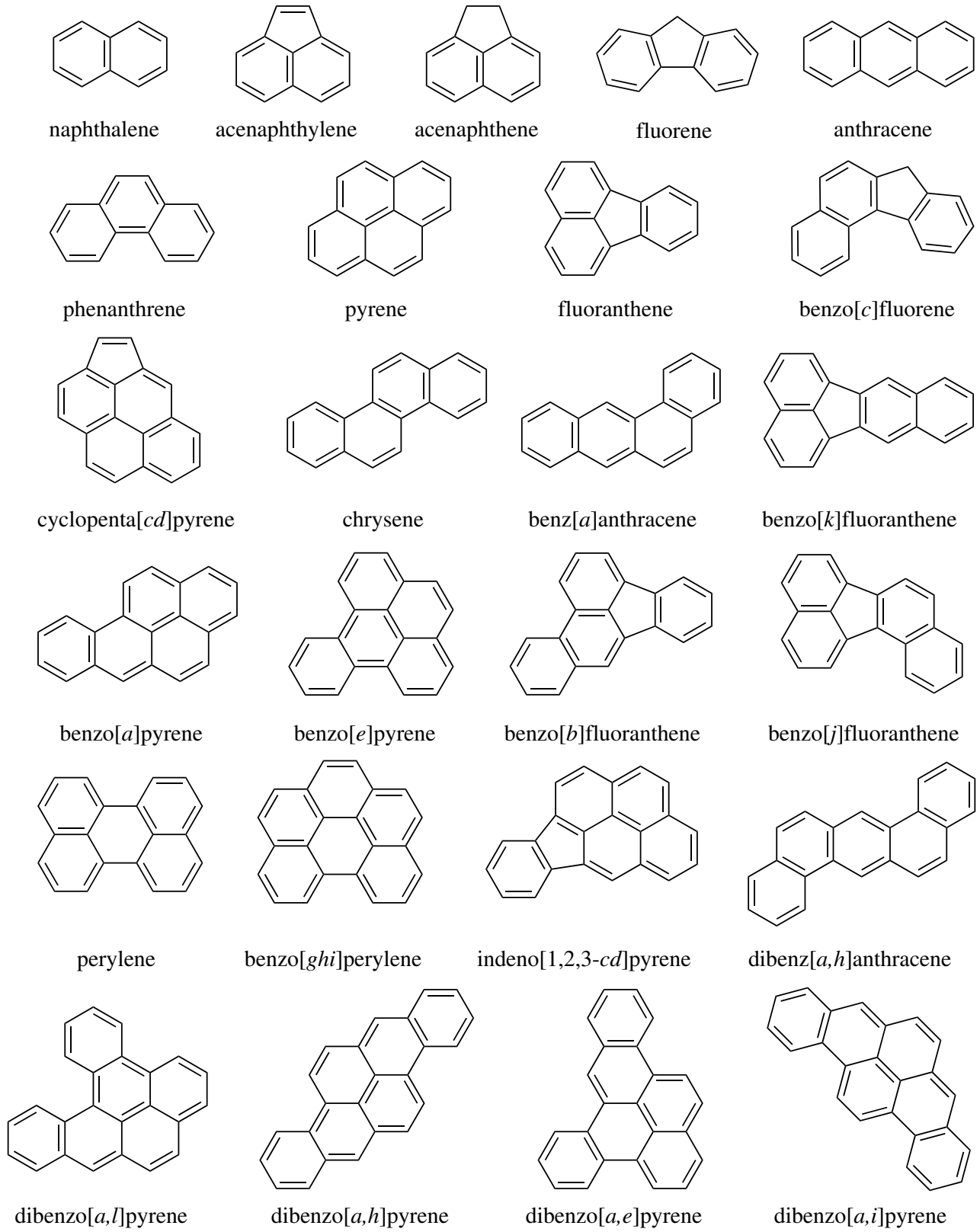

Figure 3.1: Polycyclic aromatic hydrocarbons investigated in this thesis.

Table 3.1: Polycyclic aromatic hydrocarbons investigated in this thesis. Chemical Abstracts Service Registry Number (CAS), molar mass (M), number of ring systems (five-membered rings are counted as half), logarithmic octanol-water partition coefficient (log$P$), log$P$ experimentally derived (exp) or calculated (calc) and reference (Ref.) for log$P$.

substance	**CAS**	***M* [g/mol]**	**rings**	**log*P***	**exp/calc log*P***	**Ref. log*P***
naphthalene	91-20-3	128	2	3.37	exp	[120]
acenaphthylene	208-96-8	152	2.5	4.00	exp	[120]
acenapthene	83-32-9	154	2.5	3.92	exp	[120]
fluorene	86-73-7	166	2.5	4.18	exp	[120]
anthracene	120-12-7	178	3	4.54	exp	[120]
phenanthrene	85-01-8	178	3	4.57	exp	[120]
pyrene	129-00-0	202	4	4.88	exp	[120]
fluoranthene	206-44-0	202	3.5	5.22	exp	[120]
benzo[*c*]fluorene	205-12-9	216	3.5	5.40	calc	[121]
cyclopenta[*cd*]pyrene	27208-37-3	226	4.5	5.40	calc	[121]
chrysene	218-01-9	228	4	5.86	exp	[120]
benz[*a*]anthracene	56-55-3	228	4	5.91	exp	[120]
benzo[*k*]fluoranthene	207-08-9	252	4.5	6.00	exp	[121]
benzo[*a*]pyrene	50-32-8	252	5	6.04	exp	[120]
benzo[*e*]pyrene	192-97-2	252	5	6.04	calc	[121]
benzo[*b*]fluoranthene	205-99-2	252	4.5	6.06	exp	[120]
benzo[*j*]fluoranthene	205-82-3	252	4.5	6.07	calc	[121]
perylene	198-55-0	252	5	6.25	exp	[120]
benzo[*ghi*]perylene	191-24-2	276	6	6.50	exp	[120]
indeno[1,2,3-*cd*]pyrene	193-39-5	276	5.5	6.50	exp	[120]
dibenz[*a,h*]anthracene	53-70-3	278	5	6.50	calc	[122]
dibenzo[*a,l*]pyrene	191-30-0	302	6	7.20	calc	[123]
dibenzo[*a,h*]pyrene	189-64-0	302	6	7.28	calc	[124]
dibenzo[*a,e*]pyrene	192-65-4	302	6	7.30	calc	[125]
dibenzo[*a,i*]pyrene	189-55-9	302	6	7.30	calc	[126]

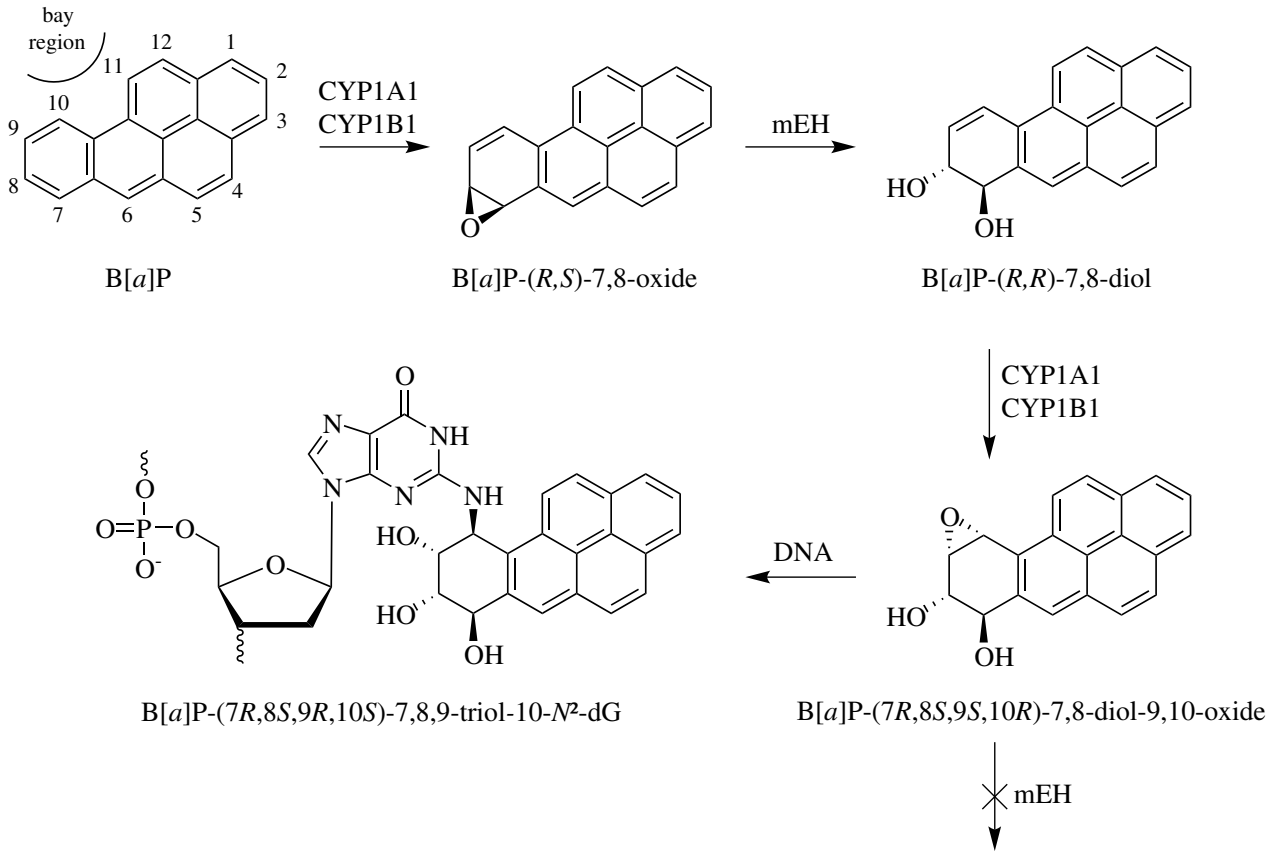

Scheme 3.1: Metabolism of benzo[*a*]pyrene (B[*a*]P) in mammalian cells.[127,128] CYP: cytochrome P450 dependent monooxygenases, mEH: microsomal epoxide hydrolases, DNA: deoxyribonucleic acid, dG: deoxyguanosine .

Metabolism of polycyclic aromatic hydrocarbons in mammals

The metabolism of organic, lipophilic xenobiotics is aimed at the conversion into hydrophilic and excretable conjugates. It follows two phases: i) the biotransformation into electrophilic intermediates and ii) the conjugation to polar molecules including glutathione, glucuronic acid, sulphate and acetic acid.[114,127] This process serves the excretion through urine. In some cases, the electrophilic intermediates are capable of covalently binding to deoxyribonucleic acid (DNA), causing mutagenic effects.[127] The metabolism and ultimate carcinogenicity of PAH is best studied for B[*a*]P.

Xenobiotics such as B[*a*]P can be metabolized by almost any cell in the human body, including viable skin cells (that is, cells beneath the s.c.).[129] In the cell, B[*a*]P acts as a ligand to the aryl hydrocarbon receptor (AhR).[127] The AhR is vital for the carcinogenicity of PAH.[115] It is a ligand induced transcription factor that activates the expression of the microsomal aryl hydrocarbon hydroxylase cytochrome P450 dependent monooxygenases (CYP).[127,130] These enzymes — for PAH most importantly CYP1A1 and CYP1B1 — oxidize B[*a*]P, leading to monoepoxides (Scheme 3.1).[131] B[*a*]P-4,5-oxide is rapidly deactivated in mammalian cells, however, B[*a*]P-7,8-oxide is far more dangerous.[128] While both are hydrolyzed by microsomal epoxide hydrolases

(mEH), B[*a*]P-4,5-diol is then conjugated and excreted, while the predominantly formed (*R,R*)-B[*a*]P-*trans*-7,8-diol can be further epoxidized.[127,128] In a second epoxidation, this compound is transformed by CYP1A1 or CYP1B1 to B[*a*]P-(7*R*,8*S*,9*S*,10*R*)-7,8-diol-9,10-oxide, the most potent mutagen among all possible diastereomers and also the preferred configuration.[127,132] Hydrolysis to B[*a*]P-7,8,9,10-tetrahydrodiol by mEH is sterically hindered by the bay region — the space between two aromatic rings in PAH (Scheme 3.1) — neighboring the epoxide.[128] This sterical hindrance is the reason for the stronger mutagenic potential of B[*a*]P-7,8-oxide compared to B[*a*]P-4,5-oxide.

Since B[*a*]P-(7*R*,8*S*,9*S*,10*R*)-7,8-diol-9,10-oxide is not rapidly biotransformed, it can bind to other molecules such as the DNA,[132] specifically to the purine bases, favoring deoxyguanosine.[133] The epoxide can be subject to *cis*- or *trans*-opening by the nucleotide with the *trans*-opening being favored.[127] This adduct is also more resistant to the nucleotide excision repair pathway (NER),[134] because it is accommodated in the minor DNA groove.[127,135] The distortion of the DNA conformation by the *trans*-adduct is thus less pronounced, leading to a tenfold reduction of NER activity compared to the *cis*-adduct.[127,136] A subsequent replication of a gene that has the potential to cause cancer (oncogene) can lead to the induction of guanine → thymin transversion.[127] One of the most important oncogenes playing a role in the formation of cancer is *TP53*, the genetic encoding for protein p53.[137] p53 plays a critical role in tumor suppression and gene stability.[138] If *TP53* is mutated, it can no longer fulfill these tasks, and indeed, it is mutated in more than 50% of all lung cancers, a type of cancer which is usually associated with B[*a*]P.[137,139]

Dermal exposure to polycyclic aromatic hydrocarbons

This section summarizes two of the four publications relevant for this dissertation: *Polycyclic aromatic hydrocarbon permeation efficiency in vitro is lower through human than pigskin and decreases with lipophilicity* and *Migration of polycyclic aromatic hydrocarbons from a polymer surrogate through the stratum corneum layer of the skin.* The published versions are available in the appendix, Sections A.2 and A.3.

Scientific basis

As far back as 1950, scientist explored the penetration of PAH into the skin. Histological analysis of newborn mice revealed that B[*a*]P partitions into the s.c. almost immediately from acetone or benzene.[140] Numerous later studies have confirmed these findings using different matrices ranging from solvents to soil.[141–146] It was shown that the matrix has an important impact on the penetration of PAH into the skin: application of B[*a*]P in soil resulted in a significantly reduced penetration into the skin when compared to the penetration of B[*a*]P applied in acetone *in vivo* (monkey) and *in vitro* (human cadaver skin).[141,143] Generally, PAH uptake from acetone was

greater than from other matrices, including lubricating oil[147,148] and coal dust.[149]

Permeation and diffusion through the skin are less governed by the matrix in which the PAH are applied. They depend more on the properties of the substances in question. For example, permeation of PAH decreases with rising log*P*, as was demonstrated for human skin *in vitro* from bitumen.[150]

The dermal uptake of PAH can cause skin cancer,[151] which is why regulations on the amount of PAH in consumer products were introduced. In the European Union, PAH content is limited to 1 mg/kg per PAH in general consumer products with intended skin contact and to 0.5 mg/kg in toys.[152] Nevertheless, PAH have been found in consumer products with designated skin contact, for example, in newspaper ink or consumer products containing rubber and plastics.[11,153] Probable contamination sources include mineral oils used as plasticizers and carbon black.[10,154–156] A study on the migration of PAH from consumer products made of rubber material revealed that B[*a*]P was able to permeate human skin *in vitro*.[25] However, about 80% of the applied B[*a*]P remained in the s.c.[25]

The understanding of the distribution of different PAH in the skin is of key importance, because it allows to asses the bioavailability of a given PAH. If PAH remain mainly in the s.c., they could form a reservoir and become bioavailable gradually. They also might be shed with the dead keratinocytes during continuous desquamation. This process is completed every 14 days, meaning that a s.c. layer takes about 14 days from its creation to the moment it is shed.[157] If, however, PAH permeate the s.c. barrier in a relatively short amount of time, they could pose a greater threat to human health.

Aim and methods

Two studies on PAH penetration through the skin by FDC assays with the aim to investigate how the intrinsic properties log*P* and *M* affect the penetration behavior through the skin were part of this thesis. Their differences are summarized in Table 3.2. All studied PAH are listed in Table 3.1.

Analytical method The analytical method applied for PAH determination in the FDC compartments was GC-MS/MS. GC is a method whereby the analytes are separated in a column according to their distribution between a gaseous phase and a stationary phase.[162] This equilibrium is dictated by the vapor pressure of the analytes and their interaction with the stationary phase. The gaseous phase acts as a carrier gas and does not interact with the analytes. Modern GC columns are capillary columns: the stationary phase is coated into a glass capillary, leaving space for the mobile phase to flow through.[162] PAH interact well with a non-polar polymer as an stationary phase due to their low polarity. If analytes exhibit weak interactions with the stationary phase, they are not effectively separated.[163] The time it takes an analyte to pass through the column is called *retention time* and is a characteristic property used for its identification.

Table 3.2: Comparison of the methodology of the studies on PAH skin penetration. Skin penetration of PAH was investigated in two different studies. The methodological differences are summarized in this table. log*P*: logarithmic octanol-water partition coefficient, PAH: polycyclic aromatic hydrocarbon, BSA: bovine serum albumin, PBS: phosphate-buffered saline.

parameter	**Simon *et al.* 2024a**[158]	**Simon *et al.* 2023b**[159]
application matrix	acetonitrile	squalane
log*P* matrix	–0.3[160]	15.6[161]
concentration in matrix	1000 ng/ml	500–1000 µg/ml
applied amount	50 ng	100–200 µg
tape strips	5	20
tape strip analysis	pooled	individually
skin type	human and pig	pig
receptor fluid	9 g/l saline solution	50 g/l BSA in PBS
PAH applied	broad range of 24 PAH	five selected PAH
incubation times	2 h, 4 h, 16 h, 24 h and 48 h	1 h and 24 h

MS/MS serves as a detection method after separation by GC. The gaseous stream of analytes coming from the GC column enters a vacuum chamber and the analytes are ionized by a stream of electrons, a process called *electron ionization*. The ions are repelled vertically and guided into the mass analyzer.[164] The most common mass analyzer for MS/MS is a hexapole called quadrupole for historic reasons. The voltage on the quadrupoles can be manipulated in such a way that only ions of a given mass-to-charge ratio (*m/z*) can pass through.[164] In MS/MS, these ions are called *precursor* ions. The selected precusor ions now enter a second quadrupole, where they are guided through a steady stream of an inert gas (for example, nitrogen) in opposite direction to the ion stream. According to their collision energy and their molecular properties, the ions dissociate, producing distinctive fragment ions. The third quadrupole filters out these ions and only lets through ions of a certain *m/z*. These ions are called *product* ions. An analyte can be identified according to this characteristic fragmentation in combination with the retention time from GC.

Dermal PAH penetration from acetonitrile Data from the quality controls of FDC assays performed for a study by Bartsch *et al.* on the penetration of PAH from consumer products were reevaluated.[25] 24 PAH had been applied in acetonitril (1000 ng/ml) onto human or pigskin in the donor compartment. Negative controls were carried out with FDC assays applying pure acetonitrile. The incubation times ranged from 2 h to 48 h with data of human skin gathered exclusively for 24 h. After the incubation, the skin was tape stripped five times and pooled. All FDC compartments were extracted and PAH content determined by GC-MS/MS. The data was then normalized to the amount taken up by the skin.

Determination of partition and diffusion coefficients The partition ($K_{sc/m}$) and diffusion coefficients (D_{sc}) of five selected PAH (naphthalene, anthracene, pyrene, B[*a*]P and DB[*a,h*]P) rep-

resenting ring sizes from two to six rings were determined. FDC assays were performed applying highly concentrated solutions in squalane onto the skin in the donor compartment. Squalane is highly lipophilic ($\log P$ = 15.6)[165] and has been used as a polymer surrogate in previous studies.[21,161,166,167] These characteristics make it suitable as a matrix for the determination of $K_{sc/m}$ of PAH for real life exposure to consumer products made of plastics. Negative controls were carried out with FDC assays applying pure squalane in the donor compartment. The receptor chamber was filled with a 50 g/l solution of bovine serum albumin (BSA) in phosphate-buffered saline (PBS). The function of BSA in bovine blood and of its human counterpart, human serum albumin, is the transport of lipophilic substances in the bloodstream. In skin penetration studies, it increases the solubility of these substances in the receptor fluid.[27,30,168] Additionally, it minimizes binding of PAH to the glass surface of the receptor chamber and reduces protein loss from the dermis.[27]

The incubation times of the FDC assays for this experiment were 1 h and 24 h (anthracene only 1 h). These time points were chosen because 1 h represented the shortest time period at which the tape stripping procedure could still be performed without taking up a significant amount of the incubation time. 24 h were considered long enough for an equilibrium to be reached between the matrix and the uppermost s.c. layer as well as the diffusion into the s.c.

After incubation, the setup was disassembled to analyze the compartments individually. The squalane solution still left on the skin was removed (donor compartment) and the skin was tape stripped 20 times. Each tape strip was extracted and analyzed individually. The remaining skin and the receptor fluid were also extracted. Each extract was then analyzed by GC-MS/MS for its PAH content.

Mathematical basis The governing principles of PAH permeation through the s.c. are the *partitioning* from the matrix into the upper most s.c. layer and the *diffusion* in the s.c. itself. The partitioning at equilibrium is described by $K_{sc/m}$ defined as

$$K_{sc/m} = \frac{c_{sc}}{c_m}, \tag{3.1}$$

where c_{sc} is the concentration of PAH in the s.c. and c_m is the concentration of PAH in the matrix (squalane). Diffusion is described by Fick's laws of diffusion.[169] Most useful to describe the diffusion behavior is the second law which reads for the case of diffusion in the s.c.

$$\frac{\partial c_{x,t}}{\partial t} = -D_{sc}\frac{\partial^2 c_{x,t}}{\partial x^2} \tag{3.2}$$

with the concentration $c_{x,t}$ in dependence of depth x in the s.c. and the time t. A solution to this differential equation is[170]

$$c_{rel,x,t} = K_{sc/m}\left[1 - \frac{x}{H_{sc}} - \frac{2}{\pi}\sum_{j=1}^{\infty}\frac{1}{j}\sin\left(\frac{j\pi}{H_{sc}}x\right)\exp\left(-\frac{j^2\pi^2 D_{sc}}{H_{sc}^2}t\right)\right] \tag{3.3}$$

with the total thickness H_{sc} of the s.c. and the concentration in the s.c. relative to c_m

$$c_{rel,x,t} = \frac{c_{x,t}}{c_m}. \tag{3.4}$$

This solution is derived by a Laplace transform and has three boundary conditions:

(i) the s.c. must be devoid of any analyte at the beginning of the incubation time at any position x: $c_{x,0} = 0$,

(ii) the concentration in the matrix c_m is considered to be constant over the incubation time,

(iii) the layers under the s.c. must act as a perfect sink. This means that the lowest layer of the s.c. must always be directly depleted of any analyte.

Condition (i) is relatively easily maintained if the skin is not contaminated with the analyte prior to the experiments. This is verififed by the analysis of the negative samples. Condition (ii) is normally achieved by infinite dose conditions, using very high starting concentrations in the application medium. Infinite dose conditions are maintained — according to the OECD — when over the total incubation period less than 10% of the applied substance penetrates the skin.[61,171] This is verified by the quantification of analyte in the donor compartment after the incubation time. Condition (iii) is the most difficult to achieve. The s.c. is a lipophilic matrix while the viable epidermis underneath is rather aqueous. Hence, hydrophilic substances can efficiently partition into the viable epidermis while lipophilic substances do not.

The parameters ($K_{sc/m}$ and D_{sc}) were calculated by fitting the concentration profile in the s.c. to equation (3.3).

The depth into the s.c. x was calculated using

$$x = 0.349 \cdot (n_{TS} - 0.5). \tag{3.5}$$

This equation was obtained in the same manner as equation (2.1), but in a separate experiment. The two equations diverge by about 12%. The subtraction of 0.5 skin layers (n_{TS}) was used to plot the middle of the s.c. layer removed by the tape strip. Furthermore, the first tape strip is dismissed from the calculation because it removes the *stratum disjunctum* (see Chapter 2).[58]

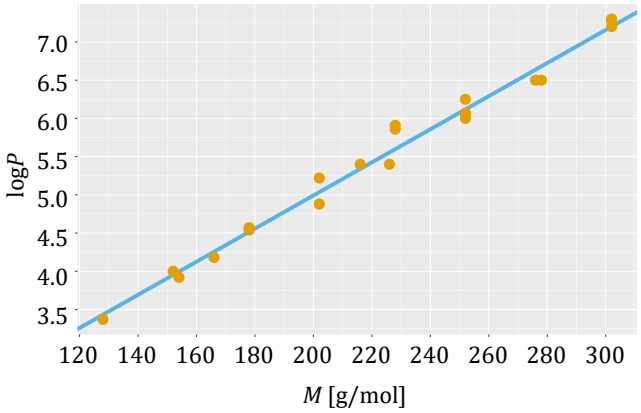

Figure 3.2: log*P* of polycyclic aromatic hydrocarbons versus their molar mass *M*. Linear regression curve: equation (3.7). For values, see Table 3.1. log*P*: logarithmic octanol-water partition coefficient.

The equation

$$y = u \cdot \mathrm{e}^{-\aleph} + w \tag{3.6}$$

served as a general equation for data fitting in both studies. y is the dependent parameter, $\aleph$ is the independent parameter and u and w are fitting parameters.

For the PAH that were investigated in the studies summarized here, log$P$ is linearly related to M (Figure 3.2) as described by

$$\log P = 0.0217 \, \frac{\mathrm{mol}}{\mathrm{g}} \cdot M + 0.660. \tag{3.7}$$

The linear regression was carried out using the data from Table 3.1 ($r^2 = 0.986$). Therefore, all interpretations regarding log$P$ could also be made for M. The largest compounds in the studies here are the dibenzopyrenes with 302 g/mol. Effective skin permeation has been shown for substances of higher M,[27,28,172] indicating that lipophilicity is a more relevant factor than M, especially when comparing to other substance classes.

Results and discussion

Dermal penetration of PAH from acetonitrile This study allowed a comparison of five incubation times, of PAH ranging in log$P$ from 3.9 to 4.2 and M ranging from 152 g/mol to 302 g/mol as well as skin from humans and pigs. The distribution in the skin layers indicate that large PAH permeate the skin less efficiently than small PAH (Figure 3.3). After 24 h, small PAH are able to permeate the s.c. almost completely with amounts in the receptor greater than those in the five uppermost layers of the s.c. Large PAH on the other hand do not permeate the skin at all: the largest amounts were found in the uppermost layers of the s.c. while the receptor fluid was devoid

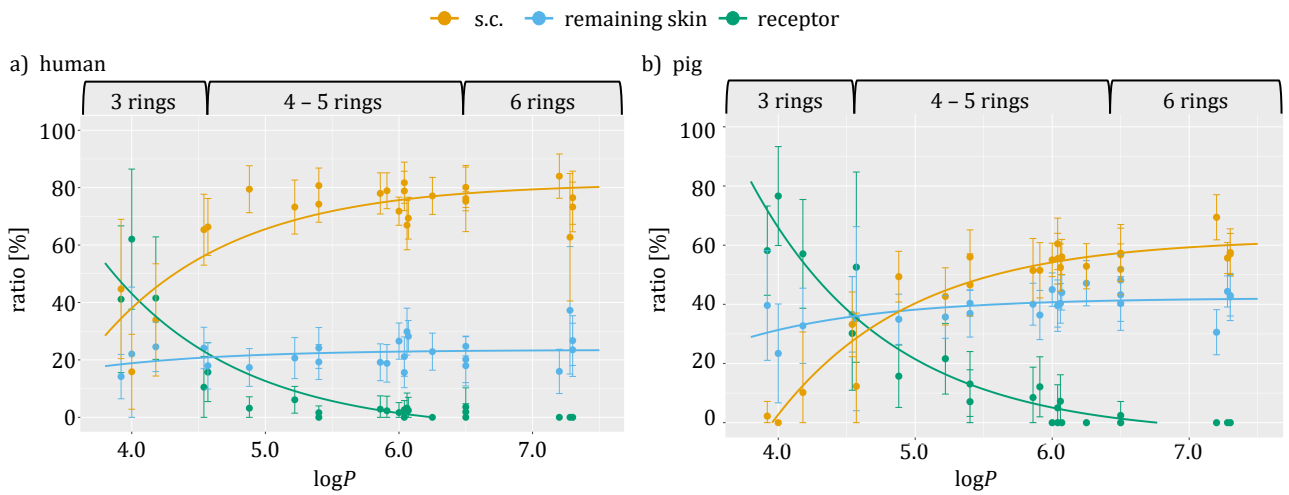

Figure 3.3: Distribution ratio of polycyclic aromatic hydrocarbons (PAH) in the skin. Distribution ratio of PAH in each compartment to total amount found in the skin (*stratum corneum* (s.c.), remaining skin) and receptor fluid after 24 h incubation time versus log*P*. Curves represent data fitted to equation (3.6). a) Human skin. b) Pigskin. log*P*: logartithmic octanol-water partition coefficient. Adapted from Simon *et al.* 2024a licensed under CC BY 4.0.[158]

of these PAH after 24 h.

Interestingly, the ratio of PAH in the remaining skin layer is almost constant over the whole log*P* range of investigated PAH (Figure 3.3, blue curve). The s.c. is not completely removed with five tape strips, as discussed above (Chapter 2, Section *Tape stripping: studying individual layers of the startum corneum*). The remaining skin therefore consists of residual s.c. as well as the complete viable epidermis and large parts of the dermis. These layers are where the partitioning between the more lipophilic s.c. and the more aqueous layers below takes place. The more lipophlic PAH presumably reside in the remaining s.c. whereas the less lipophilic PAH are distributed more evenly between the receptor fluid, dermis and viable epidermis. Hence, PAH of all sizes and lipophilicities are present to roughly equal ratios in the remaining skin.

The distribution of the PAH in the three different compartments (uppermost s.c., remaining skin, receptor fluid) can be fitted to equation (3.6) as a function of log*P*. The resulting curves are displayed in Figure 3.3 to help with visualization. The distribution ratios show a saturation at about log$P = 6$, meaning that the distribution does not change significantly for PAH of higher lipophilicity. This is consistent for skin of both species, human and pig.

The ratio of PAH in remaining human skin is lower than in remaining pigskin and the limit value is considerably higher in pigskin than in human skin (pig: 42% versus human: 24%, Figure 3.3). For small PAH, the ratio found in the receptor is higher in pigskin than in human skin. In the s.c., these ratios are reversed: the ratio of all investigated PAH in human s.c. is higher than the ratio in porcine s.c. When the ratio of PAH in human s.c. is divided by the ratio of PAH in porcine s.c. and then plotted against log*P*, the resulting curve gives an idea of how well the permeation properties of porcine s.c. resemble the properties of human s.c. (Figure 3.4).

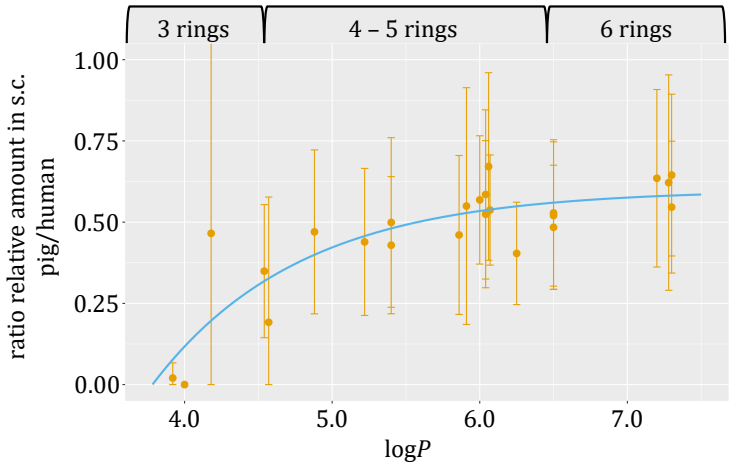

Figure 3.4: Ratio of amount in porcine *stratum corneum* (s.c.) to amount in human s.c. Curve represents data fitted to equation (3.6). log$P$: logarithmic octanol-water partition coefficient. Adapted from Simon *et al.* 2024a licensed under CC BY 4.0.[158]

The curve reaches a limit at about 0.6, which means that porcine s.c. retains a maximum of 60% of PAH that human s.c. retains according to this model. Smaller PAH are held back less strongly in porcine s.c. than in human s.c.: the smallest PAH almost completely overcome the s.c. barrier and permeate into the remaining skin. These differences between human and porcine s.c. could be rationalized by the different packing of lipids in the respective s.c. While the molar ratio of the lipids in both are comparatively equal, the packing differs: human s.c. lipids are packed orthorhombically and porcine s.c. lipids are packed hexagonally.[173] This leads to human s.c. lipids being packed more densely than their porcine counterparts.

An alternative explanation could be the different reaction of pigskin to freezing compared to human skin. A previous study demonstrated that permeation characteristics of human skin are not compromised by freezing.[174] Pigskin, however, exhibits a permeability increase of up to 25% compared to fresh pigskin when freezing and storing at −20 °C for the lipophilic substance methyl salicylate (log$P$ = 2.5).[175] A study on the direct comparison of fresh and frozen human and pigskin has not been carried out yet. However, a comparison of rat, rabbit and pigskin showed the latter to be especially vulnerable to freezing.[176]

FDC assays applying a PAH mixture in acetonitrile were carried out with incubation times from 2 h to 48 h using pigksin. In Figure 3.5 the results are displayed for three expemplary PAH of small (acenaphthene), medium (pyrene) and large (dibenzo[*a,l*]pyrene, DB[*a,l*]P) size. Acenaphthene permeates into the receptor fluid after 2 h with little retention in the s.c. The distribution does not significantly change with longer incubation times. The majority of acenaphthene is able to permeate to the receptor chamber whereas distribution between the s.c. and the remaining skin remains comparable. Other small PAH demonstrate similar penetration characteristics.

DB[*a,l*]P does not permeate the skin at all. After 2 h, the majority of DB[*a,l*]P is detected in the s.c. which is also the case for every other time point probed. No DB[*a,l*]P was recovered in the

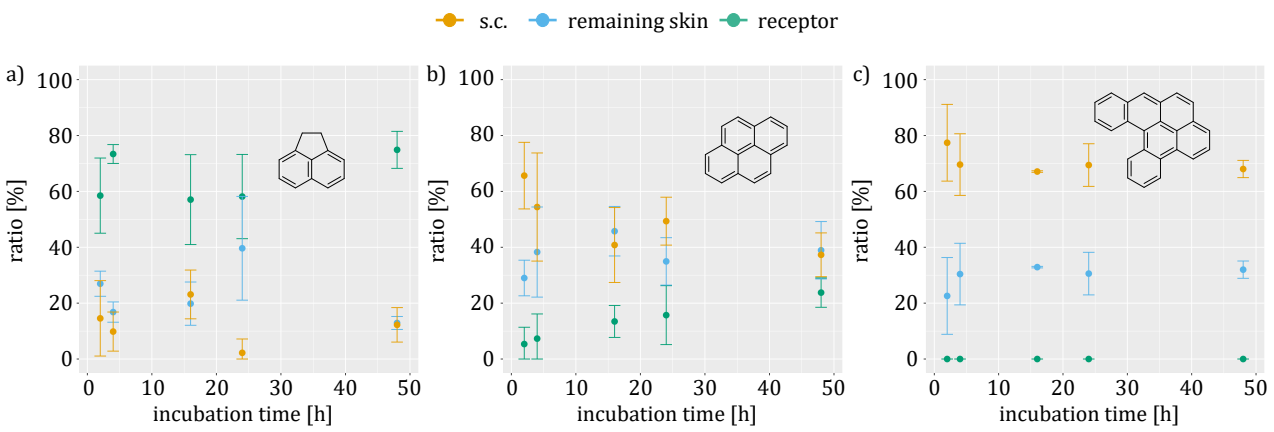

Figure 3.5: Distribution ratio of selected polycyclic aromatic hydrocarbons (PAH) in pigskin at different time points. Distribution ratio in each compartment to total amount found in the skin at different time points in pigskin. a) acenaphthene (154 g/mol, $\log P$ = 3.92), b) pyrene (202 g/mol, $\log P$ = 4.88) and c) dibenzo[*a,l*]pyrene (302 g/mol, $\log P$ = 7.20). log*P*: logarithmic octanol-water partition coefficient. Adapted from Simon *et al.* 2024a licensed under CC BY 4.0.[158]

receptor fluid. A possible explanation is the retention at the s.c./viable epidermis boundary layer. Here, DB[*a,l*]P does not efficiently partition into the more aqueous layer beneath the s.c., therefore DB[*a,l*]P can accumulate in the s.c. and form a reservoir. Over time, small amounts of it could permeate into the lower layers of the skin. The desquamation process has a turnover of 14 days, leaving two weeks for the substance to become bioavailable before it would be shed with the dead keratinocytes.[157]

The most time-dependent kinetics are offered by medium-sized PAH. At short incubation times, pyrene is found mostly in the s.c. with low amounts in the receptor fluid. The ratios in each compartment slowly converge until s.c. and remaining skin no longer significantly differ at 48 h.

Determination of partition and diffusion coefficients Five selected PAH were applied to pigskin in squalane at quasi-infinite dose conditions. Squalane was chosen as a polymer surrogate with properties close to polypropylene. Infinite dose conditions were chosen to maintain border condition (ii) of equation (3.3). The donor compartment (the share of PAH on the skin that did not penetrate) accounted for 97% to 102% of the applied dose after 1 h and for 94% to 97% after 24 h. Hence, infinite dose conditions were maintained during the complete duration of the FDC assays.[61]

Large PAH are retained by the s.c. more strongly than small PAH, as already shown above. After 1 h, the larger PAH are recovered to a higher degree in the s.c. than smaller PAH (1 h, Figure 3.6a). Only naphthalene was able to penetrate the skin and reach the receptor fluid. After 24 h, the recovery of naphthalene in the receptor fluid was an order of magnitude higher than those of the other PAH (Figure 3.6b). All PAH were about equally distributed between s.c. and remaining skin, however, the s.c. is much thinner than the remaining skin (about 15 µm in this case compared to almost 500 µm of the remaining skin). Thus the concentration of each PAH in the s.c. is higher than in the

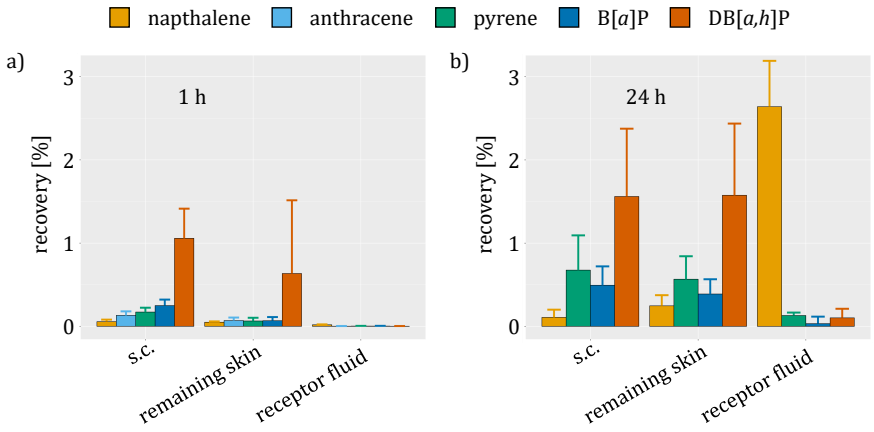

Figure 3.6: Polycyclic aromatic hydrocarbon (PAH) recovery in Franz diffusion cell (FDC) assay with squalane. Recovery of the total applied mass of each PAH in the individual compartments (donors not shown) of the FDC after application of a quasi-infinite dose in squalane. Mean ± standard deviation. a) 1 h incubation time, b) 24 h incubation time. B[*a*]P: benzo[*a*]pyrene, DB[*a,h*]P: dibenzo[*a,h*]pyrene, s.c.: *stratum corneum*. Adapted from Simon *et al.* 2023b licensed under CC BY-NC-ND 4.0.[159]

remaining skin.

The s.c. was tape stripped 20 times and the tape strips of each layer were analyzed separately, making it possible to portray concentration profiles of the PAH in the s.c. (Figure 3.7 exemplary for B[*a*]P). The concentration of PAH in each cell layer decreased with increasing depth. Due to the infinite dose conditions, the diffusive loss in the upper s.c. layers will be constantly replenished from the donor compartment. When reaching the s.c./viable epidermis boundary layer, the PAH partition into the viable epidermis according to their s.c./viable epidermis partition coefficient. Since the viable epidermis is an aqueous matrix, PAH with higher log*P* are expected to accumulate in the s.c. whereas naphthalene may partition into deeper layers, reaching the receptor more easily.

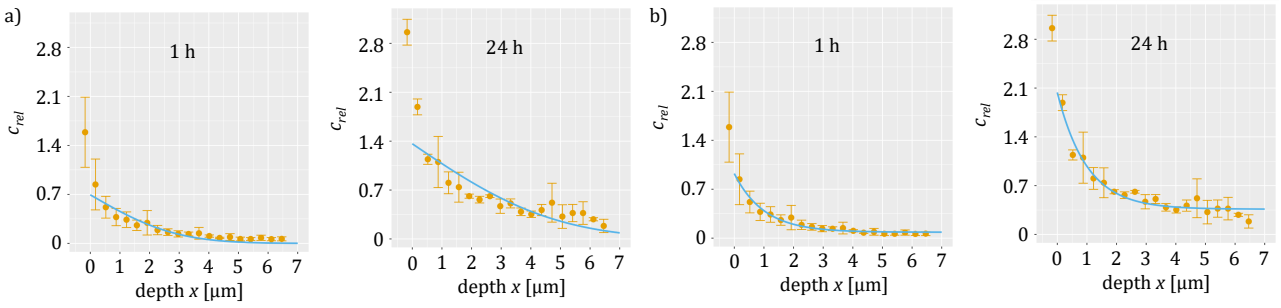

Figure 3.7: Concentration profiles of benzo[*a*]pyrene (B[*a*]P) in the *stratum corneum* (s.c.). Profile of B[*a*]P in the s.c. after incubation in squalane with 1 h and 24 h incubation time. a) Fit to equation (3.3). b) Fit to equation (3.6). The values of the first tape strip are dismissed from the calculation because it removes the *stratum disjunctum* (Chapter 2).[58] It is represented as a negative value on the *x*-axis. Mean ± standard deviation. c_{rel}: relative concentration (equation (3.4)). For all other polycyclic aromatic hydrocarbons investigated here, see the supporting information of Simon *et al.* 2023b.[159] Adapted from Simon *et al.* 2023b licensed under CC BY-NC-ND 4.0.[159]

In order to model the diffusion through the s.c., the resulting concentration profiles were fitted to equation (3.3). The resulting curves allow the determination of $K_{sc/m}$ and D_{sc} (Table 3.3 and Figure 3.8a). In theory, the obtained values for the two incubation times should be the same, however, they do not with the exception for $K_{sc/m}$ of DB[*a*,*h*]P. This discrepancy can be explained by the nature of these coefficients: partition coefficients describe a thermodynamic equilibrium. In equation (3.3), $K_{sc/m}$ is described by the relative concentration (equation (3.4)) at $x = 0$ irrespective of the time t. Hence, if equilibrium is not yet reached, calculated values for $K_{sc/m}$ are incorrect. The value after 24 h incubation period can be more plausibly expected to represent the equilibrium between donor and upper most s.c. layer.

For both time points, $K_{sc/m}$ is linearly dependent on log$P$ (Figure 3.8a). The two curves cross at log$P$ = 7.6, which is slightly above the log$P$ of DB[*a*,*h*]P (log$P$ = 7.28) and indeed, $K_{sc/m}$ values for DB[*a*,*h*]P do not differ significantly. The trend of converging linear curves indicates that the more lipophilic a PAH is, the faster it reaches equilibrium between squalane and s.c. $K_{sc/m}$ are higher for the more lipophilic PAH, which means that these PAH partition into the s.c. more strongly than the less lipophilic PAH.

Values for D_{sc} also differ for the two incubation times (Table 3.3 and Figure 3.8b). Longer incubation times diminish the contribution of the exponential term in equation (3.3). The values obtained after 1 h were thus deemed more accurate, because a variation in D_{sc} would have a stronger effect on the accuracy of the fit.

logD_{sc} of naphthalene (-10.9 ± 4.4) is considerably higher than logD_{sc} of the other investigated

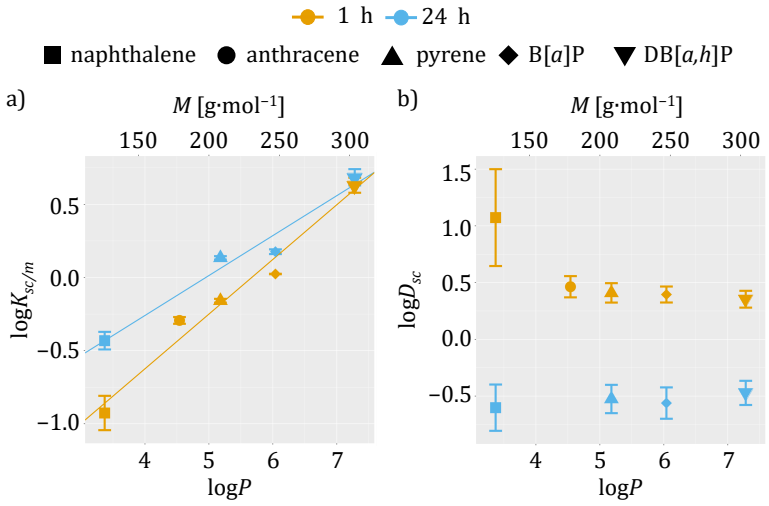

Figure 3.8: log $K_{sc/m}$ and log D_{sc} of five polycyclic aromatic hydrocarbons versus log$P$. a) log $K_{sc/m}$ versus log$P$ with linear regression curves and b) log D_{sc} versus log$P$. Means ± standard deviation. The upper x-axis shows the molar mass M, which is linearly related to the log$P$ of these PAH. Values for $K_{sc/m}$ after 1 h and D_{sc} after 24 h are considered inaccurate. s.c.: *stratum corneum*, $K_{sc/m}$: partition coefficient between squalane and s.c., D_{sc}: diffusion coefficient in the s.c., log$P$: logarithmic octanol-water partition coefficient. Adapted from Simon *et al.* 2023b licensed under CC BY-NC-ND 4.0.[159]

Table 3.3: Partition $K_{sc/m}$ and diffusion D_{sc} coefficients of five polycyclic aromatic hydrocarbons in the *stratum corneum* (s.c.). Values for $K_{sc/m}$ after 1 h and D_{sc} after 24 h are considered inaccurate. Unit of D_{sc} before logarithm: m^2/h, B[*a*]P: benzo[*a*]pyrene, DB[*a*,*h*]P: dibenzo[*a*,*h*]pyrene.

substance	log$K_{sc/m}$ 1 h	logD_{sc} 1 h	log $K_{sc/m}$ 24 h	logD_{sc} 24 h
naphthalene	-0.926 ± 0.117	-10.93 ± 4.35	-0.43 ± 0.06	-12.602 ± 4.27
anthracene	-0.293 ± 0.023	-11.54 ± 2.33	—	—
pyrene	-0.159 ± 0.013	-11.59 ± 2.42	0.13 ± 0.012	-12.526 ± 2.97
B[*a*]P	0.024 ± 0.002	-11.61 ± 2.07	0.18 ± 0.016	-12.562 ± 3.09
DB[*a*,*h*]P	0.631 ± 0.051	-11.65 ± 2.44	0.69 ± 0.056	-12.472 ± 2.81

PAH, which do not differ significantly from each other. Naphthalene is also the only PAH for which literature values of logD_{sc} exist: -9.60 ± 3.20[177] and -8.36 ± 3.89.[27,28] These formerly reported values are one and two orders of magnitude higher, respectively, than the value reported here. As already stated in these studies, the application medium plays a role for D_{sc} in these cases. Kim *et al.* applied naphthalene in jet fuel, known to damage the s.c.[177] and Ellison *et al.* applied naphthalene in 1.12% ethanol, which enhances skin permeation.[27,28] Squalane has not been reported to interfere with diffusion through the s.c.[178]

Coincidentally, equation (3.6) fits the concentration profile through the s.c. very well for both time points and for all PAH (Figure 3.7b, exemplary for B[*a*]P). Equation (3.6) is not a solution of Fick's second law. However, the data fit the equation uncommonly well. Hence, the migration of PAH through the s.c. is most probably not a purely Fickian process. The coefficients for u and w were determined for the five PAH in question and for both time points (Table 3.4).

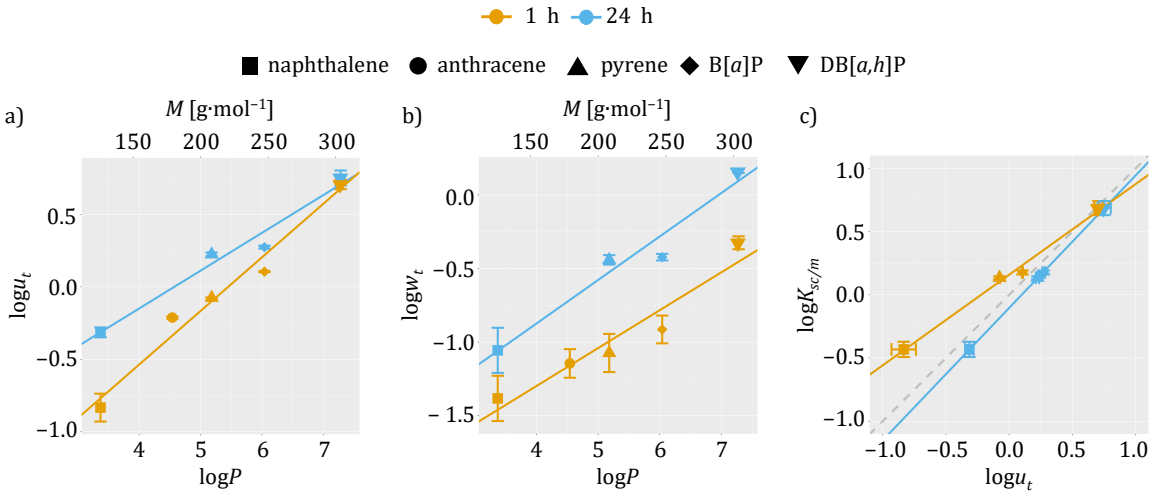

Figure 3.9: Parameters log$u$ and log$w$ of equation (3.6) versus log$P$ and log $K_{sc/m}$ of five investigated PAH. a) log$u$ versus log$P$, b) log$w$ versus log$P$ and c) log$K_{sc/m}$ versus log$u$ with respective linear regression curves. Means ± standard deviation. The upper x-axes of a) and b) show the molar mass M, which is linearly related to the log$P$ of these PAH (Figure 3.2). s.c.: *stratum corneum*, $K_{sc/m}$: partition coefficient between squalane and s.c., log$P$: logarithmic octanol-water partition coefficient. Adapted from Simon *et al.* 2023b licensed under CC BY-NC-ND 4.0.[159]

Table 3.4: Coefficients for exponential equation of five polycyclic aromatic hydrocarbons (PAH). u and w — coefficients of equation (3.6) — of the concentration profile of five PAH in the *stratum corneum*. B[*a*]P: benzo[*a*]pyrene, DB[*a,h*]P: dibenzo[*a,h*]pyrene.

substance	**log$u$ 1 h**	**log$w$ 1 h**	**log$u$ 24 h**	**log$w$ 24 h**
naphthalene	-0.833 ± 0.093	-1.383 ± 0.154	-0.314 ± 0.046	-1.056 ± 0.153
anthracene	-0.212 ± 0.018	-1.145 ± 0.097	—	—
pyrene	-0.076 ± 0.009	-1.074 ± 0.13	0.224 ± 0.016	-0.441 ± 0.032
B[*a*]P	0.105 ± 0.011	-0.914 ± 0.094	0.274 ± 0.014	-0.423 ± 0.022
DB[*a,h*]P	0.706 ± 0.095	-0.325 ± 0.044	0.751 ± 0.055	0.161 ± 0.012

The logarithmic values of the two parameters of this fit, log$u$ and log$w$, are linearly related to log$P$, again in dependence of the incubation time (Figure 3.9). Parameter w could be understood as a factor governing retention at the s.c./viable epidermis boundary layer. The time dependence of the parameter is shown by the different values for the two different time points. It can be explained by the time dependent diffusion of PAH from the surface of the skin to s.c./viable epidermis boundary layer. Furthermore, the removal rate of PAH from the lowest lying s.c. layer into the viable epidermis should have an impact on w. A high removal rate would lead to w approaching zero, corresponding to perfect sink conditions.

Parameter log$u$ is also time dependent and linearly related to log$K_{sc/m}$ (Figure 3.9). The two linear fits cross at the values for DB[*a,h*]P, similar to the fit of log$K_{sc/m}$ versus log$P$. log$u$ could be regarded as a time factor for the partitioning between the medium and the s.c. With longer incubation times, the equilibrium state is reached and the time dependent factor in log$u$ is diminished, making u and $K_{sc/m}$ equal.

Conclusion

The two studies conclusively demonstrated that skin penetration of PAH is dependent on their lipophilicity. The skin acts as a barrier for highly lipophilic PAH with the dibenzopyrenes not being able to permeate into the receptor even after long incubation times of 48 h. The main barrier is the s.c./viable epidermis boundary layer, where the liphophilic PAH are retained and do not efficiently partition into the aqueous matrix beneath the s.c.

Partitioning into the s.c., on the other hand, is favored for more lipophilic PAH. $K_{sc/m}$ is positively, linearly dependent on log$P$. D_{sc} is higher for naphthalene than for all other PAH of this study, explaining in part why it more easily reaches the receptor fluid than the other PAH.

The concentration profile in the s.c. is, however, more reliably described by equation (3.6) than by the solution of Fick's second law equation (3.3). This indicates a non-Fickian diffusion of PAH through the s.c.

4 Metal-induced allergic contact dermatitis

The mammalian immune system can be separated into two parts: the innate and the adaptive immune system. Both parts constantly interact with each other in order to protect the human body from harm. The innate immune system developed earlier evolutionarily speaking and is present in all animals, from snails to jaguars.[179] The adaptive immune system developed in jawed vertebrates more than 500 million years ago. It is part of a sophisticated system for the protection of vertebrates and thus, mammalian and human health.[179]

An allergy is an overreaction of parts of the immune system to otherwise harmless substances. They are categorized into four types.[180] A contact allergy is classified as Type IV, which causes a T cell-mediated, and thus delayed, immune response.[181] Contact allergies are associated with skin contact to the allergen.[180,181]

ACD develops, when an allergic person is exposed to their respective allergen, resulting in eczema.[3,181] The most notorious substance causing contact allergy is nickel with about 11% of the general population experiencing ACD upon contact.[9] Cobalt is the second most prominent metal contact allergen and palladium has gained traction because of its increased use in, for example, implants.[9] The allergic reaction can also be caused by other metals and chemicals, such as fragrances or biocides.[3,9,182]

For contact allergies to develop, the body must first be exposed to the allergen during the *sensitization phase*. In the case of Nickel, this most probably happens by contact to a nickel alloy in an injured part of the skin, a prime example being a piercing.[183,184]

Nickel activates Toll-like receptor 4 (TLR4), which is normally responsible for the identification of the gram-negative bacterial product lipopolysaccharide.[185,186] By an evolutionary coincidence, nickel is able to bind to primate-restricted histidines in TLR4 and thus activate the receptor.[3,187] This leads to the induction of multiple proinflammatory cytokines,[187,188] resulting in the activation of skin-resident dendritic cells.[189]

Dendritic cells are antigen-presenting cells and thus play an important role in the immune response. When nickel enters the skin, it binds to self-peptides (endogenous peptides) in a process called *haptenization*. The dendritric cells take up and process the haptenized peptide and travel to the local draining lymph node (Figure 4.1). Here, the peptide-bound nickel is presented to T cells on the major histocompatibility complex, the antigen presenting receptor of dendritic cells.[189]

T cells are highly specialized cells of the adaptive immune system that are equipped with a individual receptor for recognizing antigens presented on the major histocompatibility complex of dendritic cells.[181] Naïve $CD4^+$ and $CD8^+$ T cells that recognize the complex are activated and differentiate into effector T cells.[3] Mature $CD4^+$ cells are T helper cells that regulate the immune response, whereas $CD8^+$ cells are cytotoxic T cells, tasked with the destruction of infected cells.[189] A part of the effector T cells develop into memory T cells, which either reside in the skin tissue (skin-resident memory T cells) or distribute in the whole body (central memory T cells).[3,181] It is believed that the mechanisms for the induction of contact allergy against other contact allergens such as cobalt and palladium follow a similar route.[190]

Following a renewed contact to nickel, inflammation occurs in the *elicitation phase*: the nickel haptenizes a self-peptide and the complex is taken up by dendritic cells. They then present the nickel haptenized peptide to memory T cells, leading to the release of cytokines, promoting an allergic reaction and thus, leading to ACD.[3,181,191]

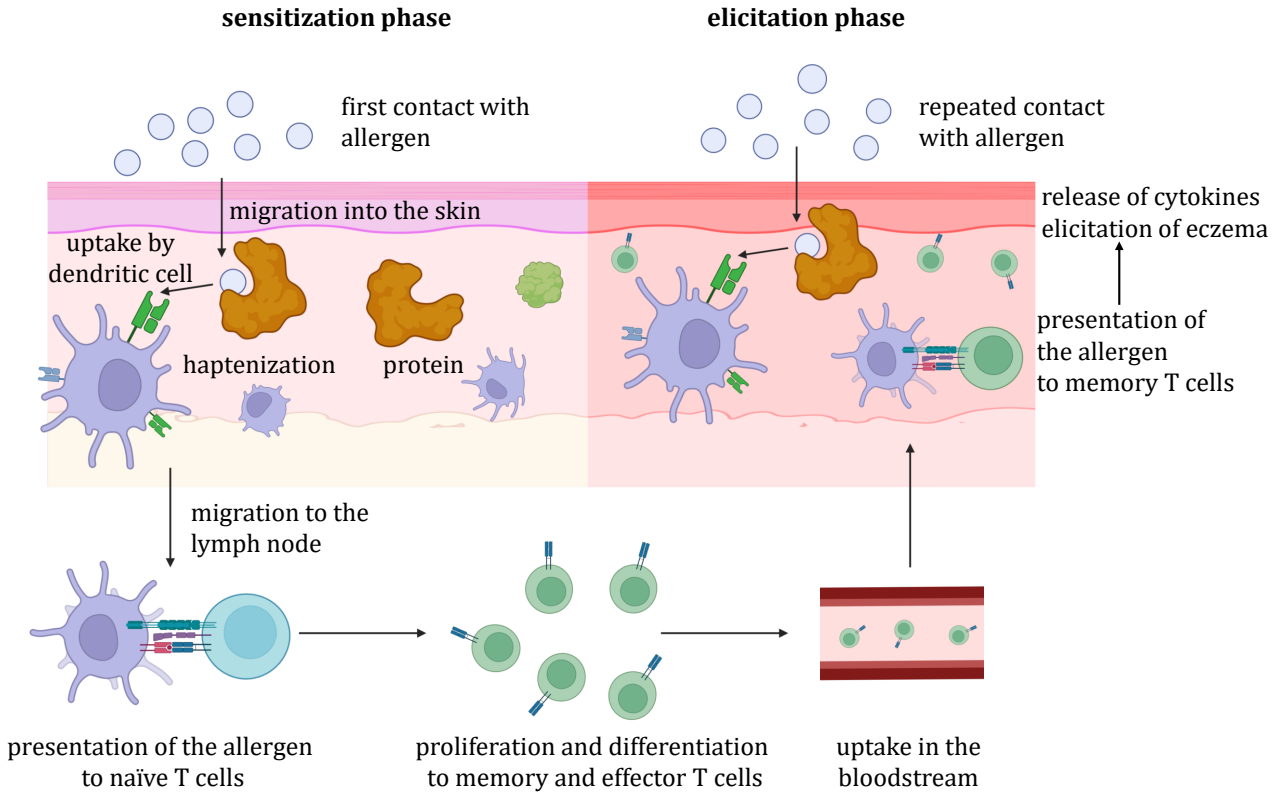

Figure 4.1: Allergic contact dermatitis. Adapted from Riedel 2022.[181] Created with BioRender.com.

Dermal penetration of metal allergens

This section summarizes one of four publications relevant for this dissertation: *Less efficient skin penetration of the metal allergen Pd^{2+} compared to Ni^{2+} and Co^{2+} from patch test preparations*. The published version is available in the appendix, Section A.4.

Scientific basis

Contact allergies are diagnosed by epicutaneous testing (patch testing), where the allergen — dispersed in a formulation such as petrolatum — is applied onto the skin for 48 h.[192,193] The application surface is examined for inflammations afterwards, which are indicative of an allergy.

The lack of global standardization of the patch test often inhibits comparability of allergy prevalence between allergens and regions.[194–199] Metal allergens are usually applied in a dispersion of a metal salt in petrolatum, called patch test preparations (PTPs) in this thesis. Nickel, cobalt and palladium are generally applied as $NiSO_4$, $CoCl_2$ and $PdCl_2$, respectively. Since $PdCl_2$ is poorly water-soluble, Na_2PdCl_4 has been discussed as a possible alternative,[200,201] even though literature lacks a reliable value for the solubility of Na_2PdCl_4.

The causes of allergies have recently been investigated in *in vitro* activation induced marker assays. It was shown that metal-specific $CD4^+$ T cell frequencies for Pd^{2+} exceed those of Ni^{2+} and Co^{2+} in human blood samples.[47,50] These frequencies were correlated to acutely allergic patients.[47] However, palladium allergies are seldom diagnosed in the general population.[202] A possible explanation for this contradiction could be the less pronounced permeation of Pd^{2+} through the skin as compared to Ni^{2+} and Co^{2+} during patch testing.

Aim and method

To test this hypothesis, diagnostic PTPs (Table 4.1) were applied to pigskin in FDC assays with an incubation time of 48 h. This corresponds to the time frame of a clinical patch test.[203] Furthermore, a solution of $NiSO_4$, $CoCl_2$ and Na_2PdCl_4 in PBS was prepared and applied in separate FDC assays.

The analytical method employed for metal quantification was ICP-MS, typically used for element quantification.[164] The analytes are atomized and ionized in an argon plasma and then guided to the mass analyzer. In most cases, the mass analyzer is a single quadrupole. ICP-MS is a very robust and sensitive method, which has lead to its wide spread adaption in the field of element analytics.[164]

For the FDC assays, the pigskin was cut to a thickness of 500 µm using a dermatome and the skin pieces were cut out using a scalpel. Contrary to the other FDC assays, the skin was not punched out. The nickel content of the cast-iron punch contaminated the skin, which was detectable in the

remaining skin.

The skin was laid atop the receptor chamber filled with fetal bovine serum, fulfilling the same function as the BSA in the PAH study (Chapter 3, Section *Dermal exposure to polycyclic aromatic hydrocarbons*). The skin's integrity was verified by the measurement of the TEWL. The donor substance was applied to the skin (20 mg of PTP or 200 µl of the metal salt solution in PBS, Table 4.1). Negative controls were carried out with FDC assays applying 20 mg of petrolatum or 200 µl of PBS. After 24 h, a 100 µl sample was taken from the receptor fluid. After 48 h, the FDCs were disassembled. The skin was cleaned of any application medium with a precision wipe and then tape stripped twenty times as described above (Chapter 2, Section *Tape stripping: studying individual layers of the startum corneum*). Four consecutive tape strips were pooled, dividing the s.c. into five investigated layers. The remaining skin and the receptor fluid were also analyzed for their metal content. The samples of all four compartments were subjected to a microwave assisted digestion in nitric acid. The acidic microwave digestion of petrolautm in presence of Pd^{2+} proved challenging, because it was not possible to fully dissolve the petrolatum in acid without residue. After many unsuccessful attempts with different acids and digestive conditions, the donor samples containing Pd^{2+} were extracted using hydrochloric acid. The resulting solutions were analyzed by ICP-MS.

To confirm the higher solubility of Na_2PdCl_4 as opposed to $PdCl_2$, saturated solutions of both salts in water were prepared and the Pd^{2+} concentration of the supernatant was quantified by ICP-MS. Water solubility is important, because the salts are dispersed in petrolatum. The salt first has to be solved in water — provided by sweat or the TEWL — for the metal to penetrate the skin.

Table 4.1: Donor substances used in Franz diffusion cell assays of metal allergen penetration: PTPs are declared as mass percentages (m/m) of the salt. Concentration metrics for each metal ion in petrolatum: mass percentages of the metal ζ, mass concentrations β and molar concentrations c_n. Applied surface concentrations β_A (mass) and c_A (molar amount) on the skin in the Franz diffusion cell assay with a skin surface area of 1.76 cm^2 and 20 mg (PTP) or 200 µl (solution) applied. PTP: patch test preparation; PBS: phosphate-buffered saline.

donor substance	ζ	β [mg/ml]	c_n [mM]	β_A [µg/cm^2]	c_A [µmol/cm^2]
$NiSO_4$ PTP (5% $NiSO_4{\cdot}6H_2O$)	1.1%	9	160	127	2.16
$CoCl_2$ PTP (1% $CoCl_2{\cdot}6H_2O$)	0.2%	2	35	28	0.48
$PdCl_2$ PTP (2% $PdCl_2$)	1.2%	10	95	136	1.28
Na_2PdCl_4 PTP (3% $Na_2PdCl_4{\cdot}H_2O$)	1.0%	9	81	116	1.09
Ni^{2+} solution ($NiSO_4{\cdot}6H_2O$ in PBS)	5 ppm	$5\cdot10^{-3}$	$8.5\cdot10^{-3}$	0.57	$17\cdot10^{-3}$
Co^{2+} solution ($CoCl_2{\cdot}6H_2O$ in PBS)	5 ppm	$5\cdot10^{-3}$	$8.5\cdot10^{-3}$	0.57	$17\cdot10^{-3}$
Pd^{2+} solution ($Na_2PdCl_4{\cdot}H_2O$ in PBS)	5 ppm	$5\cdot10^{-3}$	$4.7\cdot10^{-3}$	0.57	$9.4\cdot10^{-3}$

Results and discussion

The total recoveries in the FDC assays were in the acceptable range of 80–104% (Table 4.2).

Patch test preparations After application of the PTPs, the ions are mainly retained in the first four s.c. layers (Figure 4.2). A higher percentage of Ni^{2+} and Co^{2+} penetrated into the skin as compared to Pd^{2+} from either PTP. No metal was recovered in the receptor fluid after 24 h and no Pd^{2+} was found there after 48 h. Ni^{2+} and Co^{2+} were both detected in the receptor fluid after 48 h, suggesting that these metals permeate the skin more efficiently than Pd^{2+}. This is further underlined by the low recovery of Pd^{2+} in the remaining skin — consisting of the dermis, the viable epidermis and the lower most s.c. layers not removed by tape stripping — as compared Ni^{2+} and Co^{2+}.

There are multiple possible explanations for this. The most obvious being the solubility of the different salts. Since the salts are applied in petrolatum, the salt must first dissolve in water present on the skin (sweat, TEWL) and can then partition in ionic form into the s.c. This is why two comparative FDC assays were performed using the alternative Pd^{2+} salt Na_2PdCl_4 in petrolatum and dissolved salts in PBS. The data obtained from the solubility experiment shows that Na_2PdCl_4 is indeed better soluble in water than $PdCl_2$ ($PdCl_2$: 7.74 ± 1.17 mM of Pd^{2+}; Na_2PdCl_4: 241 ± 49 mM of Pd^{2+}). However, after application of both salts as PTPs, no Pd^{2+} was found in the receptor fluid after 48 h. In fact, the Pd^{2+} recovery only differed significantly in s.c. layers 9 to 12, where Pd^{2+} from Na_2PdCl_4 PTP was detected but not from $PdCl_2$ PTP.

Salt solution The recovery data of the salts applied in PBS reveal that the concentration of Pd^{2+} in the receptor fluid is significantly lower than the concentration of either Ni^{2+} or Co^{2+} (Figure 4.3). All three metals are mostly recovered in the four upper most s.c. layers. Ni^{2+} and Co^{2+} are also found in relatively high concentrations in the remaining skin and the receptor fluid. Co^{2+} was even shown to permeate the skin within 24 h. To conclude, even when all metals are completely

Table 4.2: Total recovery after Franz diffusion cell assays with metal allergens. Recoveries and masses of metal ions after application of patch test preparations (PTPs) or aqueous salt solutions in Franz diffusion cell assays: Mean recoveries/masses ± standard deviations. Total recoveries/masses are the sum of all compartments. PBS: phosphate-buffered saline.

donor substance	applied metal ion mass [µg]	recovered metal ion mass [µg]	recovery [%]
$NiSO_4$ PTP (5% $NiSO_4 \cdot 6H_2O$)	229 ± 5.5	219 ± 1.5	96 ± 0.5
$CoCl_2$ PTP (1% $CoCl_2 \cdot 6H_2O$)	50.6 ± 1.1	48.4 ± 0.3	96 ± 0.7
$PdCl_2$ PTP (2% $PdCl_2$)	246 ± 5.1	195 ± 1.2	80 ± 0.6
Na_2PdCl_4 PTP (3% $Na_2PdCl_4 \cdot H_2O$)	210 ± 2.3	177 ± 1.3	84 ± 0.6
Ni^{2+} solution ($NiSO_4 \cdot 6H_2O$ in PBS)	1.0	1.04 ± 0.06	104 ± 6
Co^{2+} solution ($CoCl_2 \cdot 6H_2O$ in PBS)	1.0	0.90 ± 0.05	90 ± 5
Pd^{2+} solution ($Na_2PdCl_4 \cdot H_2O$ in PBS)	1.0	0.85 ± 0.03	85 ± 3

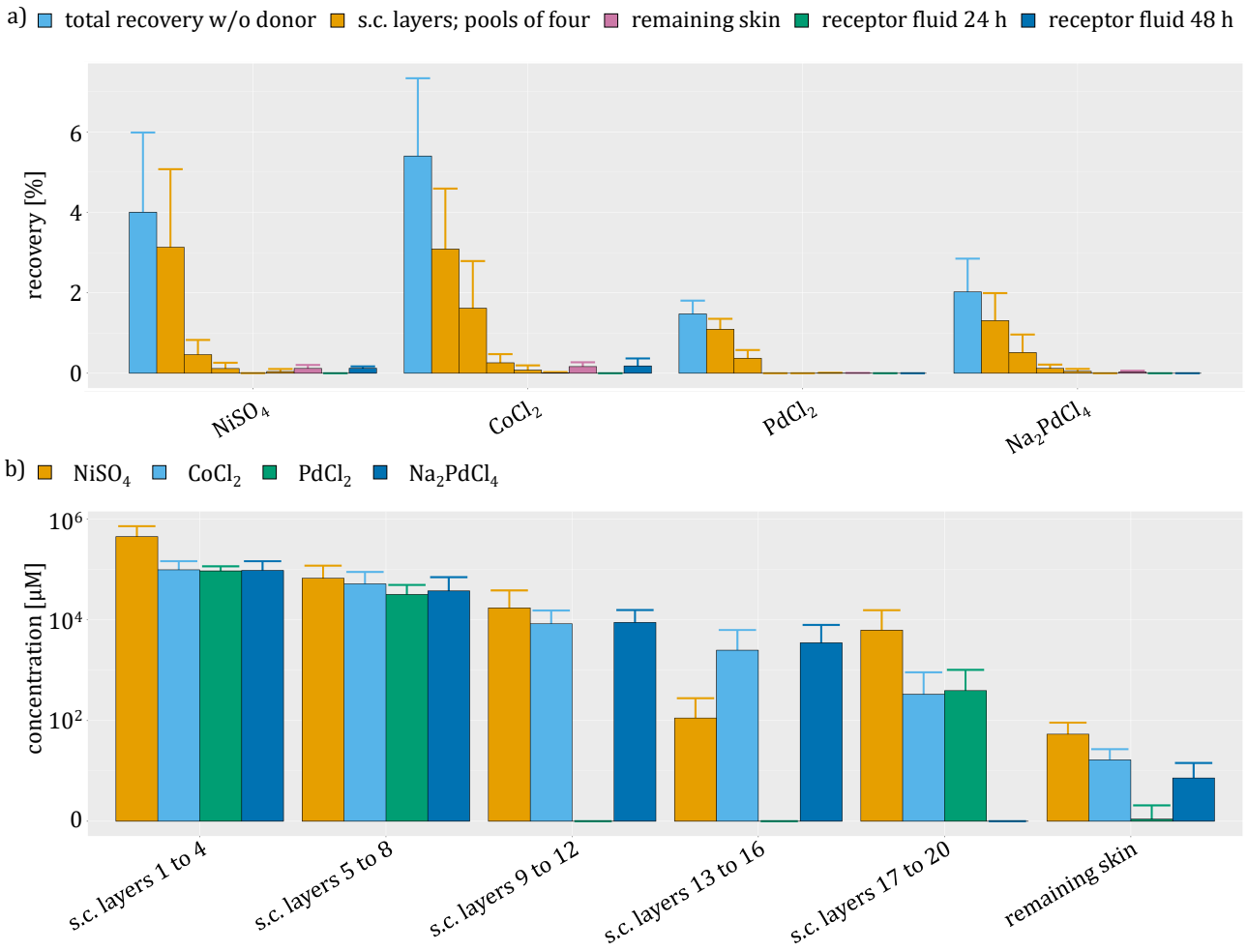

Figure 4.2: Distribution of the metal allergens nickel, cobalt and palladium in the skin after application of patch test preparations (PTP). a) Distribution of recovery in the pooled *stratum corneum* (s.c.) layers (five pools of four consecutive tape strips), the remaining skin and the receptor after 24 h and 48 h. No ions were recovered after 24 h in the receptor fluid. The light blue bar represents the total amount that penetrated the skin, that is, the sum of the recovery of all mentioned compartments. b) Concentrations in the s.c. and the remaining skin based on the volume of the respective layer; logarithmic scale. Means ± standard deviation. Adapted from Simon *et al.* 2024b licensed under CC BY-NC 4.0.[204]

dissolved in an aqueous solution, Pd^{2+} permeates the skin less efficiently than Ni^{2+} or Co^{2+}. Even though Pd^{2+} was applied in only about half the molar concentration of Ni^{2+} and Co^{2+}, the recoveries of Pd^{2+} in the receptor fluid are less than 2% and 3% of those of Ni^{2+} and Co^{2+}, respectively.

Another hypothesis regarding the lack of effective Pd^{2+} penetration through the skin could be the difference in ionic radii, which might result in a size-dependent decrease in skin permeation. However, even though Pd^{2+} has a larger ionic radius (dependent on coordination and spin, average of 0.75 ± 0.16 Å) than Ni^{2+} (0.59 ± 0.09 Å), it is not much larger than that of Co^{2+} (0.71 ± 0.11 Å).[205] Furthermore, the ionic radius of Hg^{2+} (0.95 ± 0.19 Å) is even greater and Hg^{2+} is known to quite easily overcome the skin barrier.[2,205–208]

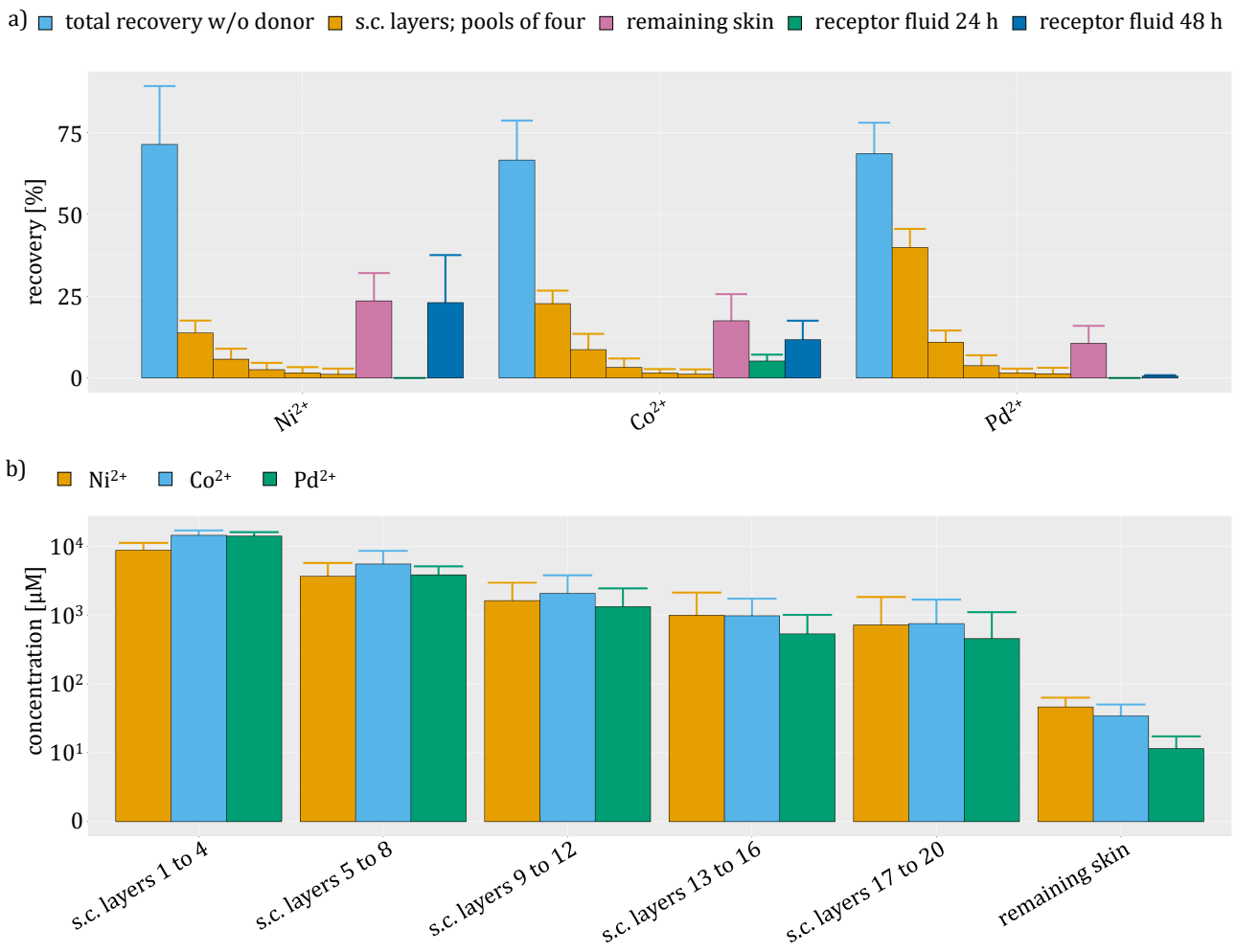

Figure 4.3: Distribution of the metal allergens nickel, cobalt and palladium in the skin after application of the metals in an aqueous solution. a) Distribution of recovery in the pooled *stratum corneum* (s.c.) layers (five pools of four consecutive tape strips), the remaining skin and the receptor after 24 h and 48 h. The light blue bar represents the total amount that penetrated the skin, that is, the sum of the recovery of all mentioned compartments. b) Concentrations in the s.c. and the remaining skin based on the volume of the respective layer; logarithmic scale. Means ± standard. Adapted from Simon *et al.* 2024b licensed under CC BY-NC 4.0.[204]

Differences in complexation properties might account for the difference in metal permeation. Chloride concentration on human skin is about 80 mM,[209] which is similar to the concentration of Pd^{2+} in the PTPs and much higher than the Pd^{2+} concentration in the PBS solution. In presence of chloride, Pd^{2+} forms complexes of the general structure $[PdCl_x(H_2O)_{4-x}]^{2-x}$ (x = 2,3,4), whereas Co^{2+} and Ni^{2+} preferably form the water adducts $[Me(H_2O)_{6-x}]^{2+}$ (Me = Ni^{2+}, Co^{2+}; x = 0,2). The Pd^{2+} complexes are negatively charged or neutral, depending on x, while the Ni^{2+} and Co^{2+} complexes are positively charged. This is crucial considering the permselective nature of skin: due to its structure, cationic transport is favored. The slightly acidic pH of the skin surface (≈ 5)[210] follows a gradient to about 7 in deeper layers.[211] The higher pH leads to more deprotonated carboxylic acid groups of proteins and free lipids. This in turn results in anion repulsion and less efficient anion transport. Therefore, cationic complexes such as those of Ni^{2+} or Co^{2+} could pass

this barrier more easily.

The immune response resulting in an allergic reaction is highly concentration-dependent. Thus, the obtained concentration of an allergen in the skin is a determining factor for the elicitation of contact dermatitis. Concentrations of all three metals after application in solution are in the range of 450 to 750 µM in the lowest s.c. layers (Figure 4.3b). Former *in vitro* studies have shown that these concentrations are sufficient to elicit activation pathways in dendtritic cells.[212]

Assuming that the patch test is a reliable diagnostic tool for Ni^{2+} contact allergy, the concentrations detected in the remaining skin and receptor of the FDC assays here can be seen as sufficient for allergy elicitation. The concentration in the remaining skin after application of $NiSO_4$ PTP is about 54 ± 37 µM Ni^{2+}. Hence, this concentration should be sufficient for the detection of contact allergy *in vitro*. And indeed, Covani *et al.* found a concentration of about 40 µM as ideal for *in vitro* nickel allergy diagnosis using a quantitative limited dilution assay.[213]

The concentration in the remaining skin of Pd^{2+} from either PTP is below 10 µM. It is probably too low to activate sufficient Pd-specific T cells and thus, an allergic reaction. This may contribute to fewer diagnoses of palladium contact allergy as compared to nickel or cobalt contact allergy.

Conclusion

This study demonstrated that the skin is less permeable for Pd^{2+} than for both Ni^{2+} and Co^{2+}. The results indicate that the lower penetration rates cannot be attributed solely to differences in solubility, as $PdCl_2$ and Na_2PdCl_4 PTPs exhibit similar penetration rates. The findings regarding skin penetration from an aqueous solution further underline that intrinsic properties of the ions such as complexation behavior are responsible for the differences in skin penetration.

The *in vitro* data provide valuable information on the concentrations in the skin after application of metal salt PTPs. This can help to understand which concentrations are needed for ACD elicitation and thus advance the development of novel *in vitro* diagnosis tools for contact allergies.

5 Conclusion

The s.c. represents the outermost part of the skin and is composed of layers of dead keratinocytes. It is an important barrier for the dermal penetration of harmful substances humans are exposed to. Consumer products are made of many different materials, including metals and plastics. They may contain harmful substances, either by design or inadvertently. PAH are a class of potentially carcinogenic compounds that have been found to contaminate consumer products dyed with carbon black or containing mineral oil.[10,12,25,45] The metal allergens nickel, cobalt and palladium are present in alloys humans are exposed to through, for example, jewelry.[4–8] In contact with the skin, these metals can cause ACD, a painful dermal rash.[9] The knowledge of the dermal penetration behavior of these harmful substances is crucial for risk assessment.

An important *in vitro* technique to investigate the dermal penetration of substances is the FDC assay. After the incubation of a substance on the skin's surface, the compartments of the FDC are extracted and the substance is quantified. Methods for quantification include GC-MS/MS for the PAH and ICP-MS for the metals in this thesis.

Both investigated substance classes, the PAH and metals, were shown to accumulate in the s.c. The s.c. is typically analyzed with the help of the tape stripping technique. A tape strip is applied to the skin's surface, pressed onto it and then removed. A layer of the s.c. is attached to the tape strip, which can be extracted and analyzed.

Tape stripping removes skin linearly up to 20 layers deep as illustrated by the histological study in the first part of this thesis. Removal of the s.c. by tape stripping and subsequent staining made it possible to measure the thickness of the remaining s.c. directly. Each tape strip removed about 0.4 µm of the s.c. Parallel bloating of the skin layers with potassium hydroxide solution (2%) allowed for the quantification of remaining skin layers and demonstrated that each tape strip removed about one layer of the s.c. The combination of these results revealed a thickness of 0.4 µm per s.c. layer — corresponding to the amount removed by each tape strip. This agrees with former measurements of the s.c. by scanning laser microscopy.[36]

Two studies on the skin penetration of PAH applying the well-established FDC assay investigated the s.c. barrier function. The data after application of 24 PAH in acetonitrile revealed that less lipophilic PAH (up to $\log P = 4.5$) effectively permeate the skin and reach the receptor chamber of the FDC within 2 h. Large PAH such as the dibenzopyrenes were not able to permeate the skin even after 48 h. They were, however, able to penetrate into the s.c., were they potentially form a

reservoir and slowly permeate the skin over time, before the s.c. layers are shed by desquamation.

The investigation of skin penetration of five selected PAH from a polymer surrogate matrix, squalane, showed that the partitioning into the s.c. is favored for larger PAH. $K_{sc/m}$ is linearly dependent on the log$P$ of the investigated PAH. Thus, the larger PAH are more likely to accumulate in the s.c. However, the diffusion in the s.c. is favored for naphthalene over the other four investigated PAH. D_{sc} of naphthalene was significantly higher than those of the other PAH, which could explain why smaller PAH reach the lower lying receptor more efficiently. An additional reason is the higher lipophilicity of the s.c. as compared to the underlying viable epidermis. The partitioning from the s.c. into the viable epidermis is thus favored for smaller and less lipophilic PAH.

For an allergen to elicit ACD, it must reach the lower layers of the s.c. In the study on the skin penetration of metal allergens, the contradiction between a low emergence of palladium contact allergies and the high frequencies of Pd-specific $CD4^+$ cells in human blood samples in *in vitro* assays was examined.[9,50] A hypothesis was that the lower skin penetration of palladium as compared to nickel and cobalt, which are widespread allergens, could account for the lower prevalence of palladium contact allergy. The FDC assays were preformed with diagnostic PTPs — featuring $NiSO_4$, $CoCl_2$, $PdCl_2$ and Na_2PdCl_4 in petrolatum — and a solution of all three metal ions in PBS. The results showed that Pd^{2+} penetrated the skin less effectively than Ni^{2+} or Co^{2+}, regardless of the type of Pd^{2+} salt or application medium. A possible reason could be the permselective nature of the skin and the favored cation transport, as Pd^{2+} tends to form anionic complexes. The concentrations determined in the skin can be used for the development of *in vitro* tools for the detection of contact allergies against these metals.

These studies investigated different aspects of *in vitro* skin penetration, ranging from methodology to the permeation of PAH and metals. They provide valuable insights for future studies such as the removal rate of s.c. cells by tape stripping, the risk assessment of consumer products with skin contact containing PAH or the development of *in vitro* allergy testing kits for metal allergens.

References

[1] "In Memoriam Karen E. Wetterhahn, Ph.D. 1948-1997" *Chem. Res. Toxicol.* **1997**, *10* (9), 923–923, doi: 10.1021/tx9704922.

[2] D. W. Nierenberg, R. E. Nordgren, M. B. Chang, R. W. Siegler, M. B. Blayney, F. Hochberg, T. Y. Toribara, E. Cernichiari, T. Clarkson, "Delayed Cerebellar Disease and Death after Accidental Exposure to Dimethylmercury" *New Engl. J. Med.* **1998**, *338* (23), 1672–1676, doi: 10.1056/nejm199806043382305.

[3] F. Riedel, M. Aparicio-Soto, C. Curato, H.-J. Thierse, K. Siewert, A. Luch, "Immunological Mechanisms of Metal Allergies and the Nickel-Specific TCR-pMHC Interface" *Int. J. Environ. Res. Public Health* **2021**, *18* (20), 10867.

[4] A. McDonagh, A. Wright, M. Cork, D. Gawkrodger, "Nickel sensitivity: the influence of ear piercing and atopy" *Br. J. Dermatol.* **1992**, *126* (1), 16–18, doi: 10.1111/j.1365-2133.1992.tb08396.x.

[5] D. J. Gawkrodger, F. M. Lewis, M. Shah, "Contact sensitivity to nickel and other metals in jewelry reactors" *J. Am. Acad. Dermatol.* **2000**, *43* (1, Part 1), 31–36, doi: 10.1067/mjd.2000.107235.

[6] P. Battaini, "The Working Properties for Jewelry Fabrication Using New Hard 950 Palladium Alloys" **2006**, https://www.santafesymposium.org/2006-santa-fe-symposium-papers/2006-the-working-properties-for-jewelry-fabrication-using-new-hard-950-palladium-alloys (accessed 15 Feb. 2024).

[7] N. H. Nielsen, T. Menné, "Nickel sensitization and ear piercing in an unselected Danish population" *Contact Dermatitis* **1993**, *29* (1), 16–21, doi: 10.1111/j.1600-0536.1993.tb04530.x.

[8] B. T. Biggs, S. S. Taylor, E. van der Lingen, "The Hardening of Platinum Alloys for Potential Jewellery Application" *Platinum Met. Rev.* **2005**, *49* (1), 2–15, doi: 10.1595/147106705X24409.

[9] F. Alinaghi, N. H. Bennike, A. Egeberg, J. P. Thyssen, J. D. Johansen, "Prevalence of contact allergy in the general population: a systematic review and meta-analysis" *Contact Dermatitis* **2019**, *80* (2), 77–85, doi: 10.1111/cod.13119.

[10] M. A. Alawi, R. A. Abdullah, I. Tarawneh, "Determination of polycyclic aromatic hydrocarbons (PAHs) in carbon black-containing plastic consumer products from the Jordanian market" *Toxin Rev.* **2018**, *37* (4), 269–277, doi: 10.1080/15569543.2017.1359628.

[11] N. Bartsch, C. Hutzler, B. Vieth, A. Luch, "Target analysis of polycyclic aromatic hydrocarbons (PAHs) in consumer products and total content of polycyclic aromatic compounds (PACs)" *Polycycl. Aromat. Comp.* **2017**, *37* (2-3), 114–121, doi: 10.1080/10406638.2016.1189440.

[12] International Agency for Research on Cancer (IARC), "Agents classified by the IARC monographs, volumes 1–113" **2018**, https://monographs.iarc.who.int/agents-classified-by-the-iarc/ (accessed 13 Aug. 2021).

[13] K. M. Mackenzie, D. M. Angevine, "Infertility in mice exposed in utero to benzo[a]pyrene" *Biol. Reprod.* **1981**, *24* (1), 183–191, doi: 10.1095/biolreprod24.1.183.

[14] J. A. Hardin, F. Hinoshita, D. H. Sherr, "Mechanisms by which benzo[a]pyrene, an environmental carcinogen, suppresses B cell lymphopoiesis" *Toxicol. Appl. Pharmacol.* **1992**, *117* (2), 155–164, doi: 10.1016/0041-008X(92)90232-H.

[15] J. Brinkmann, K. Stolpmann, S. Trappe, T. Otter, D. Genkinger, U. Bock, M. Liebsch, F. Henkler, C. Hutzler, A. Luch, "Metabolically competent human skin models: activation and genotoxicity of benzo[a]pyrene" *Toxicol. Sci.* **2012**, *131* (2), 351–359, doi: 10.1093/toxsci/kfs316.

[16] M. Rota, C. Bosetti, S. Boccia, P. Boffetta, C. L. Vecchia, "Occupational exposures to polycyclic aromatic hydrocarbons and respiratory and urinary tract cancers: an updated systematic review and a meta-analysis to 2014" *Arch. Toxicol.* **2014**, *88* (8), 1479–1490, doi: 10.1007/s00204-014-1296-5.

[17] J. Collins, J. Brown, G. Alexeeff, A. Salmon, "Potency equivalency factors for some polycyclic aromatic hydrocarbons and polycyclic aromatic hydrocarbon derivatives" *Regul. Toxicol. Pharmacol.* **1998**, *28* (1), 45–54, doi: 10.1006/rtph.1998.1235.

[18] R. D. Mosteller, "Simplified Calculation of Body-Surface Area" *New Engl. J. Med.* **1987**, *317* (17), 1098–1098, doi: 10.1056/nejm198710223171717.

[19] J. A. McGrath, R. A. J. Eady, F. M. Pope, "Anatomy and Organization of Human Skin" in "Rook's Textbook of Dermatology" Wiley-Blackwell, **2004**, 45–128, ISBN: 9780470750520, doi: 10.1002/9780470750520.ch3.

[20] T. J. Franz, "Percutaneous absorption. On the relevance of in vitro data" *J. Invest. Dermatol.* **1975**, *64* (3), 190–195, doi: 10.1111/1523-1747.ep12533356.

[21] N. Bartsch, M. Girard, L. Schneider, V. V. D. Weijgert, A. Wilde, O. Kappenstein, B. Vieth, C. Hutzler, A. Luch, "Chemical stabilization of polymers: Implications for dermal exposure to additives" *J. Environ. Sci. Health. Part A* **2018**, *53* (5), 405–420, doi: 10.1080/10934529.2017.1412192.

[22] R. L. Bronaugh, E. R. Congdon, R. J. Scheuplein, "The effect of cosmetic vehicles on the penetration of N-nitrosodiethanolamine through excised human skin" *J. Invest. Dermatol.* **1981**, *76* (2), 94–96, doi: 10.1111/1523-1747.ep12525384.

[23] S.-F. Ng, J. J. Rouse, F. D. Sanderson, V. Meidan, G. M. Eccleston, "Validation of a static Franz diffusion cell system for in vitro permeation studies" *AAPS PharmSciTech* **2010**, *11* (3), 1432–1441, doi: 10.1208/s12249-010-9522-9.

[24] C. M. Lee, S. P. Jin, E. J. Doh, D. H. Lee, J. H. Chung, "Regional Variation of Human Skin Surface Temperature" *Ann. Dermatol.* **2019**, *31* (3), 349–352, doi: 10.5021/ad.2019.31.3.349.

[25] N. Bartsch, J. Heidler, B. Vieth, C. Hutzler, A. Luch, "Skin permeation of polycyclic aromatic hydrocarbons: a solvent-based in vitro approach to assess dermal exposures against benzo[a]pyrene and dibenzopyrenes" *J. Occup. Environ. Hyg.* **2016**, *13* (12), 969–979, doi: 10.1080/15459624.2016.1200724.

[26] L. Hagvall, M. D. Pour, J. Feng, M. Karma, Y. Hedberg, P. Malmberg, "Skin permeation of nickel, cobalt and chromium salts in ex vivo human skin, visualized using mass spectrometry imaging" *Toxicol. In Vitro* **2021**, *76*, 105232, doi: 10.1016/j.tiv.2021.105232.

[27] C. A. Ellison, K. O. Tankersley, C. M. Obringer, G. J. Carr, J. Manwaring, H. Rothe, H. Duplan, C. Géniès, S. Grégoire, N. J. Hewitt, "Partition coefficient and diffusion coefficient determinations of 50 compounds in human intact skin, isolated skin layers and isolated stratum corneum lipids" *Toxicol. In Vitro* **2020**, *69*, 104990, doi: 10.1016/j.tiv.2020.104990.

[28] C. A. Ellison, K. O. Tankersley, C. M. Obringer, G. J. Carr, J. Manwaring, H. Rothe, H. Duplan, C. Géniès, S. Grégoire, N. J. Hewitt, "Corrigendum to: Partition coefficient and diffusion coefficient determinations of 50 compounds in human intact skin, isolated skin layers and isolated stratum corneum lipids" *Toxicol. In Vitro* **2021**, *71*, 105050, doi: 10.1016/j.tiv.2020.105050.

[29] L. Lemoine, D. Bayrambey, A. Roloff, C. Hutzler, A. Luch, T. Tralau, "Commensal-Related Changes in the Epidermal Barrier Function Lead to Alterations in the Benzo[a]pyrene Metabolite Profile and Its Distribution in 3D Skin" *mBio* **2021**, *12* (5), doi: 10.1128/mbio.01223-21.

[30] D. Gerstel, C. Jacques-Jamin, A. Schepky, R. Cubberley, J. Eilstein, S. Grégoire, N. Hewitt, M. Klaric, H. Rothe, H. Duplan, "Comparison of protocols for measuring cosmetic ingredient distribution in human and pig skin" *Toxicol. In Vitro* **2016**, *34*, 153–160, doi: 10.1016/j.tiv.2016.03.012.

[31] C. Herkenne, A. Naik, Y. N. Kalia, J. Hadgraft, R. H. Guy, "Pig ear skin ex vivo as a model for in vivo dermatopharmacokinetic studies in man" *Pharm. Res.* **2006**, *23* (8), 1850–1856, doi: 10.1007/s11095-006-9011-8.

[32] H. Rothe, C. Obringer, J. Manwaring, C. Avci, W. Wargniez, J. Eilstein, N. Hewitt, R. Cubberley, H. Duplan, D. Lange, "Comparison of protocols measuring diffusion and partition coefficients in the stratum corneum" *J. Appl. Toxicol.* **2017**, *37* (7), 806–816, doi: 10.1002/jat.3427.

[33] Scientific Committee on Consumer Safety (SCCS), "Basic criteria for the in vitro assessment of dermal absorption of cosmetic ingredients." *7th plenary meeting* **2010**.

[34] J. Wolf, "Die innere Struktur der Zellen des Stratum desquamans der menschlichen Epidermis" *Z. Mikrosk. Anat. Forsch.* **1939**, *46*, 170–202.

[35] A. Hughes, S. Tawfik, K. Baruah, E. O'Toole, R. O'Shaughnessy, "Tape strips in dermatology research" *Br. J. Dermatol.* **2021**, *185* (1), 26–35, doi: 10.1111/bjd.19760.

[36] U. Lindemann, K. Wilken, H.-J. Weigmann, H. Schaefer, W. Sterry, J. Lademann, "Quantification of the horny layer using tape stripping and microscopic techniques" *J. Biomed. Opt.* **2003**, *8* (4), 601–607, doi: 10.1117/1.1609200.

[37] F. Dreher, A. Arens, J. Hostýnek, S. Mudumba, J. Ademola, H. Maibach, "Colorimetric Method for Quantifying Human Stratum Corneum Removed by Adhesive-Tape-Stripping" *Acta Derm. Venereol.* **1998**, *78* (3), doi: 10.1080/000155598441495.

[38] D. A. Schwindt, K. P. Wilhelm, H. I. Maibach, "Water diffusion characteristics of human stratum corneum at different anatomical sites in vivo" *J. Invest. Dermatol.* **1998**, *111* (3), 385–389, doi: 10.1046/j.1523-1747.1998.00321.x.

[39] H.-J. Weigmann, J. Lademann, H. Meffert, H. Schaefer, W. Sterry, "Determination of the horny layer profile by tape stripping in combination with optical spectroscopy in the visible range as a prerequisite to quantify percutaneous absorption" *Skin Pharmacol. Physiol.* **1999**, *12* (1-2), 34–45, doi: 10.1159/000029844.

[40] H.-J. Weigmann, U. Lindemann, C. Antoniou, G. Tsikrikas, A. Stratigos, A. Katsambas, W. Sterry, J. Lademann, "UV/VIS absorbance allows rapid, accurate, and reproducible mass determination of corneocytes removed by tape stripping" *Skin Pharmacol. Physiol.* **2003**, *16* (4), 217–227, doi: 10.1159/000070844.

[41] U. Jacobi, H.-J. Weigmann, J. Ulrich, W. Sterry, J. Lademann, "Estimation of the relative stratum corneum amount removed by tape stripping" *Skin Res. Technol.* **2005**, *11* (2), 91–96, doi: 10.1111/j.1600-0846.2005.00094.x.

[42] U. Lindemann, H.-J. Weigmann, H. Schaefer, W. Sterry, J. Lademann, "Evaluation of the pseudo-absorption method to quantify human stratum corneum removed by tape stripping using protein absorption" *Skin Pharmacol. Physiol.* **2003**, *16* (4), 228–236, doi: 10.1159/000070845.

[43] D. Mohammed, Q. Yang, R. Guy, P. Matts, J. Hadgraft, M. Lane, "Comparison of gravimetric and spectroscopic approaches to quantify stratum corneum removed by tape-stripping" *Eur. J. Pharm. Biopharm.* **2012**, *82* (1), 171–174, doi: 10.1016/j.ejpb.2012.05.018.

[44] B. J. Finlayson-Pitts, J. J. N. Pitts, "Tropospheric air pollution: ozone, airborne toxics, polycyclic aromatic hydrocarbons, and particles" *Science* **1997**, *276* (5315), 1045–1052, doi: 10.1126/science.276.5315.1045.

[45] Stiftung Warentest, "Schminke und Klebe-Tattoos mit Schadstoffen belastet." **2016**, https://www.test.de/Fanschminke-Schminke-und-Klebe-Tattoos-mit-Schadstoffen-belastet-5024667-0/ (accessed 21 Oct. 2019).

[46] L. R. Comstedt, J. Dahlin, M. Bruze, A. Åkesson, M. Hindsén, A. Pontén, M. Isaksson, C. Svedman, "Prevalence of contact allergy to metals: nickel, palladium, and cobalt in Southern Sweden from 1995-2016" *Contact Dermatitis* **2020**, *82* (4), 218–226, doi: 10.1111/cod.13422.

[47] M. Aparicio-Soto, F. Riedel, M. Leddermann, P. Bacher, A. Scheffold, H. Kuhl, B. Timmermann, D. M. Chudakov, S. Molin, M. Worm, "TCRs with segment TRAV9-2 or a CDR3 histidine are overrepresented among nickel-specific CD4+ T cells" *Allergy* **2020**, *75* (10), 2574–2586, doi: 10.1111/all.14322.

[48] J. Swietlik, M. Reeder, "Current Quality-of-Life Tools Available for Use in Contact Dermatitis" *Dermatitis* **2016**, *27* (4), 176–185, doi: 10.1097/der.0000000000000192.

[49] B. Sætterstrøm, J. Olsen, J. D. Johansen, "Cost-of-illness of patients with contact dermatitis in Denmark" *Contact Dermatitis* **2014**, *71* (3), 154–161, doi: 10.1111/cod.12231.

[50] F. Riedel, M. Aparicio-Soto, C. Curato, L. Münch, A. Abbas, H. J. Thierse, W. K. Peitsch, A. Luch, K. Siewert, "Unique and common TCR repertoire features of Ni2+-, Co2+-, and Pd2+-specific human CD154+ CD4+ T cells" *Allergy* **2022**, *78* (1), 270–282, doi: 10.1111/all.15494.

[51] J. Gould, "Superpowered skin" *Nature* **2018**, *563* (7732), S84–S85, doi: 10.1038/d41586-018-07429-3.

[52] P. M. Elias, "Stratum corneum defensive functions: an integrated view" *J. Invest. Dermatol.* **2005**, *125* (2), 183–200, doi: 10.1111/j.0022-202X.2005.23668.x.

[53] Encyclopædia Britannica, W. Montagna, J. Ebling, "human skin" **2023**, https://www.britannica.com/science/human-skin (accessed 5 Sept. 2023).

[54] "SEER Training Modules. Skin Cancer: Melanoma" https://training.seer.cancer.gov/melanoma/anatomy/ (accessed 6 Sept. 2023).

[55] A. S. Michaels, S. K. Chandrasekaran, J. E. Shaw, "Drug permeation through human skin: Theory and in vitro experimental measurement" *AIChE Journal* **1975**, *21* (5), 985–996, doi: 10.1002/aic.690210522.

[56] A. Weerheim, M. Ponec, "Determination of stratum corneum lipid profile by tape stripping in combination with high-performance thin-layer chromatography" *Arch. Dermatol. Res.* **2001**, *293* (4), 191–199, doi: 10.1007/s004030100212.

[57] J. van Smeden, J. A. Bouwstra, "Stratum Corneum Lipids: Their Role for the Skin Barrier Function in Healthy Subjects and Atopic Dermatitis Patients" in "Skin Barrier Function" Vol. 49, (Ed.: T. Agner), S. Karger AG, **2016**, 8–26, ISBN: 978-3-318-05585-6, doi: 10.1159/000441540.

[58] H. Buist, P. Craig, I. Dewhurst, S. H. Bennekou, C. Kneuer, K. Machera, C. Pieper, D. C. Marques, G. Guillot, F. Ruffo, A. Chiusolo, "Guidance on dermal absorption" *EFSA Journal* **2017**, *15* (6), e04873, doi: 10.2903/j.efsa.2017.4873.

[59] Encyclopædia Britannica, "adipose cell" **2023**, https://www.britannica.com/science/adipose-cell (accessed 7 Sept. 2023).

[60] N. Hopf, C. Champmartin, L. Schenk, A. Berthet, L. Chedik, J. D. Plessis, A. Franken, F. Frasch, S. Gaskin, G. Johanson, "Reflections on the OECD guidelines for in vitro skin absorption studies" *Regul. Toxicol. Pharmacol.* **2020**, 104752, doi: 10.1016/j.yrtph.2020.104752.

[61] Organisation for Economic Co-operation and Development (OECD), "Guideline for the Testing of Chemicals No. 428: Skin Absorption: in vitro Method" **2004**.

[62] G. A. Simon, H. I. Maibach, "The pig as an experimental animal model of percutaneous permeation in man: qualitative and quantitative observations–an overview" *Skin Pharmacol. Appl. Skin Physiol.* **2000**, *13* (5), 229–34, doi: 10.1159/000029928.

[63] M. K. In, K. C. Richardson, A. Loewa, S. Hedtrich, S. Kaessmeyer, J. Plendl, "Histological and functional comparisons of four anatomical regions of porcine skin with human abdominal skin" *Anat. Histol. Embryol.* **2019**, *48* (3), 207–217, doi: 10.1111/ahe.12425.

[64] A. M. Barbero, H. F. Frasch, "Pig and guinea pig skin as surrogates for human in vitro penetration studies: A quantitative review" *Toxicol. In Vitro* **2009**, *23* (1), 1–13, doi: 10.1016/j.tiv.2008.10.008.

[65] S. Singh, K. Zhao, J. Singh, "In vitro permeability and binding of hydrocarbons in pig ear and human abdominal skin" *Drug Chem. Toxicol.* **2002**, *25* (1), 83–92, doi: 10.1081/dct-100108474.

[66] P. M. Elias, "Skin barrier function" *Curr. Allergy Asthma Rep.* **2008**, *8* (4), 299–305, doi: 10.1007/s11882-008-0048-0.

[67] E. A. Pinson, "Evaporation from human skin with sweat glands inactivated" *Am. J. Physiol.* **1942**, *137* (3), 492–503, doi: 10.1152/ajplegacy.1942.137.3.492.

[68] B. Idson, "In vivo measurement of trans-epidermal water-loss" *J. Soc. Cosmet. Chem.* **1978**, *29* (9), 573–580.

[69] G. E. Nilsson, "Measurement of water exchange through skin" *Med. Biol. Eng. Comput.* **1977**, *15* (3), 209–218, doi: 10.1007/BF02441040.

[70] L. O. Lamke, G. E. Nilsson, H. L. Reithner, "Insensible perspiration from the skin under standardized environmental conditions" *Scand. J. Clin. Lab. Invest.* **1977**, *37* (4), 325–331, doi: 10.3109/00365517709092637.

[71] R. P. Chilcott, C. H. Dalton, A. J. Emmanuel, C. E. Allen, S. T. Bradley, "Transepidermal water loss does not correlate with skin barrier function in vitro" *J. Invest. Dermatol.* **2002**, *118* (5), 871–875, doi: 10.1046/j.1523-1747.2002.01760.x.

[72] R. Imhof, "Method and equipment for measuring vapour flux from sufaces" United States Patent and Trademark Office, US Patent 2006/0150714 A1, **2006**.

[73] P. Xiao, H. Packham, X. Zheng, H. Singh, C. Elliott, E. P. Berg, R. E. Imhof, "Opto-thermal radiometry and condenser-chamber method for stratum corneum water concentration measurements" *Appl. Phys. B* **2007**, *86* (4), 715–719, doi: 10.1007/s00340-006-2541-2.

[74] R. E. Imhof, M. E. D. Jesus, P. Xiao, L. I. Ciortea, E. P. Berg, "Closed-chamber transepidermal water loss measurement: microclimate, calibration and performance" *Int. J. Cosmetic Sci.* **2009**, *31* (2), 97–118, doi: 10.1111/j.1468-2494.2008.00476.x.

[75] E. Elmahjoubi, Y. Frum, G. M. Eccleston, S. C. Wilkinson, V. M. Meidan, "Transepidermal water loss for probing full-thickness skin barrier function: correlation with tritiated water flux, sensitivity to punctures and diverse surfactant exposures" *Toxicol. In Vitro* **2009**, *23* (7), 1429–1435, doi: 10.1016/j.tiv.2009.06.030.

[76] R. T. Tregear, P. Dirnhuber, "The Mass of Keratin Removed from the Stratum Corneum by Stripping with Adhesive Tape" *J. Invest. Dermatol.* **1962**, *38* (6), 375–381, doi: 10.1038/jid.1962.67.

[77] E. Christophers, A. M. Kligman, "Visualization of the cell layers of the stratum corneum" *J. Invest. Dermatol.* **1964**, *42* (6), 407–409, doi: 10.1038/jid.1964.88.

[78] C. Blair, "Morphology and thickness of the human stratum corneum" *Br. J. Dermatol.* **1968**, *80* (7), 430–436, doi: 10.1111/j.1365-2133.1968.tb11978.x.

[79] C. King, S. Barton, S. Nicholls, R. Marks, "The change in properties of the stratum corneum as a function of depth" *Br. J. Dermatol.* **1979**, *100* (2), 165–172, doi: 10.1111/j.1365-2133.1979.tb05556.x.

[80] D. Bommannan, R. O. Potts, R. H. Guy, "Examination of stratum corneum barrier function in vivo by infrared spectroscopy" *J. Invest. Dermatol.* **1990**, *95* (4), 403–408, doi: 10.1111/1523-1747.ep12555503.

[81] A. Zesch, H. Schaefer, W. Hoffmann, "Barrier and resevoir function of human stratum corneum for topically applied drugs" *Arch. Dermatol. Forsch.* **1973**, *246* (2), 103–107, doi: 10.1007/BF00595526.

[82] F. Toner, G. Allan, S. S. Dimond, J. M. W. Jr, D. Beyer, "In vitro percutaneous absorption and metabolism of Bisphenol A (BPA) through fresh human skin" *Toxicol. In Vitro* **2018**, *47*, 147–155, doi: 10.1016/j.tiv.2017.11.002.

[83] H. Pinkus, "Examination of the epidermis by the strip method of removing horny layers: I. Observations on thickness of the horny layer, and on mitotic activity after stripping" *J. Invest. Dermatol.* **1951**, *16* (6), 383–386, doi: 10.1038/jid.1951.45.

[84] S.-T. R. Han, M. Haberkamp, G. L. Flynn, "Epidermal kinetics and skin condition: I. Stripping technique for quantitating stratum corneum turnover in hairless mouse skin" *J. Toxicol. Cutaneous Ocul. Toxicol.* **1989**, *8* (4), 539–553, doi: 10.3109/15569528909062958.

[85] N. Higo, A. Naik, D. B. Bommannan, R. O. Potts, R. H. Guy, "Validation of reflectance infrared spectroscopy as a quantitative method to measure percutaneous absorption in vivo" *Pharm. Res.* **1993**, *10* (10), 1500–1506, doi: 10.1023/A:1018987612155.

[86] D. Mohammed, P. Matts, J. Hadgraft, M. Lane, "Depth profiling of stratum corneum biophysical and molecular properties" *Br. J. Dermatol.* **2011**, *164* (5), 957–965, doi: 10.1111/j.1365-2133.2011.10211.x.

[87] L. Norlén, "Stratum corneum keratin structure, function and formation - a comprehensive review" *Int. J. Cosmetic Sci.* **2006**, *28* (6), 397–425, doi: 10.1111/j.1467-2494.2006.00345.x.

[88] L. Norlén, A. Al-Amoudi, "Stratum corneum keratin structure, function, and formation: the cubic rod-packing and membrane templating model" *J. Invest. Dermatol.* **2004**, *123* (4), 715–32, doi: 10.1111/j.0022-202X.2004.23213.x.

[89] Z. Ya-Xian, T. Suetake, H. Tagami, "Number of cell layers of the stratum corneum in normal skin–relationship to the anatomical location on the body, age, sex and physical parameters" *Arch. Dermatol. Res.* **1999**, *291* (10), 555–559, doi: 10.1007/s004030050453.

[90] Q. Zhang, M. Murawsky, T. LaCount, G. B. Kasting, S. K. Li, "Transepidermal water loss and skin conductance as barrier integrity tests" *Toxicol. In Vitro* **2018**, *51*, 129–135, doi: 10.1016/j.tiv.2018.04.009.

[91] U. Jacobi, M. Kaiser, H. Richter, H. Audring, W. Sterry, J. Lademann, "The number of stratum corneum cell layers correlates with the pseudo-absorption of the corneocytes" *Skin Pharmacol. Physiol.* **2005**, *18* (4), 175–179, doi: 10.1159/000085862.

[92] K. Simon, G. Oberender, A. Roloff, "Continuous removal of single cell layers by tape stripping the stratum corneum – a histological study" *Eur. J. Pharm. Biopharm.* **2023**, *188*, 48–53, doi: 10.1016/j.ejpb.2023.04.022.

[93] L. Zhang, T. Cambron, Y. Niu, Z. Xu, N. Su, H. Zheng, K. Wei, P. Ray, "MCR Approach Revealing Protein, Water, and Lipid Depth Profile in Atopic Dermatitis Patients' Stratum Corneum via in Vivo Confocal Raman Spectroscopy" *Anal. Chem.* **2019**, *91* (4), 2784–2790, doi: 10.1021/acs.analchem.8b04597.

[94] M. A. Lampe, A. L. Burlingame, J. Whitney, M. L. Williams, B. E. Brown, E. Roitman, P. M. Elias, "Human stratum corneum lipids: characterization and regional variations" *J. Lipid Res.* **1983**, *24* (2), 120–130, doi: 10.1016/S0022-2275(20)38005-6.

[95] G. Gray, H. Yardley, "Lipid compositions of cells isolated from pig, human, and rat epidermis" *J. Lipid Res.* **1975**, *16* (6), 434–440, doi: 10.1016/S0022-2275(20)34493-X.

[96] H. Fischer, I. Polikarpov, A. F. Craievich, "Average protein density is a molecular-weight-dependent function" *Protein Sci.* **2004**, *13* (10), 2825–8, doi: 10.1110/ps.04688204.

[97] P. Pott, "Chirurgical observations relative to the cataract, the polypus of the nose, the cancer of the scrotum, the different kinds of ruptures, and the mortification of the toes and feet" L. Hawes, W. Clarke and R. Collins, London, **1775**.

[98] J. R. Brown, J. L. Thornton, "Percivall Pott (1714-1788) and chimney sweepers' cancer of the scrotum" *Br. J. Dermatol.* **1957**, *14* (1), 68–70, doi: 10.1136/oem.14.1.68.

[99] H. Fujiki, "Gist of Dr. Katsusaburo Yamagiwa's papers entitled "Experimental study on the pathogenesis of epithelial tumors" (I to VI reports)" *Cancer Sci.* **2013**, *105*, doi: 10.1111/cas.12333.

[100] D. H. Phillips, "Fifty years of benzo(a)pyrene" *Nature* **1983**, *303* (5917), 468–472, doi: 10.1038/303468a0.

[101] M. L. Geiges, "Klinisch orientierte Forschung 1916–1978" in "100 Jahre Dermatologische Klinik Zürich: 100 Jahre translationale Forschung" Springer, Berlin, Heidelberg, **2017**, 1–42, ISBN: 978-3-662-53346-8, doi: 10.1007/978-3-662-53346-8_1.

[102] B. Bloch, W. Dreifuss, "Ueber die experimentelle Erzeugung vonCarcinomen mit Lymphdrüsen und Lungenmetastasen durch Teerbestandteile" *Schweiz. Med. Wochenschr.* **1921**, *51*, 1033–1037.

[103] A. Lacassagne, "Kennaway and the Carcinogens" *Nature* **1961**, *191* (4790), 743–747, doi: 10.1038/191743a0.

[104] E. L. Kennaway, "On the cancer producing factor in tar" *Br. Med. J.* **1924**, *1* (3300), 564–567, doi: 10.1136/bmj.1.3300.564.

[105] E. L. Kennaway, "Experiments on cancer-producing substances" *Br. Med. J.* **1925**, *2* (3366), 1–4, doi: 10.1136/bmj.2.3366.1.

[106] J. W. Cook, C. Hewett, I. Hieger, "Coal Tar Constituents and Cancer" *Nature* **1932**, *130* (3294), 926–926, doi: 10.1038/130926a0.

[107] J. W. Cook, C. L. Hewett, I. Hieger, "106. The isolation of a cancer-producing hydrocarbon from coal tar. Parts I, II, and III" *J. Chem. Soc.* **1933**, 395–405, doi: 10.1039/JR9330000395.

[108] J. Roberts, R. Stewart, M. Caserio, "Organic Chemistry - Methane to Macromolecules" *1*, W. A. Benjamin, New York, **1971**.

[109] A. T. Lawal, "Polycyclic aromatic hydrocarbons. A review" *Cogent Environ. Sci.* **2017**, *3* (1), 1339841, doi: 10.1080/23311843.2017.1339841.

[110] National Center for Biotechnology Information, "PubChem Compound Summary for CID 931, Naphthalene." **2024**, https://pubchem.ncbi.nlm.nih.gov/compound/Naphthalene (accessed 26 Apr. 2024).

[111] S. O. Baek, R. A. Field, M. E. Goldstone, P. W. Kirk, J. N. Lester, R. Perry, "A review of atmospheric polycyclic aromatic hydrocarbons: Sources, fate and behavior" *Water Air Soil Pollut.* **1991**, *60* (3), 279–300, doi: 10.1007/BF00282628.

[112] Y. Zhang, S. Tao, "Global atmospheric emission inventory of polycyclic aromatic hydrocarbons (PAHs) for 2004" *Atmos. Environ.* **2009**, *43* (4), 812–819, doi: 10.1016/j.atmosenv.2008.10.050.

[113] Y. Zhang, S. Tao, H. Shen, J. Ma, "Inhalation exposure to ambient polycyclic aromatic hydrocarbons and lung cancer risk of Chinese population" *Proc. Natl. Acad. Sci. USA* **2009**, *106* (50), 21063–21067, doi: 10.1073/pnas.0905756106.

[114] E. Croom, "Metabolism of Xenobiotics of Human Environments" in "Progress in Molecular Biology and Translational Science" Vol. 112, (Ed.: E. Hodgson), Academic Press, Oxford, United Kingdom, **2012**, 31–88, ISBN: 978-0-12-4158-13-9.

[115] Y. Shimizu, Y. Nakatsuru, M. Ichinose, Y. Takahashi, H. Kume, J. Mimura, Y. Fujii-Kuriyama, T. Ishikawa, "Benzo[a]pyrene carcinogenicity is lost in mice lacking the aryl hydrocarbon receptor" *Proc. Natl. Acad. Sci. USA* **2000**, *97* (2), 779–782, doi: 10.1073/pnas.97.2.779.

[116] T. Shimada, "Xenobiotic-metabolizing enzymes involved in activation and detoxification of carcinogenic polycyclic aromatic hydrocarbons" *Drug Metab. Pharmacokinet.* **2006**, *21* (4), 257–276, doi: 10.2133/dmpk.21.257.

[117] J. Kapitulnik, W. Levin, A. H. Conney, H. Yagi, D. M. Jerina, "Benzo[a]pyrene 7,8-dihydrodiol is more carcinogenic than benzo[a]pyrene in newborn mice" *Nature* **1977**, *266* (5600), 378–380, doi: 10.1038/266378a0.

[118] R. C. Wester, J. Christoffel, T. Hartway, N. Poblete, H. I. Maibach, J. Forsell, "Human Cadaver Skin Viability for In Vitro Percutaneous Absorption: Storage and Detrimental Effects of Heat-Separation and Freezing" *Pharm. Res.* **1998**, *15* (1), 82–84, doi: 10.1023/A:1011904921318.

[119] Organisation for Economic Co-operation and Development (OECD), "Series on Testing and Assesment No. 28: Guidance document for the conduct of skin absorption studies." **2004**.

[120] G.-N. Lu, X.-Q. Tao, Z. Dang, X.-Y. Yi, C. Yang, "Estimation of n-octanol/water partition coefficients of polycyclic aromatic hydrocarbons by quantum chemical descriptors" *Open Chem.* **2008**, *6* (2), 310–318, doi: 10.2478/s11532-008-0010-y.

[121] F. A. de Lima Ribeiro, M. M. C. Ferreira, "QSPR models of boiling point, octanol–water partition coefficient and retention time index of polycyclic aromatic hydrocarbons" *J. Mol. Struc. THEOCHEM* **2003**, *663* (1-3), 109–126, doi: 10.1016/j.theochem.2003.08.107.

[122] National Center for Biotechnology Information, "PubChem Compound Summary for CID 5889, Dibenz[a,h]anthracene" **2023**, https://pubchem.ncbi.nlm.nih.gov/compound/Dibenz_a_h_anthracene (accessed 11 July 2023).

[123] National Center for Biotechnology Information, "PubChem Compound Summary for CID 9119, Dibenzo[a,l]pyrene" **2023**, https://pubchem.ncbi.nlm.nih.gov/compound/Dibenzo_a_l_pyrene (accessed 11 July 2023).

[124] United Stated Environmental Protection Agency (USEPA), "Estimation Program Interface (EPI) Suite" **2012**, https://www.epa.gov/tsca-screening-tools/download-epi-suitetm-estimation-program-interface-v411 (accessed 25 Mar. 2021).

[125] National Center for Biotechnology Information, "PubChem Compound Summary for CID 9126, Dibenzo[a,e]pyrene" **2023**, https://pubchem.ncbi.nlm.nih.gov/compound/Dibenzo_a_e_pyrene (accessed 11 July 2023).

[126] National Center for Biotechnology Information, "PubChem Compound Summary for CID 9106, Dibenzo[a,i]pyrene" **2023**, https://pubchem.ncbi.nlm.nih.gov/compound/Dibenzo_A_I_pyrene (accessed 11 July 2023).

[127] A. Luch, "Nature and nurture - lessons from chemical carcinogenesis" *Nat. Rev. Cancer* **2005**, *5* (2), 113–125, doi: 10.1038/nrc1546.

[128] C. Klaassen, "Toxicology - The Basic Science of Poisons" *8*, McGraw Hill Education, **2013**, ISBN: 978-0-07-176923-5.

[129] L. Lemoine, "Modulation of polycyclic aromatic hydrocarbon toxicity by the human skin microbiome" Doctoral Thesis, Freie Universität, Berlin, **2021**.

[130] R. Haidar, F. Henkler, J. Kugler, A. Rosin, D. Genkinger, P. Laux, A. Luch, "The role of DNA-binding and ARNT dimerization on the nucleo-cytoplasmic translocation of the aryl hydrocarbon receptor" *Sci. Rep.* **2021**, *11* (1), 18194, doi: 10.1038/s41598-021-97507-w.

[131] W. M. Baird, L. A. Hooven, B. Mahadevan, "Carcinogenic polycyclic aromatic hydrocarbon-DNA adducts and mechanism of action" *Environ. Mol. Mutagen.* **2005**, *45* (2-3), 106–114, doi: 10.1002/em.20095.

[132] M. Koreeda, P. D. Moore, P. G. Wislocki, W. Levin, H. Yagi, D. M. Jerina, "Binding of benzo[a]-pyrene 7,8-diol-9,10-epoxides to DNA, RNA, and protein of mouse skin occurs with high stereoselectivity" *Science* **1978**, *199* (4330), 778–781, doi: 10.1126/science.622566.

[133] S. C. Cheng, B. D. Hilton, J. M. Roman, A. Dipple, "DNA adducts from carcinogenic and noncarcinogenic enantiomers of benzo[a]pyrene dihydrodiol epoxide" *Chem. Res. Toxicol.* **1989**, *2* (5), 334–340, doi: 10.1021/tx00011a011.

[134] E. C. Friedberg, "How nucleotide excision repair protects against cancer" *Nat. Rev. Cancer* **2001**, *1* (1), 22–33, doi: 10.1038/35094000.

[135] N. E. Geacintov, M. Cosman, B. E. Hingerty, S. Amin, S. Broyde, D. J. Patel, "NMR Solution Structures of Stereoisomeric Covalent Polycyclic Aromatic Carcinogen-DNA Adducts: Principles, Patterns, and Diversity" *Chem. Res. Toxicol.* **1997**, *10* (2), 111–146, doi: 10.1021/tx9601418.

[136] M. T. Hess, D. Gunz, N. Luneva, N. E. Geacintov, H. Naegeli, "Base pair conformation-dependent excision of benzo[a]pyrene diol epoxide-guanine adducts by human nucleotide excision repair enzymes" *Mol. Cell. Biol.* **1997**, *17* (12), 7069–76, doi: 10.1128/mcb.17.12.7069.

[137] M. F. Denissenko, A. Pao, M.-s. Tang, G. P. Pfeifer, "Preferential Formation of Benzo[a]pyrene Adducts at Lung Cancer Mutational Hotspots in P53" *Science* **1996**, *274* (5286), 430–432, doi: 10.1126/science.274.5286.430.

[138] S. Surget, M. P. Khoury, J. C. Bourdon, "Uncovering the role of p53 splice variants in human malignancy: a clinical perspective" *Onco Targets Ther.* **2013**, *7*, 57–68, doi: 10.2147/ott.S53876.

[139] M. S. Greenblatt, W. P. Bennett, M. Hollstein, C. C. Harris, "Mutations in the p53 Tumor Suppressor Gene: Clues to Cancer Etiology and Molecular Pathogenesis1" *Cancer Res.* **1994**, *54* (18), 4855–4878.

[140] K. A. I. Setälä, P. E. R. Ekwall, "Penetration of Benzpyrene through the Intact Skin of New-Born Mice" *Nature* **1950**, *166* (4213), 188–189, doi: 10.1038/166188b0.

[141] R. C. Wester, H. I. Maibach, D. A. Bucks, L. Sedik, J. Melendres, C. Liao, S. DiZio, "Percutaneous absorption of [14C] DDT and [14C] benzo[a]pyrene from soil" *Toxicol. Sci.* **1990**, *15* (3), 510–516, doi: 10.1093/toxsci/15.3.510.

[142] T. A. Roy, R. Singh, "Effect of Soil Loading and Soil Sequestration on Dermal Bioavailability of Polynuclear Aromatic Hydrocarbons" *Bull. Environ. Contam. Toxicol.* **2001**, *67* (3), 0324–0331, doi: 10.1007/s001280128.

[143] R. P. Moody, J. Joncas, M. Richardson, I. Chu, "Contaminated soils (I): In vitro dermal absorption of benzo[a]pyrene in human skin" *J. Toxicol. Environ. Health A* **2007**, *70* (21), 1858–1865, doi: 10.1080/15287390701459296.

[144] E. W. Spalt, J. C. Kissel, J. H. Shirai, A. L. Bunge, "Dermal absorption of environmental contaminants from soil and sediment: a critical review" *J. Expo. Sci. Environ. Epidemiol.* **2009**, *19* (2), 119–148, doi: 10.1038/jes.2008.57.

[145] R. P. Moody, A. V. Tytchino, A. Yip, S. Petrovic, "A Novel "By Difference" Method for Assessing Dermal Absorption of Polycyclic Aromatic Hydrocarbons from Soil at Federal Contaminated Sites" *J. Toxicol. Environ. Health A* **2011**, *74* (19), 1294–1303, doi: 10.1080/15287394.2011.589104.

[146] D. J. Beriro, M. R. Cave, J. Wragg, R. Thomas, G. Wills, F. Evans, "A review of the current state of the art of physiologically-based tests for measuring human dermal in vitro bioavailability of polycyclic aromatic hydrocarbons (PAH) in soil" *J. Hazard. Mater.* **2016**, *305*, 240–259, doi: 10.1016/j.jhazmat.2015.11.010.

[147] P. Sartorelli, A. Cenni, G. Matteucci, L. Montomoli, M. Novelli, S. Palmi, "Dermal exposure assessment of polycyclic aromatic hydrocarbons: in vitro percutaneous penetration from lubricating oil" *Int. Arch. Occup. Environ. Health* **1999**, *72* (8), 528–532, doi: 10.1007/s004200050411.

[148] D. Potter, E. D. Booth, H. C. Brandt, R. W. Loose, R. A. Priston, A. S. Wright, W. P. Watson, "Studies on the dermal and systemic bioavailability of polycyclic aromatic compounds in high viscosity oil products" *Arch. Toxicol.* **1999**, *73* (3), 129–140, doi: 10.1007/s002040050597.

[149] P. Sartorelli, L. Montomoli, A. G. Sisinni, R. Bussani, D. Cavallo, V. Foá, "Dermal exposure assessment of polycyclic aromatic hydrocarbons: in vitro percutaneous penetration from coal dust" *Toxicol. Ind. Health* **2001**, *17* (1), 17–21, doi: 10.1191/0748233701th092oa.

[150] T. A. Roy, A. J. Kriech, C. R. Mackerer, "Percutaneous Absorption of Polycyclic Aromatic Compounds from Bitumen Fume Condensate" *J. Occup. Environ. Hyg.* **2007**, *4* (sup1), 137–143, doi: 10.1080/15459620701334814.

[151] P. Boffetta, N. Jourenkova, P. Gustavsson, "Cancer risk from occupational and environmental exposure to polycyclic aromatic hydrocarbons" *Cancer Causes Control* **1997**, *8* (3), 444–472, doi: 10.1023/A:1018465507029.

[152] European Commission (EC), "Regulation No. 1272/2013 Annex XVII to Regulation (EC) No. 1907/ 2006 (REACH)" **2013**.

[153] M. Paschke, C. Hutzler, J. Brinkmann, F. Henkler, A. Luch, "Polycyclic aromatic hydrocarbons in newspaper inks: migration, metabolism, and genotoxicity in human skin" *Polycycl. Aromat. Comp.* **2015**, *35* (1), 32–40, doi: 10.1080/10406638.2014.900643.

[154] A. Diekmann, U. Giese, I. Schaumann, "Polycyclic aromatic hydrocarbons in consumer goods made from recycled rubber material: A review" *Chemosphere* **2019**, *220*, 1163–1178, doi: 10.1016/j.chemosphere.2018.12.111.

[155] S. Hamm, T. Frey, R. Weinand, G. Moninot, N. Petiniot, "Investigations on the extraction and migration behavior of polycyclic aromatic hydrocarbons (PAHs) from cured rubber formulations containing carbon black as reinforcing agent" *Rubber Chem. Technol.* **2009**, *82* (2), 214–228, doi: 10.5254/1.3548246.

[156] M. Brandt, D. Einhenkel-Arle, "Polycyclic Aromatic Hydrocarbons Harmful to the Environment! Toxic! Inevitable?" German Environment Agency (UBA), Dessau-Roßlau, **2016**.

[157] L. M. Milstone, "Epidermal desquamation" *J. Dermatol. Sci.* **2004**, *36* (3), 131–140, doi: 10.1016/j.jdermsci.2004.05.004.

[158] K. Simon, N. Bartsch, L. Schneider, V. van de Weijgert, C. Hutzler, A. Luch, A. Roloff, "Polycyclic aromatic hydrocarbon skin permeation efficiency in vitro is lower through human than pigskin and decreases with lipophilicity" *Environ. Res.* **2024**, *255*, 119118, doi: 10.1016/j.envres.2024.119118.

[159] K. Simon, L. Schneider, G. Oberender, R. Pirow, C. Hutzler, A. Luch, A. Roloff, "Migration of polycyclic aromatic hydrocarbons from a polymer surrogate through the stratum corneum layer of the skin" *Ecotoxicol. Environ. Saf.* **2023**, *262*, 115113, doi: 10.1016/j.ecoenv.2023.115113.

[160] National Center for Biotechnology Information, "PubChem Compound Summary for CID 6342, Acetonitrile" **2023**, https://pubchem.ncbi.nlm.nih.gov/compound/Acetonitrile (accessed 11 Aug. 2023).

[161] Y. S. Soebianto, Y. Katsumura, K. Ishigure, J. Kubo, T. Koizumi, H. Shigekuni, K. Azami, "Model experiment on the protection effect in polymers: radiolysis of liquid squalane in the presence and absence of additives" *Polym. Degrad. Stab.* **1993**, *42* (1), 29–40, doi: 10.1016/0141-3910(93)90022-B.

[162] U. Ritgen, "Analytische Chemie I" *1*, Springer Spektrum, Berlin, Heidelberg, **2019**, ISBN: 978-3-662-60495-3, doi: 10.1007/978-3-662-60495-3.

[163] A. Sánchez-Guijo, M. F. Hartmann, S. A. Wudy, "Introduction to Gas Chromatography-Mass Spectrometry" in "Hormone Assays in Biological Fluids" (Ed.: M. J. Wheeler), Humana Press, Totowa, New Jersey, **2013**, 27–44, ISBN: 978-1-62703-616-0, doi: 10.1007/978-1-62703-616-0_3.

[164] J. H. Gross, "Mass Spectrometry: A Textbook" *3*, Springer Cham, **2017**, 539–612, ISBN: 978-3-319-54398-7, doi: 10.1007/978-3-319-54398-7.

[165] Advanced Chemistry Development (ACD/Labs), "Octanol-Water Partition Calculation" **2021**, http://www.chemspider.com/Chemical-Structure.7798.html?rid=a22a50c7-1c8c-446d-949a-5abd6fe95e4e (accessed 20 Sept. 2021).

[166] J. Barret, P. Gijsman, J. Swagten, R. F. Lange, "A molecular study towards the interaction of phenolic anti-oxidants, aromatic amines and HALS stabilizers in a thermo-oxidative ageing process" *Polym. Degrad. Stab.* **2002**, *76* (3), 441–448, doi: 10.1016/S0141-3910(02)00047-2.

[167] S. Beißmann, M. Reisinger, K. Grabmayer, G. Wallner, D. Nitsche, W. Buchberger, "Analytical evaluation of the performance of stabilization systems for polyolefinic materials. Part I: Interactions between hindered amine light stabilizers and phenolic antioxidants" *Polym. Degrad. Stab.* **2014**, *110*, 498–508, doi: 10.1016/j.polymdegradstab.2014.09.020.

[168] R. L. Bronaugh, R. F. Stewart, "Methods for in vitro percutaneous absorption studies III: hydrophobic compounds" *J. Pharm. Sci.* **1984**, *73* (9), 1255–1258, doi: 10.1002/jps.2600730916.

[169] A. Fick, "Ueber diffusion" *Ann. Phys.* **1855**, *170* (1), 59–86.

[170] C. Herkenne, A. Naik, Y. N. Kalia, J. Hadgraft, R. H. Guy, "Ibuprofen transport into and through skin from topical formulations: in vitro–in vivo comparison" *J. Invest. Dermatol.* **2007**, *127* (1), 135–142, doi: 10.1038/sj.jid.5700491.

[171] Organisation for Economic Co-operation and Development (OECD), "OECD Environment Directorate: Health and Safety Publications Series on Testing and Assessment No. 156: Guidance Notes on Dermal Absorbtion." **2011**.

[172] R. O. Potts, R. H. Guy, "Predicting skin permeability" *Pharm. Res.* **1992**, *9* (5), 663–669, doi: 10.1023/A:1015810312465.

[173] J. Caussin, G. S. Gooris, M. Janssens, J. A. Bouwstra, "Lipid organization in human and porcine stratum corneum differs widely, while lipid mixtures with porcine ceramides model human stratum corneum lipid organization very closely" *Biochim. Biophys. Acta* **2008**, *1778* (6), 1472–1482, doi: 10.1016/j.bbamem.2008.03.003.

[174] C. Jacques-Jamin, H. Duplan, H. Rothe, O. Vaillant, J. Eilstein, S. Grégoire, R. Cubberley, D. Lange, C. Ellison, M. Klaric, N. Hewitt, A. Schepky, "Comparison of the Skin Penetration of 3 Metabolically Stable Chemicals Using Fresh and Frozen Human Skin" *Skin Pharmacol. Physiol.* **2017**, *30* (5), 234–245, doi: 10.1159/000475472.

[175] M. Morin, A. Runnsjö, T. Ruzgas, J. Engblom, S. Björklund, "Effects of storage conditions on permeability and electrical impedance properties of the skin barrier" *Int. J. Pharm.* **2023**, *637*, 122891, doi: 10.1016/j.ijpharm.2023.122891.

[176] A. C. Sintov, I. Greenberg, "Comparative percutaneous permeation study using caffeine-loaded microemulsion showing low reliability of the frozen/thawed skin models" *Int. J. Pharm.* **2014**, *471* (1), 516–524, doi: 10.1016/j.ijpharm.2014.05.040.

[177] D. Kim, M. W. Farthing, C. T. Miller, L. A. Nylander-French, "Mathematical description of the uptake of hydrocarbons in jet fuel into the stratum corneum of human volunteers" *Toxicol. Lett.* **2008**, *178* (3), 146–151, doi: 10.1016/j.toxlet.2008.03.005.

[178] K. Takahashi, T. Suzuki, H. Sakano, N. Mizuno, "Effect of vehicles on diclofenac permeation across excised rat skin" *Biol. Pharm. Bull.* **1995**, *18* (4), 571–575, doi: 10.1248/bpb.18.571.

[179] G. W. Litman, J. P. Cannon, L. J. Dishaw, "Reconstructing immune phylogeny: new perspectives" *Nat. Rev. Immunol.* **2005**, *5* (11), 866–879, doi: 10.1038/nri1712.

[180] T. Biedermann, "Grundprinzipien von Allergie- und Intoleranzreaktionen" in "Braun-Falco's Dermatologie, Venerologie und Allergologie" (Eds.: G. Plewig, T. Ruzicka, R. Kaufmann, M. Hertl), Springer, Berlin, Heidelberg, **2018**, 441–452, ISBN: 978-3-662-49544-5, doi: 10.1007/978-3-662-49544-5_25.

[181] F. Riedel, "Contact allergen-specific T cell responses and the involved T cell receptor repertoires" Doctoral Thesis, Freie Universität, Berlin, **2022**.

[182] T. H. McConnell, "The Nature of Disease: Pathology for the Health Professions" *2*, Jones and Bartlett Learning, Burlington, Massachusetts, **2013**, ISBN: 978-1609133696.

[183] J. P. Thyssen, T. Menné, "Metal Allergy-A Review on Exposures, Penetration, Genetics, Prevalence, and Clinical Implications" *Chem. Res. Toxicol.* **2010**, *23* (2), 309–318, doi: 10.1021/tx9002726.

[184] F. O. Nestle, H. Speidel, M. O. Speidel, "High nickel release from 1- and 2-euro coins" *Nature* **2002**, *419* (6903), 132–132, doi: 10.1038/419132a.

[185] L. A. J. O'Neill, A. G. Bowie, "The family of five: TIR-domain-containing adaptors in Toll-like receptor signalling" *Nat. Rev. Immunol.* **2007**, *7* (5), 353–364, doi: 10.1038/nri2079.

[186] S. Akira, S. Uematsu, O. Takeuchi, "Pathogen Recognition and Innate Immunity" *Cell* **2006**, *124* (4), 783–801, doi: 10.1016/j.cell.2006.02.015.

[187] M. Schmidt, B. Raghavan, V. Müller, T. Vogl, G. Fejer, S. Tchaptchet, S. Keck, C. Kalis, P. J. Nielsen, C. Galanos, J. Roth, A. Skerra, S. F. Martin, M. A. Freudenberg, M. Goebeler, "Crucial role for human Toll-like receptor 4 in the development of contact allergy to nickel" *Nat. Immunol.* **2010**, *11* (9), 814–819, doi: 10.1038/ni.1919.

[188] M. Saito, R. Arakaki, A. Yamada, T. Tsunematsu, Y. Kudo, N. Ishimaru, "Molecular Mechanisms of Nickel Allergy" *Int. J. Mol. Sci.* **2016**, *17* (2), 202, doi: 10.3390/ijms17020202.

[189] D. H. Kaplan, B. Z. Igyártó, A. A. Gaspari, "Early immune events in the induction of allergic contact dermatitis" *Nat. Rev. Immunol.* **2012**, *12* (2), 114–124, doi: 10.1038/nri3150.

[190] D. Rachmawati, H. J. Bontkes, M. I. Verstege, J. Muris, B. M. E. von Blomberg, R. J. Scheper, I. M. W. van Hoogstraten, "Transition metal sensing by Toll-like receptor-4: next to nickel, cobalt and palladium are potent human dendritic cell stimulators" *Contact Dermatitis* **2013**, *68* (6), 331–338, doi: 10.1111/cod.12042.

[191] M. Vocanson, A. Hennino, A. Rozières, G. Poyet, J.-F. Nicolas, "Effector and regulatory mechanisms in allergic contact dermatitis" *Allergy* **2009**, *64* (12), 1699–1714, doi: 10.1111/j.1398-9995.2009.02082.x.

[192] J. Brasch, D. Becker, W. Aberer, A. Bircher, B. Kranke, K. Jung, B. Przybilla, T. Biedermann, T. Werfel, S. M. John, P. Elsner, T. Diepgen, A. Trautmann, H. F. Merk, T. Fuchs, A. Schnuch, "Guideline contact dermatitis: S1-Guidelines of the German Contact Allergy Group (DKG) of the German Dermatology Society (DDG), the Information Network of Dermatological Clinics (IVDK), the German Society for Allergology and Clinical Immunology (DGAKI), the Working Group for Occupational and Environmental Dermatology (ABD) of the DDG, the Medical Association of German Allergologists (AeDA), the Professional Association of German Dermatologists (BVDD) and the DDG" *Allergo J. Int.* **2014**, *23* (4), 126–138, doi: 10.1007/s40629-014-0013-5.

[193] J. D. Johansen, K. Aalto-Korte, T. Agner, K. E. Andersen, A. Bircher, M. Bruze, A. Cannavó, A. Giménez-Arnau, M. Gonçalo, A. Goossens, S. M. John, C. Lidén, M. Lindberg, V. Mahler, M. Matura, T. Rustemeyer, J. Serup, R. Spiewak, J. P. Thyssen, M. Vigan, I. R. White, M. Wilkinson, W. Uter, "European Society of Contact Dermatitis guideline for diagnostic patch testing – recommendations on best practice" *Contact Dermatitis* **2015**, *73* (4), 195–221, doi: 10.1111/cod.12432.

[194] R. Gollhausen, B. Przybilla, J. Ring, "Reproducibility of patch tests" *J. Am. Acad. Dermatol.* **1989**, *21* (6), 1196–202, doi: 10.1016/s0190-9622(89)70329-7.

[195] J. Brasch, T. Henseler, W. Aberer, G. Bauerle, P. J. Frosch, T. Fuchs, V. Funfstuck, G. Kaiser, G. G. Lischka, B. Pilz, et al., "Reproducibility of patch tests. A multicenter study of synchronous left-versus right-sided patch tests by the German Contact Dermatitis Research Group" *J. Am. Acad. Dermatol.* **1994**, *31* (4), 584–91, doi: 10.1016/s0190-9622(94)70220-9.

[196] J. F. Bourke, K. Batta, L. Prais, A. Abdullah, I. S. Foulds, "The reproducibility of patch tests" *Br. J. Dermatol.* **1999**, *140* (1), 102–5, doi: 10.1046/j.1365-2133.1999.02615.x.

[197] S. I. Ale, H. I. Maibach, "Reproducibility of patch test results: a concurrent right-versus-left study using TRUE Test" *Contact Dermatitis* **2004**, *50* (5), 304–12, doi: 10.1111/j.0105-1873.2004.00351.x.

[198] A. C. de Groot, "New Contact Allergens: 2008 to 2015" *Dermatitis* **2015**, *26* (5), 199–215, doi: 10.1097/der.0000000000000144.

[199] A. C. Schaeffer, K. E. Andersen, C. Bindslev-Jensen, C. G. Mortz, "The reproducibility of nickel, cobalt and chromate sensitization in patients tested at least twice in the period 1992-2014 with TRUE Test(R)" *Contact Dermatitis* **2016**, *75* (2), 111–3, doi: 10.1111/cod.12563.

[200] J. Muris, C. J. Kleverlaan, A. J. Feilzer, T. Rustemeyer, "Sodium tetrachloropalladate as an improved test salt for palladium allergy patch testing" *Contact Dermatitis* **2008**, *58* (1), 42–46, doi: 10.1111/j.1600-0536.2007.01259.x.

[201] J. Muris, A. Goossens, M. Gonçalo, A. J. Bircher, A. Giménez-Arnau, C. Foti, T. Rustemeyer, A. J. Feilzer, C. J. Kleverlaan, "Sensitization to palladium and nickel in Europe and the relationship with oral disease and dental alloys" *Contact Dermatitis* **2015**, *72* (5), 286–296, doi: 10.1111/cod.12327.

[202] A. Faurschou, T. Menné, J. D. Johansen, J. P. Thyssen, "Metal allergen of the 21st century—a review on exposure, epidemiology and clinical manifestations of palladium allergy" *Contact Dermatitis* **2011**, *64* (4), 185–195, doi: 10.1111/j.1600-0536.2011.01878.x.

[203] A. Franken, F. C. Eloff, J. D. Plessis, J. L. D. Plessis, "In Vitro Permeation of Metals through Human Skin: A Review and Recommendations" *Chem. Res. Toxicol.* **2015**, *28* (12), 2237–2249, doi: 10.1021/acs.chemrestox.5b00421.

[204] K. Simon, P. Reichardt, A. Luch, A. Roloff, K. Siewert, F. Riedel, "Less efficient skin penetration of the metal allergen Pd2+ compared to Ni2+ and Co2+ from patch test preparations" *Contact Dermatitis* **2024**, *91* (1), 11–21, doi: 10.1111/cod.14569.

[205] R. Shannon, "Revised effective ionic radii and systematic studies of interatomic distances in halides and chalcogenides" *Acta Crystallogr. Sect. A: Found. Crystallogr.* **1976**, *32* (5), 751–767, doi: 10.1107/S0567739476001551.

[206] B. Baranowska-Dutkiewicz, "Evaluation of the skin uptake of mercuric chloride in man" *J. Appl. Toxicol.* **1982**, *2* (5), 223–225, doi: 10.1002/jat.2550020502.

[207] H. E. Boddé, M. A. M. Kruithof, J. Brussee, H. K. Koerten, "Visualisation of normal and enhanced HgCl2 transport through human skin in vitro" *Int. J. Pharm.* **1989**, *53* (1), 13–24, doi: 10.1016/0378-5173(89)90356-6.

[208] H. E. Boddé, I. van den Brink, H. K. Koerten, F. H. N. de Haan, "Visualization of in vitro percutaneous penetration of mercuric chloride; transport through intercellular space versus cellular uptake through desmosomes" *J. Control. Release* **1991**, *15* (3), 227–236, doi: 10.1016/0168-3659(91)90114-S.

[209] C. W. Eisele, L. Eichelberger, "Water, Electrolyte and Nitrogen Content of Human Skin" *Proc. Soc. Exp. Biol. Med.* **1945**, *58* (1), 97–100, doi: 10.3181/00379727-58-14856.

[210] E. Proksch, "pH in nature, humans and skin" *J. Dermatol.* **2018**, *45* (9), 1044–1052, doi: 10.1111/1346-8138.14489.

[211] H. Öhman, A. Vahlquist, "In vivo studies concerning a pH gradient in human stratum corneum and upper epidermis" *Acta Derm. Venereol.* **1994**, *74* (5), 375–379, doi: 10.2340/0001555574375379.

[212] T. Höper, K. Siewert, V. I. Dumit, M. von Bergen, K. Schubert, A. Haase, "The Contact Allergen NiSO4 Triggers a Distinct Molecular Response in Primary Human Dendritic Cells Compared to Bacterial LPS" *Front. Immunol.* **2021**, *12*, 644700, doi: 10.3389/fimmu.2021.644700.

[213] A. Cavani, D. Mei, S. Corinti, G. Girolomoni, E. Guerra, M. Giani, L. Pirrotta, P. Puddu, "Patients with Allergic Contact Dermatitis to Nickel and Nonallergic Individuals Display Different Nickel-Specific T Cell Responses. Evidence for the Presence of Effector CD8+ and Regulatory CD4+ T Cells" *J. Invest. Dermatol.* **1998**, *111* (4), 621–628, doi: 10.1046/j.1523-1747.1998.00334.x.

A Publications

A.1 Continuous removal of single cell layers by tape stripping the *stratum corneum* — a histological study

Konstantin Simon, Gila Oberender, Alexander Roloff

European Journal of Pharmaceutics and Biopharmaceutics **2023**, *188*, 48–53.

doi: 10.1016/j.ejpb.2023.04.022

This study was submitted to the journal on 12 February 2023, revised on 7 April 2023 and was accepted on 26 April 2023. Published online on 4 May 2023.

The contents of this publication are discussed in Chapter 2, Section *Tape stripping: studying individual layers of the startum corneum.* The supporting information is added following the main part.

Author contributions: **Konstantin Simon** developed the project, wrote the main parts of the manuscript, carried out experimental work and analyzed the data. Gila Oberender carried out experimental work and analyzed the data during an internship. Alexander Roloff contributed to the writing of the manuscript and analyzed the data.

Abstract

Studies on the penetration of toxicologically or pharmaceutically relevant substances through the skin and, more specifically, through the *stratum corneum* (s.c.) often rely on the well-established method of tape stripping. Tape stripping involves the removal of skin layers by means of adhesive tape, which is usually followed by quantification of dermally applied substances in these layers. However, the amount of s.c. removed by each individual tape strip is still a matter of scientific debate. While some studies imply that the amount of s.c. adhering to each tape strip decreases with

increasing depth into the s.c., others observed a constant removal rate. All these studies rely on the quantification of the amount of s.c. captured on individual or pooled tape strips. Here, we present an approach whereby we measured the amount of s.c. remaining on excised porcine skin in the process of tape stripping. Staining and bloating of the s.c. allowed to measure its thickness and to count individual s.c. layers, respectively. Histologically, we show that the s.c. remaining on the skin decreased linearly as a function of strips taken. We found that each tape strip removes about 0.4 µm of s.c., which corresponds to approximately one cellular layer. With a high coefficient of determination ($r^2 > 0.95$), we were able to linearly correlate the thickness of the remaining s.c., the number of remaining cell layers and the number of tape strips applied. Furthermore, we elaborate on possible reasons for the discrepancies reported in the scientific literature regarding the amount of s.c. removed by each tape strip.

Graphical Abstract

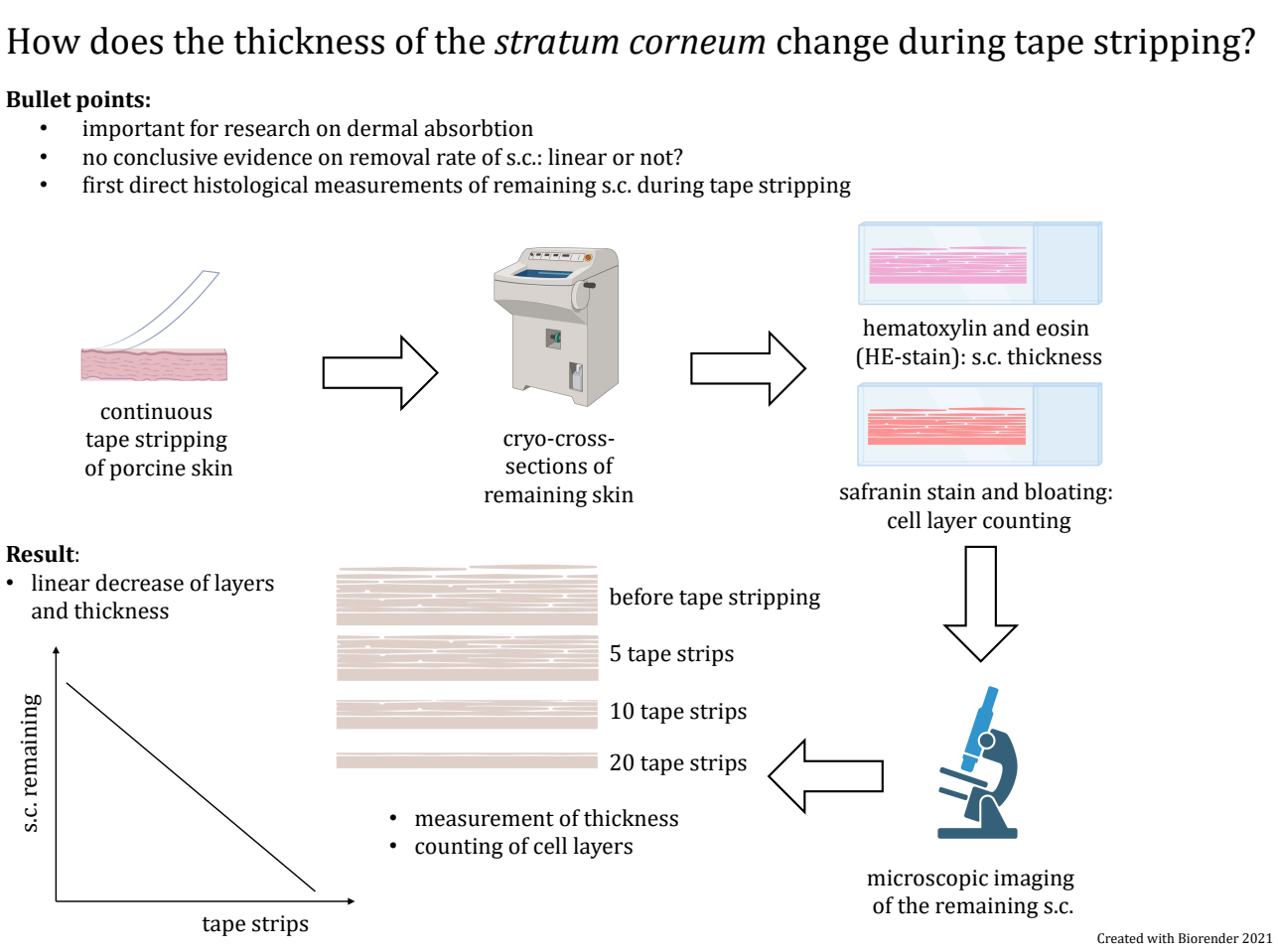

European Journal of Pharmaceutics and Biopharmaceutics 188 (2023) 48–53

Contents lists available at ScienceDirect

European Journal of Pharmaceutics and Biopharmaceutics

journal homepage: www.elsevier.com/locate/ejpb

Research paper

Continuous removal of single cell layers by tape stripping the *stratum corneum* – a histological study

Konstantin Simon [a,b,*], Gila Oberender [a,c], Alexander Roloff [a,*]

[a] German Federal Institute for Risk Assessment (BfR), Department of Chemical and Product Safety, Max-Dohrn-Str. 8-10, 10589 Berlin, Germany
[b] Institute of Pharmacy, Department of Biology, Chemistry, Pharmacy, Freie Universität Berlin, Königin-Luise-Str. 28-30, 14195 Berlin, Germany
[c] Berliner Hochschule für Technik (BHT), Luxemburger Str. 10, 13353 Berlin, Germany

ARTICLE INFO

Keywords:
Removal rate
Stratum corneum thickness
Stratum corneum layers
HE stain
Safranin stain
Skin
Histology
Tape stripping

ABSTRACT

Studies on the penetration of toxicologically or pharmaceutically relevant substances through the skin and, more specifically, through the *stratum corneum* (s.c.) often rely on the well-established method of tape stripping. Tape stripping involves the removal of skin layers by means of adhesive tape, which is usually followed by quantification of dermally applied substances in these layers. However, the amount of s.c. removed by each individual tape strip is still a matter of scientific debate. While some studies imply that the amount of s.c. adhering to each tape strip decreases with increasing depth into the s.c., others observed a constant removal rate. All these studies rely on the quantification of the amount of s.c. captured on individual or pooled tape strips. Here, we present an approach whereby we measured the amount of s.c. remaining on excised porcine skin in the process of tape stripping. Staining and bloating of the s.c. allowed to measure its thickness and to count individual s.c. layers, respectively. Histologically, we show that the s.c. remaining on the skin decreased linearly as a function of strips taken. We found that each tape strip removes about 0.4 μm of s.c., which corresponds to approximately one cellular layer. With a high coefficient of determination ($r^2 > 0.95$), we were able to linearly correlate the thickness of the remaining s.c., the number of remaining cell layers and the number of tape strips applied. Furthermore, we elaborate on possible reasons for the discrepancies reported in the scientific literature regarding the amount of s.c. removed by each tape strip.

1. Introduction

Tape stripping is a frequently used method in skin penetration research, by which the *stratum corneum* (s.c.) is successively removed by means of stripping the skin surface with adhesive tape. Earliest descriptions date back to 1939 [1]. Studies in the past have utilized tape stripping to determine the amount and corresponding concentration profiles of dermally applied substances in the s.c. [2–4], or to investigate how the barrier function of the s.c. decreases with fewer cell layers [5]. Compared to skin biopsies, it represents a method that is less invasive but still applicable in the context of *in vivo* studies [6].

Concentration profiles of substances in the s.c. crucially rely on the removal rate of the s.c. layers, that is, how much of the s.c. is taken off by each tape strip. To determine the removal rate, various methods have been applied previously, including microscopy [7], measurement of the transepidermal water loss (TEWL) [8–9], weighing [10–11], UV/vis-spectrometric characterization of the removed tape strip [12–13], infrared densitometry [14] and measuring the protein content on the removed tape strip [15–17]. Importantly, all these studies rely on the measurement of quantities retrieved from the removed cell layers. Different studies have come to opposing conclusions: While some infer that the amount of s.c. taken off by each tape strip remains constant with successive strips, others show that it decreases with increasing depth.

Colorimetric protein assays, for example, have demonstrated a uniform removal of s.c. layers [15–16]. Comparable results were obtained when the amount of s.c. removed on each tape strip was investigated via laser scanning microscopy [7]. However, several studies that focus on measuring the *pseudo*-absorption (a protologism for non-transmitted light, that is, the total of absorption, scattering, reflection and diffraction) report that the amount of s.c. removed with a tape strip decreases in deeper layers [12–13,17]. Similarly, the mass and the protein content of s.c. removed by each tape strip were found to decrease with increasing

* Corresponding authors at: German Federal Institute for Risk Assessment (BfR), Department of Chemical and Product Safety, Max-Dohrn-Str. 8-10, 10589 Berlin, Germany.
E-mail addresses: Konstantin.Simon@bfr.bund.de (K. Simon), Alexander.Roloff@bfr.bund.de (A. Roloff).

https://doi.org/10.1016/j.ejpb.2023.04.022
Received 12 February 2023; Received in revised form 7 April 2023; Accepted 26 April 2023
Available online 4 May 2023

numbers of tape strips, thereby confirming these findings [9].

On the other hand, variable results were reported when investigating the thickness of the s.c. after tape stripping of freshly excised and frozen human skin [14]. The fresh skin showed a linear decrease of the s.c. thickness with the number of tape strips whereas for the frozen skin of the same donor the decrease was not linear. For a different donor, the results were reversed. However, it was argued that the plateauing observed after a given number of applied tape strips is due to the complete removal of the s.c.

In this study, we contribute to the ongoing investigation on the removal rate of s.c. layers by tape stripping excised porcine skin. Porcine skin has been investigated as a substitute for human skin in various skin penetration studies [2–4,18–20]. It does not significantly differ from human skin in relevant permeation characteristics, including lag time, diffusion behavior of substances in the s.c. [4,18–19] and thickness of the s.c. [4,21–22], suggesting that results obtained with respect to these properties are transferrable to human skin. Porcine skin is therefore recommended by the Scientific Committee on Consumer Safety (SCCS) to be used in skin penetration studies [23]. In contrast to the aforementioned studies, which examined the amount of s.c. captured on each tape strip, we inspected the s.c. that is left behind on the skin. Cryosections of the s.c. at successive points in the tape stripping process were taken and the thickness of the remaining skin was directly measured microscopically after histological staining. Furthermore, the number of cell layers remaining were counted and the results were correlated.

2. Methods

2.1. Porcine skin

The pigskin used in this study was provided by the Charité, Universitätsmedizin Berlin. The skin was taken from the flank of female pigs, which was demonstrated to be comparable to frequently used skin from pig ears [24]. The pigs were sacrificed shortly before the skin was removed in an unrelated surgical experiment that did not influence the integrity of the skin. The excised skin was transported to our institute on ice, sheared, cut into pieces of approximately 10 × 20 cm with a scalpel, and frozen and stored at −20 °C until further use for a maximum of 12 months.

2.2. Preparation and quality control of skin samples

In preparation for tape stripping experiments, the frozen skin pieces were partially thawed and a skin sheet of 500 μm thickness was cut off using a dermatome (Aesculap AG, Tuttlingen, Germany). Sections of 25 mm diameter were punched out of the skin sheets with a stencil. Their integrity was verified visually and by measuring the TEWL. For TEWL measurements, the sections were laid atop the receptor chamber of a Franz diffusion cell (PermeGear, Hellertown, Pennsylvania, United States) filled with Dulbecco's phosphate-buffered saline (DPBS, pH 7.4, PAN Biotech, Aidenbach, Germany) containing 50 $mg{\cdot}ml^{-1}$ bovine serum albumin (BSA, Biomol, Hamburg, Germany). It was ensured that no air bubbles were present directly under the skin specimen in the receptor solution. The TEWL was measured using the AquaFlux device AF200 (Biox systems Ltd, London, United Kingdom), in accordance with OECD Guideline 428 [25]. Skin punches were excluded and replaced if the TEWL exceeded 10 $g{\cdot}m^{-2}{\cdot}h^{-1}$ [26]. The skin pieces were removed from their respective Franz diffusion cell and dried with a clean precision wipe (Kimtech Science, Kimberly-Clark, Irving, Texas, United States).

2.3. Tape stripping

The samples were cut in four sections with a scalpel and then stripped with tape strips (kristall-klar, tesafilm, tesa, Norderstedt, Germany) up to 20 times, increasing the number of tape strips by two between each sample. The tape consisted of biaxially oriented polypropylene with water-based acrylate as an adhesive [27] and has been used in previous studies for the same purpose [2–3,28]. We were able to confirm the polypropylene polymer by online-coupled pyrolysis–gas chromatography–mass spectrometry (see the Supporting Information, Figure S1). The stripping protocol was as follows: The tape strip was laid atop the skin, ensuring that the contact between the skin and the strip was complete. The tape strip was pressed onto the skin with the backside of curved tweezers by stroking the strip two times in each perpendicular direction, taking care to apply constant pressure (this procedure was carried out by the same person throughout the study). Then, the strip was removed in a single swift movement. Six replicate skin samples were used to obtain data for each investigated number of applied tape strips.

2.4. Sample preparation for histology

The skin sections were frozen in optimal cutting temperature compound (Tissue-Tek O.C.T., Sakura, Staufen, Germany) using liquid nitrogen (Linde, Pullach, Germany). Of each frozen skin section, multiple cross sections of 5 μm thickness were cut using a cryo-microtome (HM 550 OP, Thermo Fisher Scientific, Waltham, Massachusetts, United States) and laid onto microscopy slides (Epredia SuperFrost Plus, Thermo Fisher Scientific). The slides were then submerged in acetone (Sigma-Aldrich, Darmstadt, Germany) at −20 °C for 20 min to remove the optimal cutting temperature compound.

2.5. HE-Stain

For staining with hematoxylin and eosin (HE-stain), half of the slides were placed into freshly filtered (folded filters 3 hw, Ahlstrom Munksjö, Helsinki, Finland) Mayer's acidic hematoxylin solution (Carl Roth, Karlsruhe, Germany) at room temperature for 20 min. The slides were rinsed with desalinated water and then transferred into Scott's tap water substitute (23.8 mM sodium hydrogen carbonate (Sigma-Aldrich, Saint-Louis, Missouri, United States) and 166 mM magnesium sulfate heptahydrate (Carl Roth) in desalinated water, pH 8.3) for 12 min. The slides were rinsed with desalinated water and then placed into a freshly filtered (folded filters 3 hw, Ahlstrom Munksjö) 1% aqueous Eosin Y solution (Carl Roth) for 3 min. The slides were rinsed again with desalinated water and then fixed with a coverslip using FluorSave reagent (Millipore Corporation, Billerica, Massachusetts, United States). These slides were used to measure the s.c. thickness by optical microscopy (see section *Optical microscopy*).

2.6. Safranin stain

For safranin staining, the other half of the slides were treated according to an adapted protocol [29]. The slides were placed into a 1% aqueous solution of safranin (Carl Roth) for 1 min. The slides were then taken out of the solution, rinsed off with desalinated water and treated with a drop of a 2% solution of potassium hydroxide (AppliChem, Darmstadt, Germany) in desalinated water applied directly onto the skin cross sections in order to bloat the skin cells for better visualization of individual cell layers. After 20 s, a cover slip was gently pressed onto the slides, which were then immediately examined under the microscope. These slides were used to count the s.c. layers remaining after tape stripping.

2.7. Optical microscopy

In optical microscopy, the skin sections obtained with both staining methods were subjected to 10, 20 and 40-fold magnification (fluorescence microscope BX51, Olympus, Shinjuku City, Tokyo, Japan) and photographs were taken (SC50, Olympus).

The measurement of the s.c. thickness was carried out with the HE-

stained slides using CellSens standard 3.1 software (Olympus). In order to count the cell layers, the safranin-stained slides were used. Each measurement was carried out at least five times per analyzed skin sample. The measurements were performed at different positions and with different cross-sections of the same sample.

The data were analyzed using the statistical programming language R (version 4.2.1). Means and standard deviations were calculated based on all individual measurements.

2.8. Control sample (compression test)

To ensure that the measured decrease in s.c. thickness is not due to compression during tape stripping, the stripping procedure was mimicked with six skin sections. A tape strip was laid atop each skin section and the strip was pressed on with tweezers as described above. Pressing was repeated twenty times without removing the tape strip in between. Finally, the tape strips were removed in a single swift movement. The samples were then prepared for optical microscopy as described above. The individual thickness values of untreated s.c. and the control specimen were compared with the Wilcoxon rank-sum test. This test was used because the data of the compression test were not normally distributed according to a Shapiro–Wilk test ($p = 0.369 > 0.05$). The hypothesis of the Wilcoxon rank-sum test was that the two values (total thickness of s.c. vs. thickness of s.c. after compression test) are not equal, the null hypothesis assumed that the two values cannot be distinguished.

3. Results

The amount of s.c. removed after every second tape strip was determined on cryo-sections of individual skin samples in two ways. First, the thickness of the remaining s.c. on the porcine skin specimen was measured by optical microscopy after HE-staining. Second, the number of remaining s.c. layers was counted after staining with safranin and bloating the cells with a potassium hydroxide solution to better distinguish individual cell layers during microscopy.

3.1. Stratum corneum thickness

For the thickness of intact s.c. before tape stripping, we determined a value of $\delta_{sc} = 11.0 \pm 2.0$ µm. After 20 tape strips, δ_{sc} was reduced to 3.23 ± 0.76 µm (Fig. 1 and Table 1). The values for the thickness of full s.c. are in good agreement with previous studies. For example, a thickness of 11.1 to 17.4 µm was measured for healthy human s.c. [4,21], whereas a value of 10.8 ± 2.3 µm was reported for porcine s.c. [4].

The control skin sample – mimicking the compression following 20 tape strips – had a thickness of 10.6 ± 1.5 µm, which is not statistically different from δ_{sc} when no tape stripping was applied (p-value = 0.304 > 0.05). Furthermore, since the tape strip used to mimic the compression had to be removed before microscopy, the skin samples had been stripped once, explaining the slightly lower value.

The s.c. thickness, δ_{sc}, can be correlated with the number of tape strips applied, n_{TS}, with a linear function (Fig. 3a, $r^2 = 0.975$) described by:

$$\delta_{sc} = -(0.38 \pm 0.02)\ \mu m \cdot n_{TS} + (10.83 \pm 0.23)\ \mu m. \quad (1)$$

Equation (1) can be interpreted as each tape strip reducing the s.c. thickness on the skin specimen by 0.38 ± 0.02 µm on average.

3.2. Stratum corneum layers

Intact porcine s.c. before tape stripping consisted of 27.06 ± 3.21 cellular layers, n_{sc}, on average. This number was reduced to 7.72 ± 2.59 layers after 20 tape strips (Fig. 2 and Table 1). A previous report found 21 ± 5 cell layers for full thickness s.c. of porcine ear skin [30]. In that study, an average of 13 ± 3 cell layers were removed by stripping the skin 20 times, compared to about 20 cell layers removed here.

A correlation of n_{sc} and n_{TS} was also derived. The resulting linear function (Fig. 3b, $r^2 = 0.968$) is described by:

$$n_{sc} = -(0.94 \pm 0.05) \cdot n_{TS} + (26.99 \pm 0.63). \quad (2)$$

Equation (2) can be interpreted as 0.94 ± 0.05 cell layers of the s.c. being removed with each tape strip on average.

As described above, we found that not all of the s.c. layers were removed after 20 tape strips. Equations (1) and (2), however, allow estimating from their respective x-axis intercepts how many tape strips would have been required to achieve this. The resulting values of 28.50 and 27.71 tape strips from Equations (1) and (2), respectively, are in excellent agreement with each other (deviation < 3 %). This validates both equations as they support the same conclusion although being derived from different data sets obtained with different and independent methods (measurement of thickness vs. bloating and counting).

When the two data sets (δ_{sc} and n_{sc}) were directly correlated, we found a linear relationship (Fig. 3c, $r^2 = 0.977$) described by:

$$\delta_{sc} = (0.40 \pm 0.02)\ \mu m \cdot n_{sc} + (0.05 \pm 0.36)\ \mu m. \quad (3)$$

Importantly, the slope of Equation (3) can be interpreted as the thickness of a single s.c. layer. Thus, each cell layer adds on average 0.40 ± 0.02 µm to the thickness of the s.c. The function almost perfectly intercepts the origin, further validating the equation as with no remaining

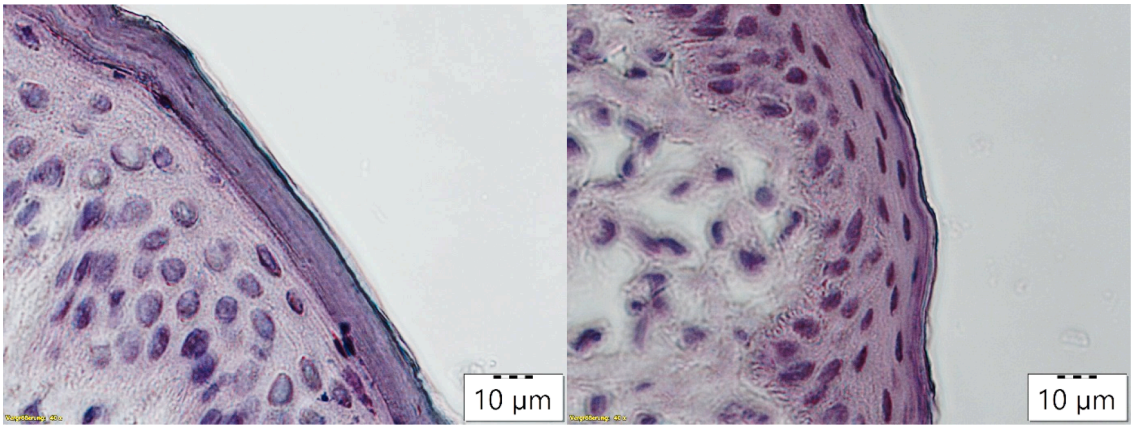

Fig. 1. Microscopy image of the upper most skin layers after hematoxylin-eosin (HE) stain at 40-fold magnification. Left: before tape stripping; right: after 20 tape strips taken off.

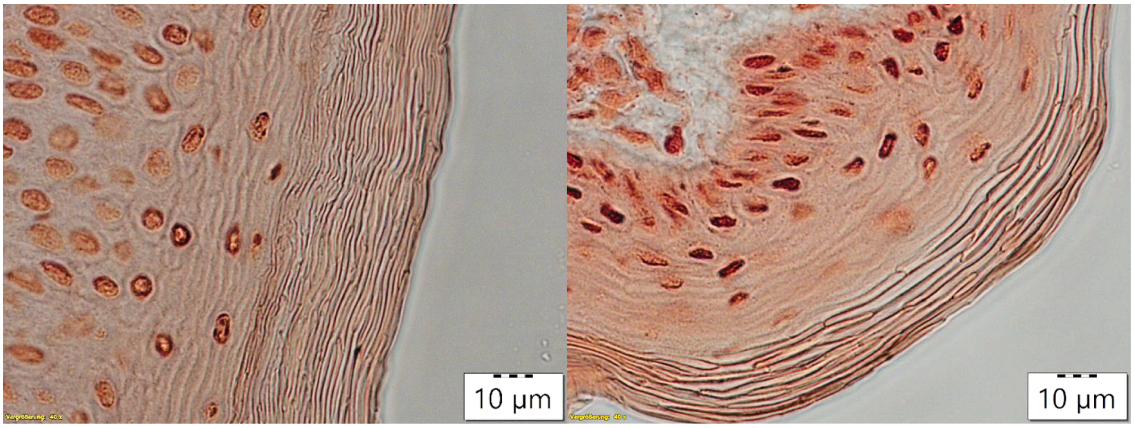

Fig. 2. Microscopy image of the upper most skin layers after safranin stain and bloating with 2% KOH_{aq} at 40-fold magnification. Left: before tape stripping; right: after 20 tape strips taken off.

Table 1
Thickness and number of layers of the *stratum corneum* (s.c.) after a given number of tape strips.

tape strips	thickness s.c. [µm]	layers s.c.
0	11.03 ± 1.99	27.06 ± 3.21
2	9.91 ± 1.90	23.09 ± 2.35
4	8.58 ± 1.35	22.57 ± 2.36
6	8.88 ± 1.64	23.20 ± 1.61
8	7.90 ± 1.02	20.54 ± 3.19
10	7.20 ± 1.49	17.57 ± 4.56
12	6.93 ± 1.48	16.40 ± 4.26
14	5.45 ± 1.48	14.46 ± 4.07
16	4.23 ± 0.98	11.14 ± 3.76
18	3.96 ± 1.15	9.33 ± 3.05
20	3.23 ± 0.76	7.72 ± 2.59
compression test: 1	10.61 ± 1.48	23.37 ± 3.00

cell layers the s.c. thickness should be zero.

4. Discussion

In previous studies, the number of applied tape strips is usually correlated with the amount of s.c. that is removed, be it by determining the mass, the cumulative *pseudo*-absorption or other measurable quantities associated with individual or pooled tape strips. These values are then converted into the depth attained within the s.c. In this study, however, the remaining s.c. layers and the s.c. thickness were directly measured. From our data and the corresponding linear regression (Equation (3)), we found that a cellular layer of porcine s.c. is on average 0.40 ± 0.02 µm thick. This is in approximate agreement with results obtained from human skin by scanning laser microscopy imaging that revealed a thickness of 0.5 µm [7]. The similarity of these results (within 20% of each other) derived by two different techniques illustrates that in terms of thickness of the s.c. layers, porcine skin is a suitable surrogate for human skin.

We report a linear correlation between the number of tape strips applied and the thickness of the remaining s.c. on the skin specimen

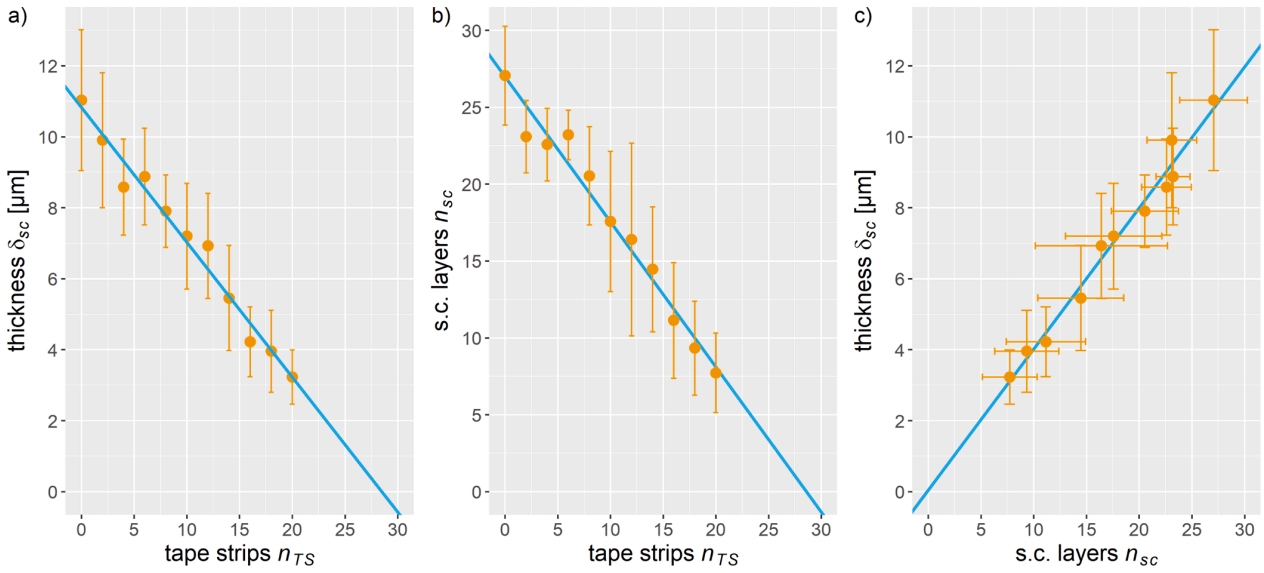

Fig. 3. Graphical representation of tape stripping data: a) thickness of the *stratum corneum* (s.c.), δ_{sc}, vs. the number of tape strips taken off, n_{TS}; b) number of s.c. layers, n_{sc}, vs. n_{TS}; c) δ_{sc} vs. n_{sc}. Individual values are reported in Table 1.

(Equation (1) and Fig. 3a), starting with the first tape strip. The data correspond to 0.38 ± 0.02 μm being removed by each tape strip, which is significantly higher than a value reported previously (0.22 ± 0.02 μm) [9]. However, the latter value was derived from the protein content on the removed tape strips. As discussed below, this might lead to an underestimation of the reduction in thickness of the s.c. by tape stripping.

Of note, our data indicate that the *stratum disjunctum* (s.d.), which represents the outer most layer of the epidermis, is removed efficiently. However, in dermal absorption studies, substances that are applied onto the skin can accumulate in the folds and furrows of the s.d. Furthermore, the s.d. is subject to constant desquamation so that substances in this layer are less likely to become bioavailable. For these reasons, the guidance of the European Food Safety Authority (EFSA) on dermal absorption recommends to exclude the first tape strip from analysis [31].

Apart from the thickness of the s.c., we also quantified the number of remaining s.c. layers after tape stripping. By linear regression of our data (Equation (2) and Fig. 3b), we found that each tape strip removed on average 0.94 ± 0.05 cellular layers, which is about one layer per tape strip. The data obtained from individual tape strips indicate that this value remained constant over at least 20 tape strips. Thus, outer s.c. layers, including those of the s.d., were removed with the same efficiency as deeper lying ones. This is in line with studies that have measured the cumulative amount of s.c. removed. For example, it was reported that the cumulative mass of s.c. removed increased linearly with the number of tape strips as determined by a colorimetric protein assay [15]. Another study concluded similarly when using a gravimetric approach to determine the number of removed s.c. layers [32].

On the other hand, variable results were obtained in a different study, with linear dependencies in some cases and plateauing observed in others [14]. It was hypothesized that for samples where the penetration depth into the s.c. plateaus, the s.c. is composed of fewer layers at the point probed. Two related reports also indicate a decrease of the amount of s.c. cells adhering to each tape strip with deeper cell layers [12,17]. Yet, in one case, data were provided for one replicate only [17]. In the other study, the deviation from linearity only starts after about 30 tape strips [12], which, according to our extrapolations (Fig. 3), would already result in the complete removal of the s.c. It is possible, however, that the observed differences are due to the different origin (human vs. porcine) and location (forearm vs. flank) of the skin samples. In a regression averaging data from 240 samples [9], the amount of s.c. removed was quantified by measuring the protein content and the weight of s.c.-related material on the tape strips. Deviations from a linear course were explained by the stronger cohesion between cells in deeper s.c. layers. However, the observed trend could also originate from a different effect.

Apart from water, proteins are the largest contributor to the mass of human s.c. (25–55% mass fraction) [33], whereas the lipid content is found to be between 2% and 10% [33–35]. The density of proteins is usually higher than 1.4 $g \cdot cm^{-3}$ [36]. This is also reflected in the density of dried s.c. which ranges from 1.4 ± 0.18 $g \cdot cm^{-3}$ [37] to 1.54 ± 0.30 $g \cdot cm^{-3}$ [38]. However, the density of the s.c. is frequently assumed to be about 1 $g \cdot cm^{-3}$ [4,9], because the s.c. is considered to be an aqueous matrix. This is despite *in vivo* confocal Raman spectroscopy of infant s.c. revealed that the protein content in the layers of the s.c. decreases from the surface of the s.c. to the viable epidermis/s.c. boundary layer [33]. Thus, it is questionable to consider the s.c. as a homogeneous aqueous matrix, given that the protein content is a major contributor to its mass. These results point to a higher density of s.c. layers lying closer to the surface of the skin. This is corroborated by observations that higher protein content correlates with higher area-specific mass of the s.c. [9,39]. In summary, these results indicate that a decreasing protein amount and, hence, a decreasing mass of the removed s.c. material on the tape strips do not necessarily correspond to less s.c. layers being stripped. In fact, this may be explained by the lower protein content and mass of layers located deeper within the s.c.

For gravimetric approaches, the evaporation of water off the tape strips between stripping and weighing could be a second contributing factor diminishing the expected mass of the removed s.c. Tape strips of deeper s.c. layers with higher water content will lose more mass due to this effect if evaporation is exhaustive.

Scanning laser microscopy measurements of the s.c. have also shown that the s.c. is relatively homogeneous regarding the thickness of individual cell layers. The average thickness of an s.c. aggregate on a tape strip was found to be independent of the depth in the s.c. [7]. Cryo-transmission electron microscopy (cryo-TEM) – a technique allowing imaging closer to the native condition than conventional TEM – showed that the thickness of the s.c. varies very little and only increases near the *stratum granulosum* [40–41]. We hypothesize that the often-cited increased cohesion in deeper layers is only relevant for those s.c. layers in direct contact with the *stratum granulosum*, and that the decreasing amount of s.c. removed per tape strip reported in many studies is at least partially due to changes in water and protein content of individual s.c. layers.

5. Conclusion

Using the well-established HE-stain, it was possible to directly measure the thickness of the remaining s.c. on excised porcine skin by optical microscopy, instead of quantifying the amount of removed s.c. on the tape strips. Thereby, potential inaccuracies associated with indirect detection methods that may, for example, result from the change in density of the s.c. as a function of depth, are circumvented. The same strategy has been used for the quantification of the remaining cell layers using a well-known histological method that involves bloating of the individual cells, thus making them better visible in light microscopy.

With this *in vitro* approach, we have conclusively shown that in excised pigskin the s.c. is indeed removed linearly, at least up to 20 tape strips. Each tape strip removes approximately 0.4 μm of s.c. which corresponds to about one cell layer on average. We have demonstrated that these results are in good agreement with existing literature on human skin, including *in vivo* studies [7,40–41], highlighting the relevance of our approach.

We envisage that future studies can benefit from the information presented in this work. The histological determination of the s.c. thickness and quantity of cell layers of scraps remaining after punching of skin samples is a quick, easy and reliable method that is practicable in many scientific and medical laboratories. With the removal rates reported here, researchers performing *in vitro* skin penetration studies could derive quick estimates of how deep in the s.c. a given concentration of analyte is found by counting the number of tape strips retrieved.

Author contributions

KS developed the project. KS and AR wrote the manuscript with main contributions from KS. KS and GO carried out the experimental work. KS, GO and AR analyzed the data. All authors contributed to the final version of the manuscript.

Declaration of competing interest

The authors declare that they have no known competing financial interests or personal relationships that could have appeared to influence the work reported in this paper.

Data availability

Data will be made available on request.

Acknowledgements

We thank Tanja Schmidt and Katja Reiter from Charité for providing

us with pigskin. We thank Lidia Schneider for help with the development of the project idea. We thank Sandra Schiewe and Nadine Dreiack for help with the cryo-microtome, staining and microscopy. We thank Markus Kirchner for conducting pyrolysis GC-MS measurements. We thank Franziska Riedel, Charlotte Kromer and Aline Rosin for proof reading and fruitful discussions. This work was funded by BfR-internal grant SFP 1322-774.

Appendix A. Supplementary material

Supplementary data to this article can be found online at https://doi.org/10.1016/j.ejpb.2023.04.022.

References

[1] J. Wolf, Die innere Struktur der Zellen des Stratum desquamans der menschlichen Epidermis, Z. Mikrosk. Anat. Forsch. 46 (1939) 170–202.
[2] N. Bartsch, J. Heidler, B. Vieth, C. Hutzler, A. Luch, Skin permeation of polycyclic aromatic hydrocarbons: a solvent-based in vitro approach to assess dermal exposures against benzo[a]pyrene and dibenzopyrenes, J. Occup. Environ. Hyg. 13 (12) (2016) 969–979, https://doi.org/10.1080/15459624.2016.1200724.
[3] N. Bartsch, M. Girard, L. Schneider, V.V. D. Weijgert, A. Wilde, O. Kappenstein, B. Vieth, C. Hutzler, A. Luch, Chemical stabilization of polymers: Implications for dermal exposure to additives, J. Environ. Sci. Heal. A 53 (5) (2018) 405–420, https://doi.org/10.1080/10934529.2017.1412192.
[4] H. Rothe, C. Obringer, J. Manwaring, C. Avci, W. Wargniez, J. Eilstein, N. Hewitt, R. Cubberley, H. Duplan, D. Lange, Comparison of protocols measuring diffusion and partition coefficients in the stratum corneum, J. Appl. Toxicol. 37 (7) (2017) 806–816, https://doi.org/10.1002/jat.3427.
[5] H. Pinkus, Examination of the epidermis by the strip method of removing horny layers: I. Observations on thickness of the horny layer, and on mitotic activity after stripping, J. Invest. Dermatol. 16 (6) (1951) 383–386, https://doi.org/10.1038/jid.1951.45.
[6] A. Hughes, S. Tawfik, K. Baruah, E. O'Toole, R. O'Shaughnessy, Tape strips in dermatology research, Br. J. Dermatol. 185 (1) (2021) 26–35, https://doi.org/10.1111/bjd.19760.
[7] U. Lindemann, K. Wilken, H.-J. Weigmann, H. Schaefer, W. Sterry, J. Lademann, Quantification of the horny layer using tape stripping and microscopic techniques, J. Biomed. Opt. 8 (4) (2003) 601–607, https://doi.org/10.1117/1.1609200.
[8] D. Mohammed, P. Matts, J. Hadgraft, M. Lane, Depth profiling of stratum corneum biophysical and molecular properties, Br. J. Dermatol. 164 (5) (2011) 957–965, https://doi.org/10.1111/j.1365-2133.2011.10211.x.
[9] D. Mohammed, Q. Yang, R. Guy, P. Matts, J. Hadgraft, M. Lane, Comparison of gravimetric and spectroscopic approaches to quantify stratum corneum removed by tape-stripping, Eur. J. Pharm. Biopharm. 82 (1) (2012) 171–174, https://doi.org/10.1016/j.ejpb.2012.05.018.
[10] D. Bommannan, R.O. Potts, R.H. Guy, Examination of stratum corneum barrier function in vivo by infrared spectroscopy, J. Invest. Dermatol. 95 (4) (1990) 403–408, https://doi.org/10.1111/1523-1747.ep12555503.
[11] N. Higo, A. Naik, D.B. Bommannan, R.O. Potts, R.H. Guy, Validation of reflectance infrared spectroscopy as a quantitative method to measure percutaneous absorption in vivo, Pharm. Res. 10 (10) (1993) 1500–1506, https://doi.org/10.1023/A:1018987612155.
[12] U. Jacobi, H.J. Weigmann, J. Ulrich, W. Sterry, J. Lademann, Estimation of the relative stratum corneum amount removed by tape stripping, Skin Res. Technol. 11 (2) (2005) 91–96, https://doi.org/10.1111/j.1600-0846.2005.00094.x.
[13] H.-J. Weigmann, U. Lindemann, C. Antoniou, G. Tsikrikas, A. Stratigos, A. Katsambas, W. Sterry, J. Lademann, UV/VIS absorbance allows rapid, accurate, and reproducible mass determination of corneocytes removed by tape stripping, Skin Pharmacol. Physiol. 16 (4) (2003) 217–227, https://doi.org/10.1159/000070844.
[14] T. Hahn, S. Hansen, D. Neumann, K.-H. Kostka, C.-M. Lehr, L. Muys, U. Schaefer, Infrared densitometry: a fast and non-destructive method for exact stratum corneum depth calculation for in vitro tape-stripping, Skin Pharmacol. Physiol. 23 (4) (2010) 183–192, https://doi.org/10.1159/000288165.
[15] F. Dreher, A. Arens, J. Hostýnek, S. Mudumba, J. Ademola, H. Maibach, Colorimetric Method for Quantifying Human Stratum Corneum Removed by Adhesive-Tape-Stripping, Acta Derm. Venereol. 78 (3) (1998), https://doi.org/10.1080/000155598441495.
[16] S.J. Bashir, A.L. Chew, A. Anigbogu, F. Dreher, H.I. Maibach, Physical and physiological effects of stratum corneum tape stripping, Skin Res. Technol. 7 (1) (2001) 40–48, https://doi.org/10.1034/j.1600-0846.2001.007001040.x.
[17] U. Lindemann, H.-J. Weigmann, H. Schaefer, W. Sterry, J. Lademann, Evaluation of the pseudo-absorption method to quantify human stratum corneum removed by tape stripping using protein absorption, Skin Pharmacol. Physiol. 16 (4) (2003) 228–236, https://doi.org/10.1159/000070845.
[18] D. Gerstel, C. Jacques-Jamin, A. Schepky, R. Cubberley, J. Eilstein, S. Grégoire, N. Hewitt, M. Klaric, H. Rothe, H. Duplan, Comparison of protocols for measuring cosmetic ingredient distribution in human and pig skin, Toxicol. In Vitro 34 (2016) 153–160, https://doi.org/10.1016/j.tiv.2016.03.012.
[19] C. Herkenne, A. Naik, Y.N. Kalia, J. Hadgraft, R.H. Guy, Pig ear skin ex vivo as a model for in vivo dermatopharmacokinetic studies in man, Pharm. Res. 23 (8) (2006) 1850–1856, https://doi.org/10.1007/s11095-006-9011-8.
[20] C. Herkenne, A. Naik, Y.N. Kalia, J. Hadgraft, R.H. Guy, Ibuprofen transport into and through skin from topical formulations: in vitro–in vivo comparison, J. Invest. Dermatol. 127 (1) (2007) 135–142, https://doi.org/10.1038/sj.jid.5700491.
[21] C. Blair, Morphology and thickness of the human stratum corneum, Br. J. Dermatol. 80 (7) (1968) 430–436, https://doi.org/10.1111/j.1365-2133.1968.tb11978.x.
[22] Y.N. Kalia, F. Pirot, R.H. Guy, Homogeneous transport in a heterogeneous membrane: water diffusion across human stratum corneum in vivo, Biophys. J. 71 (5) (1996) 2692–2700, https://doi.org/10.1016/S0006-3495(96)79460-2.
[23] SCCS (Scientific Committee on Consumer Safety): Basic criteria for the in vitro assessment of dermal absorption of cosmetic ingredients. 7th plenary meeting (2010).
[24] N.A. Monteiro-Riviere, D.G. Bristol, T.O. Manning, R.A. Rogers, J.E. Riviere, Interspecies and interregional analysis of the comparative histologic thickness and laser Doppler blood flow measurements at five cutaneous sites in nine species, J. Invest. Dermatol. 95 (5) (1990) 582–586, https://doi.org/10.1111/1523-1747.ep12505567.
[25] OECD Guideline for the Testing of Chemicals, Test No., 428: Skin Absorption: *in vitro* Method, OECD Publishing, Paris, 2004, https://doi.org/10.1787/9789264071087-en.
[26] Q. Zhang, M. Murawsky, T. LaCount, G.B. Kasting, S.K. Li, Transepidermal water loss and skin conductance as barrier integrity tests, Toxicol. In Vitro 51 (2018) 129–135, https://doi.org/10.1016/j.tiv.2018.04.009.
[27] tesafilm kristall-klar product information sheet. https://www.tesa.com/de-de/buero-und-zuhause/tesafilm-kristall-klar.html (accessed 23.03.2023).
[28] H.J. Weigmann, M.S. de Sainte Claire, S. Schanzer, A. Patzelt, M. Meinke, C. Antoniou, W. Sterry, J. Lademann, Determination of the protection efficacy and homogeneity of the distribution of sunscreens applied onto skin pre-treated with cosmetic products, Skin Res. Technol. 18 (2) (2012) 245–250, https://doi.org/10.1111/j.1600-0846.2011.00563.x.
[29] Z. Ya-Xian, T. Suetake, H. Tagami, Number of cell layers of the stratum corneum in normal skin–relationship to the anatomical location on the body, age, sex and physical parameters, Arch. Dermatol. Res. 291 (10) (1999) 555–559, https://doi.org/10.1007/s004030050453.
[30] U. Jacobi, M. Kaiser, H. Richter, H. Audring, W. Sterry, J. Lademann, The number of stratum corneum cell layers correlates with the pseudo-absorption of the corneocytes, Skin Pharmacol. Physiol. 18 (4) (2005) 175–179, https://doi.org/10.1159/000085862.
[31] H. Buist, P. Craig, I. Dewhurst, S. Hougaard Bennekou, C. Kneuer, K. Machera, C. Pieper, D. Court Marques, G. Guillot, F. Ruffo, A. Chiusolo, European Food Safety Authority (EFSA), Guidance on dermal absorption, EFSA Journal 15 (6) (2017) 4873, https://doi.org/10.2903/j.efsa.2017.4873.
[32] D.A. Schwindt, K.P. Wilhelm, H.I. Maibach, Water diffusion characteristics of human stratum corneum at different anatomical sites in vivo, J. Invest. Dermatol. 111 (3) (1998) 385–389, https://doi.org/10.1046/j.1523-1747.1998.00321.x.
[33] L. Zhang, T. Cambron, Y. Niu, Z. Xu, N. Su, H. Zheng, K. Wei, P. Ray, MCR Approach Revealing Protein, Water, and Lipid Depth Profile in Atopic Dermatitis Patients' Stratum Corneum via in Vivo Confocal Raman Spectroscopy, Anal. Chem. 91 (4) (2019) 2784–2790, https://doi.org/10.1021/acs.analchem.8b04597.
[34] M.A. Lampe, A.L. Burlingame, J. Whitney, M.L. Williams, B.E. Brown, E. Roitman, P.M. Elias, Human stratum corneum lipids: characterization and regional variations, J. Lipid Res. 24 (2) (1983) 120–130, https://doi.org/10.1016/S0022-2275(20)38005-6.
[35] G. Gray, H. Yardley, Lipid compositions of cells isolated from pig, human, and rat epidermis, J. Lipid Res. 16 (6) (1975) 434–440, https://doi.org/10.1016/S0022-2275(20)34493-X.
[36] H. Fischer, I. Polikarpov, A.F. Craievich, Average protein density is a molecular-weight-dependent function, Protein Sci. 13 (10) (2004) 2825–2828, https://doi.org/10.1110/ps.04688204.
[37] R.L. Anderson, J.M. Cassidy, Variations in physical dimensions and chemical composition of human stratum corneum, J. Invest. Dermatol. 61 (1) (1973) 30–32, https://doi.org/10.1111/1523-1747.ep12674117.
[38] D.A. Weigand, C. Haygood, J.R. Gaylor, Cell layers and density of Negro and Caucasian stratum corneum, J. Invest. Dermatol. 62 (6) (1974) 563–568, https://doi.org/10.1111/1523-1747.ep12679412.
[39] F. Dreher, B. Modjtahedi, S. Modjtahedi, H. Maibach, Quantification of stratum corneum removal by adhesive tape stripping by total protein assay in 96-well microplates, Skin Res. Technol. 11 (2) (2005) 97–101, https://doi.org/10.1111/j.1600-0846.2005.00103.x.
[40] L. Norlén, Stratum corneum keratin structure, function and formation - a comprehensive review, Int. J. Cosmet. Sci. 28 (6) (2006) 397–425, https://doi.org/10.1111/j.1467-2494.2006.00345.x.
[41] L. Norlén, A. Al-Amoudi, Stratum corneum keratin structure, function, and formation: the cubic rod-packing and membrane templating model, J. Invest. Dermatol. 123 (4) (2004) 715–732, https://doi.org/10.1111/j.0022-202X.2004.23213.x.

Continuous removal of single cell layers by tape stripping the stratum corneum – a histological study

Konstantin Simon*[1,2], Gila Oberender[1,3], Alexander Roloff*[1]

Supporting Information

Pyrolysis–gas chromatography–mass spectrometry

Pyrolysis–gas chromatography–mass spectrometry (pyrolysis GC-MS) was performed for the qualification of the polymeric tape strip material (polypropylene, according to the manufacturer). A small piece of the adhesive tape (ca. 1 mm^2) was transferred to a pyrolysis tube (Gerstel, Mülheim (Ruhr), Germany), pyrolyzed and subsequently analyzed via GC-MS according to a previously published method (inert method).[1,2] Briefly, pyrolysis was performed using a platinum filament localized in a thermal desorption unit (TDU) mounted with a Pyrolyzer Module for TDU onto a Cooled Injection System (CIS) equipped with liquid nitrogen cooling and a MultiPurpose Sampler (MPS2-XL; all items from Gerstel).[1] The sample was subjected to inert pyrolysis under a nitrogen-atmosphere (purity: 99.999%, Linde, Pullach, Germany) at 500 °C for 0.33 min. A solvent vent method was applied and 70 ml/min helium (purity: ≥99.999%, Linde) passed into the Pyrolysis-TDU-CIS complex using a pneumatic gas regulator (Gerstel) with a helium vent flow of 10 ml/min. A vent pressure of 15 kPa was applied. The pyrolysis was connected to a gas chromatograph coupled with the mass selective detector 7890A-5975C GC/MSD System (Agilent, Santa Clara, California, United States) and maintained as described previously.[1,2] We compared our results to published data on pyrolysis GC-MS of polypropylene materials.[3,4] We found characteristic peaks of polypropylene-derived fragments in the GC-MS pyrogram (Fig. S1 a, red boxes) and were able to identify characteristic mass fragments (Fig. S1 b and Table S1) in a fragmentation pattern with *m/z* differences of 14 or 15 between individual fragments, corresponding to CH_3 or CH_2 units. The most abundant fragments underlying each pyrogram peak are summarized in Table S1. These are characteristic for polypropylene.[3,4]

*Corresponding authors. E-mail: Konstantin.Simon@bfr.bund.de, Alexander.Roloff@bfr.bund.de

[1]German Federal Institute for Risk Assessment (BfR), Department of Chemical and Product Safety, Max-Dohrn-Str. 8-10, 10589 Berlin, Germany.

[2]Institute of Pharmacy, Department of Biology, Chemistry, Pharmacy, Freie Universität Berlin, 14195 Berlin, Germany.

[3]Berliner Hochschule für Technik (BHT), Luxemburger Str. 10, 13353 Berlin, Germany.

Table S1: Most abundant m/z values under characteristic peaks in chromatogram.

m/z	Compound
56	*iso*-butene
69	3-methyl-1-butene
84	3-methyl-1-pentene
97	3-methyl-1-hexene
112	3-methyl-1-heptene or 3,5-dimethyl-1-hexene
126	2,4-dimethy-1-heptene

2

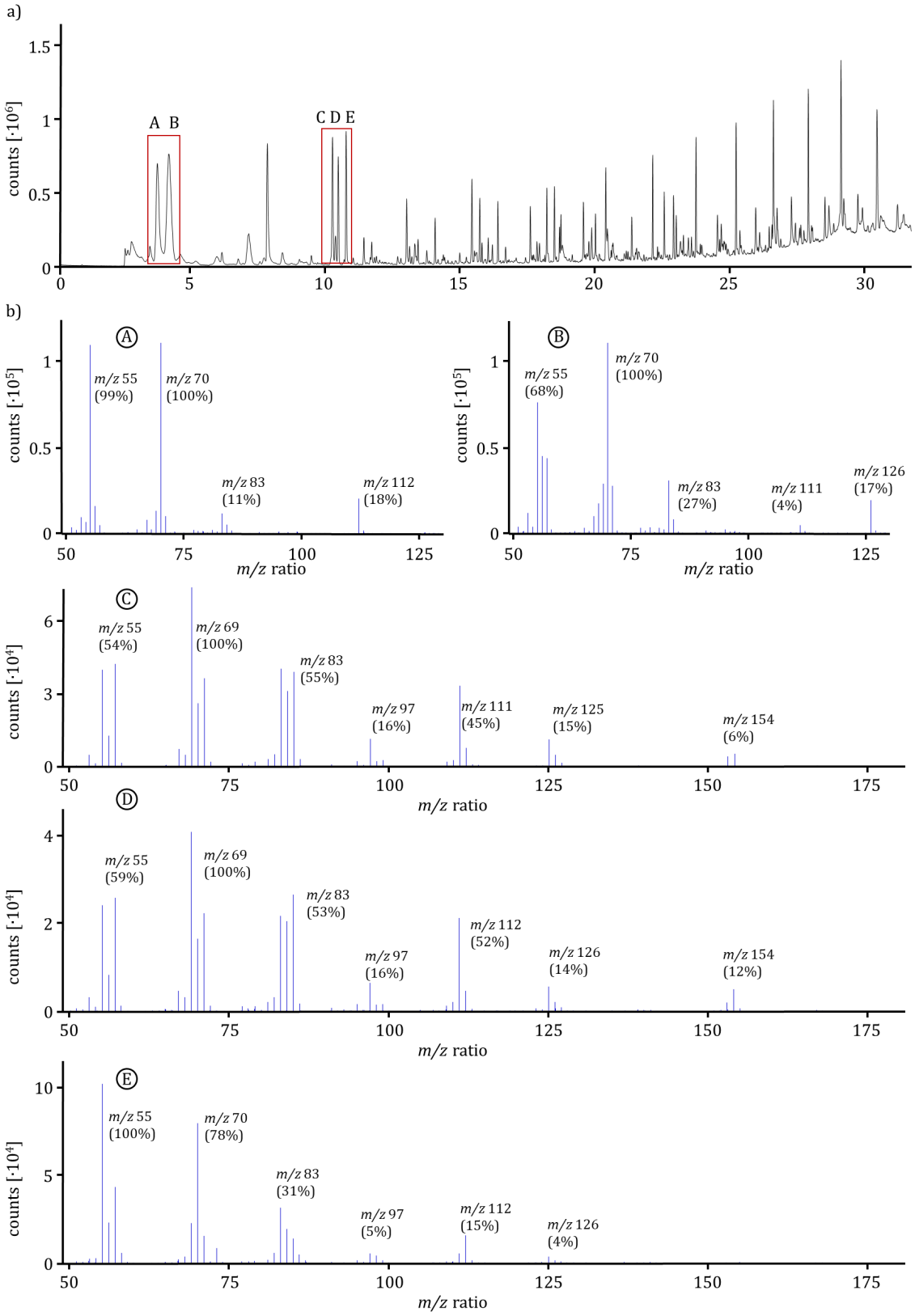

Fig. S1: a) Pyrolysis GC-MS chromatogram and b) mass spectra corresponding to the marked peaks. *m/z* values are presented together with their respective abundance as a ratio to highest peak in parentheses.

1. Bartsch, N., Girard, M., Wilde, A., Bruhn, T., Kappenstein, O., Vieth, B., Hutzler, C. & Luch, A. Thermal Stability of Polymer Additives: Comparison of Decomposition Models Including Oxidative Pyrolysis. *J. Vinyl Addit. Techn.* **25,** E12–E27. doi:10.1002/vnl.21654 (2019).

2. Paschke, M., Hutzler, C., Henkler, F. & Luch, A. Oxidative and inert pyrolysis on-line coupled to gas chromatography with mass spectrometric detection: On the pyrolysis products of tobacco additives. *International Journal of Hygiene and Environmental Health* **219,** 780–791. doi:10.1016/j.ijheh.2016.09.002 (2016).

3. Dümichen, E., Eisentraut, P., Bannick, C. G., Barthel, A. K., Senz, R. & Braun, U. Fast identification of microplastics in complex environmental samples by a thermal degradation method. *Chemosphere* **174,** 572–584. doi:10.1016/j.chemosphere.2017.02.010 (2017).

4. Soják, L., Kubinec, R., Jurdáková, H., Hájeková, E. & Bajus, M. High resolution gas chromatographic–mass spectrometric analysis of polyethylene and polypropylene thermal cracking products. *J. Anal. Appl. Pyrolysis* **78,** 387–399. doi:10.1016/j.jaap.2006.09.012 (2007).

A.2 Polycyclic aromatic hydrocarbon skin permeation efficiency *in vitro* is lower through human than pigskin and decreases with lipophilicity

Konstantin Simon, Nastasia Bartsch, Lidia Schneider, Valerie van de Weijgert, Christoph Hutzler, Andreas Luch, Alexander Roloff

Environmental Research **2024**, *255*, 119118.

doi: 10.1016/j.envres.2024.119118

This study was submitted to the journal on 30 January 2024, revised on 15 April 2024 and accepted on 8 May 2024. Published online on 17 May 2024.

The contents of this publication are discussed in Chapter 3, Section *Dermal exposure to polycyclic aromatic hydrocarbons*. The supporting information is added following the main part.

Author contributions: **Konstantin Simon:** Conceptualization, Formal analysis, Investigation, Writing — original draft, Writing — review & editing, Visualization. Nastasia Bartsch: Conceptualization, Methodology, Formal analysis, Investigation. Lidia Schneider: Methodology, Formal analysis, Investigation. Valerie van der Weijgert: Formal analysis, Investigation. Christoph Hutzler: Conceptualization, Methodology. Andreas Luch: Writing — review & editing, Resources, Funding acquisition. Alexander Roloff: Writing — original draft, Writing — review & editing, Supervision.

Abstract

Polycyclic aromatic hydrocarbons (PAH) are persistent environmental pollutants, which occasionally appear as contaminants in consumer products. Upon dermal contact, transfer of PAH into the *stratum corneum* (s.c.) and migration through the skin may occur, resulting in this class of highly toxic compounds to become bioavailable. In this study, dermal penetration through human and porcine skin of 24 PAH, comprising broad molar mass (M: 152–302 g/mol) and octanol-water partition coefficient (log$P$: 3.9–7.3) ranges, was evaluated via Franz diffusion cell *in vitro* assays. More lipophilic and potentially more toxic PAH had decreased permeation rates through the rather lipophilic s.c. into the more hydrophilic viable (epi-)dermis. Furthermore, human skin was less permeable than pigskin, a commonly used surrogate in skin penetration studies. In particular, the s.c. of human skin retains a greater share of PAH, an effect that is more pronounced for smaller PAH. Additionally, we compared the skin permeation kinetics of different PAH in pigskin.

While small PAH ($M < 230$ g/mol, log$P < 6$) permeate the skin quickly and are detected in the receptor fluid after 2 h, large PAH ($M > 252$ g/mol, log$P \geq 6$) do not fully permeate the skin up to 48 h. This indicates that highly lipophilic PAH do not become bioavailable as readily as their smaller congeners when transferred to the skin surface. Our data suggest that pigskin could be used as a surrogate for worst case scenario estimates of dermal PAH permeation through human skin.

Graphical Abstract

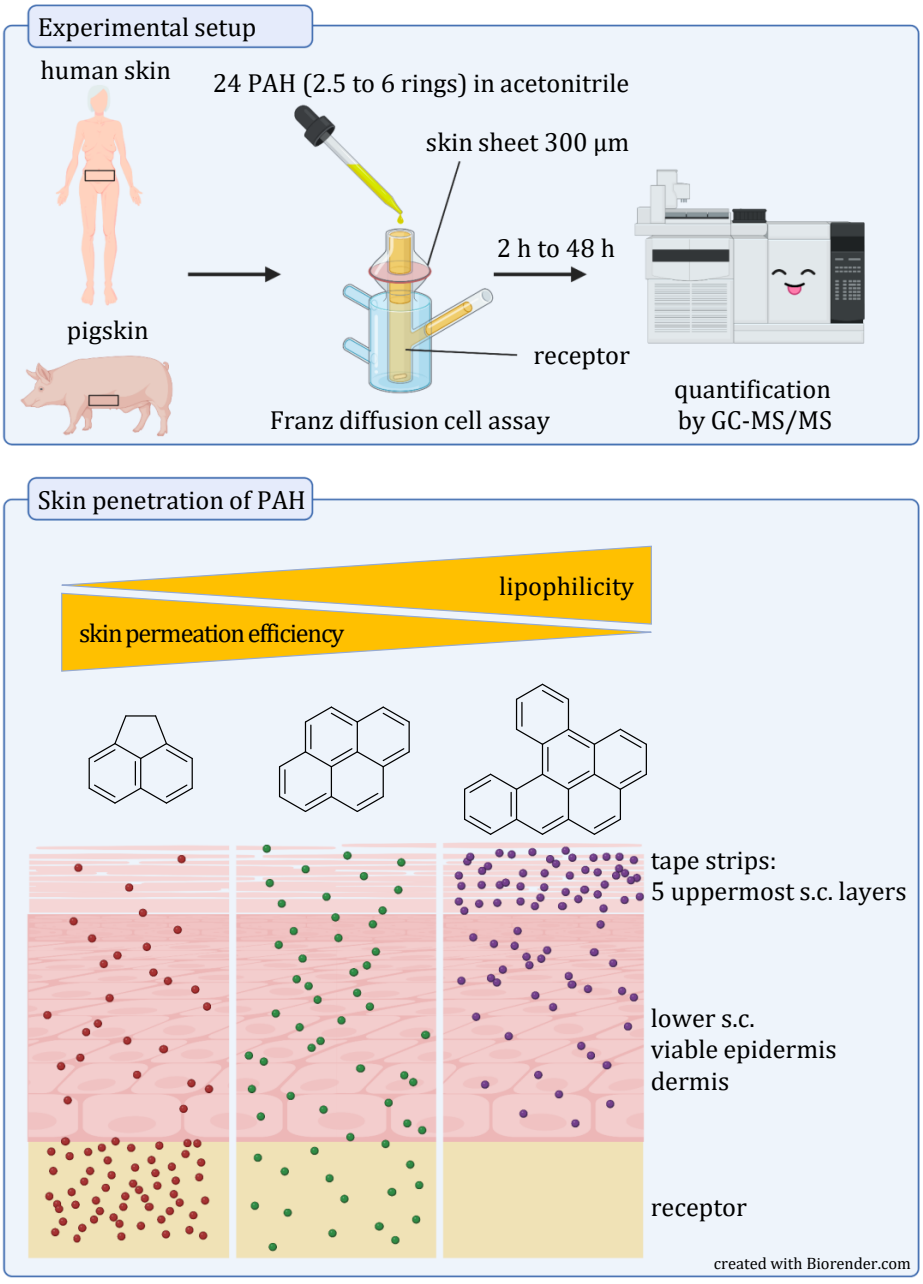

Environmental Research 255 (2024) 119118

Contents lists available at ScienceDirect

Environmental Research

journal homepage: www.elsevier.com/locate/envres

Polycyclic aromatic hydrocarbon skin permeation efficiency *in vitro* is lower through human than pigskin and decreases with lipophilicity

Konstantin Simon [a,b,*], Nastasia Bartsch [a,c], Lidia Schneider [a], Valerie van de Weijgert [a,d], Christoph Hutzler [a], Andreas Luch [a,b], Alexander Roloff [a,*]

[a] German Federal Institute for Risk Assessment (BfR), Department of Chemical and Product Safety, Max-Dohrn-Str. 8-10, 10589, Berlin, Germany
[b] Department of Biology, Chemistry, Pharmacy, Institute of Pharmacy, Freie Universität Berlin, Königin-Luise-Str. 2-4, 14195, Berlin, Germany
[c] German Federal Office of Consumer Protection and Food Safety, Bundesallee 51, 38116, Braunschweig, Germany
[d] National Institute for Public Health and the Environment (RIVM), Centre for Safety of Substances and Products, Antonie van Leeuwenhoeklaan 9, 3721, MA Bilthoven, Netherlands

ARTICLE INFO

Keywords:
Skin migration
Polycyclic aromatic hydrocarbons (PAH)
Stratum corneum
Human skin
Pigskin

ABSTRACT

Polycyclic aromatic hydrocarbons (PAH) are persistent environmental pollutants, which occasionally appear as contaminants in consumer products. Upon dermal contact, transfer of PAH into the *stratum corneum* (s.c.) and migration through the skin may occur, resulting in this class of highly toxic compounds to become bioavailable. In this study, dermal penetration through human and porcine skin of 24 PAH, comprising broad molar mass (*M*: 152–302 g/mol) and octanol-water partition coefficient (log*P*: 3.9–7.3) ranges, was evaluated *via* Franz diffusion cell *in vitro* assays. More lipophilic and potentially more toxic PAH had decreased permeation rates through the rather lipophilic s.c. into the more hydrophilic viable (epi-)dermis. Furthermore, human skin was less permeable than pigskin, a commonly used surrogate in skin penetration studies. In particular, the s.c. of human skin retains a greater share of PAH, an effect that is more pronounced for smaller PAH. Additionally, we compared the skin permeation kinetics of different PAH in pigskin. While small PAH ($M < 230$ g/mol, log$P < 6$) permeate the skin quickly and are detected in the receptor fluid after 2 h, large PAH ($M > 252$ g/mol, log$P \geq 6$) do not fully permeate the skin up to 48 h. This indicates that highly lipophilic PAH do not become bioavailable as readily as their smaller congeners when transferred to the skin surface. Our data suggest that pigskin could be used as a surrogate for worst case scenario estimates of dermal PAH permeation through human skin.

1. Introduction

Polycyclic aromatic hydrocarbons (PAH) are associated with numerous health risks (Kamal et al., 2015). Many PAH are considered to be potentially carcinogenic (IARC, 2010, 2018; Kamal et al., 2015; Kim et al., 2013; Rocha et al., 2021; WHO, 2010), including the risk of inducing skin cancer after dermal exposure (Boffetta et al., 1997). For example, benzo[*a*]pyrene (B[*a*]P) is classified as a class 1 carcinogen, whereas certain dibenzopyrenes are suspected to be even more potent toxins (Collins et al., 1998). Apart from cancer, PAH are also linked to endocrine disruption (Zhang et al., 2016), heart disease (Burstyn et al., 2005) and immunosuppression (van Grevenynghe et al., 2005), among other adverse effects (Sousa et al., 2022; WHO, 2010). Hence, multiple regulations have been implemented to limit the exposure to PAH (EC, 2006; EC, 2013; EC, 2023; US-EPA, 2021). Nonetheless, as persistent organic pollutants, PAH are ubiquitous in the environment (Haney et al., 2020; Hutzler et al., 2011; Lao et al. 2018a, 2018b; Whitehead et al., 2011) and occasionally also found as contaminants in consumer products, in particular those containing carbon black or extender oils (Alawi et al., 2018; Bartsch et al., 2017; Folgado de Lucena et al., 2018). When PAH come into contact with skin, they can become bioavailable by diffusion through the stratum corneum (s.c.) into the viable epidermis

Abbreviations: B[*a*]P, benzo[*a*]pyrene; FDC, Franz diffusion cell; GC-MS/MS, gas chromatography coupled to tandem mass spectrometry; log*P*, logarithmic octanol-water partition coefficient; *M*, molar mass; OECD, Organisation for Economic Co-operation and Development; PAH, polycyclic aromatic hydrocarbons; s.c., *stratum corneum*; SI, supporting information; TEWL, trans-epidermal water loss.

* Corresponding authors. German Federal Institute for Risk Assessment (BfR), Department of Chemical and Product Safety, Max-Dohrn-Str. 8-10, 10589, Berlin, Germany.

E-mail addresses: Konstantin.Simon@bfr.bund.de (K. Simon), Alexander.Roloff@bfr.bund.de (A. Roloff).

https://doi.org/10.1016/j.envres.2024.119118
Received 30 January 2024; Received in revised form 15 April 2024; Accepted 8 May 2024
Available online 17 May 2024

and dermis layers (Bartsch, 2018; Bartsch et al., 2016; Simon et al., 2023b).

Skin penetration is investigated either *in vivo* or *in vitro*. *In vivo* studies come with the drawback of exposing humans or animals to harmful substances and avoidable risks. Hence, *in vitro* studies involving the well-established Franz diffusion cell (FDC) assay remain an important pillar of skin penetration research (Franz, 1975; Ng et al., 2010). The FDC provides a simple set-up where the target substance, usually embedded or dissolved in a matrix, is spiked onto skin or skin models. The receptor chamber beneath is filled with a water-based fluid to mimic the subcutaneous layers and to provide a reservoir for fully permeating substances. The distribution of the substance within the skin and its concentration in the receptor compartment after specified incubation times give insights into the skin permeability.

The gold standard for FDC assays is human skin. However, human skin is not always readily available because it must be donated from plastic surgery patients (Bartsch et al., 2016; Hagvall et al., 2021) or corpses (Ellison et al., 2020, 2021). Synthetic or lab-grown skin models are alternatives that find increasing utilization in research (Lemoine et al., 2021; Ng et al., 2010), but are not yet recommended for skin permeation studies within a regulatory context (OECD, 2011). Pigskin is the most common alternative to human skin because it shares crucial properties with human skin. Thus, pigskin often provides comparable results for penetration-relevant parameters such as lag time and diffusion or partition coefficients (Gerstel et al., 2016; Herkenne et al., 2006; Rothe et al., 2017; SCCS, 2010). In addition, its procurement is relatively easy (Hopf et al., 2020). Yet, differences between human and pigskin remain (Khiao In et al., 2019). Studies have shown that pigskin is more permeable for certain substances than human skin (Barbero and Frasch, 2009; Rothe et al., 2017). A comprehensive comparison of the penetration of PAH into human and pigskin has not yet been reported.

It has been suggested that higher molecular mass (M) PAH (five or more rings: large PAH) feature lower penetration rates and fluxes through the skin than PAH with lower M (two to three rings: small PAH, Moody et al., 2011; Sartorelli et al. 1998, 1999, 2001). However, these studies either rely on small sample sizes ($n \leq 2$), involved non-human skin or reported PAH concentrations only in the receptor fluid, thus lacking information about the distribution profiles within individual skin compartments.

Here, we compiled the data of several FDC assays from a set of 24 dermally applied PAH of various ring numbers (2.5–6, $M = 152$–302 g/mol, Table A1 and Figure A1 in the Supporting Information (SI) A). Human and pigskin were incubated with PAH solutions in acetonitrile for 24 h. Pigskin was additionally incubated for various incubation times (2 h, 4 h, 16 h, 48 h), yielding insights into the migration kinetics. Subsequently, the five upper s.c. layers of treated skin samples were tape-stripped to analyze them separately from the remaining skin and the receptor fluid for their PAH content. Quantification was realized by gas chromatography coupled to tandem mass spectrometry (GC-MS/MS). Finally, the distribution of PAH in the skin layers was correlated to their logarithmic octanol-water partition coefficients (log$P$).

2. Methods

The data presented here is a compilation of quality controls which were run in parallel to FDC assays aiming to investigate dermal PAH penetration from consumer products with foreseeable skin contact (Bartsch et al., 2016). The concentration of each PAH applied to the skin specimens in acetonitrile was set at 1000 ng/ml. The method used and the materials and chemicals applied were published in the former study. Below, the method is briefly summarized for clarity.

2.1. Skin

Human skin was obtained from plastic surgery at Charité, Berlin and originated from female abdomen. The proposal to conduct permeation studies with human skin samples was reviewed and approved by an independent ethics committee (Ethics Commission Charité, Berlin, No. EA2/090/14, July 22, 2014). Flank pigskin was obtained from VION food GmbH (Perleberg, Germany) and delivered on ice. The un-scalded skin was taken from deceased pigs that would have not been used for food production. Both skin types were stored at −20 °C until use.

2.2. Franz diffusion cell assay

An FDC consists of a donor chamber for the application of a target substance in a matrix and a receptor chamber. The receptor chamber is filled with a liquid and jacketed by a water circulation system to keep the skin at a constant temperature. The skin or skin model is placed over the receptor chamber and fixed by the donor chamber cap with a clamp. Substances that reach the receptor fluid can be considered to become bioavailable. In the present study, the temperature of the receptor compartment was held at 33 ± 1 °C, which corresponds to average skin surface temperature of 32–35 °C (Lee et al., 2019). The receptor chamber was filled with an isotonic saline solution (9 g/l sodium chloride), which is considered to be a good approximation for hypodermal bodily fluids (Hoorn, 2017).

The skin was cut with a dermatome to a thickness of 300 μm and placed atop the receptor chamber. The donor cap was fixed onto the skin, resulting in an exposure area of 1.76 cm^2. The trans-epidermal water loss (TEWL) was measured to ensure skin integrity according to guideline 428 of the Organisation for Economic Co-operation and Development (OECD, 2004). If the TEWL of a skin sample was greater than 30% of the mean TEWL for the specific skin type as previously confirmed by validation experiments, the skin specimen was eliminated from the study (Bartsch et al., 2016). 50 μl of a solution containing a mixture of PAH in acetonitrile (1000 ng/ml, see Table A1 of SI A for a list of all 24 PAH) were applied onto the skin (corresponding to a dermal dose of 28 ng/cm^2) and incubated for the denoted time intervals (2–48 h, Table 1). For negative controls, 50 μl of pure acetonitrile were applied.

After the specified incubation times, all samples were spiked with internal standards (selected deuterated PAH, assignment of analytes to internal standards: Table A1 of SI A). The donor chamber was rinsed with saline solution (9 g/l sodium chloride), and the skin was removed from the assembly and stripped with five tape strips, which were then pooled. One tape strip was shown to remove one layer of the s.c. (Simon et al., 2023a), thus, the five upper s.c. layers were analyzed collectively. The tape strips were extracted using acetonitrile, which was re-extracted with n-hexane. This double extraction proved beneficial in minimizing matrix effects caused by the extraction of adhesive from the tape. The remaining skin was extracted using ethyl acetate and the receptor fluid was subjected to a solid phase extraction (reversed phase C18) followed by elution of the PAH with dichloromethane. All obtained extracts were then concentrated under a nitrogen stream, re-dissolved in acetonitrile and analyzed for their PAH content by GC-MS/MS. Further details on the measurement procedure are provided in a previous publication (Bartsch et al., 2016). This yielded PAH concentrations in three compartments: (i) upper s.c. (derived from five tape strips), (ii) remaining skin and (iii) receptor fluid.

Table 1
Number of replicates (n) of Franz diffusion cell assays performed per skin type and incubation time.

Incubation time	Origin of skin	n
2 h	pig	3
4 h	pig	3
16 h	pig	3
24 h	pig	9
24 h	human	13
48 h	pig	3

2.3. Data analysis

The data were analyzed using the statistical programming language R (version 4.2.2). Data were subjected to a Shapiro-Wilk normality test. If the data was not normally distributed, the data was tested for outliers using the Grubb's outlier test. If the test was positive, the outlier was removed. The mean and standard deviation for each PAH, skin species, compartment and incubation time were calculated from the purged data set. The results of all statistical tests are summarized in the SI B (sheets 1 and 2). Based on the amount of each PAH that penetrated into the skin (sum of all compartments, including the receptor fluid), the distribution ratio of the PAH in each compartment was calculated.

Equation (1) was used to fit the data and highlight the relationship of two variables, y and x, with u and w as regression parameters:

$$y = u \cdot e^{-x} + w. \quad (1)$$

3. Results and discussion

We compared the migration of a broad range of PAH from acetonitrile into human skin and one of its most common surrogates in skin penetration studies, pigskin (SCCS, 2010; Simon and Maibach, 2000). Furthermore, PAH were incubated on pigskin for different periods to produce a kinetic profile for each of the investigated PAH. The smallest and least lipophilic PAH in this study are acenaphthylene (M = 152 g/mol, log$P$ = 4.0, Lu et al., 2008) and acenaphthene (M = 154 g/mol, log$P$ = 3.9, Lu et al., 2008), the largest and most lipophilic PAH are the dibenzopyrenes (M = 302 g/mol, log$P$ = 7.2–7.3, PubChem, 2023b, c, d, e; US-EPA, 2012). A comprehensive list of all 24 investigated PAH is provided in Table A1 and Figure A1 (SI A). For the investigated PAH, log$P$ and M are linearly related (Figure A2 and equation (A.1), SI A). The data comprising the quantified mass, amount and ratio of each PAH at each incubation time for both species and all compartments are summarized in Sheet 3 of SI B.

The regulatory limit of the PAH content in consumer products with prolonged or repetitive short-term dermal contact is 1 mg/kg (0.5 mg/kg for toys) in the European Union (EC, 2023). However, significantly higher values in the range of up to ca. 50–270 mg/kg were measured in certain consumer products in the past (Bartsch et al., 2017; BVL, 2017). When these products are in contact with skin, dermal exposure in the range of the spiked PAH doses applied in this study (28 ng/cm^2) are expected (for example, after 24 h of skin contact, a hammer handle containing 166 mg/kg B[a]P released 102 ng/cm^2 of this PAH, Bartsch et al., 2016). In different exposure scenarios, certain sub-populations such as firefighters can be dermally exposed to even higher amounts of airborne PAH (between 4 and 1200 ng/cm^2, Sousa et al., 2022).

Previous research has shown that high concentrations of multiple PAH as well as rather complex matrices as application media (Bourgart et al., 2019; Hopf et al., 2018) can both diminish dermal penetration rates of PAH. However, the applied doses in the present study were 50-fold (Bourgart et al., 2019) and 5000-fold (Hopf et al., 2018) lower than in those studies and PAH were applied in solvent-based solutions, not in complex mixtures. Here, we investigated the relative distribution in the different skin compartments. Hence, in the following sections, we base our discussion on relative amounts normalized to the total amounts of each PAH that penetrated into the skin. This also allows for a better comparison between individual PAH in the different compartments. In addition, it compensates for the relatively high deviations that were occasionally observed in the recoveries for PAHs detected in the skin and receptor compartments compared to the amounts applied to the skin (Sheet 3 of SI B).

3.1. Distribution of dermally applied polycyclic aromatic hydrocarbons in human and pigskin

The more lipophilic the PAH, the more it is retained by the s.c. (see Fig. 1 for incubation time of 24 h; for other incubation times in pigskin, see Figure A.3, SI A). When skin migration of B[a]P and dibenzopyrenes was compared in a previous study, a similar effect was observed (Bartsch et al., 2016). Since log$P$ and M of the investigated PAH are correlated linearly, these results can be equally interpreted for the molar mass. However, since hydrophilic substances exceeding M of the most massive PAH investigated in this study were shown to efficiently permeate the skin (Ellison et al., 2020, 2021; Potts and Guy, 1992), lipophilicity is presumably a more relevant factor.

We recently demonstrated that partition coefficients characterizing the distribution of PAH between squalane and the s.c. are dependent on M and log$P$ of the respective PAH (Simon et al., 2023b). Highly lipophilic PAH partition more readily from this lipophilic matrix (log$P$ = 15.6, ACD/Labs, 2021) into the s.c. Therefore, a similar but more pronounced trend is expected for acetonitrile (log$P$ = −0.3, PubChem, 2023a), since more lipophilic compounds should partition more readily from this rather polar solvent into the hydrophobic s.c. Similarly, partition coefficients of a wide range of lipophilic (log$P$ > 3) substances for aqueous matrices and the s.c. were shown to positively correlate with log$P$ (Figure A.4 in SI A). Regarding PAH permeation into deeper skin layers, the influence of the application medium should be less relevant. However, during incubation, acetonitrile could have penetrated into the skin, selectively enhancing the permeation of smaller, less lipophilic PAH.

Since the s.c. is a relatively lipophilic matrix (Raykar et al., 1988), more lipophilic PAH should also be retained more efficiently by the s.c.

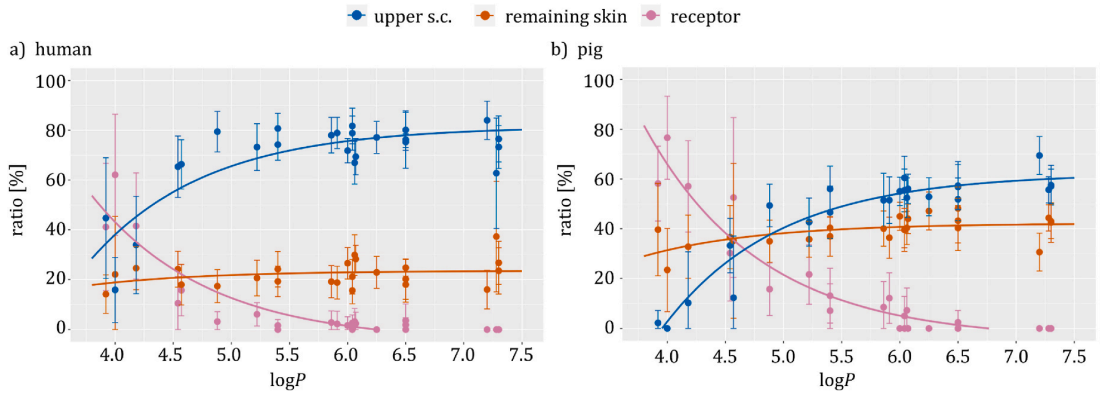

Fig. 1. Distribution ratio of polycyclic aromatic hydrocarbons in each compartment to total amount found in the skin (*stratum corneum* (s.c.), remaining skin) and receptor fluid after 24 h incubation time *versus* logarithmic octanol-water partition coefficient (log$P$). Means ± standard deviation. Curves represent data fitted to equation (1). a) Human skin (n = 13). b) Pigskin (n = 9). For other incubation times in pigskin (n = 3), see SI A, Figure A3.

at the s.c./viable epidermis boundary layer. This was confirmed experimentally: after 24 h incubation time, PAH with lower log*P* permeate the entire viable (epi-)dermis and are detected predominantly in the receptor fluid of the FDC. This effect is stronger for pigskin than for human skin. Contrarily, large PAH do not permeate the skin completely within the investigated time frame and were not found in the receptor fluid. Alternative receptor solutions that include solubility enhancers such as, for example, albumin might better dissolve these highly lipophilic PAH. Nonetheless, only minor permeation was observed even at very high applied dermal doses in the range of 6 μg/cm^2 when 50 mg/ml BSA were included in the receptor solution (Simon et al., 2023b). Since the rather aqueous layers of the viable epidermis and dermis are localized below the s.c., lipophilic substances would still have to overcome this barrier.

The ratio of the amount of each PAH in the three compartments — upper s.c., remaining skin and receptor fluid — can be approximated by fitting equation (1) to the data (Fig. 1; parameters: SI B, Sheet 4). When plotted, these curves help visualize the dependence of individual distribution ratios on log*P*. Furthermore, they show that the distribution ratios of PAH in each compartment approach a limit at about log*P* = 6.0. The distribution does not further change for larger PAH, regardless of the biological species (pig or human). A possible explanation could be favored partitioning of more lipophilic PAH into the rather lipophilic s.c. as opposed to the more aqueous epidermis beneath. Another hypothesis is a difference in the interaction with skin proteins. If larger PAH have higher affinities to these proteins, they would also be retained stronger. In principle, further physico-chemical properties could also modulate the penetration process. For example, it was shown that the molecular volume correlates with the flux of PAH through the skin, although we found no statistically relevant differences in our data (Alalaiwe et al., 2020).

The fraction detected in the remaining skin does not change substantially with log*P* values for either human or pigskin. The applied tape stripping procedure involving five tape strips only removes the five upper s.c. layers from the remaining skin (Simon et al., 2023a), which thus contains a large part of the s.c. as well as the s.c./viable epidermis boundary layer. Hence, both small and medium PAH that penetrate into the viable epidermis as well as large PAH, that are predominantly retained in the s.c. are found in this compartment.

3.2. Comparison of PAH permeation through human and pigskin

Human skin retains small PAH more effectively than pigskin. This is reflected in the greater share of small PAH in the receptor fluid after an incubation time of 24 h in pigskin than in human skin (Fig. 1). The same is true for the amount residing in the remaining skin, which on average is lower for human skin. These results are in accordance with previous studies on lipophilic compounds. For example, a study on heptane, hexadecane and xylene (log*P* > 3) found higher permeability coefficients for these three substances in pigskin than in human skin (Singh et al., 2002).

The regression curve (equation (1)), fitting the ratios of the relative amounts of PAH detected in human *versus* porcine s.c. as a function of log*P* asymptotically reaches a limit at 0.60 for highly lipophilic PAH (Fig. 2; values: Sheet 5, parameters of fit: Sheet 6 of SI B). Hence, for more lipophilic PAH, porcine s.c. better emulates human s.c. It was formerly demonstrated that lipids in the human s.c. are packed differently (orthorhombic lateral packing) and denser than in porcine s.c. (hexagonal lateral packing) even though the molar ratio of different lipids is approximately equal (Caussin et al., 2008). These more closely packed lipids could slow down the diffusion of smaller PAH in human s.c. Larger PAH, on the other hand, are retained more similarly by the s.c. of both species and the difference is less pronounced. We previously determined diffusion coefficients of PAH in porcine s.c., which were similar for PAH with log*P* > 4, while naphthalene (log*P* = 3.4) showed a significantly higher diffusion coefficient (Simon et al., 2023b). This might hint to a change of the diffusion mechanism above a given log*P*

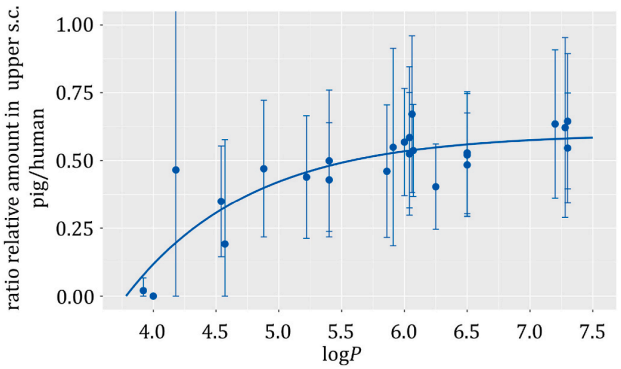

Fig. 2. Ratio of the relative amount of polycyclic aromatic hydrocarbons (PAH) found in human *stratum corneum* (s.c.) to the amount found in porcine s.c. at 24 h incubation time *versus* the logarithmic octanol-water partition coefficient (log*P*) of PAH. Means ± standard deviation. Curve represents data fitted to equation (1). Upper limit of fluorene standard deviation: 1.45.

value and thus more closely related diffusion rates in human and porcine s.c.

The anatomical site where the skin samples were obtained, however, does not seem to play a significant role in the composition of the s.c., as previous studies have shown (Khiao In et al., 2019). Furthermore, it has been reported that freezing does not significantly alter the penetration characteristics of human skin (Jacques-Jamin et al., 2017). Contrarily, pigskin was shown to be affected: freezing and storage at −20 °C increased the permeability up to 25% compared to fresh skin of the lipophilic model substance methyl salicylate (Morin et al., 2023). This is supported by a direct comparison of rat, rabbit and pigskin revealing the latter to be especially vulnerable to freezing (Sintov and Greenberg, 2014). Since we used frozen skin specimens, this effect could add to the observed higher permeation rates of PAH through pigskin compared to human skin.

3.3. Skin penetration kinetics of polycyclic aromatic hydrocarbons

In general, less lipophilic PAH permeate the skin faster than more lipophilic PAH. This is evident from the relatively high amounts of small PAH detected in the receptor compartment after incubation times of only 2 h, whereas large PAH are mostly retained by the upper s.c. up to 48 h and do not permeate into the receptor fluid at all. For example, after 2 h almost 60% of the amount of acenaphthene (a small, 2.5-ringed PAH, Fig. 3a) recovered from the skin and receptor compartments is detected in the receptor fluid and less than 20% remain in the upper s.c. Contrarily, after the same incubation time, dibenzo[*a,l*]pyrene (a large, 6-ringed PAH, Fig. 3c) is recovered to more than 75% in the upper s.c. and levels out at about 70% after 4 h, whereas it was not detectable in the receptor fluid even after 48 h. Because no considerable change in the distribution pattern was detected over a period of more than 40 h, we suspect that large PAH would not fully permeate the skin even after extended incubation times. Of note, such long exposure times are less likely to reflect realistic exposure scenarios involving PAH transfer *via* dermal contact to consumer products. Nonetheless, PAH that accumulate in the s.c. but do not penetrate deeper in the investigated time frame could form a reservoir from where migration into the skin at later time points seems possible. The turnover of s.c. cell layers is about 14 days, which leaves up to two weeks for an accumulated compound to partition into the viable skin (Milstone, 2004).

The kinetic analysis for medium PAH such as pyrene (Fig. 3b) revealed that after 2 h, only about 4% of the anmount of pyrene that penetrated into the skin reach the receptor fluid, nearly 70% are retained by the upper s.c. and 28% reside in the remaining skin. After 16

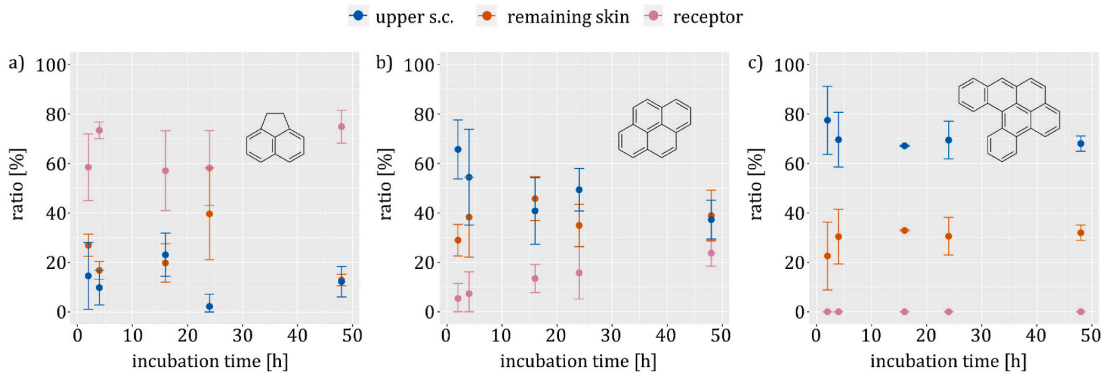

Fig. 3. Distribution ratio of selected polycyclic aromatic hydrocarbons (PAH) in each compartment to total amount found in the skin and the receptor fluid at different incubation times in pigskin. Means ± standard deviation. 24 h: $n = 9$; other incubation times: $n = 3$. a) acenaphthene (154 g/mol, log$P$ = 3.92), b) pyrene (202 g/mol, log$P$ = 4.88) and c) dibenzo[*a,l*]pyrene (302 g/mol, log$P$ = 7.20). For all other PAH, see SI A, Figures A5 to A7.

h, however, 14% reach the receptor fluid and the rest is about evenly distributed between upper s.c. and the remaining skin. After 48 h, almost a quarter of the amount of pyrene migrates into the receptor fluid. Results for skin penetration kinetics of all other investigated PAH are presented in Figures A.5–A.7 (SI A) and show similar trends.

4. Conclusion

By means of *in vitro* FDC assays involving human and pigskin, we showed that skin penetration efficiency of a broad range of PAH depends largely on log$P$, and thus, also correlates with M. At incubation times resembling time frames realistic for dermal exposure to consumer products that may be contaminated with PAH, small and to a lesser extent also medium PAH were found to reach the receptor fluid relatively fast (for example, within 2–4 h). For highly lipophilic PAH, on the other hand, the upper s.c. represents the most important barrier for permeation of PAH through the skin. These larger PAH do not partition significantly from the rather lipophilic s.c. into the more aqueous viable epidermis, and are retained effectively by the s.c. up to 48 h. This is supported by their recovery in the upper s.c. and the remaining skin, which contains a large fraction of the s.c. Since large PAH did not reach the receptor fluid in FDC assays, they would presumably not be transferred into systemic circulation *in vivo*, but eventually be removed over time by desquamation of the contaminated layers. On the other hand, formation of a reservoir in the s.c. and subsequent migration into the skin over a longer period cannot be ruled out. Furthermore, we showed that pigskin is more permeable for PAH than human skin, whereas this difference is more pronounced for small and less lipophilic PAH.

Funding

This work was funded by BfR-internal grants SFP 1322-514 and BfR-CPS-08-1322-774.

Ethics vote on the usage of human tissue

The proposal to conduct permeation studies with human skin samples was reviewed and approved by an independent ethics committee (Ethics Commission Charité, Berlin, No. EA2/090/14, July 22, 2014). Informed consent was obtained for experimentation with these skin samples from donors, respecting their privacy rights by anonymization. Experiments were in line with all relevant laws and institutional guidelines.

CRediT authorship contribution statement

Konstantin Simon: Writing – review & editing, Writing – original draft, Visualization, Investigation, Formal analysis, Conceptualization. **Nastasia Bartsch:** Methodology, Investigation, Formal analysis, Conceptualization. **Lidia Schneider:** Methodology, Investigation, Formal analysis. **Valerie van de Weijgert:** Investigation, Formal analysis. **Christoph Hutzler:** Methodology, Conceptualization. **Andreas Luch:** Writing – review & editing, Resources, Funding acquisition. **Alexander Roloff:** Writing – review & editing, Writing – original draft, Supervision.

Declaration of competing interest

The authors declare that they have no known competing financial interests or personal relationships that could have appeared to influence the work reported in this paper. We report no conflicts of interests. All data were collected at the German Federal Institut for Risk Assessment (BfR).

Data availability

All data relevant for the publication can be found in Supporting Information B.

Acknowledgements

We thank Christian Witzel from Charité, Berlin for providing us with human skin. We thank Charlotte Kromer and Franziska Riedel for fruitful discussions and Henrik Hupatz for proof reading the manuscript.

Appendix A. Supplementary data

Supplementary data to this article can be found online at https://doi.org/10.1016/j.envres.2024.119118.

References

ACD/Labs, 2021. Octanol-water partition calculation. Advanced Chemistry Development (ACD/Labs). http://www.chemspider.com/Chemical-Structure.7798.html?rid=a22a50c7-1c8c-446d-949a-5abd6fe95e4e. (Accessed 20 September 2021).

Alalaiwe, A., Lin, Y.-K., Lin, C.-H., Wang, P.-W., Lin, J.-Y., Fang, J.-Y., 2020. The absorption of polycyclic aromatic hydrocarbons into the skin to elicit cutaneous inflammation: the establishment of structure–permeation and in silico–in vitro–in vivo relationships. Chemosphere 255, 126955. https://doi.org/10.1016/j.chemosphere.2020.126955.

Alawi, M.A., Abdullah, R.A., Tarawneh, I., 2018. Determination of polycyclic aromatic hydrocarbons (PAHs) in carbon black-containing plastic consumer products from the Jordanian market. Toxin Rev. 37, 269–277. https://doi.org/10.1080/15569543.2017.1359628.

Barbero, A.M., Frasch, H.F., 2009. Pig and Guinea pig skin as surrogates for human in vitro penetration studies: a quantitative review. Toxicol. Vitro 23, 1–13. https://doi.org/10.1016/j.tiv.2008.10.008.

Bartsch, N., 2018. In: Polymer additives, contaminants and non-intentionally added substances in consumer products. Combined migration, permeation and toxicity analyses in skin. Freie Universität, Berlin.

Bartsch, N., Heidler, J., Vieth, B., Hutzler, C., Luch, A., 2016. Skin permeation of polycyclic aromatic hydrocarbons: a solvent-based in vitro approach to assess dermal exposures against benzo[a]pyrene and dibenzopyrenes. J. Occup. Environ. Hyg. 13, 969–979. https://doi.org/10.1080/15459624.2016.1200724.

Bartsch, N., Hutzler, C., Vieth, B., Luch, A., 2017. Target analysis of polycyclic aromatic hydrocarbons (PAHs) in consumer products and total content of polycyclic aromatic compounds (PACs). Polycycl. Aromat. Comp. 37, 114–121. https://doi.org/10.1080/10406638.2016.1189440.

Boffetta, P., Jourenkova, N., Gustavsson, P., 1997. Cancer risk from occupational and environmental exposure to polycyclic aromatic hydrocarbons. Cancer Causes Control 8, 444–472. https://doi.org/10.1023/A:1018465507029.

Bourgart, E., Persoons, R., Marques, M., Rivier, A., Balducci, F., von Koschembahr, A., Béal, D., Leccia, M.-T., Douki, T., Maitre, A., 2019. Influence of exposure dose, complex mixture, and ultraviolet radiation on skin absorption and bioactivation of polycyclic aromatic hydrocarbons ex vivo. Arch. Toxicol. 93, 2165–2184. https://doi.org/10.1007/s00204-019-02504-8.

Burstyn, I., Kromhout, H., Partanen, T., Svane, O., Langård, S., Ahrens, W., Kauppinen, T., Stücker, I., Shaham, J., Heederik, D., Ferro, G., Heikkilä, P., Hooiveld, M., Johansen, C., Randem, B.G., Boffetta, P., 2005. Polycyclic aromatic hydrocarbons and fatal ischemic heart disease. Epidemiology 16, 744–750. https://doi.org/10.1097/01.ede.0000181310.65043.2f.

BVL, 2017. Berichte zur Lebensmittelsicherheit Monitoring 2017. German Federal Office of Consumer Protection and Food Safety (BVL).

Caussin, J., Gooris, G.S., Janssens, M., Bouwstra, J.A., 2008. Lipid organization in human and porcine stratum corneum differs widely, while lipid mixtures with porcine ceramides model human stratum corneum lipid organization very closely. Biochim. Biophys. Acta 1778, 1472–1482. https://doi.org/10.1016/j.bbamem.2008.03.003.

Collins, J., Brown, J., Alexeeff, G., Salmon, A., 1998. Potency equivalency factors for some polycyclic aromatic hydrocarbons and polycyclic aromatic hydrocarbon derivatives. Regul. Toxicol. Pharmacol. 28, 45–54. https://doi.org/10.1006/rtph.1998.1235.

EC, 2006. Regulation No. 1907/2006 (REACH). European Commission (EC).

EC, 2013. Regulation No. 1272/2013 Annex XVII to Regulation (EC) No. 1907/2006 (REACH). European Commission (EC).

EC, 2023. Regulation No. 2023/915 of 25 April 2023 on Maximum Levels for Certain Contaminants in Food and Repealing Regulation (EC) No. 1881/2006 (Text with EEA Relevance). European Commission (EC).

Ellison, C.A., Tankersley, K.O., Obringer, C.M., Carr, G.J., Manwaring, J., Rothe, H., Duplan, H., Géniès, C., Grégoire, S., Hewitt, N.J., 2020. Partition coefficient and diffusion coefficient determinations of 50 compounds in human intact skin, isolated skin layers and isolated stratum corneum lipids. Toxicol. Vitro 69, 104990. https://doi.org/10.1016/j.tiv.2020.104990.

Ellison, C.A., Tankersley, K.O., Obringer, C.M., Carr, G.J., Manwaring, J., Rothe, H., Duplan, H., Géniès, C., Grégoire, S., Hewitt, N.J., 2021. Corrigendum to partition coefficient and diffusion coefficient determinations of 50 compounds in human intact skin, isolated skin layers and isolated stratum corneum lipids. Toxicol. Vitro 71, 105050. https://doi.org/10.1016/j.tiv.2020.105050.

Folgado de Lucena, A., Senaldi, C., Tirendi, S., Bianchi, I., Barahona, F., Barrero-Moreno, J., Aguar-Fernandez, P., Mainardi, G., Geiss, O., Leva, P., 2018. Migration of Polycyclic Aromatic Hydrocarbons (PAHs) from Plastic and Rubber Articles – Final Report on the Development of a Migration Measurement Method. European Commission Joint Research Centre Publications Office.

Franz, T.J., 1975. Percutaneous absorption. On the relevance of in vitro data. J. Invest. Dermatol. 64, 190–195. https://doi.org/10.1111/1523-1747.ep12533356.

Gerstel, D., Jacques-Jamin, C., Schepky, A., Cubberley, R., Eilstein, J., Grégoire, S., Hewitt, N., Klaric, M., Rothe, H., Duplan, H., 2016. Comparison of protocols for measuring cosmetic ingredient distribution in human and pig skin. Toxicol. Vitro 34, 153–160. https://doi.org/10.1016/j.tiv.2016.03.012.

Hagvall, L., Pour, M.D., Feng, J., Karma, M., Hedberg, Y., Malmberg, P., 2021. Skin permeation of nickel, cobalt and chromium salts in ex vivo human skin, visualized using mass spectrometry imaging. Toxicol. Vitro 76, 105232. https://doi.org/10.1016/j.tiv.2021.105232.

Haney, J.T., Forsberg, N.D., Hoeger, G.C., Magee, B.H., Meyer, A.K., 2020. Risk assessment implications of site-specific oral relative bioavailability factors and dermal absorption fractions for polycyclic aromatic hydrocarbons in surface soils impacted by clay skeet target fragments. Regul. Toxicol. Pharmacol. 113, 104649 https://doi.org/10.1016/j.yrtph.2020.104649.

Herkenne, C., Naik, A., Kalia, Y.N., Hadgraft, J., Guy, R.H., 2006. Pig ear skin ex vivo as a model for in vivo dermatopharmacokinetic studies in man. Pharm. Res. (N. Y.) 23, 1850–1856. https://doi.org/10.1007/s11095-006-9011-8.

Hoorn, E.J., 2017. Intravenous fluids: balancing solutions. J. Nephrol. 30, 485–492. https://doi.org/10.1007/s40620-016-0363-9.

Hopf, N., Champmartin, C., Schenk, L., Berthet, A., Chedik, L., Du Plessis, J., Franken, A., Frasch, F., Gaskin, S., Johanson, G., 2020. Reflections on the OECD guidelines for in vitro skin absorption studies. Regul. Toxicol. Pharmacol., 104752 https://doi.org/10.1016/j.yrtph.2020.104752.

Hopf, N.B., Spring, P., Hirt-Burri, N., Jimenez, S., Sutter, B., Vernez, D., Berthet, A., 2018. Polycyclic aromatic hydrocarbons (PAHs) skin permeation rates change with simultaneous exposures to solar ultraviolet radiation (UV-S). Toxicol. Lett. 287, 122–130. https://doi.org/10.1016/j.toxlet.2018.01.024.

Hutzler, C., Luch, A., Filser, J.G., 2011. Analysis of carcinogenic polycyclic aromatic hydrocarbons in complex environmental mixtures by LC-APPI-MS/MS. Anal. Chim. Acta 702, 218–224. https://doi.org/10.1016/j.aca.2011.07.003.

IARC, 2010. Some non-heterocyclic polycyclic aromatic hydrocarbons and some related exposures. In: IARC Monographs on the Evaluation of Carcinogenic Risks to Humans. International Agency for Research on Cancer (IARC).

IARC, 2018. Agents Classified by the IARC Monographs, Volumes 1–113. International Agency for Research on Cancer (IARC). https://monographs.iarc.who.int/agents-classified-by-the-iarc/. (Accessed 13 August 2021).

Jacques-Jamin, C., Duplan, H., Rothe, H., Vaillant, O., Eilstein, J., Grégoire, S., Cubberley, R., Lange, D., Ellison, C., Klaric, M., Hewitt, N., Schepky, A., 2017. Comparison of the skin penetration of 3 metabolically stable chemicals using fresh and frozen human skin. Skin Pharmacol. Physiol. 30, 234–245. https://doi.org/10.1159/000475472.

Kamal, A., Cincinelli, A., Martellini, T., Malik, R.N., 2015. A review of PAH exposure from the combustion of biomass fuel and their less surveyed effect on the blood parameters. Environ. Sci. Pollut. Control Ser. 22, 4076–4098. https://doi.org/10.1007/s11356-014-3748-0.

Khiao In, M., Richardson, K.C., Loewa, A., Hedtrich, S., Kaessmeyer, S., Plendl, J., 2019. Histological and functional comparisons of four anatomical regions of porcine skin with human abdominal skin. Anat. Histol. Embryol. 48, 207–217. https://doi.org/10.1111/ahe.12425.

Kim, K.-H., Jahan, S.A., Kabir, E., Brown, R.J.C., 2013. A review of airborne polycyclic aromatic hydrocarbons (PAHs) and their human health effects. Environ. Int. 60, 71–80. https://doi.org/10.1016/j.envint.2013.07.019.

Lao, J.-Y., Bao, L.-J., Zeng, E.Y., 2018a. Correction to importance of dermal absorption of polycyclic aromatic hydrocarbons derived from barbecue fumes. Environ. Sci. Technol. 52, 11439–11440. https://doi.org/10.1021/acs.est.8b04782.

Lao, J.-Y., Xie, S.-Y., Wu, C.-C., Bao, L.-J., Tao, S., Zeng, E.Y., 2018b. Importance of dermal absorption of polycyclic aromatic hydrocarbons derived from barbecue fumes. Environ. Sci. Technol. 52, 8330–8338. https://doi.org/10.1021/acs.est.8b01689.

Lee, C.M., Jin, S.P., Doh, E.J., Lee, D.H., Chung, J.H., 2019. Regional variation of human skin surface temperature. Ann. Dermatol. 31, 349–352. https://doi.org/10.5021/ad.2019.31.3.349.

Lemoine, L., Bayrambey, D., Roloff, A., Hutzler, C., Luch, A., Tralau, T., 2021. Commensal-related changes in the epidermal barrier function lead to alterations in the benzo[a]pyrene metabolite profile and its distribution in 3D skin. mBio 12. https://doi.org/10.1128/mbio.01223-21.

Lu, G.-N., Tao, X.-Q., Dang, Z., Yi, X.-Y., Yang, C., 2008. Estimation of n-octanol/water partition coefficients of polycyclic aromatic hydrocarbons by quantum chemical descriptors. Open Chem. 6, 310–318. https://doi.org/10.2478/s11532-008-0010-y.

Milstone, L.M., 2004. Epidermal desquamation. J. Dermatol. Sci. 36, 131–140. https://doi.org/10.1016/j.jdermsci.2004.05.004.

Moody, R.P., Tytchino, A.V., Yip, A., Petrovic, S., 2011. A novel “by difference” method for assessing dermal absorption of polycyclic aromatic hydrocarbons from soil at federal contaminated sites. J. Toxicol. Environ. Health 74, 1294–1303. https://doi.org/10.1080/15287394.2011.589104. A.

Morin, M., Runnsjö, A., Ruzgas, T., Engblom, J., Björklund, S., 2023. Effects of storage conditions on permeability and electrical impedance properties of the skin barrier. Int. J. Pharm. 637, 122891 https://doi.org/10.1016/j.ijpharm.2023.122891.

Ng, S.-F., Rouse, J.J., Sanderson, F.D., Meidan, V., Eccleston, G.M., 2010. Validation of a static Franz diffusion cell system for in vitro permeation studies. AAPS PharmSciTech 11, 1432–1441. https://doi.org/10.1208/s12249-010-9522-9.

OECD, 2004. Guideline for the Testing of Chemicals No. 428: Skin Absorption: *in Vitro* Method. Organisation for Economic Co-operation and Development (OECD).

OECD, 2011. Health and Safety Publications Series on Testing and Assessment No. 156: Guidance Notes on Dermal Absorbtion. Organisation for Economic Co-operation and Development (OECD).

Potts, R.O., Guy, R.H., 1992. Predicting skin permeability. Pharm. Res. (N. Y.) 9, 663–669. https://doi.org/10.1023/A:1015810312465.

PubChem, 2023a. Compound Summary for CID 6342, Acetonitrile. National Center for Biotechnology Information. https://pubchem.ncbi.nlm.nih.gov/compound/Acetonitrile. (Accessed 21 August 2023).

PubChem, 2023b. Compound Summary for CID 9106, Dibenzo[a,i]pyrene. National Center for Biotechnology Information. https://pubchem.ncbi.nlm.nih.gov/compound/Dibenzo_A_I_pyrene. (Accessed 11 July 2023).

PubChem, 2023c. Compound Summary for CID 9108, Dibenzo[a,h]pyrene. National Center for Biotechnology Information. https://pubchem.ncbi.nlm.nih.gov/compound/Dibenzo_A_H_pyrene. (Accessed 11 July 2023).

PubChem, 2023d. Compound Summary for CID 9119, Dibenzo[a,l]pyrene. National Center for Biotechnology Information. https://pubchem.ncbi.nlm.nih.gov/compound/Dibenzo_a_l_pyrene. (Accessed 11 July 2023).

PubChem, 2023e. Compound Summary for CID 9126, Dibenzo[a,e]pyrene. National Center for Biotechnology Information. https://pubchem.ncbi.nlm.nih.gov/compound/Dibenzo_a_e_pyrene. (Accessed 11 July 2023).

Raykar, P.V., Fung, M.C., Anderson, B.D., 1988. The role of protein and lipid domains in the uptake of solutes by human stratum corneum. Pharm. Res. (N. Y.) 5, 140–150. https://doi.org/10.1023/a:1015956705293.

Rocha, P.R.S., Oliveira, V.D., Vasques, C.I., dos Reis, P.E.D., Amato, A.A., 2021. Exposure to endocrine disruptors and risk of breast cancer: a systematic review. Crit. Rev. Oncol. Hematol. 161, 103330 https://doi.org/10.1016/j.critrevonc.2021.103330.

Rothe, H., Obringer, C., Manwaring, J., Avci, C., Wargniez, W., Eilstein, J., Hewitt, N., Cubberley, R., Duplan, H., Lange, D., 2017. Comparison of protocols measuring diffusion and partition coefficients in the stratum corneum. J. Appl. Toxicol. 37, 806–816. https://doi.org/10.1002/jat.3427.

Sartorelli, P., Aprea, C., Cenni, A., Novelli, M.T., Orsi, D., Palmi, S., Matteucci, G., 1998. Prediction of percutaneous absorption from physicochemical data: a model based on data of in vitro experiments. Ann. Occup. Hyg. 42, 267–276. https://doi.org/10.1016/S0003-4878(98)00021-0.

Sartorelli, P., Cenni, A., Matteucci, G., Montomoli, L., Novelli, M.T., Palmi, S., 1999. Dermal exposure assessment of polycyclic aromatic hydrocarbons: in vitro percutaneous penetration from lubricating oil. Int. Arch. Occup. Environ. Health 72, 528–532. https://doi.org/10.1007/s004200050411.

Sartorelli, P., Montomoli, L., Sisinni, A.G., Bussani, R., Cavallo, D., Foá, V., 2001. Dermal exposure assessment of polycyclic aromatic hydrocarbons: in vitro percutaneous penetration from coal dust. Toxicol. Ind. Health 17, 17–21. https://doi.org/10.1191/0748233701th092oa.

SCCS, 2010. Basic criteria for the in vitro assessment of dermal absorption of cosmetic ingredients. Scientific Committee on Consumer Safety (SCCS). 7th plenary meeting.

Simon, G.A., Maibach, H.I., 2000. The pig as an experimental animal model of percutaneous permeation in man: qualitative and quantitative observations–an overview. Skin Pharmacol. Appl. Skin Physiol. 13, 229–234. https://doi.org/10.1159/000029928.

Simon, K., Oberender, G., Roloff, A., 2023a. Continuous removal of single cell layers by tape stripping the stratum corneum – a histological study. Eur. J. Pharm. Biopharm. 188, 48–53. https://doi.org/10.1016/j.ejpb.2023.04.022.

Simon, K., Schneider, L., Oberender, G., Pirow, R., Hutzler, C., Luch, A., Roloff, A., 2023b. Migration of polycyclic aromatic hydrocarbons from a polymer surrogate through the stratum corneum layer of the skin. Ecotoxicol. Environ. Saf. 262, 115113 https://doi.org/10.1016/j.ecoenv.2023.115113.

Singh, S., Zhao, K., Singh, J., 2002. In vitro permeability and binding of hydrocarbons in pig ear and human abdominal skin. Drug Chem. Toxicol. 25, 83–92. https://doi.org/10.1081/dct-100108474.

Sintov, A.C., Greenberg, I., 2014. Comparative percutaneous permeation study using caffeine-loaded microemulsion showing low reliability of the frozen/thawed skin models. Int J Pharm 471, 516–524. https://doi.org/10.1016/j.ijpharm.2014.05.040.

Sousa, G., Teixeira, J., Delerue-Matos, C., Sarmento, B., Morais, S., Wang, X., Rodrigues, F., Oliveira, M., 2022. Exposure to PAHs during firefighting activities: a review on skin levels, in vitro/in vivo bioavailability, and health risks. Int. J. Environ. Res. Publ. Health 19. https://doi.org/10.3390/ijerph191912677.

US-EPA, 2012. Estimation Program Interface (EPI) Suite. United States Environmental Protection Agency (US-EPA). https://www.epa.gov/tsca-screening-tools/download-episuitetm-estimation-program-interface-v411 (Accessed 25 March 2021).

US-EPA, 2021. National Primary Drinking Water Regulations. United States Environmental Protection Agency (US-EPA). https://www.epa.gov/ground-water-and-drinking-water/national-primary-drinking-water-regulations#one. (Accessed 26 August 2021).

van Grevenynghe, J., Bernard, M., Langouet, S., Le Berre, C., Fest, T., Fardel, O., 2005. Human CD34-positive hematopoietic stem cells constitute targets for carcinogenic polycyclic aromatic hydrocarbons. J. Pharmacol. Exp. Therapeut. 314, 693–702. https://doi.org/10.1124/jpet.105.084780.

Whitehead, T., Metayer, C., Gunier, R.B., Ward, M.H., Nishioka, M.G., Buffler, P., Rappaport, S.M., 2011. Determinants of polycyclic aromatic hydrocarbon levels in house dust. J. Expo. Sci. Environ. Epidemiol. 21, 123–132. https://doi.org/10.1038/jes.2009.68.

WHO, 2010. Guidelines for Indoor Air Quality: Selected Pollutants. WHO European Centre for Environment and Health. World Health Organization (WHO.

Zhang, Y., Dong, S., Wang, H., Tao, S., Kiyama, R., 2016. Biological impact of environmental polycyclic aromatic hydrocarbons (ePAHs) as endocrine disruptors. Environ. Pollut. 213, 809–824. https://doi.org/10.1016/j.envpol.2016.03.050.

Supporting Information A: Polycyclic aromatic hydrocarbon permeation efficiency *in vitro* is lower through human than pigskin and decreases with lipophilicity

A1 Investigated polcyclic aromatic hydrocarbons and selected physico-chemical properties

Table A.1: Investigated polycyclic aromatic hydrocarbons. Chemical Abstracts Service Registry Number (CAS), internal standard (IStd) attributed in GC-MS/MS analysis, molar mass (M), number of ring systems (five-membered rings are counted as half), logarithmic octanol-water partition coefficient (log$P$), log$P$ experimentally derived (exp) or calculated (calc) and reference (Ref.) for log$P$. GC-MS/MS: gas chromatography coupled to tandem mass spectrometry.

substance	**CAS**	**IStd**	***M* [g/mol]**	**rings**	**log*P***	**exp/calc log*P***	**Ref. log*P***
acenaphthylene	208-96-8	acenaphthylene-d_8	152	2.5	4.00	exp	[1]
acenapthene	83-32-9	acenaphthylene-d_8	154	2.5	3.92	exp	[1]
fluorene	86-73-7	fluoranthene-d_{10}	166	2.5	4.18	exp	[1]
anthracene	120-12-7	phenanthrene-d_{10}	178	3	4.54	exp	[1]
phenanthrene	85-01-8	phenanthrene-d_{10}	178	3	4.57	exp	[1]
pyrene	129-00-0	pyrene-d_{10}	202	4	4.88	exp	[1]
fluoranthene	206-44-0	fluoranthene-d_{10}	202	3.5	5.22	exp	[1]
benzo[*c*]fluorene	205-12-9	pyrene-d_{10}	216	3.5	5.40	calc	[2]
cyclopenta[*cd*]pyrene	27208-37-3	chrysene-d_{12}	226	4.5	5.40	calc	[2]
chrysene	218-01-9	chrysene-d_{12}	228	4	5.86	exp	[1]
benz[*a*]anthracene	56-55-3	chrysene-d_{12}	228	4	5.91	exp	[1]
benzo[*k*]fluoranthene	207-08-9	benzo[*a*]pyrene-d_{12}	252	4.5	6.00	exp	[2]
benzo[*a*]pyrene	50-32-8	benzo[*a*]pyrene-d_{12}	252	5	6.04	exp	[1]
benzo[*e*]pyrene	192-97-2	benzo[*a*]pyrene-d_{12}	252	5	6.04	calc	[2]
benzo[*b*]fluoranthene	205-99-2	benzo[*a*]pyrene-d_{12}	252	4.5	6.06	exp	[1]
benzo[*j*]fluoranthene	205-82-3	benzo[*a*]pyrene-d_{12}	252	4.5	6.07	calc	[2]
perylene	198-55-0	benzo[*a*]pyrene-d_{12}	252	5	6.25	exp	[1]
benzo[*ghi*]perylene	191-24-2	benzo[*ghi*]perylene-d_{12}	276	6	6.50	exp	[1]
indeno[1,2,3-*cd*]pyrene	193-39-5	benzo[*ghi*]perylene-d_{12}	276	5.5	6.50	exp	[1]
dibenz[*a,h*]anthracene	53-70-3	benzo[*ghi*]perylene-d_{12}	278	5	6.50	calc	[3]
dibenzo[*a,l*]pyrene	191-30-0	dibenzo[*a,i*]pyrene-d_{14}	302	6	7.20	calc	[4]
dibenzo[*a,h*]pyrene	189-64-0	dibenzo[*a,i*]pyrene-d_{14}	302	6	7.28	calc	[5]
dibenzo[*a,e*]pyrene	192-65-4	dibenzo[*a,i*]pyrene-d_{14}	302	6	7.30	calc	[6]
dibenzo[*a,i*]pyrene	189-55-9	dibenzo[*a,i*]pyrene-d_{14}	302	6	7.30	calc	[7]

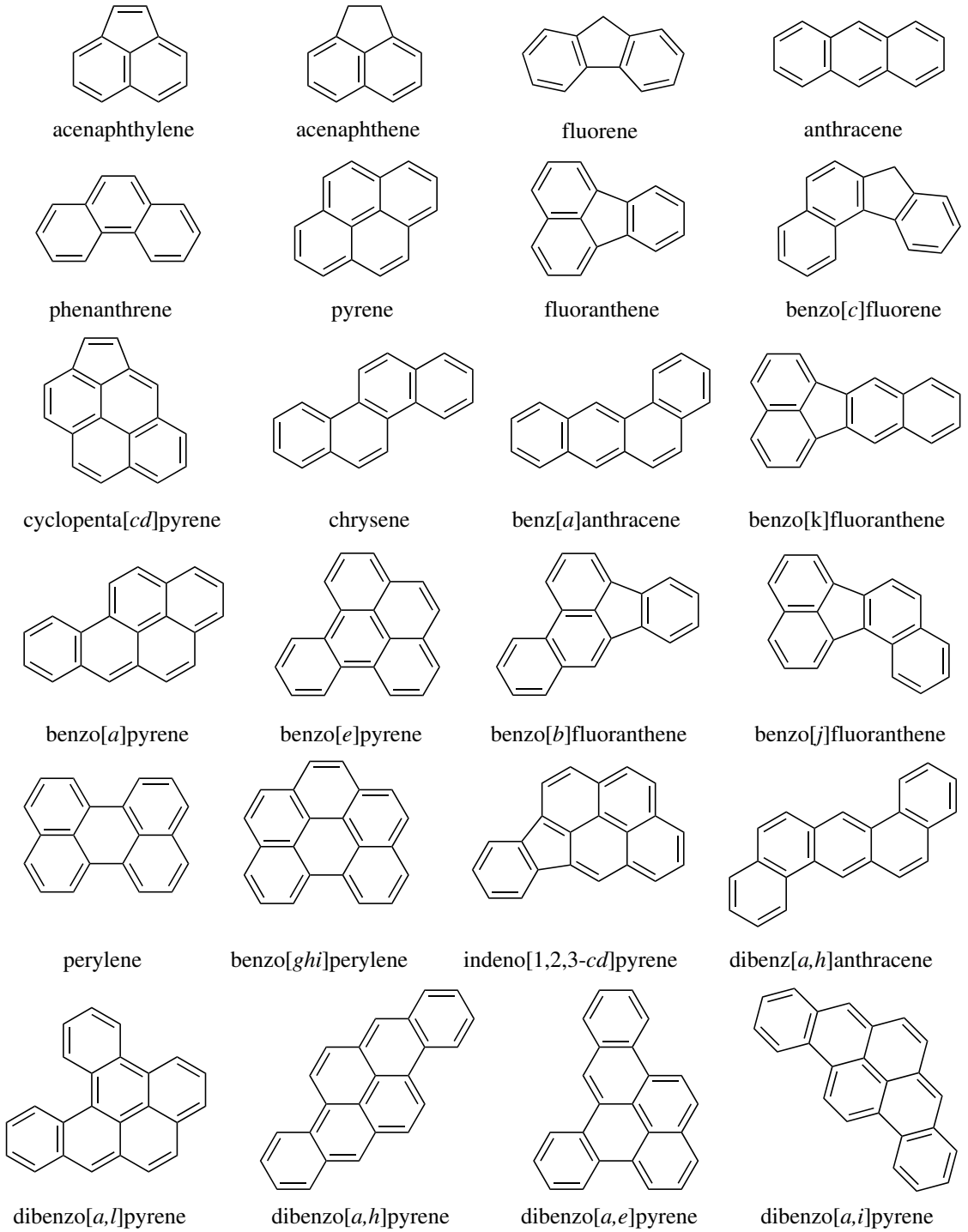

Figure A.1: Polycyclic aromatic hydrocarbons (PAH) investigated in this publication.

Linear regression of octanol-water partition coefficient ($\log P$) of 24 polycyclic aromatic hydrocarbons versus their molar mass M with coefficient of determination of $r^2 = 0.982$ (data in Table A.1.):

$$\log P = 0.0215 \frac{\text{mol}}{\text{g}} \cdot M + 0.694. \tag{A.1}$$

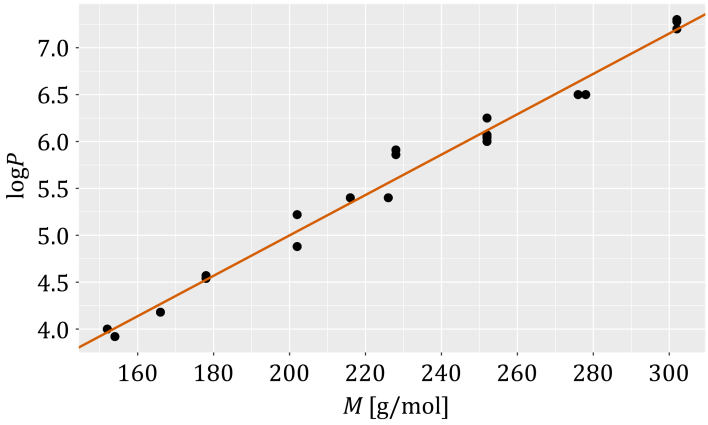

Figure A.2: Logarithmic octanol-water partition coefficient ($\log P$) of 24 polycyclic aromatic hydrocarbons versus their molar mass (M) with linear regression curve (equation (A.1)). For values, see Table A.1.

A2 Additional graphs

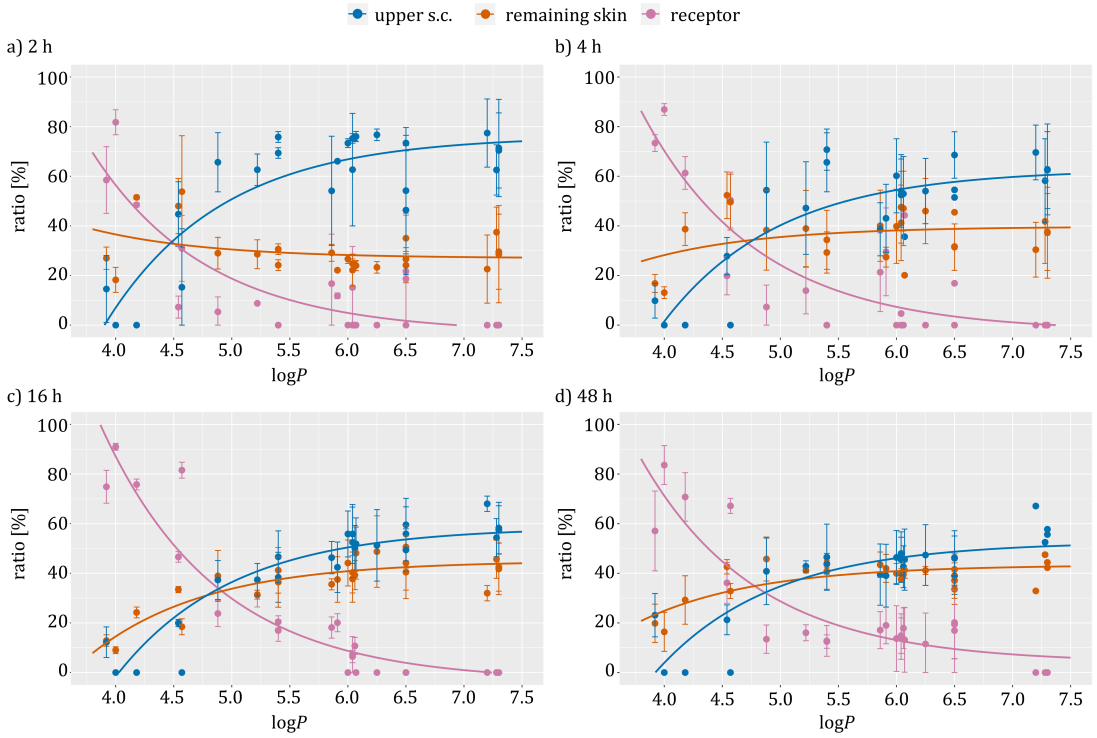

Figure A.3: Distribution ratio of polycyclic aromatic hydrocarbons in each compartment to total amount found in pigskin versus octanol water partition coefficient (log*P*). Mean ± standard deviation (24 h: $n = 9$; other incubation times: $n = 3$). Curves represent data fitted to equation (1) in the main manuscript. a) 2 h, b) 4 h, c) 16 h and d) 48 h incubation time. s.c.: *stratum corneum*.

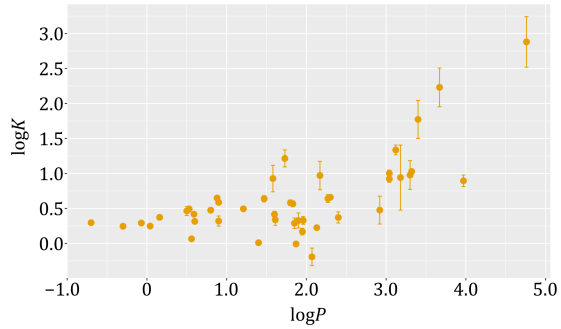

Figure A.4: Logarithmic partition coefficient (log*K*, decadic) versus logarithmic octanol/water partition coefficient (log*P*, decadic). log*K* from an aqueous medium into the *stratum corneum*. Mean ± standard deviation. log*K* data from Refs.[8, 9]. log*P* data from Pubchem (retrieved in September 2023).

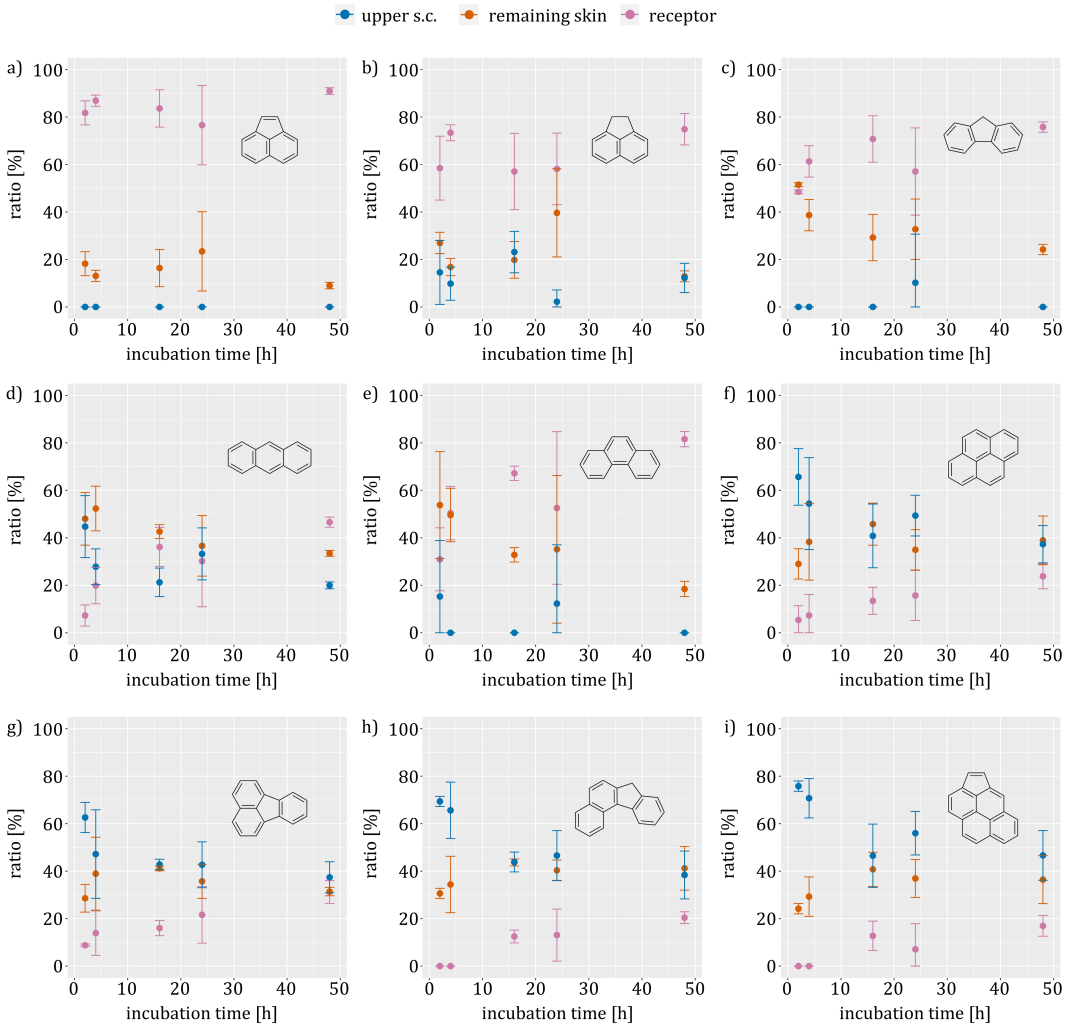

Figure A.5: Distribution ratio in each compartment to total amount found in the skin and receptor fluid at different incubation times in pigskin. Mean ± standard deviation. 24 h: $n = 9$; other incubation times: $n = 3$. a) acenaphthene, b) acenaphthylene, c) fluorene, d) anthracene, e) phenanthrene, f) pyrene, g) fluoranthene, h) benzo[*c*]fluorene and i) cyclopenta[*cd*]pyrene. s.c.: *stratum corneum*.

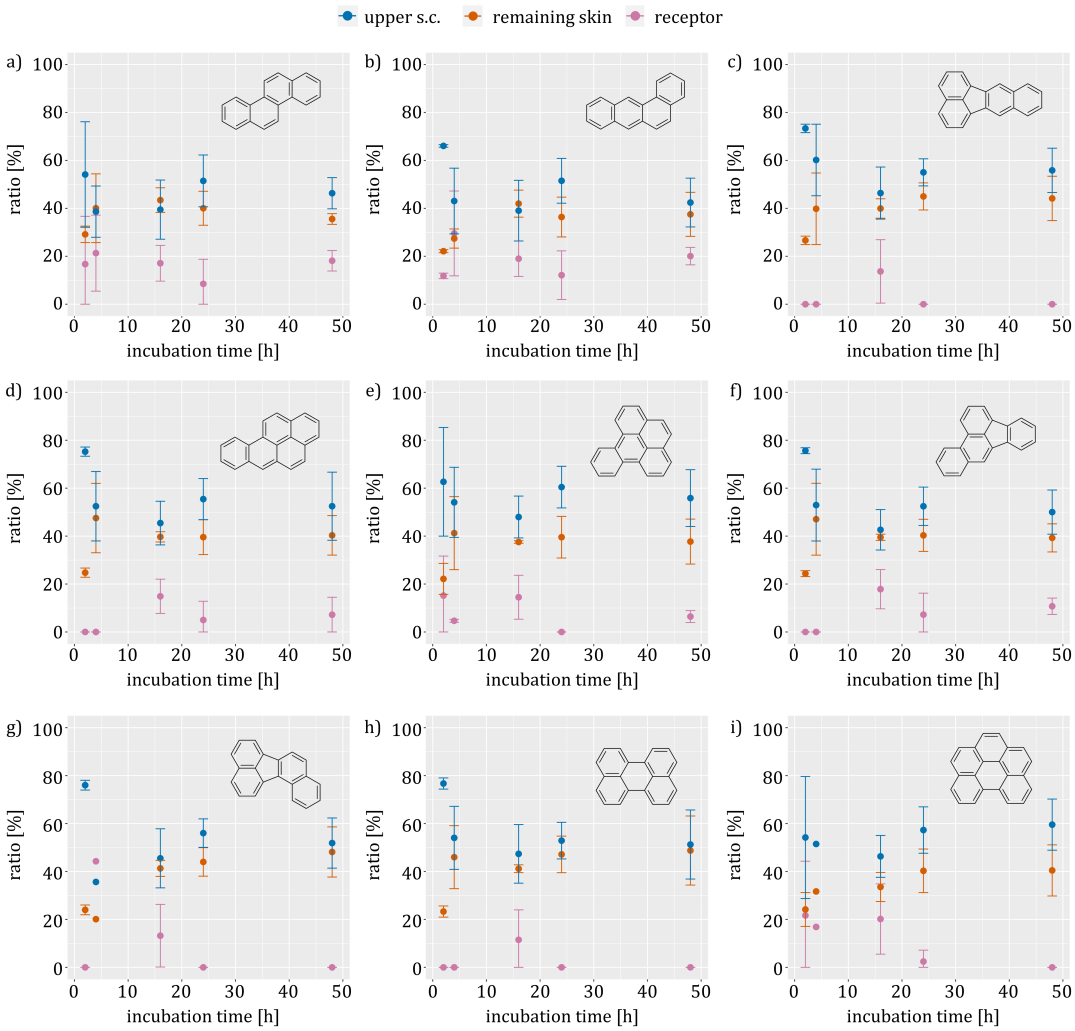

Figure A.6: Distribution ratio in each compartment to total amount found in the skin and receptor fluid at different incubation times in pigskin. Mean ± standard deviation. 24 h: $n = 9$; other incubation times: $n = 3$. a) chrysene, b) benz[*a*]anthracene, c) benzo[*k*]fluoranthene, d) benzo[*a*]pyrene, e) benzo[*e*]pyrene, f) benzo[*b*]fluoranthene, g) benzo[*j*]fluoranthene, h) perylene and i) benzo[*ghi*]perylene. s.c.: *stratum corneum*.

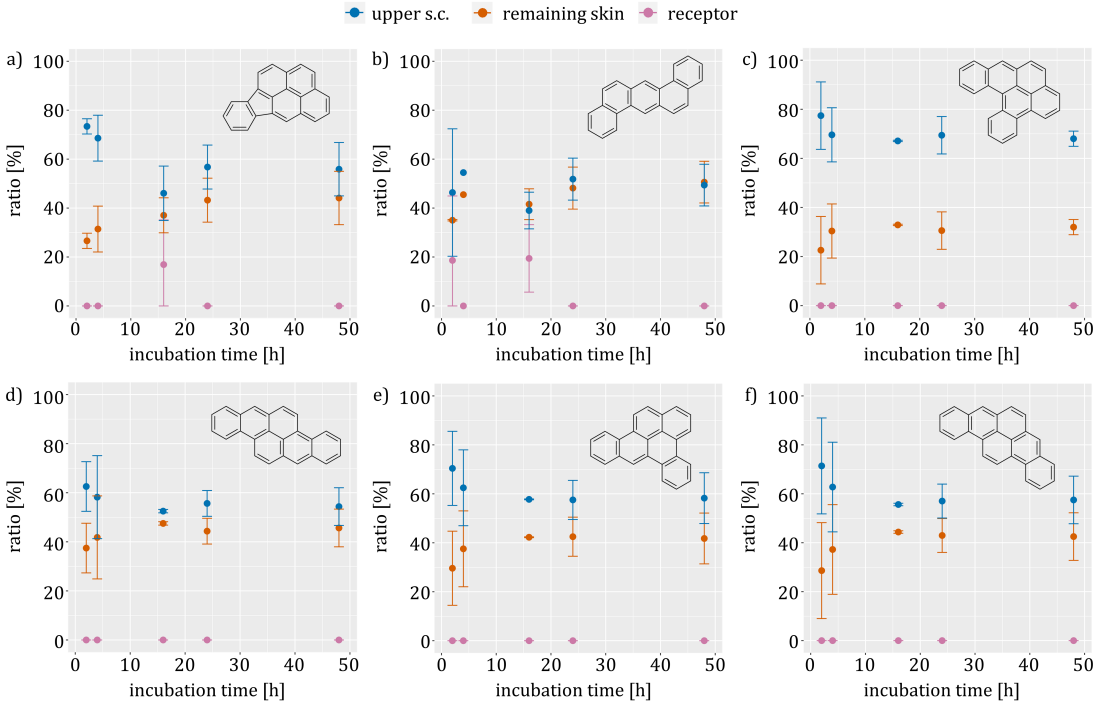

Figure A.7: Distribution ratio in each compartment to total amount found in the skin and receptor fluid at different incubation times in pigskin. Mean ± standard deviation. 24 h: $n = 9$; other incubation times: $n = 3$. a) indeno[1,2,3-*cd*]pyrene, b) dibenz[*a,h*]anthracene, c) dibenzo[*a,l*]pyrene, d) dibenzo[*a,h*]pyrene, e) dibenzo[*a,e*]pyrene and f) dibenzo[*a,i*]pyrene. s.c.: *stratum corneum*.

References

[1] G.-N. Lu, X.-Q. Tao, Z. Dang, X.-Y. Yi, C. Yang, "Estimation of n-octanol/water partition coefficients of polycyclic aromatic hydrocarbons by quantum chemical descriptors", *Open Chem.* **2008**, *6*, 310–318, doi: 10.2478/s11532-008-0010-y.

[2] F. A. de Lima Ribeiro, M. M. C. Ferreira, "QSPR models of boiling point, octanol–water partition coefficient and retention time index of polycyclic aromatic hydrocarbons", *J. Mol. Struc. THEOCHEM* **2003**, *663*, 109–126, doi: 10.1016/j.theochem.2003.08.107.

[3] National Center for Biotechnology Information, "PubChem Compound Summary for CID 5889, Dibenz[a,h]anthracene", **2023**, https://pubchem.ncbi.nlm.nih.gov/compound/Dibenz_a_h_anthracene (accessed 11 July 2023).

[4] National Center for Biotechnology Information, "PubChem Compound Summary for CID 9119, Dibenzo[a,l]pyrene", **2023**, https://pubchem.ncbi.nlm.nih.gov/compound/Dibenzo_a_l_pyrene (accessed 11 July 2023).

[5] United Stated Environmental Protection Agency (USEPA), "Estimation Program Interface (EPI) Suite", **2012**, https://www.epa.gov/tsca-screening-tools/download-epi-suitetm-estimation-program-interface-v411 (accessed 25 Mar. 2021).

[6] National Center for Biotechnology Information, "PubChem Compound Summary for CID 9126, Dibenzo[a,e]pyrene", **2023**, https://pubchem.ncbi.nlm.nih.gov/compound/Dibenzo_a_e_pyrene (accessed 11 July 2023).

[7] National Center for Biotechnology Information, "PubChem Compound Summary for CID 9106, Dibenzo[a,i]pyrene", **2023**, https://pubchem.ncbi.nlm.nih.gov/compound/Dibenzo_A_I_pyrene (accessed 11 July 2023).

[8] C. A. Ellison, K. O. Tankersley, C. M. Obringer, G. J. Carr, J. Manwaring, H. Rothe, H. Duplan, C. Géniès, S. Grégoire, N. J. Hewitt, "Partition coefficient and diffusion coefficient determinations of 50 compounds in human intact skin, isolated skin layers and isolated stratum corneum lipids", *Toxicol. In Vitro* **2020**, *69*, 104990, doi: 10.1016/j.tiv.2020.104990.

[9] C. A. Ellison, K. O. Tankersley, C. M. Obringer, G. J. Carr, J. Manwaring, H. Rothe, H. Duplan, C. Géniès, S. Grégoire, N. J. Hewitt, "Corrigendum to: Partition coefficient and diffusion coefficient determinations of 50 compounds in human intact skin, isolated skin layers and isolated stratum corneum lipids", *Toxicol. In Vitro* **2021**, *71*, 105050, doi: 10.1016/j.tiv.2020.105050.

A.3 Migration of polycyclic aromatic hydrocarbons from a polymer surrogate through the *stratum corneum* layer of the skin

Konstantin Simon, Lidia Schneider, Gila Oberender, Ralph Pirow, Christoph Hutzler, Andreas Luch, Alexander Roloff

Ecotoxicology and Environmental Safety **2023**, *262*, 115113.

doi: 10.1016/j.ecoenv.2023.115113

This study was submitted to the journal on 23 December 2022, revised on 2 June 2023 and was accepted on 4 June 2023. Published online on 12 June 2023.

The contents of this publication are discussed in Chapter 3, Section *Dermal exposure to polycyclic aromatic hydrocarbons*. The supporting information is added following the main part.

Author contributions: **Konstantin Simon:** Conceptualization, Methodology, Formal analysis, Investigation, Resources, Writing – original draft, Writing – review & editing, Visualization, Project administration. Lidia Schneider: Methodology, Formal analysis, Investigation. Gila Oberender: Formal analysis, Investigation. Ralph Pirow: Methodology, Writing – review & editing. Christoph Hutzler: Conceptualization, Methodology, Writing — review & editing. Andreas Luch: Writing — review & editing, Resources, Funding acquisition. Alexander Roloff: Conceptualization, Methodology, Formal analysis, Resources, Writing – original draft, Writing – review & editing, Supervision, Project administration, Funding acquisition.

Abstract

In this study, we determined partition ($K_{sc/m}$) and diffusion (D_{sc}) coefficients of five different polycyclic aromatic hydrocarbons (PAH) migrating from squalane into and through the stratum corneum (s.c.) layer of the skin. Carcinogenic PAH have previously been detected in numerous polymer-based consumer products, especially those dyed with carbon black. Upon dermal contact with these products, PAH may penetrate into and through the viable layers of the skin by passing the s.c. and thus may become bioavailable. Squalane, a frequent ingredient in cosmetics, has also been used as a polymer surrogate matrix in previous studies. $K_{sc/m}$ and D_{sc} are relevant parameters for risk assessment because they allow estimating the potential of a substance to become bioavailable upon dermal exposure. We developed an analytical method involving incubation of pigskin with naphthalene, anthracene, pyrene, benzo[*a*]pyrene and dibenzo[*a,h*]pyrene in

Franz diffusion cell assays under quasi-infinite dose conditions. PAH were subsequently quantified within individual s.c. layers by gas chromatography coupled to tandem mass spectrometry. The resulting PAH depth profiles in the s.c. were fitted to a solution of Fick's second law of diffusion, yielding $K_{sc/m}$ and D_{sc}. The decadic logarithm $\log K_{sc/m}$ ranged from –0.43 to +0.69 and showed a trend to higher values for PAH with higher molecular masses. D_{sc}, on the other hand, was similar for the four higher molecular mass PAH but about 4.6-fold lower than for naphthalene. Moreover, our data suggests that the s.c./viable epidermis boundary layer represents the most relevant barrier for the skin penetration of higher molecular mass PAH. Finally, we empirically derived a mathematical description of the concentration depth profiles that better fits our data. We correlated the resulting parameters to substance specific constants such as the logarithmic octanol-water partition coefficient $\log P$, $K_{sc/m}$ and the removal rate at the s.c./viable epidermis boundary layer.

Graphical Abstract

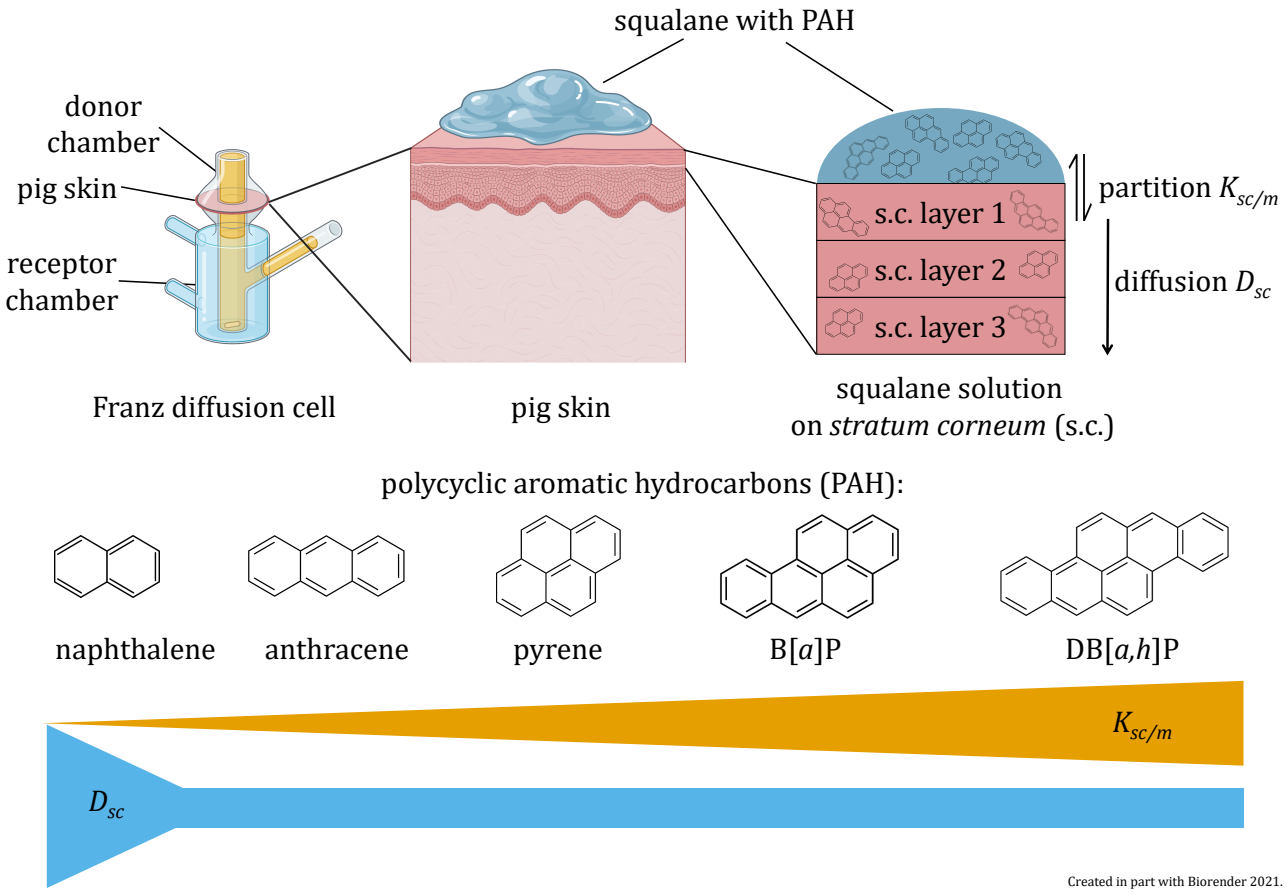

Ecotoxicology and Environmental Safety 262 (2023) 115113

Contents lists available at ScienceDirect

Ecotoxicology and Environmental Safety

journal homepage: www.elsevier.com/locate/ecoenv

Migration of polycyclic aromatic hydrocarbons from a polymer surrogate through the *stratum corneum* layer of the skin

Konstantin Simon [a,b,*], Lidia Schneider [a], Gila Oberender [a,c], Ralph Pirow [a], Christoph Hutzler [a], Andreas Luch [a,b], Alexander Roloff [a,**]

[a] German Federal Institute for Risk Assessment (BfR), Department of Chemical and Product Safety, Max-Dohrn-Str. 8–10, 10589 Berlin, Germany
[b] Department of Biology, Chemistry, Pharmacy, Institute of Pharmacy, Freie Universität Berlin, Königin-Luise-Str. 2–4, 14195 Berlin, Germany
[c] Berliner Hochschule für Technik (BHT), Luxemburger Str. 10, 13353 Berlin, Germany

ARTICLE INFO

Editor: Dr Hyo-Bang Moon

Keywords:
stratum corneum
skin migration
polycyclic aromatic hydrocabons (PAH)
partition
diffusion

ABSTRACT

In this study, we determined partition ($K_{sc/m}$) and diffusion (D_{sc}) coefficients of five different polycyclic aromatic hydrocarbons (PAH) migrating from squalane into and through the *stratum corneum* (s.c.) layer of the skin. Carcinogenic PAH have previously been detected in numerous polymer-based consumer products, especially those dyed with carbon black. Upon dermal contact with these products, PAH may penetrate into and through the viable layers of the skin by passing the s.c. and thus may become bioavailable. Squalane, a frequent ingredient in cosmetics, has also been used as a polymer surrogate matrix in previous studies. $K_{sc/m}$ and D_{sc} are relevant parameters for risk assessment because they allow estimating the potential of a substance to become bioavailable upon dermal exposure. We developed an analytical method involving incubation of pigskin with naphthalene, anthracene, pyrene, benzo[*a*]pyrene and dibenzo[*a,h*]pyrene in Franz diffusion cell assays under quasi-infinite dose conditions. PAH were subsequently quantified within individual s.c. layers by gas chromatography coupled to tandem mass spectrometry. The resulting PAH depth profiles in the s.c. were fitted to a solution of Fick's second law of diffusion, yielding $K_{sc/m}$ and D_{sc}. The decadic logarithm log$K_{sc/m}$ ranged from −0.43 to +0.69 and showed a trend to higher values for PAH with higher molecular masses. D_{sc}, on the other hand, was similar for the four higher molecular mass PAH but about 4.6-fold lower than for naphthalene. Moreover, our data suggests that the s.c./viable epidermis boundary layer represents the most relevant barrier for the skin penetration of higher molecular mass PAH. Finally, we empirically derived a mathematical description of the concentration depth profiles that better fits our data. We correlated the resulting parameters to substance specific constants such as the logarithmic octanol-water partition coefficient log*P*, $K_{sc/m}$ and the removal rate at the s.c./viable epidermis boundary layer.

1. Introduction

Understanding the migration of polycyclic aromatic hydrocarbons (PAH) from consumer products through the skin is of key importance to support risk assessment of this ubiquitous class of contaminants. Exposure to PAH is linked to several relevant toxicological endpoints. For example, benzo[*a*]pyrene (B[*a*]P), one of the best studied PAH, can cause reproductive toxicity (Mackenzie and Murray Angevine, 1981), immune system suppression (Hardin et al., 1992), genotoxicity (Brinkmann et al., 2012) and cancer (Rota et al., 2014), among other adverse

Abbreviations: B[*a*]P, benzo[*a*]pyrene; c_m, concentration in medium; c_{sc}, concentration in *stratum corneum*; $c_{x,t}$, concentration at depth x and time t; c_{rel}, relative concentration; DB[*a,h*]P, dibenzo[*a,h*]pyrene; D_{sc}, diffusion coefficient in the *stratum corneum*; EFSA, European Food Safety Authority; FDC, Franz diffusion cell; GC-MS/MS, gas chromatography coupled to tandem mass spectrometry; H_{sc}, total thickness of *stratum corneum*; IARC, International Agency for Research on Cancer; $K_{sc/m}$, partition coefficient between stratum corneum and medium; log*P*, octanol-water partition coefficient; LOQ, limit of quantification; *M*, molecular mass; OECD, Organization for Economic Co-operation and Development; PAH, polycyclic aromatic hydrocarbons; s.c., *stratum corneum*; SCCS, Scientific Committee on Consumer Safety; SD, standard deviation; SI, supporting information; *t*, time; *x*, depth in *stratum corneum*; σ, residual standard deviation.

* Corresponding author at: German Federal Institute for Risk Assessment (BfR), Department of Chemical and Product Safety, Max-Dohrn-Str. 8–10, 10589 Berlin, Germany.
** Corresponding author.
E-mail addresses: Konstantin.Simon@bfr.bund.de (K. Simon), Alexander.Roloff@bfr.bund.de (A. Roloff).

https://doi.org/10.1016/j.ecoenv.2023.115113
Received 23 December 2022; Received in revised form 2 June 2023; Accepted 4 June 2023
Available online 12 June 2023

conditions (Collins et al., 1998). The International Agency for Research on Cancer (IARC) classifies B[*a*]P as a class 1 carcinogen, whereas many other PAH are considered to be possibly carcinogenic to humans (IARC, 2010; IARC, 2018). Multiple regulations have limited the amount of PAH in consumer products (Regulation (EC), 2006: Regulation (EU) 2013), although there is no safe exposure level for genotoxic carcinogens (BfR, 2019). Unfortunately, PAH are still detectable in certain commodities made of synthetic polymers, such as tools and toys (Alawi et al., 2018; Bartsch et al., 2017).

Upon dermal contact, these PAH have been shown to migrate through the *stratum corneum* (s.c.) into viable human skin layers, where they potentially become bioavailable (Bartsch et al., 2016). Most studies, however, investigated skin uptake from aqueous matrices (Luo et al., 2020; Roy et al., 2007; Sousa et al., 2022) or organic solvents such as acetone (Moody et al., 1995, 2011; Ng et al., 1991; Sartorelli et al., 1998), which are only of limited relevance for PAH exposure from consumer products. To the best of our knowledge, concentration profiles of these substances in the s.c. after dermal exposure have never been reported. Accordingly, we decided to study skin penetration of PAH from squalane. Squalane is a suitable surrogate for aliphatic polymers that has been used previously to investigate the stability of polymer additives (Barret et al., 2002; Soebianto et al., 1993; Bartsch, 2018; Beißmann et al., 2014). It is highly lipophilic (calculated octanol-water partition coefficient log$P$ = 15.6, Octanol-Water Partition Calculation, 2021) and resembles an extended and branched alkyl chain (Zafar and Chickos, 2019). Furthermore, it is frequently used as an ingredient in cosmetic articles, such as anti-aging creams, lotions and shampoos (Bergfeld et al., 2019; Kim and Karadeniz, 2012).

Upon first contact of a substance with the skin, partitioning occurs from the applied medium into the s.c., the outermost layer of the skin representing a crucial barrier for skin penetration (Sousa et al., 2022). This process is described by the partition coefficient $K_{sc/m}$, which is defined as the ratio of the concentration in the s.c. (c_{sc}) to the concentration in the medium (c_m; here: squalane) at chemical equilibrium. $K_{sc/m}$ is strongly dependent on the physicochemical properties of the medium in which the substance of interest is applied to the skin. Because the s.c. is comparatively lipophilic (Raykar et al., 1988), lipophilic substances are expected to have a higher partition coefficient, as was shown exemplarily by Rothe et al. (2017) for partitioning from aqueous media.

Partitioning of a substance into the upper most layer of the s.c. is followed by diffusion into deeper layers. This process is governed by Fick's (1855) laws of diffusion. The second law describes the concentration profile of a substance in a medium as a function of time:

$$\frac{\partial c_{x,t}}{\partial t} = -D_{sc}\frac{\partial^2 c_{x,t}}{\partial x^2}, \tag{1}$$

where $c_{x,t}$ is the concentration at depth x of the s.c. and time t, and D_{sc} is the diffusion coefficient in the s.c. D_{sc} is a measure of how fast a substance will move through the s.c. and reach the viable epidermis, where it will potentially become bioavailable.

In silico methods aiming to model partitioning and diffusion of substances through the skin crucially rely on input parameters — including $K_{sc/m}$ and D_{sc} — to predict skin permeation accurately. They can represent helpful alternatives to tedious *in vivo* studies on dermal exposure to toxic substances. However, *in vitro* skin permeation studies are needed to determine realistic input parameters. The present study contributes to this work with experimentally derived values for $K_{sc/m}$ and D_{sc} of highly lipophilic PAH (log$P$ = 3.4–7.4 (de Lima Ribeiro and Ferreira, 2003; US EPA, 2012) by employing Franz diffusion cell (FDC) assays (Franz, 1975). We investigated partitioning and diffusion of naphthalene, anthracene, pyrene, B[*a*]P and dibenzo[*a,h*]pyrene (DB[*a,h*]P) from squalane matrices into and through the s.c. of excised pigskin. These PAH feature molecules consisting of two to six condensed aromatic rings. To the best of our knowledge, this study is the first to measure these parameters for substances with a high carcinogenic potential applied in a matrix that is relevant for real-life exposure to polymer-based consumer products and cosmetics.

2. Methods

The following section summarizes the method applied in this work. A detailed description can be found in the supporting information (SI, section A.2 *Method*). The FDC assays were carried out with two different incubation times (1 h and 24 h) in replicates with $n = 4$ (24 h: naphthalene, pyrene, DB[*a,h*]P), $n = 8$ (24 h: B[*a*]P) and $n = 5$ (1 h: all PAH).

2.1. Principle of the Franz diffusion cell assay

The FDC assay (Franz, 1975) is a well-established method to investigate dermal absorption (Bartsch et al., 2018; Bronaugh et al., 1981, 1986, Bronaugh and Stewart, 1984, 1986; Ng et al., 2010) and was previously established for PAH at our institute (Bartsch et al., 2016). In this study, the receptor chamber at the bottom of the FDC (Fig. S1) contained bovine serum albumin (BSA; 50 mg·ml^{-1}) in Dulbecco's phosphate buffered saline (DPBS). BSA is known to increase the solubility of lipophilic substances in aqueous solutions, which is also its primary function in the bloodstream (Bronaugh and Stewart, 1984; Ellison et al., 2020, 2021; Gerstel et al., 2016). Furthermore, it can compensate for loss of protein in the dermis, and reduce binding of PAH to the glass surface of the receptor chamber (Ellison et al., 2020, 2021). The BSA solution was freshly prepared before each FDC assay.

The receptor chamber is enclosed by a water jacket to regulate the temperature at 32 ± 1 °C corresponding to average skin surface temperature (Lee et al., 2019). The skin was laid atop the upper opening of the FDC so that it covered the receptor chamber. It was fixed by a donor chamber cap and a clamp. The sample solution was added to the donor chamber to start the incubation and the FDCs were occluded with parafilm. After the incubation time, the set-up was disassembled and the compartments were analyzed for their respective analyte concentrations individually: the donor solution was removed and the skin was taken off. The s.c. was stripped off layer by layer with tape strips, which is a common method to determine the concentration profile in the s.c. (Hopf et al., 2020; Simon et al., 2023). The donor solution, the tape strips and the remaining skin were then extracted with acetonitrile. The BSA in the receptor solution was denatured with saturated ethanolic potassium hydroxide, followed by extraction with cyclohexane. Deuterated internal standards were used to compensate for analyte losses throughout sample preparation (SI, section A.2 *Methods*). All resulting solutions were analyzed for their PAH content by gas chromatography coupled to tandem mass spectrometry (GC-MS/MS).

We applied PAH at high concentrations dissolved in squalane (saturated solution for DB[*a,h*]P, 500–1000 μg/ml for other PAH; for exact concentrations, see Table S1) to the skin and incubated for 1 h and 24 h, respectively. For technical reasons, 1 h was the shortest incubation time for which tape stripping could be performed without significant deviations in the incubation times for individual s.c. layers. The 24 h incubation period was chosen because at this time point the system was considered to have approached a steady state.

2.2. Mathematical analysis and calculation

The diffusion of PAH through the s.c. was modelled with an analytical solution to Fick's (1855) second law of diffusion (Eq. (1)). A solution for the one-dimensional diffusion in x-direction through a plane sheet of thickness H_{sc} representing the s.c. is (Herkenne et al., 2007)

$$c_{rel,x,t} = K_{sc/m}\left[1 - \frac{x}{H_{sc}} - \frac{2}{\pi}\sum_{j=1}^{\infty}\frac{1}{j}\sin\left(\frac{j\pi}{H_{sc}}x\right)\exp\left(-\frac{j^2\pi^2 D_{sc}}{H_{sc}^2}t\right)\right], \tag{2}$$

with

$$c_{rel,x,t} = \frac{c_{x,t}}{c_m}, \quad (3)$$

where $c_{x,t}$ is the concentration at a certain depth x at time t in the s.c., c_m is the concentration in the medium applied in the donor chamber, $K_{sc/m}$ is the partition coefficient between the s.c. and the medium, H_{sc} is the thickness of the s.c., j is the index of the infinite series and D_{sc} is the diffusion coefficient in the s.c. The boundary and initial conditions are: (i) c_m is assumed to remain constant over the duration of the incubation period. This is achieved by applying high concentrations close to the solubility limit of the PAH in squalane, that is, quasi-infinite dose conditions. (ii) The s.c. does not contain any analyte at $t = 0$ at any position in x-direction: $c_{x,0} = 0$. This assumption is verified by including negative controls. (iii) The viable epidermis is assumed to act as a perfect sink, with any substance reaching the last layer of the s.c. being removed immediately: $c_{Hsc,t} = 0$.

$K_{sc/m}$ and D_{sc} were obtained by fitting the measured concentration profiles in the s.c. with Eq. (2). The number of terms used in the infinite series was set to 10 000, which was considered sufficiently large to approximate the solution. The data were analyzed using the statistical programming language R (version 4.03), using the non-linear least squares approach.

2.3. Infinite dose conditions

For the determination of $K_{sc/m}$ and D_{sc}, the Organization for Economic Co-operation and Development (OECD) recommends to apply infinite dose conditions in their guidelines on skin penetration studies employing FDC assays (OECD, 2004a, 2004b). This assures that the concentration in the donor solution stays quasi-constant during the course of the experiment. In consequence, steady-state conditions are established at the boundary layer between the medium and the s.c. (Anissimov et al., 2013). We therefore used highly concentrated solutions of PAH in squalane in the present study. Naphthalene, anthracene, pyrene and B[*a*]P were readily dissolved at a concentration of 1 mg·ml^{-1} in squalane after treatment in an ultrasonic bath for 30 min at 70 °C. Due to the lower solubility of DB[*a,h*]P in squalane, a solution of 1 mg·ml^{-1} in dichloromethane was prepared and mixed 1:1 with squalane. Evaporation of dichloromethane under reduced pressure (50 mbar) at 55 °C in a parallel evaporation concentrator (Syncore Analyst, Büchi, Labortechnik AG, Flawil, Switzerland, cooler set to 10 °C) yielded a saturated solution of DB[*a,h*]P. Final PAH concentrations of the applied squalane solutions were determined analytically by GC-MS/MS (Table S1).

2.4. Skin

The skin used in the FDC assays was provided by the Charité , Universitätsmedizin Berlin and treated as described previously (Simon et al., 2023). Briefly, the skin was taken from the flank of female pigs, which had been sacrificed shortly before the skin was removed in an unrelated surgical experiment that did not affect the skin. The excised skin was transported to our laboratory on ice, sheared, cut into pieces of approximately 10 × 20 cm with a knife, and stored at − 20 °C before use. The storage time did not exceed 12 months and skin integrity was thoroughly checked by monitoring the trans-epidermal water loss in line with OECD Guideline 428 (SI, section A.2.3 *Franz diffusion cell protocol*, OECD, 2004b; Zhang et al., 2018).

Pigskin has been used as a substitute for human skin in various previous skin penetration studies (Bartsch et al., 2016, 2018; Gerstel et al., 2016; Herkenne et al., 2006, 2007; Rothe et al., 2017). It was shown that pigskin does not significantly differ from human skin in relevant penetration properties, such as lag time and diffusion of substances in the s.c. (Gerstel et al., 2016; Herkenne et al., 2006; Rothe et al., 2017). For these reasons, the Scientific Committee on Consumer Safety (SCCS) also recommends pigskin to be used in skin penetration studies (SCCS, 2010).

2.5. Thickness of the stratum corneum

The thickness of the porcine s.c. was determined histologically (SI, section A.2.8 *Determination of stratum corneum thickness*). It amounted to 10.14 ± 1.88 μm (mean ± SD, $n = 25$ measurements with three biological replicates, Fig. S2). This is in line with previous studies: Blair (1968) found a thickness of 12.5–17.4 μm for healthy human s.c., Kalia et al. (1996) found a thickness of 9.5–16.1 μm (human s.c.) and Rothe et al. (2017) found 11.1 ± 1.1 μm (human s.c.) and 10.8 ± 2.3 μm (porcine s.c.). During tape stripping, each tape strip removes about one layer of the s.c so that the depth attained is a linear function of the number of tape strips (equation (S6), Simon et al., 2023). The concentrations of PAH in individual s.c. layers as depicted in Figs. 1 and 3 were derived from PAH amounts extracted from individual tape strips and determined via GC-MS/MS. The volume of a single s.c. layer in the FDC assay was calculated assuming an average height of 0.349 μm and a permeation area of 1.76 cm^{-2} of the FDC (see SI, section A.2.3 and equations S5 and S6).

2.6. Concentration of polycyclic aromatic hydrocarbons in the stratum disjunctum

The guidance on dermal absorption of the European Food Safety Authority (EFSA) recommends to dismiss the first tape strip from analysis. The first tape strips removes cells of the *stratum disjunctum* (Buist et al., 2017), the upper most layer of the s.c. which is subject to permanent desquamation. Substances can accumulate in the folds and furrows of the *stratum disjunctum*, which can lead to an over-determination of the concentration in the upper layer of the s.c. In this study, we therefore calculated $K_{sc/m}$ and D_{sc} considering data points from the second tape strip onwards. We expect this to yield more accurate coefficients for a rather homogeneous s.c. The measured concentrations of the first tape strip are represented at negative x-values in the graphs.

3. Results and discussion

3.1. Recovery of PAH in Franz diffusion cell assays

To determine whether quasi-infinite dose conditions were maintained throughout the incubation period, the total PAH recovery across all compartments was calculated (Fig. S3 and Table S1). After 1 h, 97–102% of the applied dose remained in the donor chamber. After 24 h, recovery in the donor compartment ranged between 94% and 97%. These values are in compliance with the OECD guideline that stipulates less than 10% donor depletion to be sufficient for infinite dose conditions (OECD, 2004b).

The viable epidermis and the dermis were found to represent a significant barrier for the higher molecular mass PAH. The concentration of each PAH in the s.c. after 1 h and 24 h exposure was about two to three orders of magnitude higher than the concentration in the remaining skin (see Table 1 for measured PAH concentrations in individual compartments). After 1 h, naphthalene was already detected in the receptor solution whereas only trace amounts of the higher molecular mass PAH were found. After 24 h, the concentration of naphthalene in the receptor solution was more than an order of magnitude higher than the concentration of the other PAH. More lipophilic PAH are thus retained by the rather lipophilic s.c., whereas the comparatively less lipophilic naphthalene is better able to permeate through these compartments. This can be explained by the higher lipophilicity of the s.c. compared to that of the remaining skin, (Gartner, 2021) since PAH are highly lipophilic substances (log$P$ > 3.3, de Lima Ribeiro and Ferreira, 2003; US EPA, 2012).

Interestingly, the concentrations of pyrene and B[*a*]P in the

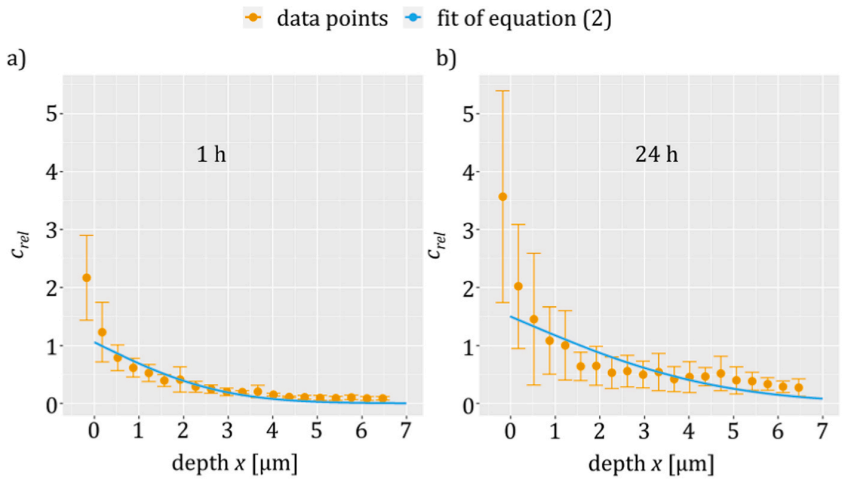

Fig. 1. Measured relative concentrations c_{rel} of B[*a*]P (yellow, mean ± SD) at depth x in the *stratum corneum* and the corresponding fit of the solution of Fick's second law of diffusion (Eq. (2), light blue) after an incubation time of a) 1 h and b) 24 h. The first data points at negative x-values represent the *stratum disjunctum* and were omitted from analysis. For other PAH, see Fig. S4. SD: standard deviation, PAH: polycyclic aromatic hydrocarbons, B[*a*]P: benzo[*a*]pyrene, c_{rel}: see Eq. (3).

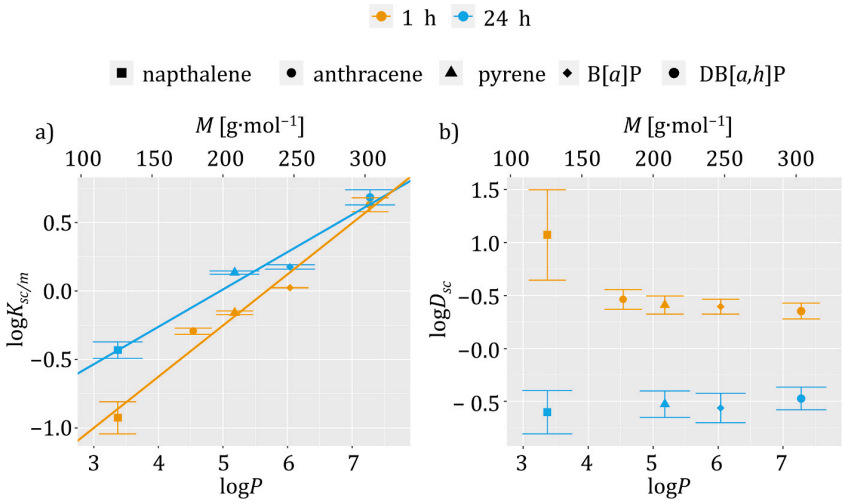

Fig. 2. Calculated a) partition coefficients log$K_{sc/m}$ (mean ± SD) with linear regression curves and b) diffusion coefficients logD_{sc} (mean ± SD) of five PAH for incubation times of 1 h and 24 h (upper x-axis: molecular mass (M), lower x-axis: octanol-water partition coefficient (log$P$). log$P$ and M are linearly related for these PAH (Fig. S5). SD: standard deviation, PAH: polycyclic aromatic hydrocarbons, B[*a*]P: benzo[*a*]pyrene, DB[*a,h*]P: dibenzo[*a,h*]pyrene.

remaining skin after 24 h are significantly higher than that of naphthalene. This might be due to these compounds accumulating at the interface between the s.c. and the viable epidermis. The s.c. of pigskin is not completely removed by 20 tape strips (Simon et al., 2023). Presumably, these compounds are retained in the remaining s.c. layers, diffusing slower into deeper layers of the skin and can thus not reach the receptor in comparable quantities.

3.2. Concentration depth profiles in the stratum corneum

The measured concentrations of PAH in the s.c. decrease with increasing depth (see Fig. 1 for B[*a*]P and Fig. S4 for other investigated PAH). Because the concentration in the donor compartment is quasi-constant (infinite dose conditions), the diffusive loss of PAH in the upper layers of the s.c. will constantly be replenished with PAH from the donor compartment. At the lower end of the s.c. ($x = H_{sc}$), the PAH partition into the viable epidermis. Hence, a constant flux of PAH through the s.c. is maintained in a dynamic equilibrium (steady state), avoiding saturation of s.c. layers.

3.3. Partition coefficients $K_{sc/m}$

The values of $K_{sc/m}$ determined for an incubation time of 1 h are lower than after 24 h (Fig. 2a and Table S2). Partition coefficients describe concentration ratios at chemical equilibrium, which presumably is not yet reached after 1 h. Eq. (2) describes the diffusion through the s.c. at equilibrium between the medium and the most upper s.c. layer. Thus, only when equilibrium is reached, can $K_{sc/m}$ be calculated accurately. After an extended incubation time of 24 h, the system better resembles the steady state. Hence, we consider the values calculated for 24 h as the more realistic partition coefficients $K_{sc/m}$.

Values of log$K_{sc/m}$ for the two different incubation time points linearly depend on log$P$ and the two linear relationships converge for higher log$P$ values (Fig. 2). By extension, log$K_{sc/m}$ is also linearly dependent on the molecular mass M, because log$P$ and M are linearly related for the investigated PAH (Fig. S5, de Lima Ribeiro and Ferreira, 2003; US EPA,

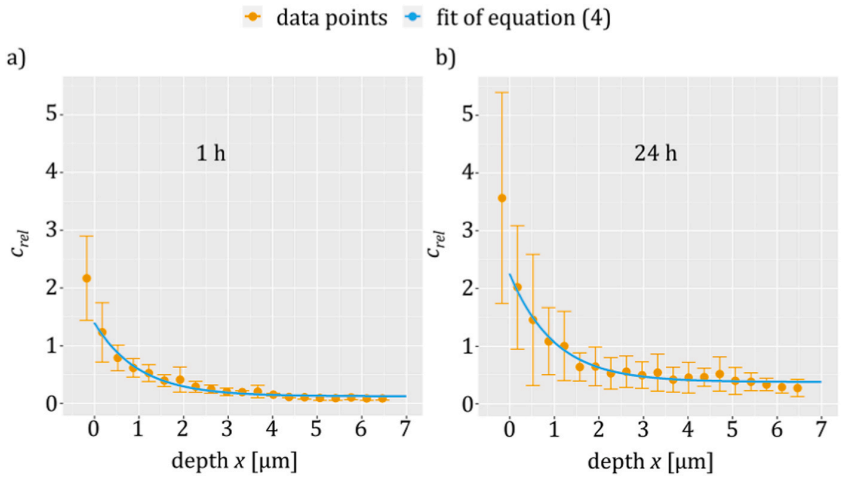

Fig. 3. Alternative fit of an empirically determined function (Eq. (4), light blue) of the relative concentration c_{rel} of B[*a*]P (yellow, mean ± SD) at depth x in the *stratum corneum* after incubation times of a) 1 h and b) 24 h. The first data points at negative x-values represent the *stratum disjunctum* and were omitted from analysis. For other PAH, see Fig. S4. SD: standard deviation, PAH: polycyclic aromatic hydrocarbons, B[*a*]P: benzo[*a*]pyrene, c_{rel}: see Eq. (3).

Table 1
Measured concentrations (mean ± SD) of PAH in different compartments after incubation time t_i. SD: standard deviation, PAH: polycyclic aromatic hydrocarbons, s.c.: *stratum corneum*, B[*a*]P: benzo[*a*]pyrene, DB[*a,h*]P: dibenzo[*a,h*]pyrene, LOQ: limit of quantification; please note the different units of PAH concentrations in individual compartments.

substance	t_i [h]	donor [µg·ml^{-1}]	s.c. [µg·ml^{-1}]	remaining skin [ng·ml^{-1}]	receptor [ng·ml^{-1}]
naphthalene	1	1028 ± 30	63 ± 28	112 ± 24	3.05 ± 0.83
anthracene	1	1027 ± 20	152 ± 55	162 ± 85	0.225 ± 0.304
pyrene	1	532 ± 6	104 ± 31	79 ± 47	0.235 ± 0.245
B[*a*]P	1	644 ± 12	185 ± 53	102 ± 66	0.261 ± 0.331
DB[*a,h*]P	1	51.3 ± 2.7	60 ± 20	74 ± 102	<LOQ
naphthalene	24	916 ± 71	116 ± 100	542 ± 28	425 ± 89
pyrene	24	851 ± 15	679 ± 419	1156 ± 562	19 ± 5
B[*a*]P	24	838 ± 35	499 ± 229	799 ± 364	5 ± 13
DB[*a,h*]P	24	37 ± 25	88 ± 46	181 ± 99	0.86 ± 0.92

2012). DB[*a,h*]P (0.685 ± 0.056) and naphthalene (−0.432 ± 0.060) feature the highest and lowest values for log$K_{sc/m}$, respectively. Notably, the two values derived for DB[*a,h*]P (24 h: 0.685 ± 0.056 vs. 1 h: 0.631 ± 0.052) are not significantly different. This trend indicates that under quasi-infinite dose conditions the more lipophilic PAH also reach steady state faster.

The experimentally determined value for log$K_{sc/m}$ of naphthalene (−0.432 ± 0.060) is considerably lower than reported previously (0.98 ± 0.19, Ellison et al., 2020, 2021) where naphthalene was applied to the skin surface in a 0.88% solution of ethanol in DPBS. Here, we used squalane, which is highly lipophilic (log$P$ = 15.59, Octanol-Water Partition Calculation, 2021). A higher lipophilicity of the medium reduces log$K_{sc/m}$ for lipophilic substances such as PAH. Importantly, squalane represents a medium that is better suited to mimic skin contact to polymer-based consumer products (Barret et al., 2002; Bartsch et al., 2018; Beißmann et al., 2014; Soebianto et al., 1993) and cosmetics, where it is frequently used as an ingredient (Kim and Karadeniz, 2012; Zafar and Chickos, 2019).

3.4. Diffusion coefficients D_{sc}

The calculated values for D_{sc} vary for the two different incubation times (Fig. 2 and Table S2). Eq. (2) requires that the cellular layers beyond the s.c. function as a sink for PAH (boundary condition iii). The flux through the s.c. should thus not be diminished by the solubility of the PAH in the rather hydrophilic viable epidermis. The sink conditions are more likely to be fulfilled at shorter incubation times. Hence, D_{sc} values obtained after 1 h more accurately describe the diffusion process in the s.c. The curvature of the function associated with Eq. (2) is dependent on D_{sc}. With longer incubation times, the contribution of the exponential term (containing D_{sc}) to the measured value of $c_{rel,x,t}$ decreases significantly, leading to a better fit of Eq. (2) at shorter incubation times. Lower residual standard deviations σ of the fit of Eq. (2) describing the concentration profiles measured after 1 h support this conclusion (Table S3).

The presented values for D_{sc} represent the first experimentally determined diffusion coefficients for PAH in the s.c., with the exception of naphthalene. For naphthalene, values between $[2.35 \pm 1.06]\cdot10^{-9}$ m^2·h^{-1} (Ellison et al., 2020, 2021) and $[2.52 \pm 0.84]\cdot10^{-10}$ m^2·h^{-1} (Kim et al., 2008) were reported. These significantly higher coefficients can be attributed to the medium in which naphthalene was applied to the skin. Ellison et al. (2020, 2021) used a 1.12% solution of ethanol in DPBS. Ethanol is known to enhance skin penetration (OECD, 2011). Kim et al. (2006) applied jet fuel as a medium, which has been shown to damage the s.c. (Singh et al., 2003). It is of note that the mentioned studies acknowledge these limitations (Ellison et al., 2020, 2021; Kim et al., 2008). Squalane, on the other hand, is a medium which was shown to not substantially enhance the permeation of applied drugs (Takahashi et al., 1995). D_{sc} for naphthalene ($[1.183 \pm 0.471]\cdot10^{-11}$ m^2·h^{-1}) is higher than for any of the other PAH that were analyzed. Thus, upon dermal exposure, it potentially becomes bioavailable more quickly. However, the lower value for log$K_{sc/m}$ implies lower total amounts of naphthalene in the s.c. compared to the higher molecular mass PAH upon skin contact.

3.5. Simplified mathematical description of diffusion in the stratum corneum

Fick's (1855) laws are the mathematical basis for each discussion of diffusion. As discussed, Eq. (2) represents a solution to Fick's second law. Boundary condition iii states that the viable epidermis must act as a perfect sink. Hence, the concentration at the boundary layer between the s.c. and the viable epidermis (at depth $x = H_{sc} \approx 10$ µm) must always be zero. The viable epidermis, however, is an aqueous matrix and therefore

less lipophilic than the s.c. Thus, after a certain time is passed, a non-zero concentration of PAH in the deepest investigated s.c. layer builds up, even after the shorter incubation period of 1 h (Fig. 1 and Fig. S4). This is supported by the observed underprediction of the concentrations in deeper s.c. layers by the fit of Eq. (2).

We propose a simplified alternative to Eq. (2) to deal with this problem:

$$c_{rel,x,t} = u_t \cdot e^{-x} + w_t, \quad (4)$$

where $c_{rel,x,t}$ is the concentration at depth x and time t divided by the concentration in the donor solution (compare Eq. (3)). The parameters u_t and w_t are time-dependent factors. Eq. (4) describes the data more accurately than Eq. (2) as implied by the lower residual standard deviation σ of the fit (Table S3). It represents an excellent fit to our data for two different time points and for five different substances. We thus hypothesize that Eq. (4) could be used for modelling diffusion through the skin if more data were made available to confirm its suitability for other substance classes.

The parameter w_t can be interpreted as a measure for the retention of a given PAH at the boundary between the s.c. and the viable epidermis. It is time-dependent because the amount of PAH retained at this boundary depends on the amount which is already diffused to this position. We suspect that it is related to the inverse of the removal rate and the viable epidermis/s.c. partition coefficient $K_{ve/sc}$. High removal rates or large coefficients $K_{ve/sc}$, as required for sink conditions, would lead to w_t approaching zero.

logw_t is linearly dependent on log$P$ (Fig. 4b). Since the s.c. is a more lipophilic matrix than the viable epidermis (Gartner, 2021), substances with higher lipophilicity are retained more strongly in the s.c., as observed for the trend of logw_t for different PAH. The parameter logu_t is also linearly correlated with log$P$ (Fig. 4a), as is log$K_{sc/m}$ derived from Eq. (2) (Fig. 2a). Thus, the two parameters are linearly related (Fig. S6).

Eq. (4) does not obey Fick's second law, since that would require w_t to be time-independent (SI, section A2.6 *Mathematical analysis of* Eq. (4)). However, w_t is time-dependent (Fig. 4b). Hence, Eq. (4) describes the diffusion in the s.c. only approximately. Still, this approximation represents an excellent fit to the experimental data. It can be directly correlated to physico-chemical properties, including log$P$ and log$K_{sc/m}$. Additionally, it shows a sound theorized correlation to the removal rate at the s.c./viable epidermis boundary layer and appeals with its simplicity.

4. Conclusion

We demonstrated that the viable epidermis and dermis represent the main barrier for the penetration of higher molecular mass PAH through the skin. Our results indicate that $K_{sc/m}$ can only be calculated reliably from measured concentration profiles of dermally applied substances in the s.c. when a sufficiently long incubation time (for example 24 h) is maintained. Furthermore, for the investigated PAH, log$K_{sc/m}$ is linearly related to log$P$ and M. Values for D_{sc} are highest for naphthalene. For PAH with three or more condensed rings, D_{sc} is lower but comparable to each other. We suspect that naphthalene, due to its low molecular mass and molar volume, features an exceptionally fast diffusion compared to PAH with more extended aromatic ring systems.

We empirically derived a simplified mathematical description of the measured concentration profiles, which fits our data better than the solution to Fick's second law. Its parameters can be correlated to substance- and matrix-specific physico-chemical parameters such as log$P$, $K_{sc/m}$ and the removal rate at the s.c./viable epidermis boundary layer. Future work includes the determination of these constants for other relevant substances in consumer products, such as degradation products of polymer additives.

CRediT authorship contribution statement

Konstantin Simon: Conceptualization, Methodology, Formal analysis, Investigation, Resources, Writing – original draft, Writing – review & editing, Visualization, Project administration. **Lidia Schneider:** Methodology, Formal analysis, Investigation. **Gila Oberender:** Formal analysis, Investigation. **Ralph Pirow:** Methodology, Writing – review & editing. **Christoph Hutzler:** Conceptualization, Methodology, Writing – review & editing. **Andreas Luch:** Writing – review & editing, Resources, Funding acquisition. **Alexander Roloff:** Conceptualization, Methodology, Formal analysis, Resources, Writing – original draft, Writing – review & editing, Supervision, Project administration, Funding acquisition.

Declaration of Competing Interest

The authors declare that they have no known competing financial interests or personal relationships that could have appeared to influence the work reported in this paper.

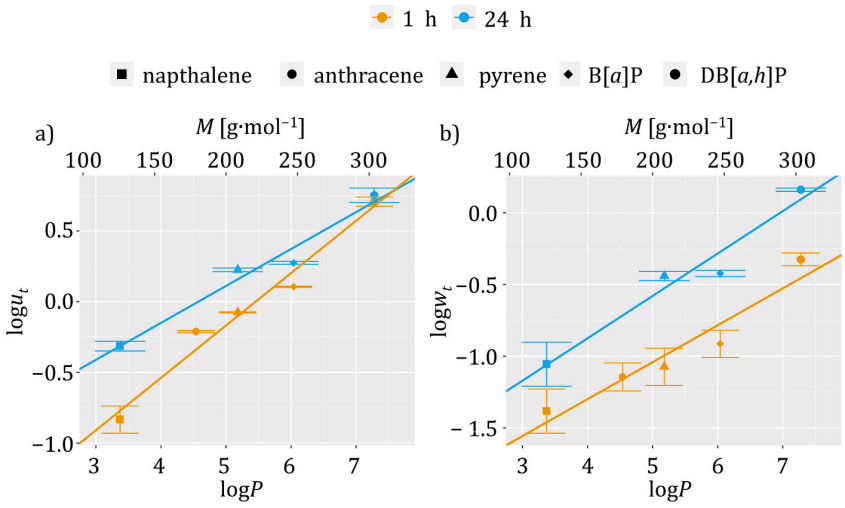

Fig. 4. a) logu_t (mean ± SD) vs. octanol-water partition coefficient (log$P$) with linear regression curves and b) logw_t (mean ± SD) vs. log$P$ of five PAH for incubation times of 1 h and 24 h (upper x-axis: molecular mass (M), lower x-axis: log$P$. log$P$ and M are linearly related for these PAH (Fig. S5). SD: standard deviation, PAH: polycyclic aromatic hydrocarbons, B[a]P: benzo[a]pyrene, DB[a,h]P: dibenzo[a,h]pyrene.

Data availability

Data will be made available on request.

Acknowledgements

We thank Tanja Schmidt and Katja Reiter from Charité for providing us with pigskin. We thank Klaudia Michna and Svetlana Kruschinski for excellent technical assistance. We thank Franziska Riedel, Benjamin-Christoph Krause, Charlotte Kromer, Aline Rosin and Nadja Mallock for proof reading and fruitful discussions. This work was funded by BfR-internal grants BfR-CPS-08-1322–514 and BfR-CPS-08-1322–774.

Appendix A. Supporting information

Supplementary data associated with this article can be found in the online version at doi:10.1016/j.ecoenv.2023.115113.

References

Alawi, M.A., Abdullah, R.A., Tarawneh, I., 2018. Determination of polycyclic aromatic hydrocarbons (PAHs) in carbon black-containing plastic consumer products from the Jordanian market. Toxin Rev. 37 (4), 269–277. https://doi.org/10.1080/15569543.2017.1359628.

Anissimov, Y.G., Jepps, O.G., Dancik, Y., Roberts, M.S., 2013. Mathematical and pharmacokinetic modelling of epidermal and dermal transport processes. Adv. Drug Del. Rev. 65 (2), 169–190. https://doi.org/10.1016/j.addr.2012.04.009.

Barret, J., Gijsman, P., Swagten, J., Lange, R.F., 2002. A molecular study towards the interaction of phenolic anti-oxidants, aromatic amines and HALS stabilizers in a thermo-oxidative ageing process. Polym. Degrad. Stab. 76 (3), 441–448. https://doi.org/10.1016/S0141-3910(02)00047-2.

Bartsch, N. Polymer additives, contaminants and non-intentionally added substances in consumer products: Combined migration, permeation and toxicity analyses in skin. Doctoral dissertation, Freie Universität, Berlin, 2018.

Bartsch, N., Hutzler, C., Vieth, B., Luch, A., 2017. Target analysis of polycyclic aromatic hydrocarbons (PAHs) in consumer products and total content of polycyclic aromatic compounds (PACs). Polycycl. Aromat. Compd. 37 (2–3), 114–121. https://doi.org/10.1080/10406638.2016.1189440.

Bartsch, N., Heidler, J., Vieth, B., Hutzler, C., Luch, A., 2016. Skin permeation of polycyclic aromatic hydrocarbons: a solvent-based in vitro approach to assess dermal exposures against benzo[a]pyrene and dibenzopyrenes. J. Occup. Environ. Hyg. 13 (12), 969–979. https://doi.org/10.1080/15459624.2016.1200724.

Bartsch, N., Girard, M., Schneider, L., Weijgert, V.V.D., Wilde, A., Kappenstein, O., Vieth, B., Hutzler, C., Luch, A., 2018. Chemical stabilization of polymers: Implications for dermal exposure to additives. J. Environ. Sci. Heal. A 53 (5), 405–420. https://doi.org/10.1080/10934529.2017.1412192.

Beißmann, S., Reisinger, M., Grabmayer, K., Wallner, G., Nitsche, D., Buchberger, W., 2014. Analytical evaluation of the performance of stabilization systems for polyolefinic materials. Part I: Interactions between hindered amine light stabilizers and phenolic antioxidants. Polym. Degrad. Stab. 110, 498–508. https://doi.org/10.1016/j.polymdegradstab.2014.09.020.

Wilma F. Bergfeld, D. V. B, Ronald A. Hill, Curtis D. Klaassen, Daniel C. Liebler, James G. Marks, Jr., Ronald C. Shank, Thomas J. Slaga, and Paul W. Snyder In Safety Assessment of Squalane and Squalene *as Used in Cosmetics*, 2019.

Blair, C., 1968. Morphology and thickness of the human stratum corneum. Br. J. Dermatol. 80 (7), 430–436. https://doi.org/10.1111/j.1365-2133.1968.tb11978.x.

Brinkmann, J., Stolpmann, K., Trappe, S., Otter, T., Genkinger, D., Bock, U., Liebsch, M., Henkler, F., Hutzler, C., Luch, A., 2012. Metabolically competent human skin models: activation and genotoxicity of benzo[*a*]pyrene. Toxicol. Sci. 131 (2), 351–359. https://doi.org/10.1093/toxsci/kfs316.

Bronaugh, R.L., Stewart, R.F., 1984. Methods for in vitro percutaneous absorption studies III: hydrophobic compounds. J. Pharm. Sci. 73 (9), 1255–1258. https://doi.org/10.1002/jps.2600730916.

Bronaugh, R.L., Stewart, R.F., 1986. Methods for in vitro percutaneous absorption studies VI: preparation of the barrier layer. J. Pharm. Sci. 75 (5), 487–491. https://doi.org/10.1002/jps.2600750513.

Bronaugh, R.L., Congdon, E.R., Scheuplein, R.J., 1981. The effect of cosmetic vehicles on the penetration of N-nitrosodiethanolamine through excised human skin. J. Invest. Dermatol. 76 (2), 94–96. https://doi.org/10.1111/1523-1747.ep12525384.

Comission Regulation (EU) No 1272/2013 amending Annex XVII to Regulation (EC) No 1907/2006 (REACH). Official Journal of the European Union 328, 2013, 69–71.

Bronaugh, R.L., Stewart, R.F., Simon, M., 1986. Methods for in vitro percutaneous absorption studies VII: use of excised human skin. J. Pharm. Sci. 75 (11), 1094–1097. https://doi.org/10.1002/jps.2600751115.

Buist, H.; Craig, P.; Dewhurst, I.; Hougaard Bennekou, S.; Kneuer, C.; Machera, K.; Pieper, C.; Court Marques, D.; Guillot, G., Guidance on dermal absorption. In EFSA Journal, European Food Safety Authority, Ed. 2017; Vol. 15, p e04873.

Bundesinstitut für Risikobewertung (BfR): PAH levels in consumer products should be as low as possible. 2019 ⟨https://www.bfr.bund.de/en/press_information/2019/29/pah_levels_in_consumer_products_should_be_as_low_as_possible-241757.html⟩ (accessed 26.08.2021).

Collins, J., Brown, J., Alexeeff, G., Salmon, A., 1998. Potency equivalency factors for some polycyclic aromatic hydrocarbons and polycyclic aromatic hydrocarbon derivatives. Regul. Toxicol. Pharmacol. 28 (1), 45–54. https://doi.org/10.1006/rtph.1998.1235.

Ellison, C.A., Tankersley, K.O., Obringer, C.M., Carr, G.J., Manwaring, J., Rothe, H., Duplan, H., Géniès, C., Grégoire, S., Hewitt, N.J., 2020. Partition coefficient and diffusion coefficient determinations of 50 compounds in human intact skin, isolated skin layers and isolated stratum corneum lipids. Toxicol. Vitr. 69, 104990 https://doi.org/10.1016/j.tiv.2020.104990.

Ellison, C.A., Tankersley, K.O., Obringer, C.M., Carr, G.J., Manwaring, J., Rothe, H., Duplan, H., Géniès, C., Grégoire, S., Hewitt, N.J., 2021. Corrigendum to partition coefficient and diffusion coefficient determinations of 50 compounds in human intact skin, isolated skin layers and isolated stratum corneum lipids. Toxicol. Vitr. 71, 105050 https://doi.org/10.1016/j.tiv.2020.105050.

Fick, A., 1855. Ueber diffusion. Ann. Phys. (Leipz.) 170 (1), 59–86.

Franz, T.J., 1975. Percutaneous absorption. On the relevance of in vitro data. J. Invest. Dermatol. 64 (3), 190–195. https://doi.org/10.1111/1523-1747.ep12533356.

Gartner, L.P., 2021. Integument. *Textbook of Histology*, 5 ed..,. Elsevier,.

International Agency for Research on Cancer (IARC), 2010. Some non-heterocyclic polycyclic aromatic hydrocarbons and some related exposures. IARC Monogr. Eval. Carcinog. Risks Hum. 92, 1.

Gerstel, D., Jacques-Jamin, C., Schepky, A., Cubberley, R., Eilstein, J., Grégoire, S., Hewitt, N., Klaric, M., Rothe, H., Duplan, H., 2016. Comparison of protocols for measuring cosmetic ingredient distribution in human and pig skin. Toxicol. Vitr. 34, 153–160. https://doi.org/10.1016/j.tiv.2016.03.012.

Hardin, J.A., Hinoshita, F., Sherr, D.H., 1992. Mechanisms by which benzo[*a*]pyrene, an environmental carcinogen, suppresses B cell lymphopoiesis. Toxicol. Appl. Pharmacol. 117 (2), 155–164. https://doi.org/10.1016/0041-008X(92)90232-H.

Herkenne, C., Naik, A., Kalia, Y.N., Hadgraft, J., Guy, R.H., 2006. Pig ear skin ex vivo as a model for in vivo dermatopharmacokinetic studies in man. Pharm. Res. 23 (8), 1850–1856. https://doi.org/10.1007/s11095-006-9011-8.

Herkenne, C., Naik, A., Kalia, Y.N., Hadgraft, J., Guy, R.H., 2007. Ibuprofen transport into and through skin from topical formulations: in vitro–in vivo comparison. J. Invest. Dermatol. 127 (1), 135–142. https://doi.org/10.1038/sj.jid.5700491.

Hopf, N., Champmartin, C., Schenk, L., Berthet, A., Chedik, L., Du Plessis, J., Franken, A., Frasch, F., Gaskin, S., Johanson, G., 2020. Reflections on the OECD guidelines for in vitro skin absorption studies. Regul. Toxicol. Pharmacol., 104752 https://doi.org/10.1016/j.yrtph.2020.104752.

International Agency for Research on Cancer (IARC), 2018, Agents classified by the IARC monographs, volumes 1–113. https://monographs.iarc.who.int/agents-classified-by-the-iarc/ (accessed 13.08.2021).

Kalia, Y.N., Pirot, F., Guy, R.H., 1996. Homogeneous transport in a heterogeneous membrane: water diffusion across human stratum corneum in vivo. Biophys. J. 71 (5), 2692–2700. https://doi.org/10.1016/S0006-3495(96)79460-2.

Kim, D., Andersen, M.E., Nylander-French, L.A., 2006. Dermal absorption and penetration of jet fuel components in humans. Toxicol. Lett. 165 (1), 11–21. https://doi.org/10.1016/j.toxlet.2006.01.009.

Kim, D., Farthing, M.W., Miller, C.T., Nylander-French, L.A., 2008. Mathematical description of the uptake of hydrocarbons in jet fuel into the stratum corneum of human volunteers. Toxicol. Lett. 178 (3), 146–151. https://doi.org/10.1016/j.toxlet.2008.03.005.

Kim, S.-K., Karadeniz, F., 2012. Biological importance and applications of squalene and squalane. Adv. Food Nutr. Res 65, 223–233. https://doi.org/10.1016/B978-0-12-416003-3.00014-7.

Lee, C.M., Jin, S.P., Doh, E.J., Lee, D.H., Chung, J.H., 2019. Regional Variation of Human Skin Surface Temperature. Ann. Dermatol. 31 (3), 349–352. https://doi.org/10.5021/ad.2019.31.3.349.

de Lima Ribeiro, F.A., Ferreira, M.M.C., 2003. QSPR models of boiling point, octanol–water partition coefficient and retention time index of polycyclic aromatic hydrocarbons. J. Mol. Struc. -THEOCHEM 663 (1–3), 109–126. https://doi.org/10.1016/j.theochem.2003.08.107.

Luo, K., Zeng, D., Kang, Y., Lin, X., Sun, N., Li, C., Zhu, M., Chen, Z., Man, Y.B., Li, H., 2020. Dermal bioaccessibility and absorption of polycyclic aromatic hydrocarbons (PAHs) in indoor dust and its implication in risk assessment. Environ. Pollut. 264, 114829 https://doi.org/10.1016/j.envpol.2020.114829.

Mackenzie, K.M., Murray Angevine, D., 1981. Infertility in mice exposed in utero to benzo[*a*]pyrene. Biol. Reprod. 24 (1), 183–191. https://doi.org/10.1095/biolreprod24.1.183.

Moody, R.P., Nadeau, B., Chu, I., 1995. In vivo and in vitro dermal absorption of benzo [a]pyrene in rat, guinea pig, human and tissue-cultured skin. J. Dermatol. Sci. 9 (1), 48–58. https://doi.org/10.1016/0923-1811(94)00356-J.

Moody, R.P., Tytchino, A.V., Yip, A., Petrovic, S., Novel, A., 2011. "By Difference" Method for Assessing Dermal Absorption of Polycyclic Aromatic Hydrocarbons from Soil at Federal Contaminated Sites. J. Toxicol. Environ. Health, A 74 (19), 1294–1303. https://doi.org/10.1080/15287394.2011.589104.

Ng, K.M.E., Bronaugh, R.L., Franklin, C.A., Somers, D.A., 1991. Percutaneous absorption/metabolism of phenanthrene in the hairless guinea pig: Comparison of in vitro and in vivo results. Fundam. Appl. Toxicol. 16 (3), 517–524. https://doi.org/10.1016/0272-0590(91)90092-I.

Ng, S.-F., Rouse, J.J., Sanderson, F.D., Meidan, V., Eccleston, G.M., 2010. Validation of a static Franz diffusion cell system for in vitro permeation studies. AAPS PharmSciTech 11 (3), 1432–1441. https://doi.org/10.1208/s12249-010-9522-9.

Octanol-Water Partition Calculation. ⟨http://www.chemspider.com/Chemical-Structure.7798.html?rid=a22a50c7–1c8c-446d-949a-5abd6fe95e4e⟩ (accessed 20.09.2021).

OECD Series on Testing and Assesment No. 28: Guidance document for the conduct of skin absorption studies. OECD Publishing: Paris, 2004a.
OECD Guideline for the Testing of Chemicals No. 428: Skin Absorption: in vitro Method. OECD Publishing: Paris, 2004b.
OECD Environment Directorate: Health and Safety Publications Series on Testing and Assessment No. 156: Guidance Notes on Dermal Absorbtion. OECD Publishing: Paris, 2011.
Raykar, P.V., Fung, M.C., Anderson, B.D., 1988. The role of protein and lipid domains in the uptake of solutes by human stratum corneum. Pharm. Res 5 (3), 140–150. https://doi.org/10.1023/a:1015956705293.
Regulation (EC) Nr. 1907/2006 (REACH). In Official Journal of the European Union, 2006; Vol. 136, pp 3–280.
Rota, M., Bosetti, C., Boccia, S., Boffetta, P., La Vecchia, C., 2014. Occupational exposures to polycyclic aromatic hydrocarbons and respiratory and urinary tract cancers: an updated systematic review and a meta-analysis to 2014. Arch. Toxicol. 88 (8), 1479–1490. https://doi.org/10.1007/s00204-014-1296-5.
Rothe, H., Obringer, C., Manwaring, J., Avci, C., Wargniez, W., Eilstein, J., Hewitt, N., Cubberley, R., Duplan, H., Lange, D., 2017. Comparison of protocols measuring diffusion and partition coefficients in the stratum corneum. J. Appl. Toxicol. 37 (7), 806–816. https://doi.org/10.1002/jat.3427.
Roy, T.A., Kriech, A.J., Mackerer, C.R., 2007. Percutaneous absorption of polycyclic aromatic compounds from bitumen fume condensate. J. Occup. Environ. Hyg. 4 (sup1), 137–143. https://doi.org/10.1080/15459620701334814.
Sartorelli, P., Aprea, C., Cenni, A., Novelli, M.T., Orsi, D., Palmi, S., Matteucci, G., 1998. Prediction of percutaneous absorption from physicochemical data: a model based on data of in vitro experiments. Ann. Occup. Hyg. 42 (4), 267–276. https://doi.org/10.1016/S0003-4878(98)00021-0.
SCCS (Scientific Committee on Consumer Safety): Basic criteria for the in vitro assessment of dermal absorption of cosmetic ingredients. 7th plenary meeting 2010.
Simon, K., Oberender, G., Roloff, A., 2023. Continuous removal of single cell layers by tape stripping the stratum corneum – a histological study. Eur. J. Pharm. Biopharm. 188, 48–53. https://doi.org/10.1016/j.ejpb.2023.04.022.
Singh, S., Zhao, K., Singh, J., 2003. In vivo percutaneous absorption, skin barrier perturbation, and irritation from JP-8 jet fuel components. Drug Chem. Toxicol. 26 (2), 135–146. https://doi.org/10.1081/DCT-120020408.
Soebianto, Y.S., Katsumura, Y., Ishigure, K., Kubo, J., Koizumi, T., Shigekuni, H., Azami, K., 1993. Model experiment on the protection effect in polymers: radiolysis of liquid squalane in the presence and absence of additives. Polym. Degrad. Stab. 42 (1), 29–40. https://doi.org/10.1016/0141-3910(93)90022-B.
Sousa, G., Teixeira, J., Delerue-Matos, C., Sarmento, B., Morais, S., Wang, X., Rodrigues, F., Oliveira, M., 2022. Exposure to PAHs during Firefighting Activities: A Review on Skin Levels, In Vitro/In Vivo Bioavailability, and Health Risks. Int. J. Environ. Res. Public Health 19 (19). https://doi.org/10.3390/ijerph191912677.
Takahashi, K., Suzuki, T., Sakano, H., Mizuno, N., 1995. Effect of vehicles on diclofenac permeation across excised rat skin. Biol. Pharm. Bull. 18 (4), 571–575. https://doi.org/10.1248/bpb.18.571.
US EPA. Estimation Program Interface (EPI) Suite. Ver. 4.11. 2012, Available from, as of Sept 13, 2016: ⟨https://www2012.epa.gov/tsca-screening-tools⟩.
Zafar, A., Chickos, J., 2019. The vapor pressure and vaporization enthalpy of squalene and squalane by correlation gas chromatography. J. Chem. Thermodyn. 135, 192–197. https://doi.org/10.1016/j.jct.2019.03.032.
Zhang, Q., Murawsky, M., LaCount, T., Kasting, G.B., Li, S.K., 2018. Transepidermal water loss and skin conductance as barrier integrity tests. Toxicol. Vitr. 51, 129–135. https://doi.org/10.1016/j.tiv.2018.04.009.

A. Supporting Information

A.1 Additional Images, Tables and Graphs

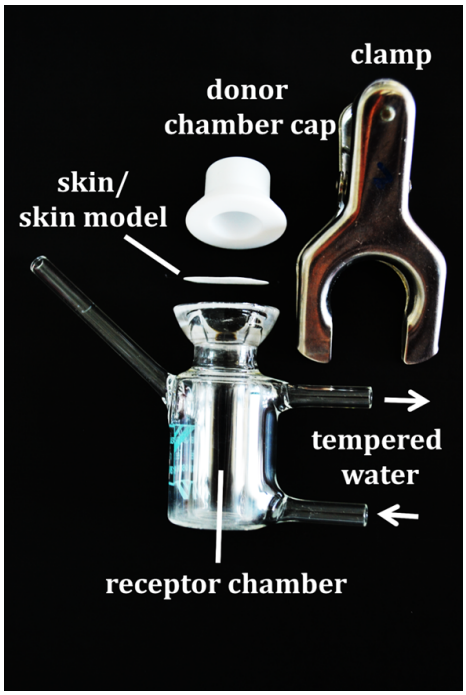

Fig. S1: Overview of the components of the disassembled Franz diffusion cell.

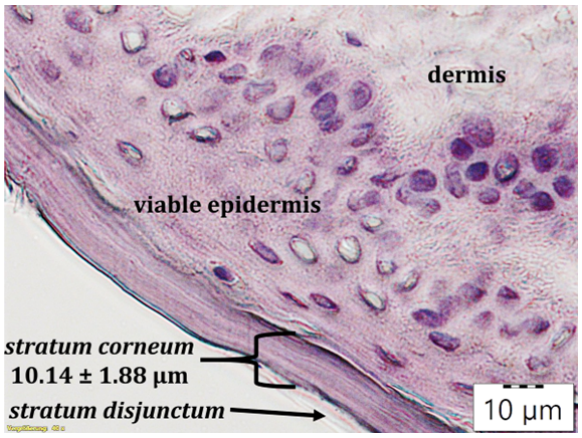

Fig. S2: Cross section of pigskin for the determination of the thickness of the stratum corneum and visible stratum disjunctum, viable epidermis and dermis. 40-fold magnification.

Table S1: Starting concentrations cm of the different PAH in the donor solutions (mean ± SD, $n = 3$), recovery in the different compartments, and over-all recovery (mean ± SD) after incubation time ti. SD: standard deviation, PAH: polycyclic aromatic hydrocarbons, s.c.: stratum corneum, B[*a*]P: benzo[*a*]pyrene, DB[*a,h*]P: dibenzo[*a,h*]pyrene; please note the different units of PAH concentrations in individual compartments.

substance	t_i **[h]**	c_m **[µg·ml^{-1}]**	**donor [%]**	**s.c. [‰]**	**remaining skin [‰]**	**receptor [‰]**	**sum [%]**
naphthalene	1	1005 ± 36	102.3 ± 3	0.559 ± 0.244	0.488 ± 0.103	0.182 ± 0.05	102.4 ± 3
anthracene	1	1030 ± 46	99.7 ± 1.9	1.317 ± 0.477	0.69 ± 0.36	0.015 ± 0.018	99.9 ± 2
pyrene	1	541 ± 8	98.4 ± 1.1	1.171 ± 0.518	0.639 ± 0.385	0.025 ± 0.038	98.6 ± 1.2
B[a]P	1	661 ± 4	97.4 ± 1.8	2.491 ± 0.718	0.675 ± 0.437	0.024 ± 0.03	97.7 ± 2
DB[a,h]P	1	50.9 ± 0.9	100.9 ± 5.4	10.6 ± 3.5	6.345 ± 8.797	0.012 ± 0.02	102.6 ± 6.6
naphthalene	24	965 ± 34	94.95 ± 7.4	1.08 ± 0.92	2.47 ± 1.28	26.4 ± 5.51	98.05 ± 7.52
pyrene	24	895 ± 24	95 ± 1.4	6.76 ± 3.62	5.67 ± 2.39	1.3 ± 0.3	96.37 ± 0.85
B[a]P	24	900 ± 27	93.78 ± 4	6.98 ± 2.62	4.7 ± 2.43	0.97 ± 0.89	95.05 ± 3.77
DB[a,h]P	24	50.5 ± 1.5	97.04 ± 4.5	15.61 ± 7.06	15.75 ± 7.46	1.02 ± 0.94	99.89 ± 4.75

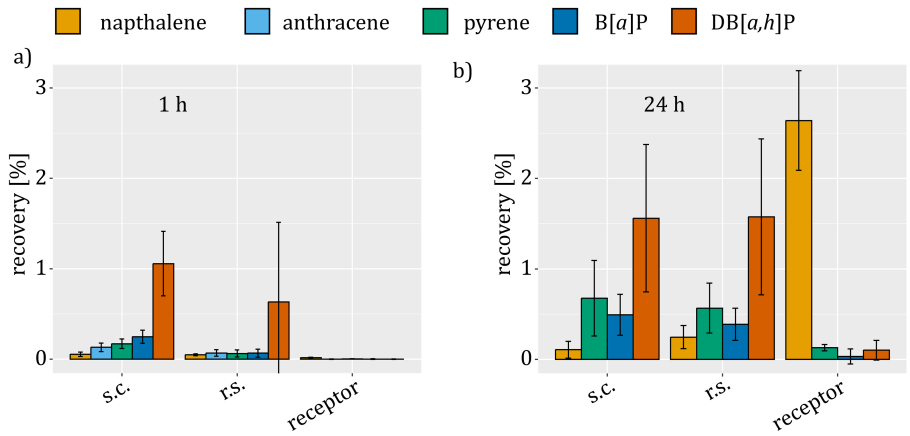

Fig. S3: Recovery of the total applied mass of each PAH in each compartment. a) 1 h incubation time (mean ± SD); b) 24 h incubation time (mean ± SD). Donors not shown, see Table S1 for values. SD: standard deviation, PAH: polycyclic aromatic hydrocarbons, B[a]P: benzo[*a*]pyrene, DB[*a,h*]P: dibenzo[*a,h*]pyrene, s.c.: *stratum corneum*, r.s.: remaining skin.

2

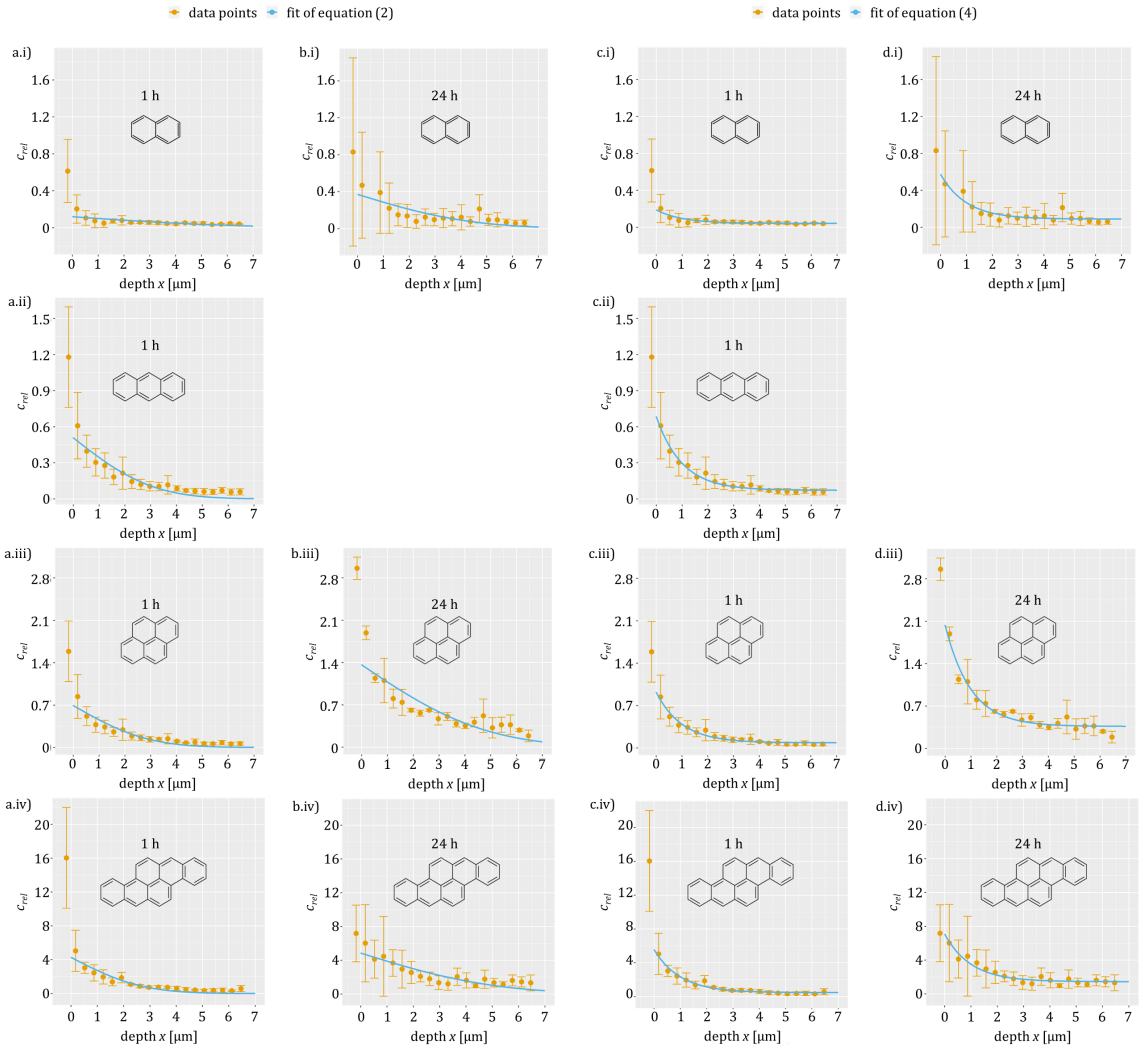

Fig. S4: Measured relative concentrations c_{rel} of the PAH (yellow, means ± SD): i) naphthalene, ii) anthracene, iii) pyrene, iv) dibenzo[*a*,*h*]pyrene (for benzo[*a*]pyrene see Fig. 1 and 3 of the main paper) at depth x in the *stratum corneum* and after an incubation time 1 h (a) and c)) and 24 h (b) and d)) and the corresponding fit of equation (1) (a) and b)) and equation (3) (c) and d)). Fits in light blue. The first data points at negative *x*-values represent the *stratum disjunctum* and were omitted from mathematical analysis. SD: standard deviation, PAH: polycyclic aromatic hydrocarbons, c_{rel}: see equation (3).

Table S2: Molecular mass (M), logarithmic octanol-water partition coefficient (log$P$), decadic logarithmic partition coefficient log$K_{sc/m}$ of medium and *stratum corneum* and diffusion coefficient D_{sc} for the different PAH (mean ± SD). SD: standard deviation, PAH: polycyclic aromatic hydrocarbons, B[*a*]P: benzo[*a*]pyrene, DB[*a,h*]P: dibenzo[*a,h*]pyrene.

substance	M [g·mol^{-1}]	log$P$	log$K_{sc/m}$ 1 h	$D_{sc}\cdot 10^{12}$ [m$^2\cdot$h^{-1}] 1 h	log$K_{sc/m}$ 24 h	$D_{sc}\cdot 10^{12}$ [m$^2\cdot$h^{-1}] 24 h
naphthalene	128	3.37[1]	−0.926 ± 0.117	11.83 ± 4.71	−0.432 ± 0.06	0.250 ± 0.085
anthracene	178	4.54[1]	−0.293 ± 0.023	2.908 ± 0.587	—	—
pyrene	202	5.18[1]	−0.159 ± 0.013	2.567 ± 0.536	0.134 ± 0.012	0.298 ± 0.071
B[*a*]P	252	6.04[1]	0.024 ± 0.002	2.483 ± 0.443	0.176 ± 0.016	0.274 ± 0.067
DB[*a,h*]P	302	7.28[2]	0.631 ± 0.052	2.257 ± 0.473	0.685 ± 0.056	0.337 ± 0.076

Table S3: Molecular mass (M), logarithmic octanol-water partition coefficient (log$P$), decadic logarithmic partition coefficient log$K_{sc/m}$ of medium and *stratum corneum* and diffusion coefficient D_{sc} for the different PAH (mean ± SD). SD: standard deviation, PAH: polycyclic aromatic hydrocarbons, B[*a*]P: benzo[*a*]pyrene, DB[*a,h*]P: dibenzo[*a,h*]pyrene.

substance	**σ equation (2) 1 h**	**σ equation (4) 1 h**	**ratio 1 h**	**σ equation (2) 24 h**	**σ equation (4) 24 h**	**ratio 24 h**
naphthalene	0.02709	0.01676	1.617	0.07333	0.04629	1.584
anthracene	0.05465	0.02213	2.47	—	—	—
pyrene	0.07471	0.03708	2.015	0.22703	0.09548	2.089
B[*a*]P	0.09637	0.0458	2.104	0.67331	0.07266	3.125
DB[*a,h*]P	0.44753	0.232	1.929	0.22703	0.38404	1.753

Table S4: Parameters calculated from equation (4) (value ± SD). SD: standard deviation, B[*a*]P: benzo[*a*]pyrene, DB[*a,h*]P: dibenzo[*a,h*]pyrene.

substance	**log u_t 1 h**	**log w_t 1 h**	**log u_t 24 h**	**log w_t 24 h**
naphthalene	−0.833 ± 0.093	−1.383 ± 0.154	−0.314 ± 0.046	−1.056 ± 0.153
anthracene	−0.212 ± 0.018	−1.145 ± 0.097	—	—
pyrene	−0.076 ± 0.009	−1.074 ± 0.13	0.224 ± 0.016	−0.441 ± 0.032
B[a]P	0.105 ± 0.011	−0.914 ± 0.094	0.274 ± 0.014	−0.423 ± 0.022
DB[a,h]P	0.707 ± 0.095	−0.325 ± 0.044	0.751 ± 0.055	0.161 ± 0.012

4

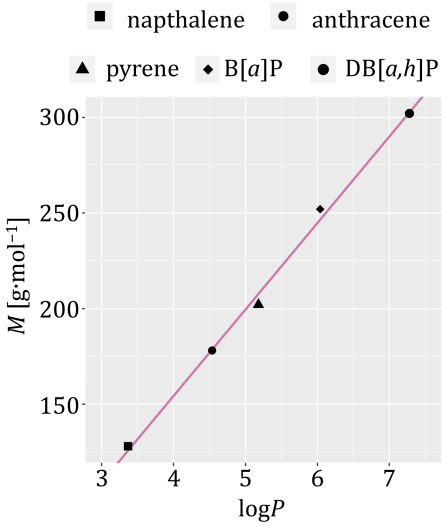

Fig. S5: Molar mass (M) vs. octanol-water partition coefficient ($\log P$).[1,2] For the investigated PAH, the two are linearly related as indicated by the purple trend line described by $M = (45.199 \cdot \log P - 26.341)\,\mathrm{g \cdot mol^{-1}}$ with coefficient of determination $r^2 = 0.995$. PAH: polycyclic aromatic hydrocarbons, B[a]P: benzo[a]pyrene, DB[a,h]P: dibenzo[a,h]pyrene.

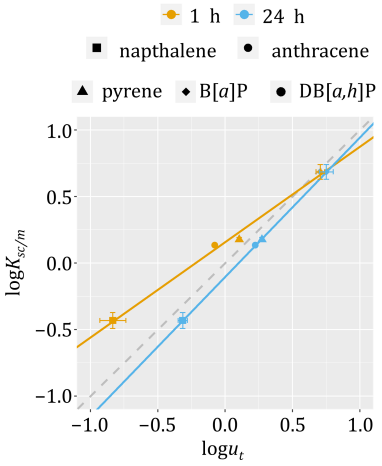

Fig. S6: Decadic logarithmic partition coefficient $\log K_{sc/m}$ vs. $\log u_t$ (see equation (4), mean ± SD) with linear regressions for both time points (dashed line: $y = x$). SD: standard deviation, B[a]P: benzo[a]pyrene, DB[a,h]P: dibenzo[a,h]pyrene.

A.2 Method

A.2.1 Chemicals

Naphthalene (CAS: 91-20-3) was acquired from Merck Group (Darmstadt, Germany), B[a]P-d12 (63466-71-7), bovine serum albumin (9048-46-8), magnesium sulfate heptahydrate (10034-99-8), naphthalen-d8 (1146-65-2), pyrene (129-00-0), pyrene-d_{10} (1718-52-1), and sodium hydrogen carbonate (144-55-8) were purchased from Sigma-Aldrich (Saint-Louis, Missouri, United States). Dibenzo[*a,h*]pyrene (189-64-0), dibenzo[*a,e*]pyrene (192-65-4), and squalane (111-01-3) were acquired from Tokyo Chemical Industry (TCI, Tokyo, Japan). B[*a*]P (50-32-8) and citric acid (77-92-9) were acquired from Fluka (Honeywell, Charlotte, North Carolina, United States), cyclohexane (110-82-7), ethanol (64-17-5), and acetonitrile (75-05-8) were acquired from Supelco (Bellefonte, Pennsylvania, United States), dichloro-methane (75-09-2), 1% aqueous Eosin Y solution, and acidic hematoxylin solution by Meyer were acquired from Carl Roth (Karlsruhe, Germany). Potassium hydroxide (1310-58-3) was acquired from AppliChem (Darmstadt, Germany). Dulbecco's phosphate-buffered saline (without calcium and magnesium) was purchased from PAN Biotech (Aidenbach, Germany).

A.2.2 Quantification of donor solutions

The actual PAH concentration of the applied donor liquid was verified individually for each experiment in triplicate. The test solution in squalane was centrifuged before use to eliminate any formed precipitate (15430 g, 6 min, Centrifuge 5427 R, Eppendorf, Hamburg, Germany). 200 µl of the supernatant were transferred to 6 ml of acetonitrile (ACN) and spiked with internal standard solution (1000 µg·ml^{-1} of the respective deuterated compound in squalane; in the case of anthracene: phenanthrene-d_{10}, in the case of DB[*a,h*]P: 10 µg·ml^{-1} dibenzo[*a,e*]pyrene (DB[*a,e*]P) in squalane). The solution was shaken vigorously, placed in an ultrasonic bath for 15 min at room temperature, and then centrifuged (3700 g, 0 °C, 15 min, Heraeus Multifuge, Thermo Fisher Scientific, Waltham, Massachusetts, United States). The upper ACN layer was removed and the extraction process was repeated once with 6 ml ACN. The combined ACN phases were diluted 1:100 with ACN (1:10 in the case of DB[a,h]P). An aliquot of 100 µl was filled into a vial with insert for PAH quantification by GC-MS/MS. The internal stand-ard concentration in the final solution was 100 ng·ml^{-1}.

A.2.3 Franz diffusion cell assay protocol

The FDC assay was carried out as follows: six FDCs (PermeGear, Hellertown, PA, United States) with 15 mm diameter (1.76 cm^2 permeation area) and a receptor volume of 12 ml were used (see Fig. S1). Each FDC assay was carried out as quadruplicate experiments with additional duplicate negative controls (24 h incubation time; B[*a*]P: n = 8 FDC assays) or as a quintuplicate experiments with one negative control (1 h incubation time). The receptor solution (50 mg·ml^{-1} of BSA in DPBS)

of 12 ml was continuously stirred magnetically. It was maintained at 32 ± 1 °C by an externally heated water jacket throughout the incubation period.
The frozen skin pieces were partially thawed and a 500 µm thick skin sheet was cut off using a dermatome (Aesculap AG, Tuttlingen, Ger-many). Sections of 25 mm diameter were punched out of the skin sheets with a stencil. Their integrity was visually verified and then laid atop the filled receptor chamber. It was visually ensured that no air bubbles were present directly under the skin in the receptor solution. To verify the integrity of the skin, the trans-epidermal water loss (TEWL) was measured using an AquaFlux device AF200 (Biox systems Ltd, London, United Kingdom), in line with OECD Guideline 428.[3] Skins were excluded and replaced if the TEWL exceeded 10 $g \cdot m^{-2} \cdot h^{-1}$.[4]
The test solution in squalane was centrifuged before use to avoid that any formed precipitate is applied to the skin (15430 g, 6 min, Centrifuge 5427 R, Eppendorf). 200 µl of the supernatant were added onto the skin with a syringe (Hamilton, Bonaduz, Switzerland, for concentra-tions, see Table S1). 200 µl of pure squalane were added onto the skin of negative controls. All cells were covered with parafilm (American National Can, Greenwich, Connecticut, United States) and incubated for 1 h or 24 h.

A.2.4 Disassembly and Extraction

After the incubation period, the four compartments of the Franz cell (donor, s.c., remaining skin, receptor) were treated as follows: The remaining donor liquid was removed with a Pasteur pipette and transferred into a screw top glass jar. The donor chamber was washed with 3 × 1 ml of ACN and the washes were added to the glass jar. The donor chamber cap was wiped off using a precision wipe (Kimtech Science, Kimberly-Clark, Irving, Texas, United States). The wipe was then folded in on itself and used to wipe off any residual squalane from the skin and added to the squalane/ACN mixture. An internal standard solution (1000 $\mu g \cdot ml^{-1}$ of the respective deuterated compound or phenan-threne-d10 in squalane; in the case of DB[*a*,*h*]P: 10 $\mu g \cdot ml^{-1}$ DB[*a*,*e*]P in squalane) was added and the jars were placed into an ultrasonic bath for 30 min at room temperature. The liquid phases were transferred into a centrifugal tube and centrifuged (3720 g, 0 °C, 15 min). The ACN phase was transferred into a 10 ml volumetric flask and the extraction was repeated once with 5 ml of ACN. The combined solution was filled up to 10 ml and diluted 1:100 with ACN (1:10 in the case of DB[*a*,*h*]P). An aliquot of 100 µl was filled into a vial with insert for PAH quantification by GC-MS/MS. The internal standard concentration in the final solution was 100 $ng \cdot ml^{-1}$.
The s.c. was stripped 20 times using tape strips (kristall-klar, tesafilm, Norderstedt, Germany). Each tape was placed into a separate screw top jar filled with 6 ml of ACN and an internal standard solution (500 $ng \cdot ml^{-1}$ of the respective deuterated compound, phenanthrene-d_{10} or DB[*a*,*e*]P in ACN). The tapes were extracted in an ultrasonic bath for 30 min at room temperature. The liquid phases were transferred into centrifugal tubes. The tape strips were discarded and the jars were rinsed with 5 ml of cyclohexane that was added into the centrifugal tubes. The tubes were shaken, then centrifuged (3720 g, 0 °C, 15 min) and the cyclohexane phases were transferred into 10 ml

volumetric flasks (tape strips 1–5) or in test tubes (tape strips 6–20; in the case of DB[*a*,*h*]P: all solutions were directly given into test tubes). The extraction was repeated once with 5 ml of cyclohexane. The solutions in the volumetric flasks were filled up to the mark and an aliquot (1 ml for tape strips 1–3; 2.5 ml for tape strips 4 and 5) was taken and transferred to test tubes. The solutions in the test tubes were then evaporated close to dryness under a stream of nitrogen (35–70 kPa, 35 °C) using a concentration workstation (Turbovap, Biotage, Uppsala, Sweden) as published by Bartsch *et al.*[5] The residue was taken up with 100 µl of cyclohexane and transferred into 1 ml vials with 100 µl inserts for PAH quantification by GC-MS/MS. The internal standard concentration in the final solution was 100 ng·ml^{-1}. The skin remaining after the tape stripping was transferred to a screw top jar filled with 6 ml of ACN and an internal standard solution (10 µg·ml^{-1} of the respective deuterated compound, phenanthrene-d_{10} or DB[*a*,*e*]P in ACN). The jar was placed into an ultrasonic bath for 30 min at room temperature. The liquid phase was transferred into a 10 ml volumetric flask. The skin was rinsed twice with 2 ml of ACN, which was added to the volumetric flask. The flask was filled up to the mark. An aliquot of 100 µl was filled into a vial with insert for PAH quantification by GC-MS/MS. The internal standard concentration in the final solution was 100 ng·ml^{-1}.

2 ml of the receptor solution were transferred into a centrifugal tube. An internal standard solution (10 µg·ml^{-1} of the respective deuterated compound, phenanthrene-d_{10} or DB[*a*,*e*]P in ACN) was added to the receptor chamber and stirred for 20 min. The solution in the receptor chamber was then added to the centrifugal tube and the receptor chamber was rinsed twice with 2 ml of ACN. 12 ml of a saturated, ethanolic potassium hydroxide solution were added into the centrifugal tube to denature the BSA. The solution was extracted twice with 12 ml and 6 ml of cyclohexane, respectively, which were transferred into a fresh centrifugal tube. The resulting solution was washed with 12 ml of aqueous citric acid (100 mg·ml^{-1}) to neutralize the solution and with 12 ml of water. The cyclohexane phase was then dried with magnesi-um sulfate and the solution was filtered into glass tubes with graduated appendices (1 ml). The solution was concentrated to < 1 ml under reduced pressure (150 mbar) at 55 °C in a parallel evaporation concentrator with the cooler set to 10 °C. The solutions were then filled up to 1 ml. An aliquot of 100 µl was filled into a vial with insert for PAH quantification by GC-MS/MS. The internal standard concentration in the final solution was 100 ng·ml^{-1}.

A.2.5 GC-MS/MS Analysis

The solutions obtained in the above described protocols were quantified using online-coupled gas chromatography electron ionization tandem mass spectrometry (GC7890A-MS7000A, Agilent, Santa Clara, California, United States) in multiple reaction monitoring (MRM) mode. For chromatographic separation, a DB-EUPAH GC-column (20 m × 0.18 mm inner diameter; 0.14 µm film thickness; Agilent) attached to a pre-column (10 m × 0.25 mm inner diameter; Phenomenex, Aschaffenburg, Germany) was used. Helium (purity ≥ 99.999%, Linde, Pullach, Germany) acted as carrier gas. The following GC temperature program was applied: 70 °C for 2 min, structured ramp:

8

20 °C·min^{-1} to 100 °C, 50 °C·min^{-1} to 340 °C with a hold time of 12 min. For more parameters, see table S5. For time segments, see table S6. For details on the MRM-settings, see table S7.
The instrument was connected to an autosampler MPS 2XL (MultiPurpose Sampler; Gerstel, Mülheim, Ruhr, Germany). A cooled injection system (CIS, programmed temperature vaporizing type; Gerstel) was used with an initial injection temperature of 45 °C, followed by a ramp of 12 °C·s^{-1} to 340 °C with a hold time of 5 min. The injection volume was 1 µl. The syringe was rinsed four times before and after each injection with cyclohexane or ACN. GC-MS/MS data were acquired using the Enhanced MassHunter Version 10.0 software (Build 10.0.384.1, Agilent) and Maestro 1.4.56.6/35 software (Gerstel). MassHunter workstation software (Quantitative Analysis Version 10.0.707.0, Agilent) was used to analyze the GC-MS/MS data. Selected qualifier and quantifier ions were extracted and automatically integrated accompanied by manual control (Table S7 and Fig. S7). A deviation of up to 20% from the quantifier to qualifier ratio was deemed acceptable. For all analytes, a linear regression calibration for the concentration range from 0.50 to 500 ng·ml^{-1} was performed. For the calibration, the relative concentration was determined by dividing the theoretical concentration by the concentration of the internal standard (10 ng·ml^{-1}). The relative response was calculated by dividing the response by the response of the internal standard. The relative response was then plotted against the relative concentration and a linear regression weighted by one over the relative concentration was calculated (Table S6 and Fig. S8).

Table S5: General GC-MS/MS parameters.

parameter	**value**
source temperature	280 °C
GC gas	helium
collision gas	nitrogen at 1.5 ml·min^{-1}
flow rate GC	1.8 ml·min^{-1}
gain factor	15
ionization energy	70 eV
transfer line temperature	320 °C
quadrupole temperature	150 °C
purge flow to split valve	50 ml·min^{-1} after 5 min
quench gas flow	helium at 2.25 ml·min^{-1}

Table S6: MRM time segments used in the GC-MS/MS program and factors for linear regression for the calibration curve of each compound ($y = m \cdot x + e$): m: slope of linear regression, e: y-axis intercept, r^2: coefficient of determination, MRM: multiple reaction monitoring, B[*a*]P: benzo[*a*]pyrene, DB[*a,h*]P: dibenzo[*a,h*]pyrene.

time segment	substance	start time	end time	m	e	r^2
1	naphthalene	4.00 min	6.00 min	0.942905	–0.029400	0.9993
2	anthracene	6.00 min	7.40 min	0.93847	–0.049893	0.9991
3	pyrene	7.40 min	8.80 min	1.305984	0.004525	0.9993
4	B[*a*]P	8.80 min	11.50 min	2.032834	–0.151048	0.9986
5	DB[*a,h*]P	11.50 min	20.30 min	0.792002	–0.021443	0.9986

Table S7: Time segments, quantifiers and qualifiers for each compound: *m/z*: mass to charge ratio; TS: time segment; t_r: retention time; qaunt pre ion: *m/z* quantifier precursor ion; quant prod ion: *m/z* quantifier product ion; qual pre ion: *m/z* qualifier precursor ion; qual prod ion: *m/z* qualifier product ion; CE: collision energy; qual/quant: ratio of qualifier response to quantifier response, B[*a*]P: benzo[*a*]pyrene, DB[*a,h*]P: dibenzo[*a,h*]pyrene.

compound	TS	t_r [min]	dwell [ms]	qaunt pre ion	quant prod ion	CE [V]	qual pre ion	qual prod ion	CE [V]	qual/quant [%]
naphthalene	1	4.996	5	128	128	20	128	102	20	55
naphthalene-d8	1	4.982	5	136	136	20	136	108	20	44
anthracene	2	6.911	10	178	178	20	178	177	20	23
phenanthrene-d10	2	6.881	10	188	188	20	188	186	20	22
pyrene	3	7.729	15	202	202	15	202	201	20	18
pyrene-d10	3	7.717	15	212	212	15	212	210	20	13
B[a]P	4	9.401	25	252	252	15	252	250	20	15
B[a]P-d12	4	9.377	25	264	264	15	264	260	20	10
DB[a,h]P	5	13.798	40	302	302	30	302	300	47	55
DB[a,e]P	5	13.14	40	302	302	30	302	300	47	66

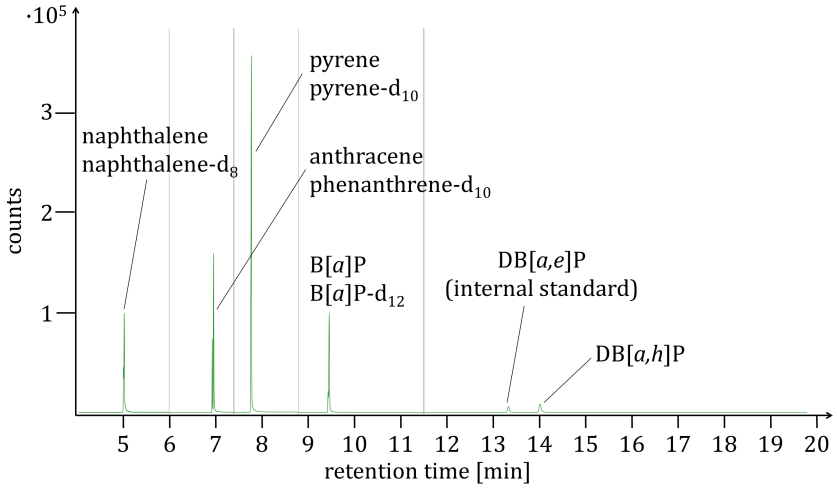

Fig. S7: Chromatogram of the five investigated compounds at a concentration of 240 ng·ml^{-1} (internal standard concentration: 100 ng·ml^{-1}). B[*a*]P: benzo[*a*]pyrene, DB[*a,h*]P: dibenzo[*a,h*]pyrene, DB[*a,e*]P: dibenzo[*a,e*]pyrene.

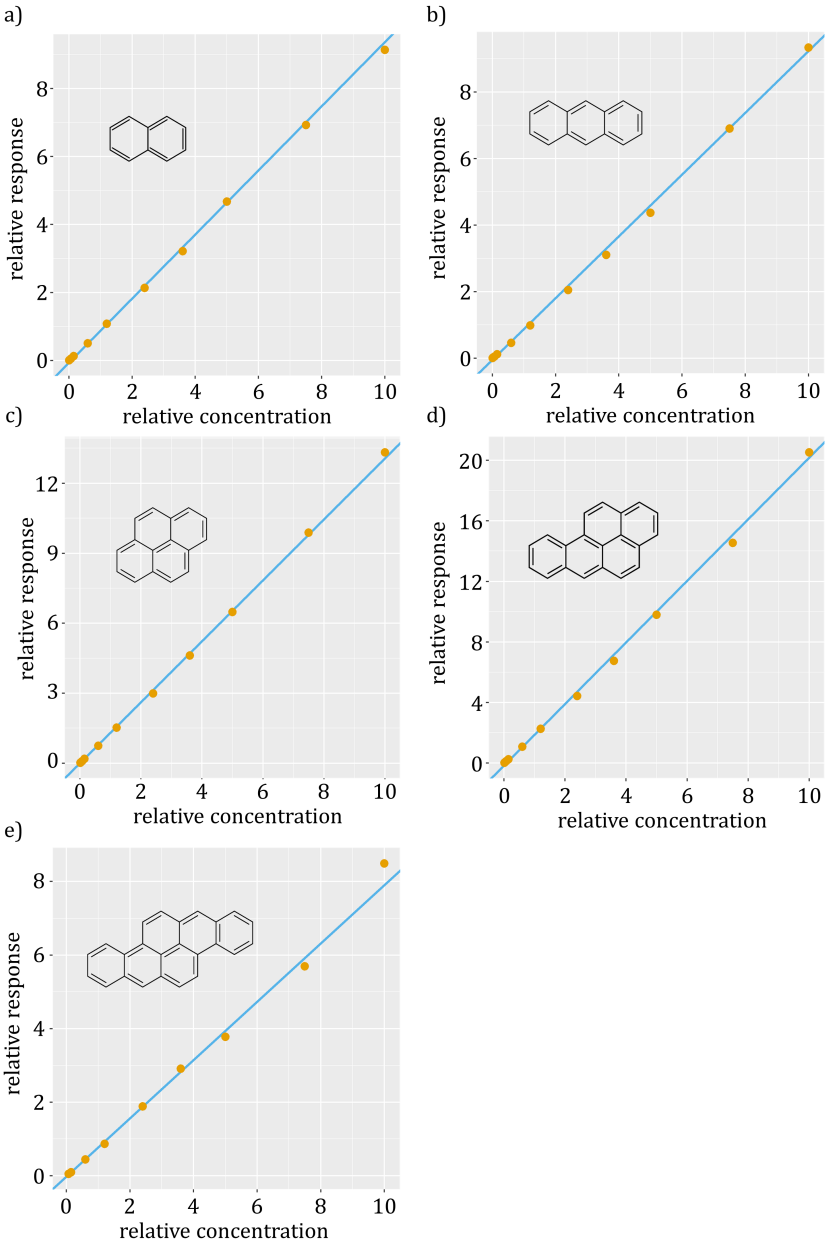

Fig. S8: Calibration curves of a) naphthalene, b) anthracene, c) pyrene, d) benzo[*a*]pyrene and e) dibenzo[*a*,*h*]pyrene. Relative response: response of compound divided by response of internal standard. Relative concentration: theoretical concentration divided by concentration of internal standard (100 ng·ml^{-1}).

A.2.6 Mathematical analysis of equation (4)

For an equation to obey Fick's second law, the equation

$$\frac{\partial c_{x,t}}{\partial t} = -D_{sc}\frac{\partial^2 c_{x,t}}{\partial x^2} \tag{A.1}$$

must be fulfilled. The second derivative of equation (3) with respect to the depth x is

$$\frac{\partial c_{rel,x,t}}{\partial x^2} = u_t \cdot e^{-x}. \tag{A.2}$$

The first derivative of equation (4) with respect to t is

$$\frac{\partial C_{rel,x,t}}{\partial t} = \frac{\partial u_t}{\partial t}e^{-x} + \frac{\partial w_t}{\partial t}. \tag{A.3}$$

The first derivative of w_t with respect to t cannot yield zero unless w_t would be a time-independent constant. Our data show that w_t is time-dependent (compare Fig. 4b). Thus,

$$-D \cdot u_t \cdot e^{-x} \neq \frac{\partial u_t}{\partial t} \cdot e^{-x} + \frac{\partial w_t}{\partial t}, \tag{A.4}$$

and equation (4) does not obey Fick's second law.

A.2.7 Determination of *stratum corneum* thickness

The thickness and the removal rate of the s.c. was determined histologically, as previously described.[6] Briefly, the scraps of the punched out skin sheets were stripped up to 20 times, increasing the number of tape strips by two between each sample. Then, a section of about 5 × 5 mm was cut out using a scalpel. It was frozen in an optimal cutting temperature compound (Tissue-Tek O.C.T., Sakura, Staufen, Germany) using liquid nitrogen. Of each frozen skin section, multiple cross sections of 5 µm were cut using a cryotom (HM 550 OP, Thermo Fisher Scientific) and fixed onto microscopy slides (Epredia SuperFrost Plus, Thermo Fischer Scientific). The slides were submersed in acetone at –20 °C for 20 min. The slides were placed into an acidic hematoxylin solution by Meyer (filtered before use) at room temperature for 20 min. The slides were rinsed with desalinated water and then transferred into Scott's Tap Water Substitute (23.8 mM sodium hydrogen carbonate and 166 mM magnesium sulfate heptahydrate in desalinated water, pH = 8.3) for 12 min. The slides were rinsed with desalinated water and then placed into a 1% aqueous Eosin Y solution for 3 min. The slides were rinsed again with desalinated water and then fixed with a coverslip using FluorSave Reagent (Millipore Corporation, Billerica, Massachusetts, United States). The skin sections were magnified to 10, 20 and 40-fold magnification (Fluorescence microscope

BX51, Olympus, Shinjuku City, Tokyo, Japan) and photographs were taken (SC50, Olympus, compare Fig. S2). The measurement of the s.c. was carried out using CellSens standard 3.1 (Olympus). The thickness of the s.c. δ_{sc} was then plotted against the number of tape strips n_{TS}, thus calculating the thickness of a single s.c. layer (0.349 µm). This way, the depth d attained can be calculated with

$$d = 0.349\ \mu\text{m} \cdot n_{TS}. \tag{A.5}$$

Because the first tape strip is discarded and because we considered the depth x in our calculations to be on average in the middle of a given s.c. layer, the equation is adjusted to

$$x = 0.349\ \mu\text{m} \cdot (n_{TS} - 1) - 0.5 \cdot 0.349\ \mu\text{m} = 0.349\ \mu\text{m} \cdot (n_{TS} - 0.5). \tag{A.6}$$

1. De Lima Ribeiro, F. A. & Ferreira, M. M. C. QSPR models of boiling point, octanol–water partition coefficient and retention time index of polycyclic aromatic hydrocarbons. *J. Mol. Struc.-THEOCHEM* **663,** 109–126. doi:10.1016/j.theochem.2003.08.107 (2003).
2. *Estimation Program Interface (EPI) Suite* 2012. https://www.epa.gov/tsca-screening-tools/download-epi-suitetm-estimation-program-interface-v411.
3. OECD. *OECD Guideline for the Testing of Chemicals No. 428: Skin Absorption: in vitro Method* Legal Rule or Regulation. 2004.
4. Zhang, Q., Murawsky, M., LaCount, T., Kasting, G. B. & Li, S. K. Transepidermal water loss and skin conductance as barrier integrity tests. *Toxicol. In Vitro* **51,** 129–135. doi:10.1016/j.tiv.2018.04.009 (2018).
5. Bartsch, N., Girard, M., Schneider, L., Weijgert, V. V. D., Wilde, A., Kappenstein, O., Vieth, B., Hutzler, C. & Luch, A. Chemical stabilization of polymers: Implications for dermal exposure to additives. *J. Environ. Sci. Heal. A* **53,** 405–420. doi:10.1080/10934529.2017.1412192 (2018).
6. Simon, K., Oberender, G. & Roloff, A. Continuous removal of single cell layers by tape stripping the stratum corneum – a histological study. *Eur. J. Pharm. Biopharm.* **188,** 48–53. doi:10.1016/j.ejpb.2023.04.022 (2023).

14

A.4 Less efficient skin penetration of the metal allergen Pd^{2+} compared to Ni^{2+} and Co^{2+} from patch test preparations

Konstantin Simon, Philipp Reichardt, Andreas Luch, Alexander Roloff, Katherina Siewert, Franziska Riedel

Contact Dermatitis **2024**, *91*(1), 11–21.

doi: 10.1111/cod.14569

This study was submitted to the journal on 14 December 2023, revised on 01 March 2024 and accepted on 17 April 2024. Published online on 27 April 2024.

The contents of this publication are discussed in Chapter 4, Section *Dermal penetration of metal allergens*. The supporting information is added following the main part.

Author contributions: **Konstantin Simon:** Conceptualization, Methodology, Formal analysis, Investigation, Resources, Writing — original draft, Writing — review & editing, Visualization, Project administration. Philipp Reichhardt: Methodology, Investigation. Andreas Luch: Conceptualization, Writing — review & editing, Resources, Funding acquisition. Alexander Roloff: Conceptualization, Methodology, Writing — review & editing, Supervision, Project administration, Funding acquisition. Katherina Siewert: Conceptualization, Writing — review & editing, Supervision, Project administration, Project administration, Funding acquisition. Franziska Riedel: Conceptualization, Methodology, Formal analysis, Investigation, Resources, Writing — original draft, Writing — review & editing, Visualization, Project administration.

Abstract

Background: Contrary to Ni^{2+}- and Co^{2+}-induced allergic contact dermatitis (ACD), reactions against Pd^{2+} are rare. However, Pd^{2+} activates a larger T cell fraction *in vitro*, suggesting an inefficient skin penetration.

Objectives: This study compares Ni^{2+}, Co^{2+} and Pd^{2+} skin penetration from commonly used diagnostic patch test preparations (PTPs) and aqueous metal salt solutions.

Methods: Using Franz diffusion cell assays, we applied the metals in PTPs (5% $NiSO_4$, 1% $CoCl_2$, 2% $PdCl_2$ and 3% Na_2PdCl_4) and in solution to pigskin for 48 h, thereby mirroring the time frame

of a patch test. The different compartments were analysed individually by inductively coupled plasma mass spectrometry.

Results: Metal ions were mainly retained in the upper *stratum corneum* layers. After application of PTPs, concentrations in the viable skin were lower for Pd^{2+} (1 and 7 µM) compared to Ni^{2+} and Co^{2+} (54 and 17 µM).

Conclusions: Ni^{2+} and Co^{2+} penetrated the skin more efficiently than Pd^{2+} and thus may sensitize and elicit allergic contact dermatitis more easily. This was observed for ions applied in petrolatum and aqueous solutions. We hypothesize that the differently charged metal complexes are responsible for the varying skin penetration behaviors.

Graphical Abstract

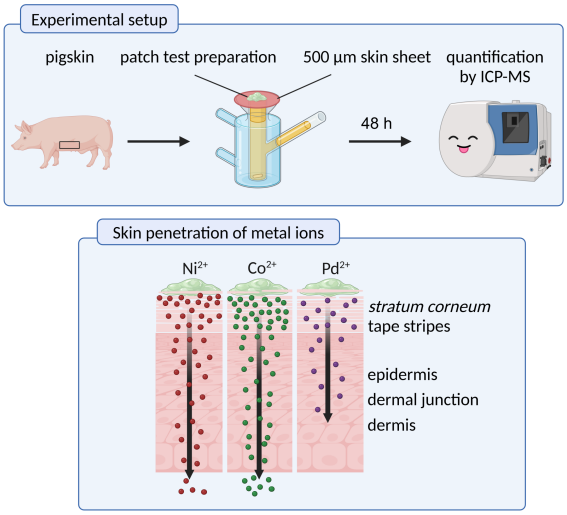

- Skin penetration of allergenic metals from petrolatum and aqueous solution was analysed by *in vitro* Franz diffusion cell assay followed by inductively coupled plasma mass spectrometry analysis.
- Ni^{2+} and Co^{2+} penetrate skin more effectively than Pd^{2+}, regardless of the matrix.
- The lower penetration rates might contribute to lower palladium allergy prevalence.

Received: 14 December 2023 | Revised: 1 March 2024 | Accepted: 17 April 2024

DOI: 10.1111/cod.14569

ORIGINAL ARTICLE

CONTACT DERMATITIS | WILEY

Less efficient skin penetration of the metal allergen Pd^{2+} compared to Ni^{2+} and Co^{2+} from patch test preparations

Konstantin Simon[1,2] | **Philipp Reichardt**[1] | **Andreas Luch**[1,2] | **Alexander Roloff**[1] | **Katherina Siewert**[1] | **Franziska Riedel**[1]

[1]Department of Chemical and Product Safety, German Federal Institute for Risk Assessment (BfR), Berlin, Germany

[2]Department of Biology, Chemistry, Pharmacy, Institute of Pharmacy, Freie Universität Berlin, Berlin, Germany

Correspondence
Alexander Roloff and Franziska Riedel, Department of Chemical and Product Safety, German Federal Institute for Risk Assessment (BfR), Berlin, Germany.
Email: alexander.roloff@bfr.bund.de and franziska.riedel@bfr.bund.de

Funding information
BfR-Internal Grants SFP, Grant/Award Numbers: 1322-774, 1322-719; Deutsche Forschungsgemeinschaft, Grant/Award Number: 500312706

Abstract

Background: Contrary to Ni^{2+}- and Co^{2+}-induced allergic contact dermatitis (ACD), reactions against Pd^{2+} are rare. However, Pd^{2+} activates a larger T cell fraction *in vitro*, suggesting an inefficient skin penetration.

Objectives: This study compares Ni^{2+}, Co^{2+} and Pd^{2+} skin penetration from commonly used diagnostic patch test preparations (PTPs) and aqueous metal salt solutions.

Methods: Using Franz diffusion cell assays, we applied the metals in PTPs (5% $NiSO_4$, 1% $CoCl_2$, 2% $PdCl_2$ and 3% Na_2PdCl_4) and in solution to pigskin for 48 h, thereby mirroring the time frame of a patch test. The different compartments were analysed individually by inductively coupled plasma mass spectrometry.

Results: Metal ions were mainly retained in the upper *stratum corneum* layers. After application of PTPs, concentrations in the viable skin were lower for Pd^{2+} (1 and 7 µM) compared to Ni^{2+} and Co^{2+} (54 and 17 µM).

Conclusions: Ni^{2+} and Co^{2+} penetrated the skin more efficiently than Pd^{2+} and thus may sensitize and elicit ACD more easily. This was observed for ions applied in petrolatum and aqueous solutions. We hypothesize that the differently charged metal complexes are responsible for the varying skin penetration behaviours.

KEYWORDS
Franz diffusion cell assay; metal allergy; Ni, Co, Pd; patch test preparation; skin penetration; T cell activation

1 | INTRODUCTION

Contact allergies are T cell-mediated diseases and are estimated to affect about 20% of the population.[1] Common contact allergens include metals such as nickel and cobalt which can be released from a variety of consumer products.[1] Therefore, nearly everyone is frequently exposed to metal allergens and thus at risk of allergic sensitization.

We recently quantified metal-specific CD4+ T cells by an *in vitro* activation-induced marker assay and identified the underlying interactions with conserved T cell receptor residues.[2,3] The particularly high frequencies we observed for Ni^{2+} and Co^{2+} were further exceeded by those of Pd^{2+}-specific T cells at optimal concentrations (ca. 400 µM

Abbreviations: ACD, allergic contact dermatitis; FDC, Franz diffusion cell; ICP-MS, inductively coupled plasma mass spectrometry; LOD, limit of detection; LOQ, limit of quantification; PBS, phosphate-buffered saline; PTP, patch test preparation; s.c., *stratum corneum*; TLR4, Toll-like receptor 4.

Katherina Siewert and Franziska Riedel shared the last authors.

Pd^{2+}). However, palladium allergy is rarely diagnosed in the general population, which may be due to less efficient skin penetration of Pd^{2+}.

Patch testing—also known as epicutaneous testing—is used as a diagnostic tool to identify contact allergies.[4,5] Although it is the current diagnostic standard, the test has several limitations. Patch testing is supposed to induce the elicitation phase of allergic contact dermatitis (ACD) by delivering a critical amount of allergen into the skin to activate immune cells on a small test area. Antigen-specific tissue-resident memory T cells emerge during sensitization and become reactivated by renewed allergen exposure, for example, during patch testing.[6,7] Tissue-resident memory T cells predominantly reside in the epidermis near the dermal junction or in the dermis. However, it remains unclear whether metal ion concentrations on the skin eliciting ACD in real-life exposure scenarios and those used in patch testing are similar. As a result, the clinical relevance of a positive patch test remains unknown.

Patch test preparations (PTPs) of metals are undissolved metal salts dispersed in petrolatum, which are applied to the back of a patient. Various PTPs of different compositions used globally can potentially deliver varying amounts of metal ions into the skin thereby hindering the comparison of allergy prevalence.[8–13] Substance properties, including particle size and solubility of the metal salt, have a significant impact on the release and penetration of metal ions into the skin.[14,15] Therefore, using an inappropriate substance can lead to false positive or false negative patch test results, which can ultimately result in incorrect allergy diagnoses. For instance, the European Society of Contact Dermatitis guideline recommends the use of undissolved $PdCl_2$ in petrolatum as a PTP.[5] As $PdCl_2$ is poorly soluble in water, it is possible that not enough Pd^{2+} is migrating into the skin during patch testing. This can lead to false negative results when employing $PdCl_2$ as test substance. As an alternative for palladium-based PTPs, the water-soluble Na_2PdCl_4 has been suggested. Positive patch test results obtained with $PdCl_2$ were generally confirmed by Na_2PdCl_4. Furthermore, Na_2PdCl_4 allowed for the diagnosis of additional patients with palladium allergy. The results were obtained despite the fact that $PdCl_2$ was applied to the skin in dissolved form and Na_2PdCl_4 was applied dispersed in petrolatum.[16–18] In the literature, the permeation of metal ions through skin (human, pig and mouse) has been analysed mainly via Franz diffusion cell (FDC) assays. Most of these experiments were carried out with incubation times of 24 h, making it difficult to predict metal permeation rates after 48 h, which is the typical duration of the patch test.[19] Since most studies are designed to mimic real-life human exposure, mainly undissolved metal salts or metal nanoparticles in artificial sweat formulations have been investigated.[19–21] The analysis of skin penetration from artificial sweat is not representative of the metal ion release from PTPs into the skin because of the different physicochemical properties of the formulations. For instance, when investigating the penetration properties of 5% $NiSO_4$ PTPs, no Ni^{2+} was found in the receptor phase after 48 h.[22]

In the present study, the metal ion penetration of the patch test salts $NiSO_4$, $CoCl_2$, $PdCl_2$ and Na_2PdCl_4 into pigskin was determined using FDC assays combined with inductively coupled plasma mass spectrometry (ICP-MS) analysis. In a setting mimicking clinical use, the metal salts were applied as PTPs under occlusion for 48 h. In addition, metal salt solutions in phosphate-buffered saline (PBS) were tested. According to the *Registration, Evaluation, Authorisation and Restriction of Chemicals* legislation of the European Union, products that have direct and prolonged contact with the skin are restricted to release nickel to a maximum of 0.5 μg/(cm^2·week).[23] We used a salt solution in PBS to apply a similar concentration of 0.57 μg/cm^2 Ni^{2+} to the skin. Therefore, it can be assumed that the penetration of Ni^{2+} into the remaining skin provides an exposure scenario close to the regulatory limit. Co^{2+} and Pd^{2+} were applied in equal amounts for comparison.

After the incubation period, the FDCs were disassembled and the *stratum corneum* (s.c.) was separated from the remaining skin by tape stripping. The disassembly produced four compartments: donor, s.c., remaining skin and receptor fluid, with the remaining skin containing the dermal junction between the epidermis and dermis.

On the basis of our results, the accuracy of patch test-based diagnoses of metal contact allergies was evaluated. Furthermore, potential causes of the observed differences in the prevalence of metal contact allergies are discussed. The determined metal ion concentrations in the different FDC compartments can guide the selection of appropriate metal ion concentrations for *in vitro* studies, including diagnostic T cell assays.

2 | METHODS

For chemicals and materials, confer to the supporting information (SI) I, section A.1 Chemicals. The experimental strategy is summarized in Figure 1.

2.1 | Pigskin

Pigskin from two female pigs was received from Charité, Universitätsmedizin Berlin. Several earlier skin penetration investigations have substituted pigskin for human skin.[24–30] Pigskin and human skin do not significantly differ in terms of relevant penetration features for organic chemicals,[31] such as lag time and diffusion of drugs in the s.c.[26–28] Because pigskin shares key permeation characteristics with human skin, the Scientific Committee on Consumer Safety advises using it in tests of skin penetration.[32] Metal penetration was found to be qualitatively similar in pigskin as compared to human skin, indicating that pigskin is a suitable experimental model for human skin.[33] The skin was treated as published before.[34] Briefly, sows were sacrificed without impact on the skin's integrity after an unrelated surgical procedure. Flank skin was removed without delay and brought to our facility on ice. There, the skin was shaved and cut into pieces of about 10 × 20 cm^2 with a knife. These pieces were frozen in plastic bags and kept at a temperature of −20°C for up to 12 months.

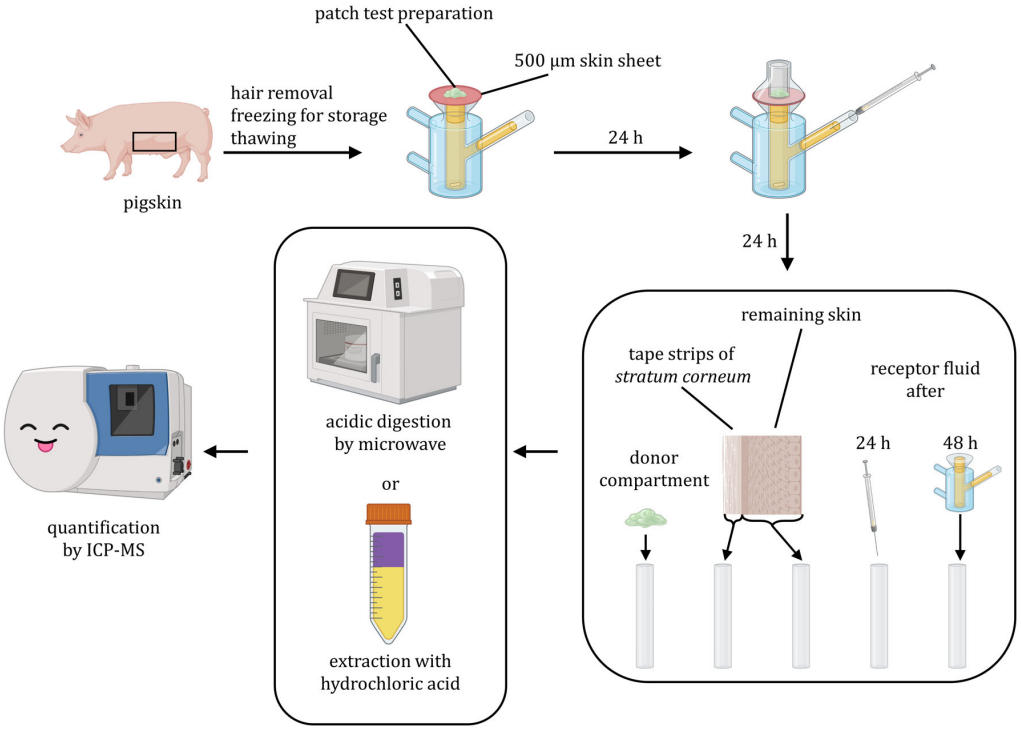

FIGURE 1 Experimental strategy. Donor substances were applied onto flank pigskin in Franz diffusion cell assays. After 24 h, a sample of the receptor fluid was taken. After 48 h, the compartments were separated including tape stripping of the *stratum corneum*. All compartments were digested with nitric acid in a microwave or extracted using hydrochloric acid. The metal contents of the resulting solutions were quantified by inductively coupled plasma mass spectrometry (ICP-MS). Created in part with BioRender.com.

TABLE 1 Donor substances used in Franz diffusion cell assays.

Donor substance	ζ	β (mg/mL)	c_n (mM)	β_A (µg/cm^2)
$NiSO_4$ PTP (5% $NiSO_4 \cdot 6H_2O$)	1.1%	9	160	127
$CoCl_2$ PTP (1% $CoCl_2 \cdot 6H_2O$)	0.2%	2	35	28
$PdCl_2$ PTP (2% $PdCl_2$)	1.2%	10	95	136
Na_2PdCl_4 PTP (3% $Na_2PdCl_4 \cdot H_2O$)	1.0%	9	81	116
Ni^{2+} solution ($NiSO_4 \cdot 6H_2O$ in PBS)	5 ppm	$5 \cdot 10^{-3}$	$8.5 \cdot 10^{-3}$	0.57
Co^{2+} solution ($CoCl_2 \cdot 6H_2O$ in PBS)	5 ppm	$5 \cdot 10^{-3}$	$8.5 \cdot 10^{-3}$	0.57
Pd^{2+} solution ($Na_2PdCl_4 \cdot H_2O$ in PBS)	5 ppm	$5 \cdot 10^{-3}$	$4.7 \cdot 10^{-3}$	0.57

Note: PTPs are declared as mass percentages (m/m). Concentration metrics for each metal ion: mass percentages of the metal ζ, mass concentrations β, molar concentrations c_n and applied surface concentrations β_A on the skin in the Franz diffusion cell assay with a skin surface area of 1.76 cm^2. Molar masses: SI II sheet 8.
Abbreviations: PBS, phosphate-buffered saline; PTP, patch test preparation.

2.2 | Donor substances

For this study, commercially available and clinically applied PTPs (ChemotechniqueMB Diagnostics AB, Vellinge, Sweden) were used (concentrations: Table 1). The amount of PTP applied to the skin was 20 mg as recommended by the European Society of Contact Dermatitis.[5] Furthermore, a solution of the three metals in PBS was used. The solution was prepared by solving the respective metal salts in hydrochloric acid (6.7%, salt concentration: $NiSO_4 \cdot 6H_2O$: 3.36 g/mL, $CoCl_2 \cdot 6H_2O$: 3.03 g/mL and $Na_2PdCl_4 \cdot H_2O$: 2.21 g/mL) and subsequent dilution in PBS to a concentration of 5 µg/mL (pH ≈ 7). About 200 µL of this solution was applied to the skin. The resulting surface concentrations on the skin after the application of PTPs or PBS solutions are summarized in Table 1.

2.3 | FDC assay

The FDC assay is commonly applied in skin penetration studies. Here, we illustrate an overview of the used method (Figure 1). The assays were carried out as six (per individual metal PTP) or seven (metal salt solution in PBS) independent experiments. For details on the experimental design and microwave digestion of samples, see the SI I, section A.2 Protocol of Franz diffusion cell assay.

For the assay, the receptor chamber (12 mL) of the FDC was filled with fetal bovine serum and a piece of dermatomed pigskin (1.5 × 1.5 cm^2, 500 µm thick) was placed onto the cell and fixed with the donor chamber cap, resulting in an application area of 1.76 cm^2. The skin integrity was assured monitoring the trans-epidermal water loss, using the AquaFlux device AF200 (Biox Systems Ltd, London, UK) in accordance with Guideline 428 of the Organisation for Economic Co-operation and Development.[35] Skin pieces were excluded and replaced if the trans-epidermal water loss exceeded 13 $g{\cdot}m^{-2}{\cdot}h^{-1}$.

The PTPs or the metal salt solution in PBS were applied to the skin and the cell was incubated at 32°C. After 24 h, a 100 µL sample was taken from the receptor chamber using a syringe. After a total incubation time of 48 h, the FDC was disassembled and the s.c. was separated from the remaining skin by tape stripping (20 strips, four consecutive strips were pooled to obtain five groups). All compartments were processed by microwave digestion with nitric acid or an extraction with hydrochloric acid (conditions: Tables S1–S3 in SI I). The samples were then quantified using ICP-MS.

2.4 | Tape stripping and skin layer volume calculation

The s.c. was separated from the skin by tape stripping.[34,36,37] Each tape strip removes about one layer of the s.c., corresponding to ca. 0.38 µm of s.c. removed per tape strip, as determined in our recent study.[34] In this study, four consecutive tape strips were pooled. Thus, every pooled sample corresponds to approximately 1.52 µm of s.c. removed. Given the 1.76 cm^2 permeation area in the FDC, this amounts to a volume of 268 nL. After 20 tape strips, 7.60 µm of the 500 µm thick skin sheet is removed, leaving a volume of 86.7 µL for the remaining skin. These values were used for the calculation of the concentrations of metal ions in the different skin layers. Importantly, 20 tape strips were found to not completely remove the s.c. but leave behind about seven layers in pigskin.[34]

2.5 | Establishment of sample preparation for quantification

Sample treatments were optimized to ensure an efficient digestion, especially for palladium, and metal ion recoveries for each compartment of the FDC assays were determined from spiked matrix samples applying optimized conditions. Recoveries were within the range of 100 ± 15%, except for the recovery of palladium from the tape strip matrix (42.1 ± 2.2%, Table S4). For quantification, the determined recovery values were used to correct for losses during sample preparation. Limits of detection (LODs) and limits of quantification (LOQs) were determined for each of the metals from noise levels of blank solutions of 3% nitric acid (Table S5). A detailed description can be found in SI I, section A.3 Establishment of sample preparation for ICP-MS.

2.6 | Solubility assessment of palladium salts in water

To determine the water solubility of the palladium salts used in the PTPs ($PdCl_2$ and Na_2PdCl_4), aqueous saturated solutions of both salts were prepared. The Pd^{2+} concentrations of the supernatants were determined by ICP-MS yielding the solubility of each salt. For details on the experimental set-up, see SI I, section A.5 Solubility of palladium salts.

2.7 | Inductively coupled plasma mass spectrometry

A quadrupole ICP-MS (iCAP Q, Thermo Fisher Scientific GmbH, Dreieich, Germany) with a perfluoroalkoxy alkane ST-Nebulizer, a quartz cyclonic spray chamber and a 2.5 mm quartz O-ring-free injector (all from Elemental Service and Instruments GmbH, Mainz, Germany) was used. The sample solutions were injected at a flow rate of 0.4 mL/min. A performance report was evaluated on each measurement day and the instrument was tuned if necessary. All isotopes were measured with collision gas (5 mL/min, H_2: 7 vol%; He: 93 vol%) in kinetic energy discrimination mode. Calibration solutions were prepared in nitric acid (3.5%) ranging from 0.2 to 120 ng/mL. Blank solutions (3.5% nitric acid, 1% hydrochloric acid) were measured before and after the calibration solutions as well as after the analysis of every five samples. Solutions were injected using a prepFast dilution system (Elemental Scientific, Omaha, Nebraska). The system was tuned using a diluted solution of Tune B (Thermo Fisher Scientific Co. LLC Waltham, Massachusetts) at a concentration of 1 ppb in 2% isopropanol. For more details, confer to the SI I, section A.5 ICP-MS quantification.

2.8 | Data analysis and statistics

Exported raw data (comma-separated values files) were analysed in R (version 4.2.2) and data points corresponding to metal concentrations below the LODs (Table S5) were marked as below LOD (<LOD). In the next step, the means of the concentrations of the negative control FDC assay results (pure petrolatum applied) were calculated and these values were subtracted (negative values are documented in SI II sheet 1) from the values obtained from the FDC cells loaded with metal-containing donor substances. From these background-corrected

values, the total metal ion masses in each of the compartments were calculated. The data were then subjected to a Shapiro–Wilk normality test.[38] If the Shapiro–Wilk normality test failed, the dataset was checked for outliers using boxplots (Figures S1–S3 in SI I). Outliers were excluded from the data set if the data were not normally distributed and if the data point was outside 1.5 times the interquartile range of the boxplot (outside of whiskers). Differences were considered significant when a *t*-test resulted in $p < 0.05$. Data given in the text are reported as means ± standard deviations.

3 | RESULTS

The aim of this study was to quantitatively compare skin penetration of Ni^{2+}, Co^{2+} and Pd^{2+} ions from both common diagnostic PTPs and an aqueous salt solution. Following incubation of pigskin in FDC assays for 48 h, the metal contents of all compartments including different s.c. layers and the remaining skin were analysed by ICP-MS. Total recoveries are in the range of 80%–104% (Table 2) illustrating that the metal ion contents were reliably quantified.

3.1 | Skin penetration of metal ions from patch test preparations

When applied in PTPs with metal ion concentrations used in clinical patch testing, Ni^{2+} and Co^{2+} more effectively penetrate into the skin than Pd^{2+} from $PdCl_2$ PTP (Figure 2A,B, SI II sheets 2 and 3). A greater share of Ni^{2+} and Co^{2+} than Pd^{2+} from either PTP was absorbed into the skin, corresponding to the recovery of all compartments but the donor compartment, even though the difference between $NiSO_4$ and Na_2PdCl_4 was not significant ($NiSO_4$: 3.98 ± 2.09%; $CoCl_2$: 5.40 ± 2.64%; $PdCl_2$: 1.47 ± 0.45%; Na_2PdCl_4: 2.00 ± 0.99%, SI II sheet 4 for *p* values). Furthermore, a greater share of Ni^{2+} and Co^{2+} was found in the remaining skin after tape stripping ($NiSO_4$: 0.120 ± 0.045%; $CoCl_2$: 0.166 ± 0.105%) compared with Pd^{2+} ($PdCl_2$: 0.004 ± 0.004%; Na_2PdCl_4: 0.032 ± 0.031%, SI II sheet 5 for *p* values). No Pd^{2+} was found in the receptor fluid after 48 h incubation, while recoveries of Ni^{2+} and Co^{2+} above the LOQ were determined (Ni^{2+}: 0.182 ± 0.186%; Co^{2+}: 0.124 ± 0.045%). No recoveries above the LOD of Ni^{2+}, Co^{2+} or Pd^{2+} were found in the receptor fluid after 24 h incubation time.

The first four tape strips contain the highest amount of any metal ion regardless of the PTP (Figure 2B). Ni^{2+} and Co^{2+} show very similar results, however, the decrease after the first four tape strips is more pronounced for Ni^{2+} than for Co^{2+}. After incubation with $PdCl_2$ PTP, Pd^{2+} was only found in the first eight tape strips in amounts above the LOD. After incubation with Na_2PdCl_4 PTP, the amount of Pd^{2+} decreased less rapidly and Pd^{2+} was detected up to 16 tape strips deep.

The concentration of Ni^{2+} in the first s.c. layers is significantly ($p = 0.025$) higher than the other metals probably due to the higher concentration in the PTP (Figure 2C, Table 3 for values of s.c. layers 17–20 and the remaining skin, SI II sheet 6 for all values). Molar concentrations in deeper s.c. layers do not differ significantly with few exceptions (SI II sheet 7). Pd^{2+} from $PdCl_2$ was not detected in tape strips nine through 16 and then again in tape strips 17–20.

Pd^{2+} from $PdCl_2$ PTP was found in a significantly lower concentration in the remaining skin than Ni^{2+} and Co^{2+} from their respective PTPs ($p = 0.02$). Contrarily, the Pd^{2+} concentration in the remaining skin from Na_2PdCl_4 PTP is only significantly different from Ni^{2+} ($p = 0.03$, $NiSO_4$: 53 ± 37 μM; $CoCl_2$: 17 ± 10 μM; $PdCl_2$: 1.1 ± 1.0 μM; Na_2PdCl_4: 11.5 ± 5.8 μM).

3.2 | Skin penetration of metal ions from metal salt solutions in PBS

To investigate the different skin penetration capabilities of the metal ions independent from salt solubility in water, FDCs applying an aqueous solution of the salts in PBS were performed (Figure 3). Metal salts were dissolved in PBS to maintain a stable, neutral pH. Since we found no reliable values in the literature, the solubilities of $PdCl_2$ and Na_2PdCl_4 in water were determined. The values obtained are 7.74

TABLE 2 Total recovery and absolute masses of metal ions after application of patch test preparations (PTPs) and aqueous salt solutions in Franz diffusion cell assays.

Application	Applied metal ion mass (μg)	Recovered metal ion mass (μg)	Total recovery (%)
$NiSO_4$ PTP	229 ± 5.5	219 ± 1.5	96 ± 0.5
$CoCl_2$ PTP	50.6 ± 1.1	48.4 ± 0.3	96 ± 0.7
$PdCl_2$ PTP	246 ± 5.1	195 ± 1.2	80 ± 0.6
Na_2PdCl_4 PTP	210 ± 2.3	177 ± 1.3	84 ± 0.6
Ni^{2+} solution in PBS	1.0	1.04 ± 0.06	104 ± 6
Co^{2+} solution in PBS	1.0	0.90 ± 0.05	90 ± 5
Pd^{2+} solution in PBS	1.0	0.85 ± 0.03	85 ± 3

Note: Mean recoveries/masses ± standard deviations with $n = 6$ (PTP) or $n = 7$ (solution) independent experiments. Total recoveries/masses represent the sum of the quantified metal contents in all analysed compartments.
Abbreviation: PBS, phosphate-buffered saline.

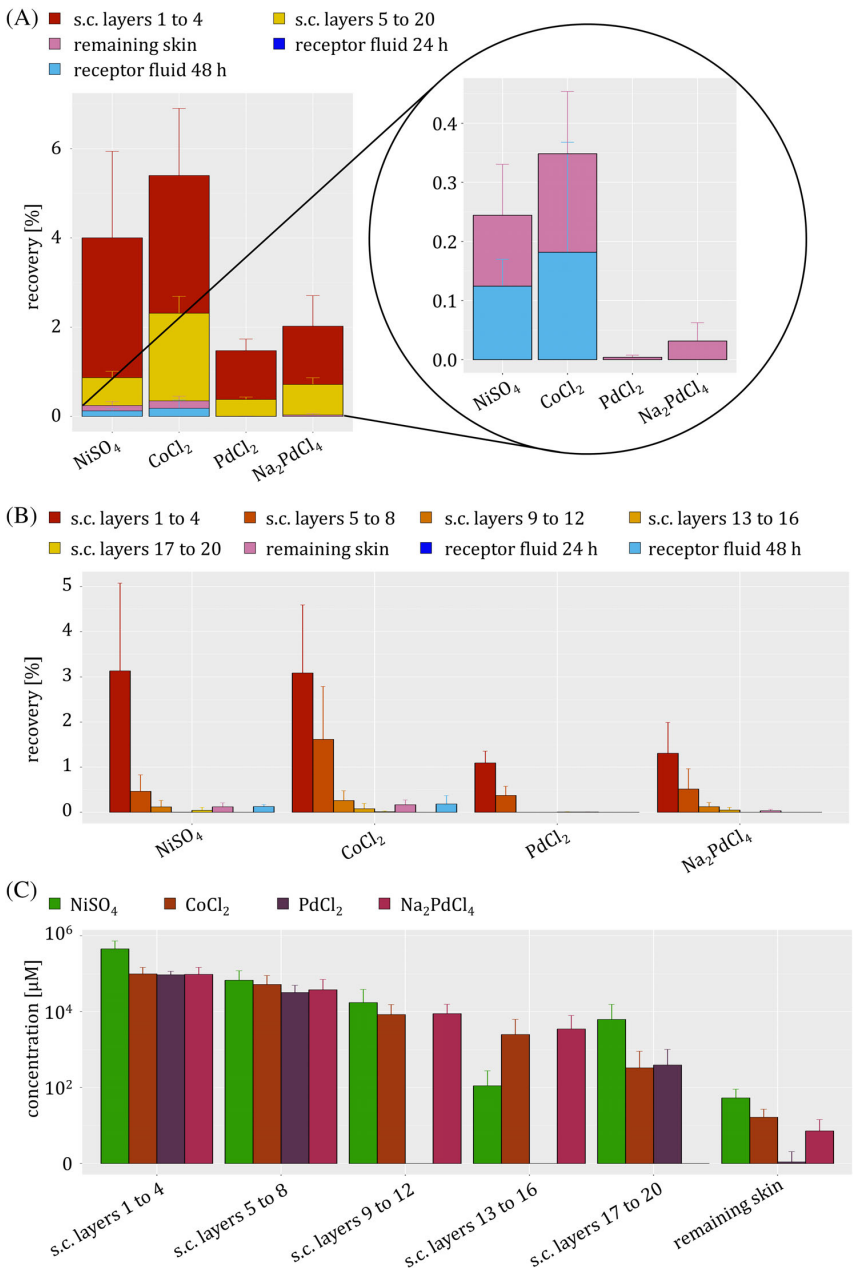

FIGURE 2 Recoveries of Ni^{2+}, Co^{2+} and Pd^{2+} after the application of different patch test preparations (PTPs, see Table 1 for metal concentration) in a Franz diffusion cell assay after 48 h of incubation. (A) Stacked diagram. Magnification: data from the *stratum corneum* (s.c.) were omitted for clarity. (B) Bar diagram of recoveries to compare different compartments and layers of the s.c. (C) Bar diagram showing micromolar concentrations in the respective skin layers to compare different PTPs; logarithmic scale. No ions were recovered after 24 h in the receptor fluid. Means ± standard deviation with $n = 6$ independent experiments.

± 1.17 mM of Pd^{2+} for $PdCl_2$ and 241 ± 49 mM of Pd^{2+} for Na_2PdCl_4. The values determined here are used as guidance to show that Na_2PdCl_4 is indeed better soluble in water than $PdCl_2$. For comparison, the water solubilities of $NiSO_4$ and $CoCl_2$ are 1.9 M of Ni^{2+} and 4.08 M of Co^{2+}, respectively.[39,40]

Notably, the proportion of the applied ions that was detected in the entire skin after 48 h did not significantly differ between the metals (Ni^{2+}: 64.5 ± 16.4%; Co^{2+}: 69.4 ± 16.2%; Pd^{2+}: 68.5 ± 7.3%). However, the distribution in individual skin compartments is different: the recoveries in the uppermost s.c. layers (tape strips one to four) significantly vary for all three ions with Pd^{2+} being retained the most, which is followed by Co^{2+} and Ni^{2+} ($p < 0.02$, Ni^{2+}: 13.8 ± 3.8%; Co^{2+}: 22.7 ± 4.0%; Pd^{2+}: 39.9 ± 5.7%). In s.c. layers 5–20, the three metals are statistically equally abundant (Ni^{2+}: 11.0 ± 2.2%; Co^{2+}: 14.7 ± 2.5%; Pd^{2+}: 17.5 ± 2.5%). A higher recovery of Ni^{2+} compared to Pd^{2+} is found in the remaining skin ($p = 0.006$); Co^{2+} recovery does not significantly differ from both (Ni^{2+}: 23.6 ± 8.5%; Co^{2+}: 17.5 ± 8.1%; Pd^{2+}: 10.6 ± 5.4%). In the receptor fluid after 24 h, the only metal that was detected above LOD was Co^{2+} (5.18 ± 1.96%). After 48 h, only a small recovery of Pd^{2+} was detected in the receptor fluid

TABLE 3 Metal concentrations in the lower *stratum corneum* (s.c.) layers and the remaining skin.

	s.c. layers 17–20		Remaining skin	
Donor substance	**(µM)**	**(µg/ml)**	**(µM)**	**(µg/ml)**
$NiSO_4$ PTP	6263 ± 9349	368 ± 549	53.5 ± 37.4	3.14 ± 2.20
$CoCl_2$ PTP	333 ± 576	19.6 ± 33.9	16.5 ± 10.5	0.97 ± 0.62
$PdCl_2$ PTP	394 ± 622	41.9 ± 66.2	1.1 ± 1.0	0.12 ± 0.10
Na_2PdCl_4 PTP	<LOD	<LOD	7.2 ± 7.1	0.77 ± 0.76
Ni^{2+} solution in PBS	718 ± 1110	42.2 ± 65.1	46.3 ± 16.7	2.72 ± 0.98
Co^{2+} solution in PBS	753 ± 923	44.4 ± 54.4	34.2 ± 15.9	2.02 ± 0.94
Pd^{2+} solution in PBS	454 ± 645	48.3 ± 68.6	11.5 ± 5.8	1.22 ± 0.62

Note: Mean concentrations ± standard deviations with $n = 6$ (PTP) or $n = 7$ (solution) independent experiments. Molar masses: SI II sheet 8.
Abbreviations: PBS, phosphate-buffered saline; PTP, patch test preparation.

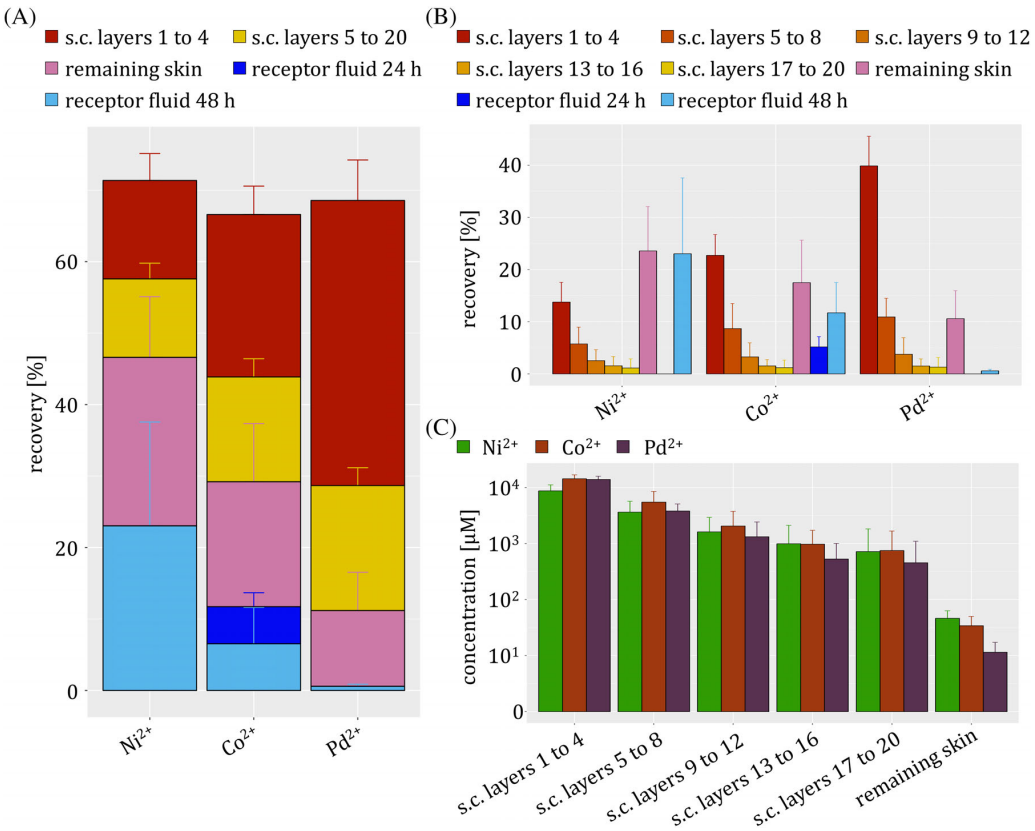

FIGURE 3 Recovery of Ni^{2+}, Co^{2+} and Pd^{2+} after application of a solution of the three metals (see Table 1 for metal concentration) in a Franz diffusion cell assay at 48 h incubation time. (A) Stacked diagram. Recovery after 24 h was subtracted from recovery after 48 h. (B) Bar diagram of recoveries to compare different compartments and layers of the *stratum corneum* (s.c.). (C) Bar diagram of micromolar concentrations in the respective skin layers to compare different metals; logarithmic scale. Means ± standard deviation with $n = 7$ independent experiments.

compared to Ni^{2+} and Co^{2+} ($p < 0.013$; Ni^{2+}: 23.0 ± 14.5%; Co^{2+}: 11.7 ± 5.8%; Pd^{2+}: 0.59 ± 0.29%).

The distribution profile in the s.c. after incubation of the metals dissolved in PBS is similar for Ni^{2+} and Co^{2+} (Figure 3B). Molar concentrations (Figure 3C; Table 3 for values of s.c. layers 17–20 and remaining skin) on the other hand do not differ significantly in the different s.c. layers, except for lower Ni^{2+} concentration in the uppermost s.c. layers ($p = 0.002$). The molar concentration of Pd^{2+} in the remaining skin is significantly lower than that of the other two metals ($p < 0.01$). Even though the applied molar concentration of Pd^{2+} is

about half of that of Ni^{2+} and Co^{2+}, the molar concentration of Pd^{2+} in the s.c. is similar. The drop in Pd^{2+} concentration in the remaining skin is thus not due to a lower applied concentration but shows less efficient Pd^{2+} penetration through the skin.

4 | DISCUSSION

Here, we present an investigation of the skin penetration of Ni^{2+}, Co^{2+} and Pd^{2+} from commonly applied PTPs. Using FDC assays, we incubated pigskin with the PTPs for 48 h, mimicking the settings of diagnostic patch testing as recommended by the European Society of Contact Dermatitis guidelines.[5] Pigskin served as an often used alternative to human skin, as it is similar in relevant penetration features.[31] The skin penetration of metal ions from a solution in PBS was analysed to investigate penetration independent from water solubility. Based on the results, we attempt to understand the link between metal ion penetration and epicutaneous patch testing results for metal-mediated contact allergies.

4.1 | Chemical factors influencing metal penetration rates

Ni^{2+} and Co^{2+} from $NiSO_4$ and $CoCl_2$ PTPs penetrated the s.c. and the viable skin much more efficiently than Pd^{2+} from $PdCl_2$ or Na_2PdCl_4 PTPs (Figure 2A). This can be explained by the different metal salt water solubilities, which are reported to be in the molar range for $NiSO_4$ and $CoCl_2$ but measured to be in the mid to low millimolar range for the two palladium salts.[39,40] In PTPs, the metal salts are dispersed in petrolatum, while for skin penetration, it is feasible to assume a dissolution in an aqueous medium such as sweat prior to being taken up into the skin. In FDC assays, the necessary water is provided by the transepidermal water loss (measured at about 10 g/(h·m^2)). Thus, the higher water solubilities of Ni^{2+} and Co^{2+} salts compared to Pd^{2+} salts contribute to higher recoveries of Ni^{2+} and Co^{2+} in the different s.c. layers and the remaining skin.

The water solubility of metal salts was not the only factor leading to a lower skin penetration of Pd^{2+} into the skin. Previous research on the skin penetration of dissolved metal salts indicates that metal ions are retained in the s.c.[14,41–43] The effect, where Pd^{2+} was not detected in tape strips 9–16 of the s.c., but in tape strips 17–20, could be due to the s.c./viable epidermis boundary layer. Here, the diffusion from the s.c. into the viable epidermis is slow. A similar trend was observed for Ni^{2+}, whose concentration in the s.c. also increased when approaching this boundary layer. In the literature, the middle and lower s.c. layers have been shown to provide a barrier to metals, for example chromium.[44] Histidine-rich filaggrin proteins strongly chelate nickel, which is hypothesized to slow down skin penetration. The effective retention of metal ions may therefore be attributed to the barrier effect of filaggrin.[44–46]

Infinite dose conditions,[35] which occur due to the excessive abundance of metal salts in PTPs, could compensate for the lower solubility. We observed that the majority (>90%) of the metal ions remain in the donor compartment and do not penetrate the skin. The metal salt concentration of the PTPs is therefore likely not the determining factor for the efficient delivery of Pd^{2+} into the remaining skin. Hence, the difference between the penetration of Ni^{2+} and Co^{2+} on the one hand and Pd^{2+} on the other hand must at least partially be due to physico-chemical differences in the ions—such as radius or complexation behaviour—and biochemical properties determining their interactions with the skin.

The skin is a permselective membrane preferring cation transport.[47,48] The chloride concentration in the skin is around 79.9 ± 4.8 mM,[49] approximately corresponding to the molar Pd^{2+} concentration in the PTPs. Since Pd^{2+} prefers complexation with chloride, it is plausible to assume that dermally applied Pd^{2+} will form complexes with the general structure of $[PdCl_x(H_2O)_{4-x}]^{2-x}$ ($x = 2, 3, 4$).[50,51] These chloropalladate complexes are negatively charged or neutral. Ni^{2+} and Co^{2+} on the other hand form complexes with the general structure of $[M(H_2O)_{6-x}]^{2+}$ ($M = Ni^{2+}$, Co^{2+}, $x = 0, 2$).[52] These complexes are always positively charged. We thus hypothesize that the difference in charge of the metal ion complexes contributes to the observed differences in penetration rates through the skin.

This hypothesis is supported by the skin penetration data for metal salts in buffered solutions. While the molar concentrations in the s.c. are similar for all three metal salts ($NiSO_4$, $CoCl_2$ and Na_2PdCl_4), the concentration of Pd^{2+} in the remaining skin is significantly lower than that of Ni^{2+} and Co^{2+}. This difference can be explained with the pH gradient of the skin: the s.c. surface pH is acidic, ranging from 4.1 to 5.8.[53] In deeper cell layers, the pH rises to about 7.[54] A higher pH corresponds to more deprotonated carboxylic acid groups and the membrane becomes more permselective for cations. This effect is intensified by the application medium (PBS), with a pH of about 7. At this point, the negatively charged Pd^{2+} complexes are retained stronger while the positively charged Ni^{2+} and Co^{2+} complexes are able to penetrate more readily through the skin into the receptor fluid, which was held at a physiological pH of 7.4.

4.2 | Potential immunological interactions

Determining the concentration of metal ions in skin layers is crucial because immune system interactions that trigger metal allergies are concentration-dependent. During sensitization, the innate immune system becomes activated, resulting in the maturation of dendritic cells such as epidermal Langerhans cells. The dendrites of Langerhans cells can extend outwards into the lower layers of the s.c.[53] In this study, concentrations of about 450–750 μM of Ni^{2+}, Co^{2+} and Pd^{2+} were determined in the lower layers of the s.c. (strips 17–20). Such concentrations were shown to activate a plethora of pathways in dendritic cells *in vitro*, for example, due to reactive oxygen species formation.[55] *In vitro* studies demonstrated that THP-1 cells were activated by 500 μM Ni^{2+} and Co^{2+}, while human Toll-like receptor 4 (TLR4) activation occurred at 250 μM Ni^{2+} and 750 μM Co^{2+} in HEK293 cells.[56] TLR4 is not expressed on freshly isolated Langerhans cells or keratinocytes,[57] but

TLR4-expressing cells in the dermis may be in contact with similarly high metal ion concentrations in case of skin injury. Our results thus demonstrate that exposure to a Ni^{2+} solution in PBS at concentrations comparable to the regulatory limit may lead to Ni^{2+} concentrations in the skin relevant for dendritic cell activation.

Using the novel activation-induced marker assay, our previous research has shown that T cell activation is highly concentration-dependent, peaking at about 400 μM for all three metal ions.[3] Notably, at this concentration, Pd^{2+} activates a large fraction of the T cell pool. To ensure an accurate allergy diagnosis, PTPs must release metals to yield concentrations in the viable epidermis comparable to those that elicit ACD to re-activate tissue-resident memory T cells. In healthy skin of nickel allergic donors, as little as 7.7 μg/cm^2 Ni^{2+} was sufficient to elicit ACD.[58,59] However, these concentrations may not be the same as those for optimal *in vitro* T cell activation.

In our FDC assays using the $NiSO_4$ PTP, a Ni^{2+} concentration of about 54 μM was found in the remaining skin. A concentration within the same range could therefore be optimal for replicating patch test results *in vitro*. Consequently, this concentration could be utilized for an alternative *in vitro* assay for diagnosing contact allergies. In accordance with our results, Cavani et al. identified approximately 40 μM Ni^{2+} as the most suitable concentration for conducting a nickel allergy diagnosis using a quantitative limited dilution assay.[60] Such a quantitative approach may reveal an increased blood frequency of Ni^{2+}-specific T cells in allergic individuals and thereby enable allergy diagnosis.

Conventional lymphocyte transformation test protocols use lower metal salt concentrations. Higher concentrations may lead to ambiguous results due to an allergy non-related T cell proliferation caused by the presence of Ni^{2+} reactive cells in each individual.[61,62] In FDC assays using $CoCl_2$ PTP, we found considerably less Co^{2+} in the remaining skin compared to Ni^{2+}. Hence, lower concentrations than those used for Ni^{2+} may be necessary in *in vitro* experiments to replicate the results of patch tests.

Of the three metals analysed, Pd^{2+} had the lowest concentration in the remaining skin, regardless of whether PTPs or a metal salt solution were applied. This suggests that even though Pd^{2+} has the ability to activate a large portion of the T cell pool, only a very small fraction of Pd^{2+}-specific T cells become engaged at the low Pd^{2+} concentrations in the skin.[3] This may explain why palladium allergies are less common than nickel allergies, in addition to a generally lower dermal exposure. On the other hand, individuals may become sensitized to higher Pd^{2+} concentrations (for example, in case of skin injury), but $PdCl_2$ PTP may not deliver enough ions to enable diagnoses. This may lead to false negative results when employing $PdCl_2$ in a PTP. Previous research by Muris et al. suggested higher reliability in patch tests conducted with Na_2PdCl_4 compared to $PdCl_2$,[18] proposing the use of the water-soluble Na_2PdCl_4 for patch testing.[16,17]

4.3 | Limitations

Due to the experimental set-up, only 100 μL of the receptor solution was sampled for analysis after 24 h. As a result of this small volume, it is possible that the metal ions in this aliquot were below the LODs of the ICP-MS method and therefore the migrated amount of metal ions could not be determined. This limitation does not apply to the receptor solution after 48 h.

FDC assays were carried out using either a solution of equal mass of Ni^{2+}, Co^{2+} and Pd^{2+} in PBS or diagnostic PTPs. An alternative approach would be the use of equimolar solutions and PTPs. If the penetration of the metal ions is concentration-dependent, an evaluation of higher concentrated solutions could lead to diverging concentrations in the skin. However, we do not believe that the overall trend (Pd^{2+} penetrates the skin less efficiently than Ni^{2+} and Co^{2+}) would change. We base this on the similar trend in penetration after the application of the PBS solution and the PTPs.

The obtained results could further be verified with human skin. However, the literature indicates that pigskin is a good surrogate for human skin, yielding qualitatively comparable results.[33]

An additional limitation is the use of skin from only two pigs. Data from a higher number of specimens could better account for variability between different individuals, even though we found no variance between the two analysed individuals.

5 | CONCLUSION

In conclusion, we elucidate a lower skin penetration capacity of Pd^{2+} compared to Ni^{2+} and Co^{2+}. The approach allows the comparison of metal ion penetration into healthy pigskin from aqueous solutions to that of metal ion penetration from diagnostic PTPs. Our results provide orientation values on local metal ion concentration in different layers of the skin, which are important for an understanding of metal allergies and the patch testing procedure. The less efficient skin penetration of Pd^{2+} could potentially result in lower sensitization rates or underdiagnoses of contact allergies through patch testing on intact skin, which could partially be addressed by employing Na_2PdCl_4-based PTPs. Our findings can guide the further development of *in vitro* testing strategies and the choice of relevant concentrations for cross-reactivity assessment, given that metal ion interactions with the immune system are highly concentration-dependent.

AUTHOR CONTRIBUTIONS

Konstantin Simon: Conceptualization; methodology; formal analysis; investigation; resources; writing – original draft; writing – review and editing; visualization; project administration. **Philipp Reichardt:** Methodology; investigation. **Andreas Luch:** Conceptualization; writing – review and editing; resources; funding acquisition. **Alexander Roloff:** Conceptualization; methodology; writing – review and editing; supervision; project administration; funding acquisition. **Katherina Siewert:** Conceptualization; writing – review and editing; supervision; project administration; funding acquisition. **Franziska Riedel:** Conceptualization; methodology; formal analysis; investigation; resources; writing – original draft; writing – review and editing; visualization; project administration.

ACKNOWLEDGEMENTS

We thank Tanja Schmidt and Katja Reiter from Charité, Berlin, for providing us with pigskin. We thank Nadine Dreiack and Mohammad Al-Khatib for excellent technical assistance and Roman Schmidt for help with the ICP-MS analysis. We thank Benjamin-Christoph Krause for help with initial method development and Charlotte Kromer for proof reading and fruitful discussions. This work was funded by BfR-Internal Grants SFP 1322-774, SFP 1322-719 and Deutsche Forschungsgemeinschaft grant 500312706 (to K. Siewert). Open Access funding enabled and organized by Projekt DEAL.

CONFLICT OF INTEREST STATEMENT

The authors have no conflict of interest to declare.

DATA AVAILABILITY STATEMENT

All data are made available in the tables provided in the Supporting Information.

ORCID

Konstantin Simon https://orcid.org/0000-0001-7409-5004
Philipp Reichardt https://orcid.org/0000-0002-0159-5814
Alexander Roloff https://orcid.org/0000-0003-1886-3288
Katherina Siewert https://orcid.org/0000-0003-0380-1594
Franziska Riedel https://orcid.org/0000-0002-2395-5454

REFERENCES

1. Alinaghi F, Bennike NH, Egeberg A, Thyssen JP, Johansen JD. Prevalence of contact allergy in the general population: a systematic review and meta-analysis. *Contact Dermatitis*. 2019;80(2):77-85. doi:10.1111/cod.13119
2. Aparicio-Soto M, Riedel F, Leddermann M, et al. TCRs with segment TRAV9-2 or a CDR3 histidine are overrepresented among nickel-specific CD4+ T cells. *Allergy*. 2020;75(10):2574-2586. doi:10.1111/all.14322
3. Riedel F, Aparicio-Soto M, Curato C, et al. Unique and common TCR repertoire features of Ni(2+) -, Co(2+) -, and Pd(2+) -specific human CD154+ CD4+ T cells. *Allergy*. 2023;78(1):270-282. doi:10.1111/all.15494
4. Brasch J, Becker D, Aberer W, et al. Guideline contact dermatitis: S1-Guidelines of the German Contact Allergy Group (DKG) of the German Dermatology Society (DDG), the Information Network of Dermatological Clinics (IVDK), the German Society for Allergology and Clinical Immunology (DGAKI), the Working Group for Occupational and Environmental Dermatology (ABD) of the DDG, the Medical Association of German Allergologists (AeDA), the Professional Association of German Dermatologists (BVDD) and the DDG. *Allergo J Int*. 2014;23(4):126-138. doi:10.1007/s40629-014-0013-5
5. Johansen JD, Aalto-Korte K, Agner T, et al. European Society of Contact Dermatitis guideline for diagnostic patch testing—recommendations on best practice. *Contact Dermatitis*. 2015;73(4):195-221. doi:10.1111/cod.12432
6. Gaide O, Emerson RO, Jiang X, et al. Common clonal origin of central and resident memory T cells following skin immunization. *Nat Med*. 2015;21(6):647-653. doi:10.1038/nm.3860
7. Ono E, Lenief V, Lefevre M-A, et al. Topical corticosteroids inhibit allergic skin inflammation but are ineffective in impeding the formation and expansion of resident memory T cells. *Allergy*. 2024;79:52-64. doi:10.1111/all.15819
8. de Groot AC. New contact allergens: 2008 to 2015. *Dermatitis*. 2015;26(5):199-215. doi:10.1097/der.0000000000000144
9. Gollhausen R, Przybilla B, Ring J. Reproducibility of patch tests. *J Am Acad Dermatol*. 1989;21(6):1196-1202. doi:10.1016/s0190-9622(89)70329-7
10. Brasch J, Henseler T, Aberer W, et al. Reproducibility of patch tests. A multicenter study of synchronous left-versus right-sided patch tests by the German Contact Dermatitis Research Group. *J Am Acad Dermatol*. 1994;31(4):584-591. doi:10.1016/s0190-9622(94)70220-9
11. Bourke JF, Batta K, Prais L, Abdullah A, Foulds IS. The reproducibility of patch tests. *Br J Dermatol*. 1999;140(1):102-105. doi:10.1046/j.1365-2133.1999.02615.x
12. Ale SI, Maibach HI. Reproducibility of patch test results: a concurrent right-versus-left study using TRUE Test. *Contact Dermatitis*. 2004;50(5):304-312. doi:10.1111/j.0105-1873.2004.00351.x
13. Schaeffer AC, Andersen KE, Bindslev-Jensen C, Mortz CG. The reproducibility of nickel, cobalt and chromate sensitization in patients tested at least twice in the period 1992-2014 with TRUE Test(R). *Contact Dermatitis*. 2016;75(2):111-113. doi:10.1111/cod.12563
14. Tanojo H, Hostýnek JJ, Mountford HS, Maibach HI. In vitro permeation of nickel salts through human stratum corneum. *Acta Derm Venereol*. 2001;81(212):19-23. doi:10.1080/000155501753279596
15. Larese F, Gianpietro A, Venier M, Maina G, Renzi N. In vitro percutaneous absorption of metal compounds. *Toxicol Lett*. 2007;170(1):49-56. doi:10.1016/j.toxlet.2007.02.009
16. Muris J, Goossens A, Gonçalo M, et al. Sensitization to palladium and nickel in Europe and the relationship with oral disease and dental alloys. *Contact Dermatitis*. 2015;72(5):286-296. doi:10.1111/cod.12327
17. Muris J, Kleverlaan CJ, Feilzer AJ, Rustemeyer T. Sodium tetrachloropalladate (Na2[PdCl4]) as an improved test salt for palladium allergy patch testing. *Contact Dermatitis*. 2008;58(1):42-46. doi:10.1111/j.1600-0536.2007.01259.x
18. Muris J, Kleverlaan CJ, Rustemeyer T, et al. Sodium tetrachloropalladate for diagnosing palladium sensitization. *Contact Dermatitis*. 2012;67(2):94-100. doi:10.1111/j.1600-0536.2012.02061.x
19. Franken A, Eloff FC, Du Plessis J, Du Plessis JL. In vitro permeation of metals through human skin: a review and recommendations. *Chem Res Toxicol*. 2015;28(12):2237-2249. doi:10.1021/acs.chemrestox.5b00421
20. Champmartin C, Chedik L, Marquet F, Cosnier F. Occupational exposure assessment with solid substances: choosing a vehicle for in vitro percutaneous absorption experiments. *Crit Rev Toxicol*. 2022;52(4):294-316. doi:10.1080/10408444.2022.2097052
21. Crosera M, Mauro M, Bovenzi M, et al. In vitro permeation of palladium powders through intact and damaged human skin. *Toxicol Lett*. 2018;287:108-112. doi:10.1016/j.toxlet.2018.02.009
22. Fullerton A, Andersen JR, Hoelgaard A. Permeation of nickel through human skin in vitro—effect of vehicles. *Br J Dermatol*. 1988;118(4):509-516. doi:10.1111/j.1365-2133.1988.tb02460.x
23. ANNEX XVII TO REACH—Conditions of Restriction; Entry 27: Nickel. 2016.
24. Bartsch N, Heidler J, Vieth B, Hutzler C, Luch A. Skin permeation of polycyclic aromatic hydrocarbons: a solvent-based in vitro approach to assess dermal exposures against benzo[a]pyrene and dibenzopyrenes. *J Occup Environ Hyg*. 2016;13(12):969-979. doi:10.1080/15459624.2016.1200724
25. Bartsch N, Girard M, Schneider L, et al. Chemical stabilization of polymers: implications for dermal exposure to additives. *J Environ Sci Health A*. 2018;53(5):405-420. doi:10.1080/10934529.2017.1412192
26. Rothe H, Obringer C, Manwaring J, et al. Comparison of protocols measuring diffusion and partition coefficients in the stratum corneum. *J Appl Toxicol*. 2017;37(7):806-816. doi:10.1002/jat.3427
27. Gerstel D, Jacques-Jamin C, Schepky A, et al. Comparison of protocols for measuring cosmetic ingredient distribution in human and pig skin. *Toxicol in Vitro*. 2016;34:153-160. doi:10.1016/j.tiv.2016.03.012
28. Herkenne C, Naik A, Kalia YN, Hadgraft J, Guy RH. Pig ear skin ex vivo as a model for in vivo dermatopharmacokinetic studies in

man. *Pharm Res*. 2006;23(8):1850-1856. doi:10.1007/s11095-006-9011-8
29. Herkenne C, Naik A, Kalia YN, Hadgraft J, Guy RH. Ibuprofen transport into and through skin from topical formulations: in vitro–in vivo comparison. *J Invest Dermatol*. 2007;127(1):135-142. doi:10.1038/sj.jid.5700491
30. Simon K, Schneider L, Oberender G, et al. Migration of polycyclic aromatic hydrocarbons from a polymer surrogate through the stratum corneum layer of the skin. *Ecotoxicol Environ Saf*. 2023;262:115113. doi:10.1016/j.ecoenv.2023.115113
31. Simon GA, Maibach HI. The pig as an experimental animal model of percutaneous permeation in man: qualitative and quantitative observations—an overview. *Skin Pharmacol Appl Skin Physiol*. 2000;13(5):229-234. doi:10.1159/000029928
32. SCCS. Scientific Committee on Consumer Safety (SCCS): Basic criteria for the in vitro assessment of dermal absorption of cosmetic ingredients; 7th Plenary Meeting. 2010.
33. Magnano GC, Marussi G, Pavoni E, Adami G, Larese Filon F, Crosera M. Percutaneous metals absorption following exposure to road dust powder. *Environ Pollut*. 2022;292(Pt B):118353. doi:10.1016/j.envpol.2021.118353
34. Simon K, Oberender G, Roloff A. Continuous removal of single cell layers by tape stripping the stratum corneum—a histological study. *Eur J Pharm Biopharm*. 2023;188:48-53. doi:10.1016/j.ejpb.2023.04.022
35. OECD. *OECD Guideline for the Testing of Chemicals No. 428: Skin Absorption: In Vitro Method*. OECD Publishing; 2004.
36. Hughes A, Tawfik S, Baruah K, O'Toole E, O'Shaughnessy R. Tape strips in dermatology research. *Br J Dermatol*. 2021;185(1):26-35. doi:10.1111/bjd.19760
37. Keurentjes AJ, Jakasa I, Kezic S. Research techniques made simple: stratum corneum tape stripping. *J Invest Dermatol*. 2021;141(5):1129-1133.e1. doi:10.1016/j.jid.2021.01.004
38. Shapiro SS, Wilk MB. An analysis of variance test for normality (complete samples). *Biometrika*. 1965;52(3–4):591-611. doi:10.1093/biomet/52.3-4.591
39. PubChem Compound Summary for CID 24586, Nickel Sulfate. National Center for Biotechnology Information; 2023.
40. PubChem Compound Summary for CID 3032536, Cobaltous Chloride. National Center for Biotechnology Information; 2023.
41. Hostýnek JJ, Dreher F, Nakada T, Schwindt D, Anigbogu A, Maibach HI. Human stratum corneum adsorption of nickel salts. *Acta Derm Venereol*. 2001;81(212):11-18. doi:10.1080/000155501753279587
42. Malmberg P, Guttenberg T, Ericson MB, Hagvall L. Imaging mass spectrometry for novel insights into contact allergy—a proof-of-concept study on nickel. *Contact Dermatitis*. 2018;78(2):109-116. doi:10.1111/cod.12911
43. Hagvall L, Pour MD, Feng J, Karma M, Hedberg Y, Malmberg P. Skin permeation of nickel, cobalt and chromium salts in ex vivo human skin, visualized using mass spectrometry imaging. *Toxicol In Vitro*. 2021;76:105232. doi:10.1016/j.tiv.2021.105232
44. Kubo A, Ishizaki I, Kubo A, et al. The stratum corneum comprises three layers with distinct metal-ion barrier properties. *Sci Rep*. 2013;3(1):1731. doi:10.1038/srep01731
45. Julander A, Liljedahl ER, Korres de Paula H, et al. Nickel penetration into stratum corneum in FLG null carriers—a human experimental study. *Contact Dermatitis*. 2022;87(2):154-161. doi:10.1111/cod.14137
46. Ross-Hansen K, Østergaard O, Tanassi JT, et al. Filaggrin is a predominant member of the denaturation-resistant nickel-binding proteome of human epidermis. *J Invest Dermatol*. 2014;134(4):1164-1166. doi:10.1038/jid.2013.445
47. Marro D, Guy RH, Delgado-Charro MB. Characterization of the iontophoretic permselectivity properties of human and pig skin. *J Control Release*. 2001;70(1–2):213-217. doi:10.1016/s0168-3659(00)00350-3
48. Wong TW. Electrical, magnetic, photomechanical and cavitational waves to overcome skin barrier for transdermal drug delivery. *J Control Release*. 2014;193:257-269. doi:10.1016/j.jconrel.2014.04.045
49. Eisele CW, Eichelberger L. Water, electrolyte and nitrogen content of human skin. *Proc Soc Exp Biol Med*. 1945;58(1):97-100. doi:10.3181/00379727-58-14856
50. van Middlesworth JM, Wood SA. The stability of palladium(II) hydroxide and hydroxy–chloride complexes: an experimental solubility study at 25–85°C and 1 bar. *Geochim Cosmochim Acta*. 1999;63(11):1751-1765. doi:10.1016/S0016-7037(99)00058-7
51. Drew Tait C, Janecky DR, Rogers PSZ. Speciation of aqueous palladium(II) chloride solutions using optical spectroscopies. *Geochim Cosmochim Acta*. 1991;55(5):1253-1264. doi:10.1016/0016-7037(91)90304-N
52. Riedel E. *Anorganische Chemie*. 5th ed. Walter de Gruyter; 2002.
53. Proksch E. pH in nature, humans and skin. *J Dermatol*. 2018;45(9):1044-1052. doi:10.1111/1346-8138.14489
54. Öhman H, Vahlquist A. In vivo studies concerning a pH gradient in human stratum corneum and upper epidermis. *Acta Derm Venereol*. 1994;74(5):375-379. doi:10.2340/0001555574375379
55. Höper T, Siewert K, Dumit VI, von Bergen M, Schubert K, Haase A. The contact allergen NiSO4 triggers a distinct molecular response in primary human dendritic cells compared to bacterial LPS. *Front Immunol*. 2021;12:644700. doi:10.3389/fimmu.2021.644700
56. Oblak A, Pohar J, Jerala R. MD-2 determinants of nickel and cobalt-mediated activation of human TLR4. *PLoS One*. 2015;10(3):e0120583. doi:10.1371/journal.pone.0120583
57. Vennegaard MT, Dyring-Andersen B, Skov L, et al. Epicutaneous exposure to nickel induces nickel allergy in mice via a MyD88-dependent and interleukin-1-dependent pathway. *Contact Dermatitis*. 2014;71(4):224-232. doi:10.1111/cod.12270
58. Ahlström MG, Thyssen JP, Menné T, et al. Short contact with nickel causes allergic contact dermatitis: an experimental study. *Br J Dermatol*. 2018;179(5):1127-1134. doi:10.1111/bjd.16935
59. Ahlström MG, Midander K, Menné T, et al. Nickel deposition and penetration into the stratum corneum after short metallic nickel contact: an experimental study. *Contact Dermatitis*. 2019;80(2):86-93. doi:10.1111/cod.13136
60. Cavani A, Mei D, Corinti S, et al. Patients with allergic contact dermatitis to nickel and nonallergic individuals display different nickel-specific T cell responses. Evidence for the presence of effector CD8+ and regulatory CD4+ T cells. *J Invest Dermatol*. 1998;111(4):621-628. doi:10.1046/j.1523-1747.1998.00334.x
61. Blomberg-Van Der Flier MV, Burg CKHVD, Pos O, et al. In vitro studies in nickel allergy: diagnostic value of a dual parameter analysis. *J Invest Dermatol*. 1987;88(4):362-368. doi:10.1111/1523-1747.ep12469023
62. Ständer S, Oppel E, Thomas P, Summer B. Evaluation of lymphocyte transformation tests as compared with patch tests in nickel allergy diagnosis. *Contact Dermatitis*. 2017;76(4):228-234. doi:10.1111/cod.12751

SUPPORTING INFORMATION

Additional supporting information can be found online in the Supporting Information section at the end of this article.

How to cite this article: Simon K, Reichardt P, Luch A, Roloff A, Siewert K, Riedel F. Less efficient skin penetration of the metal allergen Pd^{2+} compared to Ni^{2+} and Co^{2+} from patch test preparations. *Contact Dermatitis*. 2024;91(1):11-21. doi:10.1111/cod.14569

Supporting information I: Less efficient skin penetration of the metal allergen Pd^{2+} compared to Ni^{2+} and Co^{2+} from patch test preparations

A Methods

A.1 Chemicals

Water was treated with a MilliPore water treatment system (Merck MilliPore, Merck KGaA, Darmstadt, Germany). Acids and hydrogen peroxide were always used in the concentration declared in this section, unless stated otherwise. Metal standards were bought as reference standards for inductively coupled plasma mass spectrometry (ICP-MS). Metal salts were bought in reagent grade (>98%). Nitric acid (69%) was bought from VWR International LLC (Darmstadt, Germany) in technical quality and then distilled in a sub-boiling aperture (MLS GmbH, Leutkirch, Germany) before use. Sulfuric acid (98%, ultrapur) and hydrochloric acid (30%, suprapur) were acquired from Merck KGaA (Darmstadt, Germany). Hydrogen peroxide (30%, suprapur), iso-propanol (hypergrade) as well as cobalt and indium standards were bought from Supelco Inc. (Bellefonte, Pennsylvania). Dichloromethane (rotisolv pestilyse) and palladium standard were acquired from Carl Roth GmbH & Co. KG (Karlsruhe, Germany). Nickel standard was bought from Inorganic Ventures (I.V. Labs Inc., Christiansburg, Virginia). Fetal bovine serum Good and phosphate-buffered saline (without Ca and Mg; PBS) were purchased from PAN Biotech GmbH (Aidenbach, Germany). Petrolatum (Ph. Eur.), cobalt(II) chloride hexahydrate, nickel(II) sulfate hexahydrate and sodium tetrachloropalladate(II) monohydrate were acquired from Sigma-Aldrich (Merck KGaA). Patch test preparations (PTPs) were acquired from Chemotechnique MB Diagnostics AB (Vellinge, Sweden).

A.2 Protocol of Franz diffusion cell assay

Each Franz diffusion cell (FDC) assay consisted of seven FDCs: one negative control (petrolatum) and six PTP or metal salt solution applications. The skin was partially thawed and a sheet of 500 µm thickness was cut off using a dermatome (Aesculap AG, Tuttlingen, Germany). The sheet was cut into 15 × 15 mm pieces with a scalpel (paragon, neoLab Migge GmbH, Heidelberg, Germany) and the integrity of the pieces was visually controlled. The receptor chamber of the FDCs (PermeGear Inc., Hellertown, Pennsylvania) with a 15 mm diameter (1.76 cm^2 permeation area) was filled with 12 ml of fetal bovine serum. The receptor fluid was continually magnetically stirred. A skin piece (*stratum corneum* (s.c.) side up) was laid atop each receptor chamber and fixed with the polytetrafluorethylene (PTFE) donor

cap and a clamp. It was visually ensured that no air bubbles were present directly under the skin in the receptor fluid. To further verify the integrity of the skin, the trans-epidermal water loss was measured using the AquaFlux device AF200 (Biox systems Ltd, London, United Kingdom) in accordance with Guideline 428 of the Organisation for Economic Co-operation and Development.[1] Skin pieces were excluded and replaced if the trans-epidermal water loss exceeded 13 $g \cdot m^{-2} \cdot h^{-1}$.
Either 20 mg of the respective PTP was weighed onto a cardboard sample cutout (14 mm diameter, TownStix, Singapore), which was placed PTP facing the skin onto the skin, or 200 µl of a 5 µg/ml solution of Ni^{2+}, Co^{2+} and Pd^{2+} in PBS were given onto the skin. The FDC was then incubated for 48 h at 32 ± 1 °C maintained by an externally heated water jacket.
After an incubation time of 24 h, a sample of 100 µl was taken from the receptor chamber with a syringe (Hamilton Bonaduz AG, Bonaduz, Switzerland). After a total of 48 h, the FDCs were disassembled.

Sample preparation of Franz diffusion cell assays with $CoCl_2$ and $NiSO_4$ patch test preparations

The cardboard and the remaining PTP were transferred into a PTFE microwave tube (MLS GmbH, Leutkirch, Germany). The skin and the donor chamber cap were taken off the FDC and wiped dry with a precision tissue (Kimtech Science, Kimberly-Clark Inc., Irving, Texas), which was also added to the microwave tube.
The skin was then stripped 20 times with tape strips (kristall-klar, tesafilm, Tesa SE, Norderstedt, Germany). Four consecutive strips each were placed into a PTFE microwave tube. The remaining skin was also transferred into a PTFE microwave tube. The receptor fluid was filled into a 20 ml volumetric flask (Brand GmbH und Co. KG, Wertheim, Germany). The emptied receptor chamber was rinsed twofold with 2 ml of water, which was filled into the volumetric flask. The flask was filled up to the mark and an aliquot of 6 ml was transferred into a PTFE microwave tube. The receptor fluid sample taken after 24 h was also transferred into a PTFE microwave tube. Internal standard (donor samples: 40 µl of 1000 µg/ml of indium in 3.5% nitric acid; all other samples: 100 µl of 1000 ng/ml of indium in 3.5% nitric acid), nitric acid (donor samples: 3.5 ml; all other samples: 2.5 ml), hydrogen peroxide (donor samples: none; all other samples: 1 ml) and water (tape strip, remaining skin and receptor fluid 24 h samples: 1 ml; donor and receptor fluid sample 48 h: none) were added to each of the microwave tubes. The samples were placed into a microwave autoclave (MLS GmbH) with a baseload of 320 ml of water, 30 ml of hydrogen peroxide and 2 ml of sulfuric acid. For the digestion program, see Table S1 for donor and tape strip samples and Table S2 for remaining skin and receptor fluid samples. After the digestion and cool down, the sample solutions were transferred into 50 ml polypropylene tubes (Corning Science Inc.), rinsed

twice with 2 ml of water and filled up with water. The donor samples were further diluted: 125 µl of the solution were filled up to 50 ml with nitric acid (3.5%). The samples were then quantified by ICP-MS. The PTFE microwave tubes were subject to a cleanup microwave digestion using nitric acid, hydrogen peroxide and water (program: Table S3).

Table S1: Microwave digestion program for donor compartment and tape strip samples. P_{max} is the maximum power of the microwave radiation, T_1 is the target temperature in the samples after the specified time t, T_2 is the maximum allowed temperature in the cooling water and p is the maximum pressure inside the microwave.

step	t [min]	P_{max} [W]	T_1 [°C]	T_2 [°C]	p [bar]
1	6.00	1000	110	60	100
2	10.00	1000	160	60	120
3	15.00	1000	200	60	160
4	45.00	1000	200	60	160
5	50.00	cooling down			

Table S2: Microwave digestion program for remaining skin and receptor fluid samples. P_{max} is the maximum power of the microwave radiation, T_1 is the target temperature in the samples after the specified time t, T_2 is the maximum allowed temperature in the cooling water, and p is the maximum pressure inside the microwave.

step	t [min]	P_{max} [W]	T_1 [°C]	T_2 [°C]	p [bar]
1	10.00	700	85	50	100
2	9.00	500	145	50	100
3	4.00	1000	200	50	150
4	14.00	1000	200	50	160
5	cooling down				

Table S3: Microwave digestion program for cleanup. P_{max} is the maximum power of the microwave radiation, T_1 is the target temperature in the samples after the specified time t, T_2 is the maximum allowed temperature in the cooling water, and p is the maximum pressure inside the microwave.

step	t [min]	P_{max} [W]	T_1 [°C]	T_2 [°C]	p [bar]
1	3.00	700	85	50	100
2	9.00	500	145	50	100
3	4.00	1000	180	50	150
4	14.00	1000	180	50	160
5			cooling down		

Sample preparation of Franz diffusion cell assays with $PdCl_2$ and Na_2PdCl_4 patch test preparations

The cardboard and remaining PTP were placed into 50 ml polypropylene centrifugal tubes. The skin and the donor chamber cap were taken off the FDC and wiped dry with a precision tissue, which was also added to the tube. The donor samples were extracted using hydrochloric acid: internal standard (40 µl of 1000 µg/ml of indium in 3.5% nitric acid) was given into the tubes, along with 5 ml of dichloromethane. The tubes were mixed (vortex, Scientific Industries Inc., Bohemia, New York) until the petrolatum of the PTP was dissolved. The liquid phase was transferred into a second 50 ml tube. 15 ml of hydrochloric acid was added into the first tube to extract the tissue and the cardboard as well as remaining residues. The tube was shaken and the hydrochloric acid was transferred into the second tube to extract the dichloromethane. The tube was shaken, centrifuged (2900 rcf, 5 min, room temperature; Hettich GmbH und Co. KG) and the aqueous phase was transferred into a third tube. The extraction using hydrochloric acid was repeated twice. The pooled aqueous phases were filled up to 50 ml with hydrochloric acid. 1.5 ml of this solution was passed through a nylon syringe filter (0.2 µm, Merck) and 125 µl of the filtrate were filled up to 50 ml with 3.5% nitric acid. The diluted solutions were then used for quantification by ICP-MS.
The skin was stripped 20 times with tape strips. Four consecutive strips each were given into a glass test tube. The remaining skin was also given into a glass test tube (VWR International LLC, Darmstadt, Germany).
The receptor fluid was filled into a 20 ml volumetric flask. The emptied receptor chamber was rinsed twofold with 2 ml of water, which was filled into the volumetric flask. The flask was filled up to the mark and an aliquot of 6 ml was given into a glass test tube.
Internal standard (100 µl of 1000 ng/ml of indium in 3.5% nitric acid), nitric acid (2.5 ml), hydrogen peroxide (1 ml) and water (receptor fluid 48 h samples: none; all other samples:

1 ml) were added to each of the glass test tubes. The samples were placed into a microwave autoclave with a baseload of 320 ml of water, 30 ml of hydrogen peroxide and 2 ml of sulfuric acid. For the digestion program, see Table S1 for tape strips and Table S2 for all other samples. After the digestion and cool down, the sample solutions were transferred into 50 ml tubes, rinsed twice with 2 ml of water and filled up with water. The samples were then quantified by ICP-MS. The glass tubes were discarded after use.

Franz diffusion cell with metal salt solutions in phosphate-buffered saline

The skin and the donor chamber cap were taken off the FDC and wiped dry with a precision tissue, which was transferred to a 50 ml polypropylene centrifugal tube. The donor samples were extracted using hydrochloric acid: internal standard (500 µl of 1000 ng/ml of indium in 3.5% nitric acid) was given into the tubes, along with 10 ml of hydrochloric acid. The tubes were shaken (vortex) and the liquid phase was transferred into a second 50 ml tube. The extraction using hydrochloric acid was repeated twice. The pooled aqueous phases were filled up to 50 ml with water. 15 ml of this solution was passed through a polyethersulfone syringe filter (0.45 µm, Merck) and 10 ml of the filtrate along with 2.5 ml of nitric acid were filled up to 50 ml with water. The diluted solutions were then used for quantification by ICP-MS.

The skin was stripped 20 times with tape strips. Four consecutive strips each were given into a glass test tube. The remaining skin was also given into a glass test tube.

The receptor fluid was filled into a 20 ml volumetric flask and rinsed twofold with 2 ml of water. The flask was filled up to the mark and an aliquot of 6 ml was given into a glass test tube.

Internal standard (100 µl of 1000 ng/ml of indium in 3.5% nitric acid), nitric acid (2.5 ml), hydrogen peroxide (1 ml) and water (receptor fluid samples 48 h: none; all other samples: 1 ml) were added to each of the glass test tubes. The samples were placed into a microwave autoclave with a baseload of 320 ml of water, 30 ml of hydrogen peroxide and 2 ml of sulfuric acid. For the digestion program, see Table S1 for tape strips and Table S2 for all other samples. After the digestion and cool down, the sample solutions were transferred into 50 ml tubes, rinsed twice with 2 ml of water and filled up with water. The samples were then quantified by ICP-MS. The glass tubes were discarded after use.

A.3 Establishment of sample preparation for quantification

In a series of experiments, the digestion of the different matrices was tested. The results are summarized here. For a detailed description of the developed method, see section A.2 *Protocol of Franz diffusion cell assay*. The matrices were spiked with the analytes and subjected

to a microwave digestion using acids. Two different microwave programs were used (Table S1 and S2) since petrolatum and the tape strips needed more aggressive conditions than the remaining skin and the receptor fluid.

Acidic microwave digestion of the petrolatum proved challenging in the presence of Pd^{2+}. Different acids in different ratios were tested but the digested solution always contained an unidentified, insoluble, white substance. After numerous trials to digest petrolatum in presence of Pd^{2+}, a different approach was chosen: the PTP was extracted with hydrochloric acid and filtered. This approach proved to be successful and reproducible. The microwave digestion of the PTP in nitric acid containing Ni^{2+} and Co^{2+} was unproblematic. Digestion of the tape strips was successful up to a maximum of four tape strips, which is why four consecutive tape strips were pooled. The digestion of the remaining skin showed that nickel was present in the blank matrix. This was eliminated by using a scalpel to cut out the skin samples instead of the commonly used cast iron punch. The digestion of the receptor fluid needed no adjustments.

During the digestion trials in PTFE microwave tubes, Pd^{2+} showed a very strong carry-over effect. This lead to the usage of single use glass test tubes whenever Pd^{2+} was present. However, Ni^{2+} was detected in the digestion fluid when using the glass tubes. Hence, PTFE tubes were used for nickel and cobalt set-ups. In the FDC assays of the metal salt solutions, Ni^{2+} and Pd^{2+} were both present in the samples. Thus, the glass tubes were subject to a cleanup microwave digestion using nitric acid, hydrogen peroxide and water (program: Table S3). This eliminated contamination with Ni^{2+} successfully. All matrices were digested as blank samples and measured by ICP-MS according to protocol (see section A.2 *Protocol of Franz diffusion cell assay*) to assure that they were free of the investigated metals.

Recovery Experiments

To determine the recovery of each metal after digestion, the different matrices were spiked with a reference standard solution (1000 µg/ml) of the respective metal ion. Then the matrices were digested or extracted according to protocol (see section A.2 *Protocol of Franz diffusion cell assay*). After the digestion and extraction, the digestion fluids and the extracts were quantified by ICP-MS and the recovery was recorded (see Table S4). The recovery was used to correct the calculated masses of the respective ions in the FDC assays.

Table S4: Recoveries after sample preparation of spiked matrices. n = 5 replicates per matrix. PTP: patch test preparation, PBS: phosphate buffered saline.

matrix	recovery [%]		
	Ni^{2+}	Co^{2+}	Pd^{2+}
$NiSO_4$ PTP	98.5 ± 1.3	—	—
$CoCl_2$ PTP	—	102.2 ± 1.6	—
$PdCl_2$ PTP	—	—	105.1 ± 3.4
Na_2PdCl_4 PTP	—	—	114.9 ± 2.8
PBS with Ni^{2+}, Co^{2+}, Pd^{2+}	95.9 ± 0.9	93.0 ± 0.2	82.0 ± 1.2
tape strips	101.1 ± 5.1	96.4 ± 0.6	42.1 ± 2.2
remaining skin	104.0 ± 4.8	98.7 ± 1.9	87.6 ± 2.1
receptor fluid	104.0 ± 4.8 (sic)	94.4 ± 3.9	100.2 ± 0.6

Limit of detection and limit of quantification

The limits of detection (LOD) and limits of quantification (LOQ) of the ICP-MS for each metal were determined and are summarized in Table S5. Blank nitric acid solutions (3.5%) were quantified by ICP-MS. The LOD is defined as the noise plus three times its standard deviation and the LOQ as the noise plus ten times its standard deviation.[2]

Table S5: Limit of detection (LOD) and limit of quantification (LOQ).

ion	LOD [ng/ml]	LOQ [ng/ml]
Ni^{2+}	0.05	0.12
Co^{2+}	<0.01	<0.01
Pd^{2+}	0.05	0.10

A.4 Solubility of palladium salts

30 mg of $PdCl_2$ were weighed into a 15 ml polypropylene centrifugal tube (Corning Science Inc., Reynosa, Mexico). 100 mg of Na_2PdCl_4 were weighed into a 1 ml polypropylene centrifugal tube (Eppendorf SE, Hamburg, Germany). The tubes were filled up to the respective mark with water, shaken and placed into an ultrasonic bath for 15 min at room temperature. The tubes were then stored at room temperature for 60 h and transferred into a shaker (35 rpm, Turbula, Bachofen AG, Muttenz, Switzerland) for 94 h. The solutions were centrifuged ($PdCl_2$: 2900 rcf, 5 min, room temperature; Hettich GmbH und Co. KG, Tuttlingen, Germany, Na_2PdCl_4: 16000 rcf, 5 min, room temperature, Eppendorf SE) and the

supernatant was filtered (polyethersulfone syringe filter, 0.22 µm, Merck). The solution was diluted $1:1\cdot10^6$ with water and the metal ion concentrations were determined by ICP-MS. The experiment was performed in five replicates.

A.5 ICP-MS quantification

The samples were quantified using internal and external calibration. The ICP-MS system was set up with a Prep-Fast system, which introduced the sample solutions. The solutions were all spiked with indium as internal standard (see section A.2 *Protocol of Franz diffusion cell assay*). The spiked internal standard concentration was set to 2 ng/ml of indium in the final solutions. Furthermore, the final concentrations were divided by the mean recoveries found during the method development (see Table S4) to correct for sample loss. The calibration was performed using a weighted linear regression (weighted by c^{-1}).

B Box plots for outlier analysis

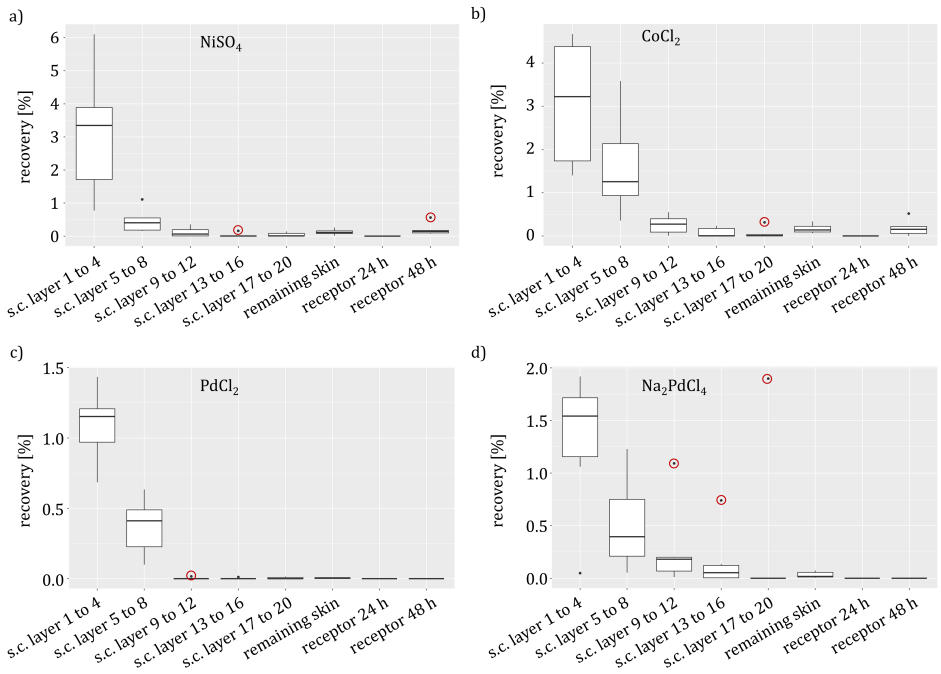

Figure S1: Boxplots showing the recovery of Ni^{2+}, Co^{2+} and Pd^{2+} in the different compartments of the FDC assays with PTP applied. a) $NiSO_4$ PTP, b) $CoCl_2$ PTP, c) $PdCl_2$ PTP, d) Na_2PdCl_4 PTP. Concentrations in donor samples were much higher and are thus depicted in a separate figure (Fig. S2). $n = 6$ replicates. PTP: patch test preparation, FDC: Franz diffusion cell, s.c.: *stratum corneum*. Outliers were circled in red and not included in further data analysis.

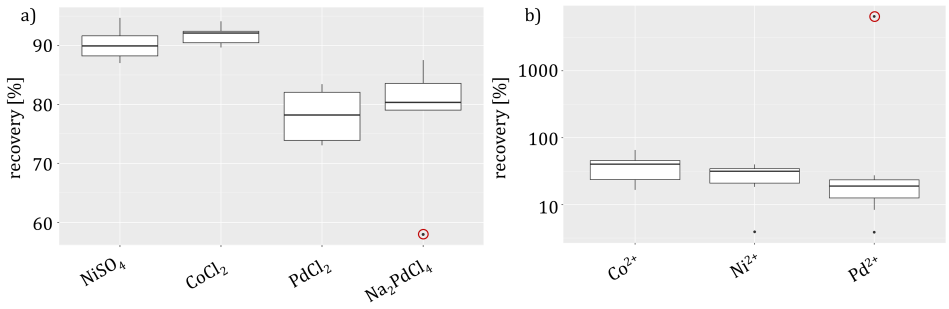

Figure S2: Boxplots showing the recovery of Ni^{2+}, Co^{2+} and Pd^{2+} in the donor compartment samples. a) Donor compartments of the different PTPs. b) Donor compartments of the metal salt solution (logarithmic scale). $n = 6$ replicates. PTP: patch test preparation. Outliers were circled in red and not included in further data analysis.

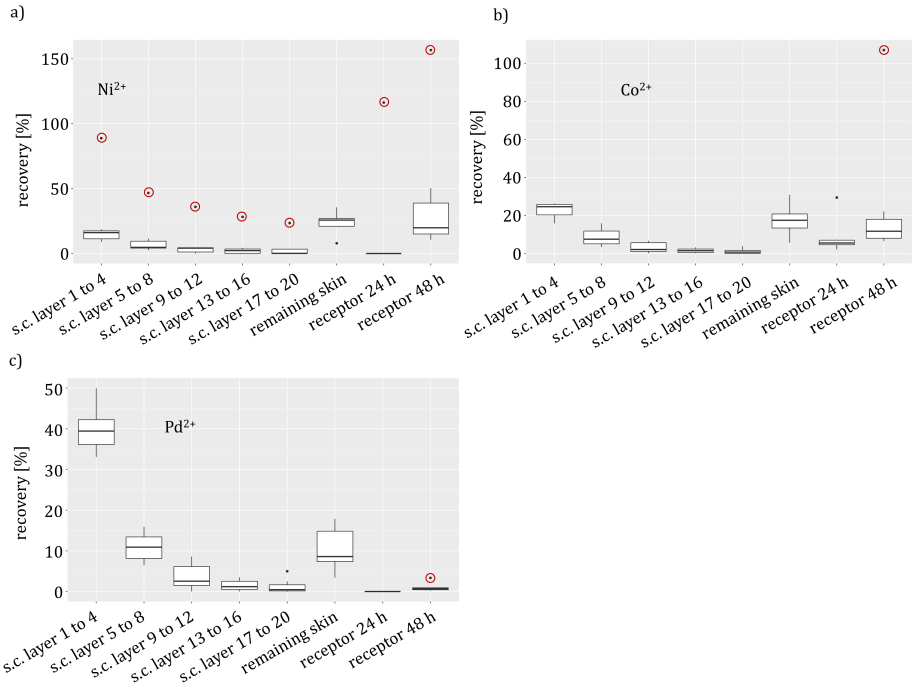

Figure S3: Boxplots showing the recovery of a) Ni^{2+}, b) Co^{2+} and c) Pd^{2+} in the different compartments of the FDC assay with the metal salt solutions. Concentrations in donor samples were much higher and are thus depicted in a separate figure (Fig. S2). FDC: Franz diffusion cell, s.c.: *stratum corneum*. $n = 6$ replicates. Outliers were circled in red and not included in further data analysis.

References

1. *OECD Guideline for the Testing of Chemicals No. 428: Skin Absorption: in vitro Method* 2004.
2. Kaiser, H. Zum Problem der Nachweisgrenze. *Fresenius' Zeitschrift für analytische Chemie* **209,** 1–18. doi:10.1007/BF00508735 (1965).